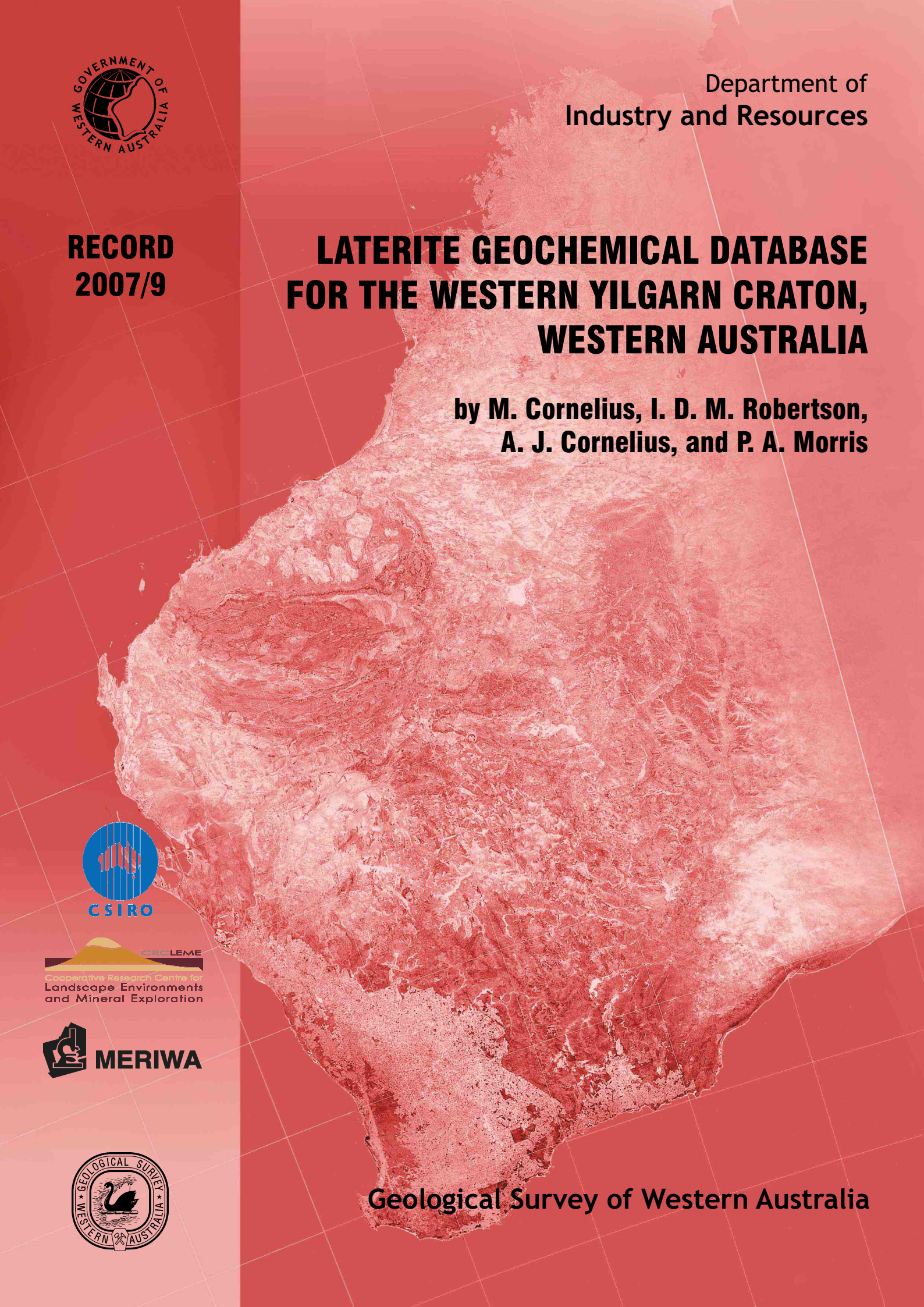

Department of
Industry and Resources

RECORD
2007/9

LATERITE GEOCHEMICAL DATABASE FOR THE WESTERN YILGARN CRATON, WESTERN AUSTRALIA

by M. Cornelius, I. D. M. Robertson,
A. J. Cornelius, and P. A. Morris

CSIRO

CRCLEME
Cooperative Research Centre for
Landscape Environments
and Mineral Exploration

MERIWA

Geological Survey of Western Australia

GEOLOGICAL SURVEY OF WESTERN AUSTRALIA

Record 2007/9

LATERITE GEOCHEMICAL DATABASE FOR THE WESTERN YILGARN CRATON, WESTERN AUSTRALIA

by
M. Cornelius[1], I. D. M. Robertson[1], A. J. Cornelius[1], and P. A. Morris

[1] CSIRO Exploration and Mining, PO Box 1130, Bentley, W.A. 6102

Perth 2007

MINISTER FOR RESOURCES
Hon. Francis Logan MLA

DIRECTOR GENERAL, DEPARTMENT OF INDUSTRY AND RESOURCES
Jim Limerick

EXECUTIVE DIRECTOR, GEOLOGICAL SURVEY OF WESTERN AUSTRALIA
Tim Griffin

CRC LEME Reference: Open File Report 116
CSIRO Exploration and Mining Reference: Report P2007/202

REFERENCE
The recommended reference for this publication is:
CORNELIUS, M., ROBERTSON, I. D. M., CORNELIUS, A. J., and MORRIS, P. A., 2007, Laterite geochemical database for the western Yilgarn Craton, Western Australia: Western Australia Geological Survey, Record 2007/9, 44p.

National Library of Australia Card Number and ISBN 978 1 74168 102 4

Grid references in this publication refer to the Geocentric Datum of Australia 1994 (GDA94). Locations mentioned in the text are referenced using Map Grid Australia (MGA) coordinates, Zone 50. All locations are quoted to at least the nearest 100 m.

Cover image modified from Landsat data, courtesy of ACRES

Published 2007 by Geological Survey of Western Australia
This Record is published in digital format (PDF), as part of a digital dataset on DVD, and is available online at www.doir.wa.gov.au/GSWA/publications. Laser-printed copies can be ordered from the Information Centre for the cost of printing and binding.

Further details of geological publications and maps produced by the Geological Survey of Western Australia are available from:
Information Centre
Department of Industry and Resources
100 Plain Street
EAST PERTH, WESTERN AUSTRALIA 6004
Telephone: +61 8 9222 3459 Facsimile: +61 8 9222 3444
www.doir.wa.gov.au/GSWA/publications

Contents

Appendices

Figures

Tables

Laterite geochemical database for the western Yilgarn Craton, Western Australia

by

M. Cornelius[1], I. D. M. Robertson[1], A. J. Cornelius[1], and P. A. Morris

Abstract

This Record is the final release of a 53-element dataset for approximately 3150 laterite samples (59-element dataset for selected samples) from the western Yilgarn Craton. Samples were taken at a nominal 9-km spacing on an approximately triangular grid, with each sample comprising about 1 kg of ferruginous nodules and pisoliths from lateritic residuum, lag formed from lateritic residuum, or of ferruginous gravel contained in locally derived colluvium. Some authigenic pisoliths and nodules formed in depositional regimes might have been included inadvertently.

The laterite geochemical database is designed to provide a regional geochemical framework at a sample spacing sufficiently close to recognize regional geochemical trends and major lithological differences. The wide-spaced sampling may also provide an indication of broad geochemical dispersion patterns from mineralized systems. However, the 9-km spacing was not designed to detect individual geochemical halos, for which 1-km or 500-m spacing is more appropriate. The sample spacing is wide enough to cover a substantial part of the Yilgarn Craton and still provide useful data for exploration and environmental purposes.

There are several significant results of the sampling completed in the southwest and northwest quadrants of the Yilgarn Craton. These include: a) increased Au abundances in the northeast part of the sampling area that cluster around known gold deposits; their extent might mean more widespread mineralization in these areas; b) the chalcophile element index (CHI6*) illustrates potential for Au and base metal mineralization in the westernmost part of the Yilgarn Craton; the pegmatophile PEG4* index shows a regional northwest trend north of the Saddleback greenstone belt; c) chromium abundances in nominally granitic terrain might indicate mafic–ultramafic remnants outside the known greenstone belts; d) a regional Hg anomaly (as yet unexplained) trends northwest over more than 500 km.

This final report, together with the release of the digital analytical data as a database, provides information about the sampling strategy, preparation methods, analysis, and some new element-distribution patterns with significance to exploration.

KEYWORDS: Archean, Yilgarn Craton, Western Australia, laterites, geochemistry.

Introduction

Background

The main objective of the laterite geochemical database is to stimulate mineral exploration in the Yilgarn Craton. Data for the western Yilgarn Craton (the 'survey area') are intended to demonstrate the feasibility and value of low-density geochemical maps of the whole Yilgarn Craton and adjacent terrains, using a consistent sample medium.

This Record accompanies the final release of 'laterite'* geochemical data from the western Yilgarn Craton. Data for the southwest Yilgarn Craton was released in February 2006 as an interim report (Cornelius et al., 2006). There was strong interest by industry in the first release and within four weeks of this release, approximately 25 exploration licences covering some 20 000 km^2 were applied for, representing an approximate three-fold increase in pegging compared to the month preceding the data release.

Statistical examination of laterite geochemistry data from the CSIRO–AGE database (Smith et al., 1992; Geological Survey of Western Australia, 1998), covering the southwest Yilgarn Craton, demonstrated that low-density sampling (9 × 9-km spacing or one sample per 70 km^2) can outline regional geochemical trends (Cornelius et al., 2001) that are of value to the mineral exploration industry. This has important implications for mineral exploration as most of the western Yilgarn Craton can be sampled at this spacing because there are small remnants of lateritic residuum, even in largely eroded terrains. In colluvial–depositional terrains, ferruginous

[1] CSIRO Exploration and Mining, PO Box 1130, WA 6102

* The term 'laterite', as used in this Record, refers to lateritic residuum (ferruginous duricrust, nodules, and pisoliths), lag formed from lateritic residuum, and nodules and pisoliths that have become part of colluvium in the context of laterite geochemistry. Some of the materials classified here as lateritic residuum might have experienced local transport of about 100–200 m, or might have formed in sediment.

nodules and pisoliths can form part of the colluvium or might form lenses within it. This material, although no longer residual, has regional geochemical relevance at the sampling interval used.

The southwest Yilgarn Craton was selected as the starting point, as there is much existing data and access is relatively easy due to a well-developed road and track network. Apart from the world-class bauxite deposits, the Boddington Au mine, and the Greenbushes rare metal pegmatite, the southwest Yilgarn Craton has an apparent lesser mineral endowment than its eastern counterpart. This might, in part, reflect less intense exploration. Following completion of sampling in the southwest Yilgarn Craton, sampling progressed into the northwest Yilgarn Craton. There, access north and east of the agricultural areas was along tracks and fence lines, mainly on pastoral leases. Sampling progress was slower than in the southwest Yilgarn Craton and parts of the northwest Yilgarn Craton (Belele*, Murgoo, Byro, and Cue) were excised from the program due to shortage of funds and staff. Sampling is incomplete on Jackson, Southern Cross, Bencubbin, Ninghan, Barlee, Sandstone, and Youanmi.

The geochemical database will provide baseline data for comparison with both existing and new datasets. The data might also prove useful for bedrock identification, and for environmental purposes such as the regional distribution of Se for agriculture and geomedical studies.

The choice of analytes and analytical methods was based on the expected abundances and likely mineral hosts in this ferruginous sample medium. For a few elements, compromise was needed between the most suitable method and budget constraints. However, field reference material and pulps are stored with the Geological Survey of Western Australia for further analysis.

Climate

Inland, the western half of the Yilgarn Craton is semi-arid; whereas closer to the coast and in the southwest the climate is typically Mediterranean with dry summers and cool winters. Mean annual rainfall ranges from greater than 1000 mm near the coast and in the southwest to 200 mm inland (Fig. 1).

Geology of the western Yilgarn Craton

The western part of the Archean Yilgarn Craton consists of variably metamorphosed igneous and sedimentary rocks. Supracrustal sequences include metamorphosed mafic volcanic rocks, with less common ultramafic rocks, chemical and siliciclastic sedimentary rocks, and intermediate to felsic volcanic rocks (Fig. 2). Mineralization includes structurally controlled and, less commonly, stratabound gold deposits, stratabound nickel and base metal deposits, and supergene-enriched iron ore deposits. Gold mineralization, in particular, shows a strong spatial relationship with regional structures and greenstones, and areas of potential for platinum group element (PGE) and vanadium mineralization are also associated with greenstones.

A combination of detailed mapping, and new geochronological, isotopic, geophysical, and geochemical data has improved the understanding of the tectonic evolution of the Yilgarn Craton (Fig. 3), which has recently been summarized by Cassidy et al., (2006). They have used an hierarchical scheme to subdivide the Yilgarn Craton into six terranes (some of which contain domains), three of which are grouped into the Eastern Goldfields Superterrane. This terminology follows Neuendorf et al. (2005), where a terrane is a series of regional-scale fault-bounded rock bodies with a different geological history to adjacent associations, and domains are fault-bounded geologically contiguous blocks within terranes (Cassidy et al., 2005). The western part of the Yilgarn Craton (i.e. the focus of this survey; west of latitude 120°E and south of longitude 28°S) comprises the South West Terrane and part of the Youanmi Terrane, the latter consisting of the Southern Cross and Murchison Domains. This subdivision is similar to that of Tyler and Hocking (2001), although their Southern Cross and Murchison Granite–Greenstone Terranes have been recast as the Southern Cross and Murchison Domains respectively.

The South West Terrane, which largely comprises granitic rocks (including granitic gneiss) with crystallization ages of 2.75 to 2.72 Ga (Nemchin and Pidgeon, 1997), has undergone multiple phases of late-Archean deformation. Supracrustal rocks of the South West Terrane are mid- to late Archean (3.2 to 2.8 Ga; Chittering, Jimperding, Balingup belts), although older detrital zircons have been dated from quartzites in the Jimperding metamorphic belt (Wilde et al., 1996). Wilde et al. (1996) grouped these rocks into the Jimperding, Chittering and Balingup metamorphic belts, but Cassidy et al. (2006) did not continue this subdivision, arguing that the boundaries between the belts are poorly defined. These metamorphic rocks are dominated by ortho- and paragneiss, with localized gradations to quartzites, quartz–mica schists, and banded iron-formation (BIF), with pelitic rocks more common in some belts (Wilde et al., 1996). Small pockets of greenstones consist of volcanic and sedimentary rocks. The Wongan Hills greenstone belt, east of New Norcia, is dominated by mafic volcanic rocks, with less common felsic volcanic rocks, chemical sedimentary rocks, mica schists, and ultramafic intrusive rocks. Mafic rocks also dominate the Morangup greenstone belt near Toodyay, with intermediate volcanic rocks and some metasedimentary rocks. The Saddleback greenstone belt, near Boddington, is very poorly exposed due to deep weathering and a generally well-preserved residual regolith (Anand, 1994). According to a summary presented by Hassan (1998), it is dominated by mafic volcanic rocks, in addition to siliciclastic sedimentary rocks, acidic volcanic rocks, and high-level intrusive rocks. Geochronological data for the Saddleback greenstone belt indicates two periods of igneous activity at c. 2700 and 2675 Ma (Allibone et al., 1996). Wilde et al. (1996) argued that the Morangup greenstone belt was of a similar age.

* Capitalized names refer to standard 1:250 000 map sheets.

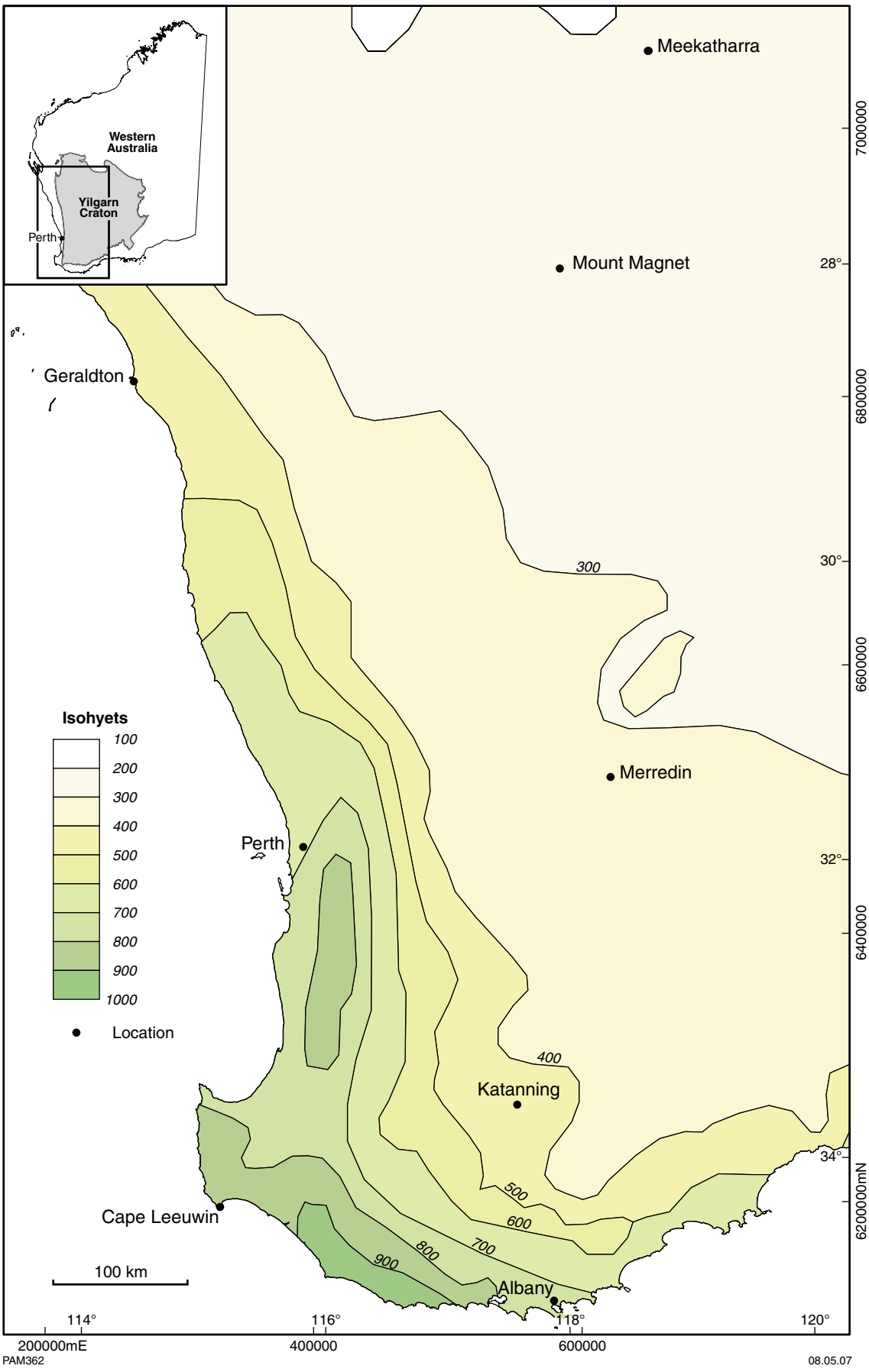

Figure 1. Contoured average rainfall for the western Yilgarn Craton (after Australian Bureau of Meteorology website)

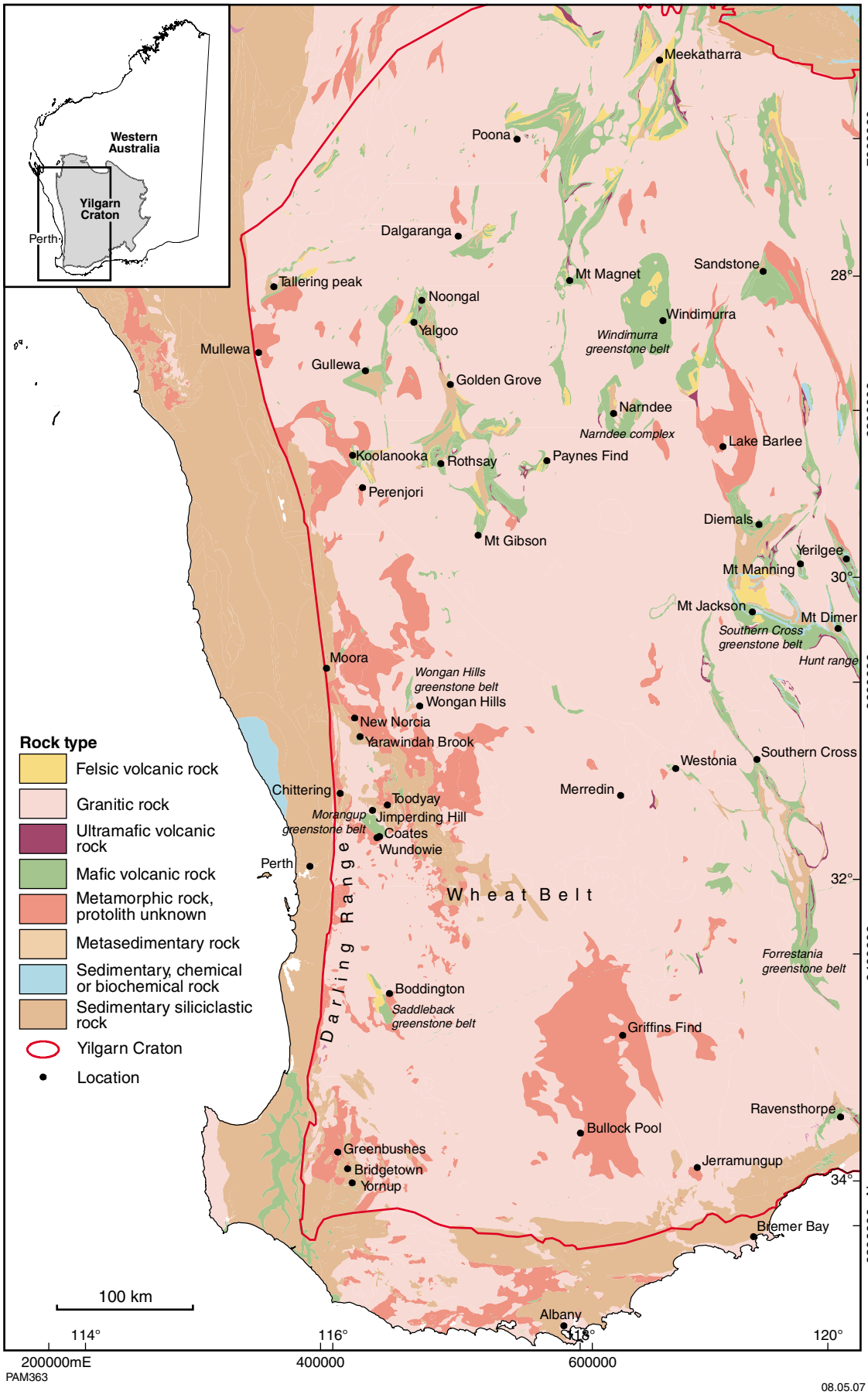

Figure 2. Geology of the western Yilgarn Craton (after Wilde et al., 1996; Myers and Hocking, 1998)

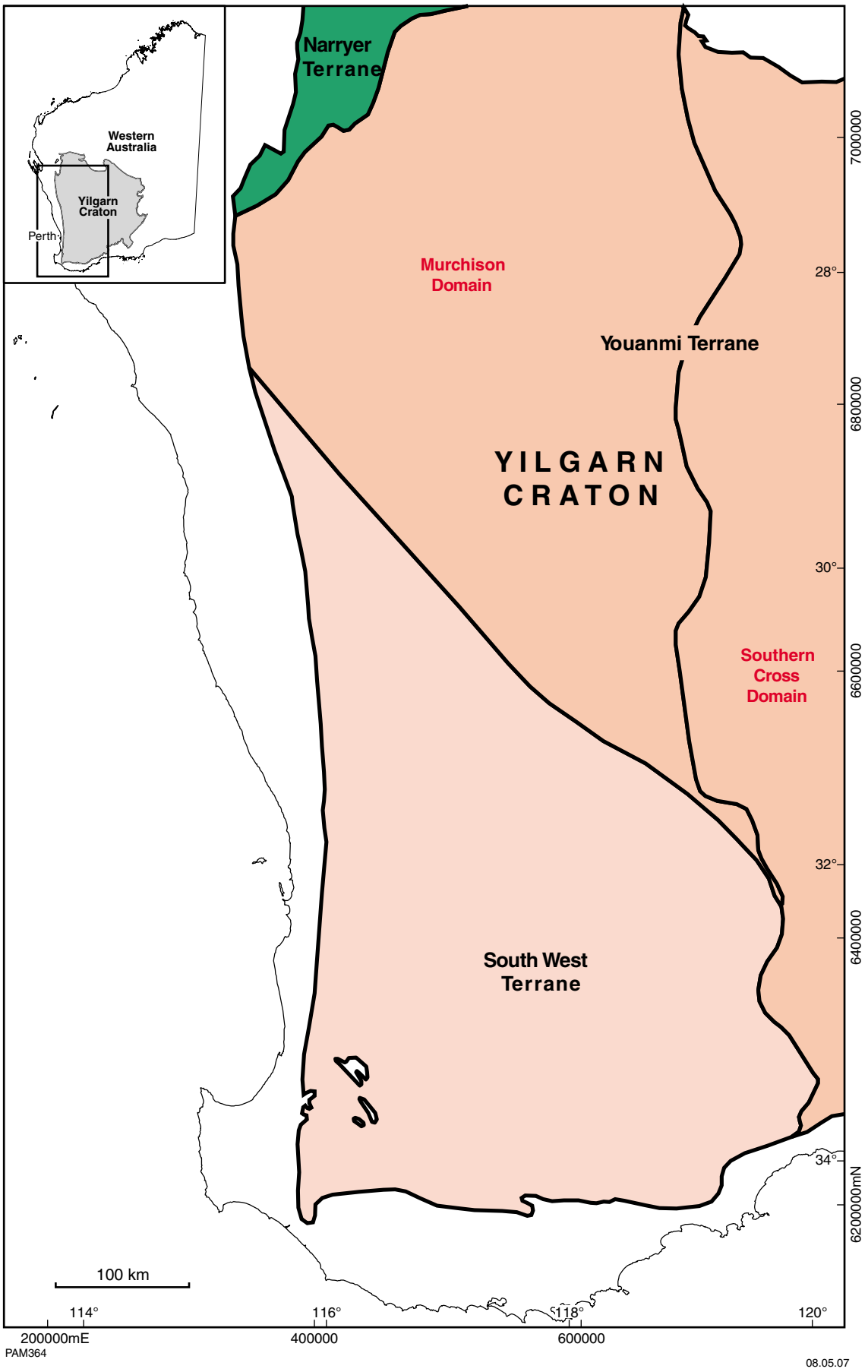

Figure 3. Tectonic and structural provinces of the western Yilgarn Craton (after Cassidy et al., 2006)

Granitic rocks and granitic gneiss are also found in both domains of the Youanmi Terrane. Both rock types are associated with more common and extensive, northeast-oriented, elongate greenstone belts (Cassidy et al., 2006). In the Murchison area, Watkins (1990) identified two greenstone successions and four granitoid suites. Granitic rocks comprise a granodiorite–monzogranite (metamorphosed to a pegmatite-banded gneiss), a deformed and metamorphosed monzogranite, and two compositionally variable suites of post-deformational granitic rocks. In a summary of greenstone belt lithologies, Watkins (1990) and Watkins and Hickman (1990) noted the dominance of mafic volcanic and intrusive rocks, with only small amounts of ultramafic rocks. They also noted that felsic volcanic and sedimentary rocks are generally found together, many forming thick successions. Although there is agreement that the lower parts of greenstone successions in the Murchison Domain have more BIF than the upper part (the latter being dominated by mafic volcanic rocks, with less common intermediate volcanic rocks and komatiitic basalt; e.g. Pidgeon and Hallberg, 2000), the more formalized approach to greenstone stratigraphy proposed by Watkins and Hickman (1990) has been disputed. They divided greenstones into the Luke Creek and Mount Farmer Groups (together making up the Murchison Supergroup), but Pidgeon and Hallberg (2000), amongst others, have argued that structural complexity and separation of greenstone successions by granitic rocks makes stratigraphic correlation unreliable. Instead, they proposed an informal stratigraphic subdivision based on packages of greenstones termed assemblages. The three stratigraphically lowest assemblages comprise ultramafic, mafic and intermediate volcanic rocks, with the overlying fourth assemblage consisting of felsic volcanic rocks, generally of a more limited extent. Zircon chronology indicates periods of emplacement at 3.0–2.9, 2.747, and 2.719 Ga (Cassidy et al., 2006).

Unlike the South West Terrane, depositional ages of greenstones in the Youanmi Terrane span a wider interval, including c. 3.05–2.93, 2.81, and 2.76–2.72 Ga (Cassidy et al., 2006, and references therein). Granitic rocks and granitic gneiss were emplaced in the mid- to late Archean (Cassidy et al., 2002; Geological Survey of Western Australia, 2005), and zircon ages as old as 4.3 Ga (Wyche et al., 2004) show that the Youanmi Terrane might contain some of the oldest known crustal components.

In terms of lithostratigraphy, greenstone belts generally consist of a lower succession dominated by mafic and less common ultramafic volcanic rocks (underlain by quartzite), BIF, and a minor felsic volcanic component. Localized younger greenstone successions (e.g. in the Marda–Diemals area of the Southern Cross Domain) have a larger felsic volcanic and sedimentary rock component.

Individual greenstone belts have been described by a variety of authors. The Wongan Hills greenstone belt was briefly described by Watkins (1990), largely based on the work of Carter and Lipple (1982) and Lipple (1982). These rocks comprise mafic and felsic volcanic rocks, in addition to siliciclastic and chemical sedimentary rocks. Pidgeon and Wilde (1985, 1986) report ages of c. 3.00 Ga and c. 2.70–2.60 Ga for porphyry and granitic rocks.

The regional geology of the Forrestania greenstone belt, which forms part of the Southern Cross greenstone belt (Fig. 2), is a series of six ultramafic belts comprising cumulate flow units, pyroxenitic and gabbroic rocks, quart–mica schists (interpreted as metamorphosed tuffs), and mafic volcanic flows and tuffs (Perring et al., 1996).

Greenstones in the northern part of the Southern Cross greenstone belt have been described by Wyche et al. (2001), Riganti and Chen (2002), and Chen and Wyche (2003). The best exposed and most extensive is the Marda–Diemals greenstone belt that consists of a lower succession of mafic volcanic rocks and BIF, which can be subdivided into three lithostratigraphic packages and is dated at c. 3.0 Ga (Cassidy et al., 2006). The lower succession is unconformably overlain by a succession of intermediate to felsic volcanic rocks (Marda Complex), and siliciclastic sedimentary rocks (Diemals Formation), dated at 2.73 Ga (Cassidy et al., 2006). Chen and Wyche (2003) suggested other greenstone belts in this area (Hunt Range, Mount Manning, and the Yerilgee greenstone belts) could be stratigraphically correlated with parts of the Marda–Diemals greenstone belt.

Layered mafic intrusions (i.e. at Windimurra and Narndee) are located in the eastern part of the Murchison Domain. The disposition and lithological content of these intrusions have been described by Ahmat (1990) and Ruddock (1990) respectively. Both intrusions are located close to the margin of the Murchison and Southern Cross Domains. The Windimurra Complex is a layered gabbroic intrusion greater than 2300 km^2 in size. It contains vanadiferous and titaniferous magnetite bands up to 10 m thick, and localized chromite-rich segregations. According to Ahmat (1990), the complex represents an intrusion of tholeiitic magma at high levels during a period of crustal extension. The Narndee Complex comprises structurally disturbed peridotitic and pyroxenitic units exposed over a strike of 40 km, with a thickness of about 9 km (Ruddock, 1990). Although an igneous stratigraphy is difficult to determine, due to poor outcrop and deformation, the complex appears to represent multiple phases of intrusion of basic and more acidic magma.

Mineral deposits

The mineral resources in the northwest of the survey area were described by the Geological Survey of Western Australia (GSWA; Flint et al., 2000) as part of a summary of the Mid West region. The region hosts a number of mineral commodities such as alumina, coal, gold, mineral sands, base metals, rare metals, silver, talc, chromite, petroleum products, lime sand, limestone, and clay. A review of the mineralization and mineral potential of southwest Western Australia is given in Hassan (1998).

In the western Yilgarn Craton, economic gold mineralization is associated with Archean greenstones and most gold deposits are structurally controlled, associated with faults, shears or fractures. In a summary of the spatial distribution of gold deposits in the Murchison area, Watkins and Hickman (1990) noted that most gold deposits were found within 1 km of structures hosted

by greenstones, and many deposits were within 2–3 km of granite–greenstone contacts. They also noted that mines with higher production were found in chemical sedimentary rocks. In addition to these bedrock deposits, chemical weathering has developed supergene ore. Flint et al. (2000) noted that dispersion of material from these bedrock and supergene deposits has also provided substantial geochemical halos that are targeted by exploration. At the Mount Gibson deposit, gold mineralization is, in part, hosted by laterite developed on a bedrock resource. The Boddington gold deposit (approximately 100 km south of Perth, with total contained gold estimated at 19.7 Moz with 790 kt of Cu; Flint and Abeysinghe, 2006) is largely hosted in regolith that formed on mineralized bedrock of the Saddleback greenstone belt (Anand, 1994; Symons et al., 1990).

Although most known nickel-sulfide ore bodies are in the Kalgoorlie Terrane, there is significant primary nickel mineralization also in greenstones in the southeast part of the Southern Cross Domain, in particular the Forrestania region (Abeysinghe and Flint, in prep.). Here, nickel sulfide mineralization is associated with ultramafic volcanic and sedimentary rocks.

Economic iron-ore deposits in the western part of the Yilgarn Craton are restricted to supergene hematite–goethite developed from weathering of magnetite in BIF. Resource assessments have been made at Koolanooka, Mungada, Tallering Peak, Nunierra Range, Weld Range, Mount Gibson, Robinson Range, Mount Hale, and Mount Taylor, with the first two having been utilized previously. Other deposits are known from Boolygoo and Windarling Range (Flint et al., 2000).

Platinum-group mineral and chromite mineralization have been reported from several areas in the survey area, including the Yornup area in the southwest (Cornelius et al., 1987) and the Yarawindah Brook area near New Norcia (Cornelius et al., 1987; Harrison, 1984), the latter in the Jimperding metamorphic belt. In the northwest part of the Yilgarn Craton, platinoid and chromite mineralization has been reported (Flint et al., 2000) in greenstones of the Weld Range greenstone belt (part of the Luke Creek Group). Flint et al. (2000) drew comparisons between the geology of the Narndee and Windimurra intrusions and that of the Bushveld and Stillwater Complexes, and suggested PGE potential. Both the Narndee and Windimurra intrusions have potential for nickel and cobalt mineralization.

Archean and Proterozoic rocks in Western Australia host several rare-metal pegmatite bodies, including the world-class Greenbushes Sn–Ta–Li deposit located approximately 270 km south of Perth (Fig. 2). According to Freeman and Donaldson (2004), the Greenbushes mineral field has produced more than 2150 t of tantalite and more than 54 000 t of spodumene. The combined production from the Greenbushes mine and the Wodgina mine in the Pilbara accounts for 65% of world tantalum production. Although economic abundances of tin, tantalum, niobium, beryllium, and lithium are known from the Poona and Noongal areas of the Mid West region (Flint et al., 2000), the main pegmatite-related product has been beryl. Flint et al. (2000) speculated that Sn–Ta-bearing pegmatites at Dalgaranga could be related to intrusion of post-folding granitic magma, whereas the overall distribution of other pegmatites might be spatially related to granite–greenstone contacts.

Geomorphology

Dominant landforms of the Yilgarn Craton (Anand and Paine, 2002) are sandplains, plateaus, breakaways, colluvial and alluvial plains, ridges of greenstones, granitic hills and rises with extensive debris fans, large salt lakes, and dunes along broad valleys. The craton has a gently undulating low relief with sheet floodplains tributary to major valleys, partly occupied by chains of playas. The low relief is broken by low breakaways, dunes, granite tors and north-northwesterly striking ridges of greenstone. Along the western margin of the craton, the fault escarpment of the Darling Range separates it from the Phanerozoic rocks of the coastal plain to the west. The elevation of the Yilgarn Craton ranges from 300 to 650 m above mean sea level, with most of the terrain being of the order of 350–550 m, and a progressive decrease southwards. It is partitioned by a meridional continental divide.

Regolith–landform history

The present, relatively flat surface of the Yilgarn Craton indicates little of the complex regolith beneath that has now been revealed by mapping, drilling, and mining. Four broad stages of regolith–landform evolution have taken place since the Late Paleozoic (Anand and Paine (2002) and references therein).

Pre-Tertiary weathering

There appears to have been significant weathering in the Paleozoic but, despite substantial erosion, only small remnants of this regolith survive. The protolith from which the present landscape evolved was largely the ice-scoured terrain that emerged from the Permian–Carboniferous glaciation, when there was significant sedimentation. The Late Permian to Middle Jurassic was a period of weathering with little sedimentation, when hills and broad, shallow valleys formed with saprolites, lateritic residuum and ferricrete. These materials were later eroded and dispersed into younger (Triassic – Early Eocene) drainages as accumulations of ferruginous gravel. Some ferricretes in valleys were subject to relief inversion. Partial stripping of the regolith took place in the mid-Jurassic and Early Eocene, with uplift and incision leaving remnants of lateritic residuum and ferricrete.

Early to mid-Tertiary erosion and sedimentation

By the Eocene, 'younger' channels, 1–3 km wide and many kilometres long had formed, set on broad paleovalleys. These filled with fluvial, estuarine, marine and lacustrine sediments. They included fluvial 'sandy' basal units and a thick upper 'clay' deposited in lacustrine to swampy

conditions, which ultimately choked the drainage system. The composition of the clay seems related to that of the surrounding local Archean basement. The development of the clay may be attributed, in part, to regional tilting in the Late Eocene or Jurassic.

The landscape, following sedimentation, comprised slightly elevated, dissected areas of pre-Tertiary terrain surrounded by lower elevation sediment-covered terrain. Deposition penetrated as far inland as the Yandal greenstone belt. The sediments are all quite similar throughout the Yilgarn Craton, implying similar regional conditions. The change from sandy to clay facies is probably related to a change in base level in the Middle Eocene.

Mid- to Late Tertiary weathering

Paleomagnetic data indicate weathering in the Miocene. Eocene sediments and the underlying bedrock were weathered, ferruginized and silicified to mottled duricrusts and silcretes under more contrasting seasons, resulting in paleosols, leaching and mottling. Dolocretes formed at the base of some paleochannel sediments.

Late Tertiary to Quaternary sedimentation and weathering

Tectonic uplift and a shift to semi-arid to arid conditions caused instability and erosion, dissecting the land surface. Fluvial, colluvial and eolian sediments were deposited. Some regolith units have been indurated and cemented to lateritic duricrust, silcrete and ferricrete, but many remained soft and unconsolidated. Existing superficial deposits inland were retained in the absence of competent drainage, but significant erosion has taken place nearer the coast. In the Darling Range, abundant duricrust has provided a barrier to erosion.

Patches of shallow, sandy clay to sandy sediments overlie paleochannel sediments and weathered basement. Inland, topographically low areas were cemented by Fe, Si, and Ca to form ferricrete, ferruginous saprolite, silcrete, red-brown hardpan and calcrete; some of this is now topographically inverted. With increased aridity, drainages became restricted and the ground-waters saline. Major valleys became chains of salt lakes with dunes and parnas. There are significant eolian, smectite, and calcrete components to most soils, and deflation has left pavements of lag.

Vegetation

The vegetation of the extreme southwest part of the western Yilgarn Craton and along the Darling scarp is dominated by open eucalypt forest. The Wheat Belt, from the Darling Range to southwest of a diagonal between Jerramungup in the southeast to Mullewa in the northwest, is largely cleared agricultural land interspersed with remnants of eucalypt woodland in the south and stands of acacia in the north. The remainder, to the northeast of the diagonal, is dominated by acacia woodland, largely on sandplain, and some eucalypts between and chenopod and samphire shrubs in the extreme north. Mallee woodlands grow in the southeast (Butt, 2005, fig. 1; and Australian Native Vegetation Assessment, 2001).

Regolith of the western Yilgarn Craton

Weathering, mainly during the Tertiary, produced a thick regolith that typically comprises weakly weathered bedrock or saprock, saprolite (commonly bleached in its upper part), and a clay-rich zone, in places mottled, that gives way to a ferruginous, siliceous or bauxitic upper zone. In the inland, particularly over granite–gneiss terrain, sandplain covers the residual profile; sands and silts forming the sandplain were largely derived from the residual profile (with some colluvial and eolian input) and vary in thickness from less than 1 m to tens of metres (Li Shu et al., 1998). In many parts of the craton, the regolith is more complex due to erosion, deposition, and multiple weathering events. However, this laterite sampling program generally targeted residual settings with a preserved or largely preserved profile. A discussion of the regolith geology of the Yilgarn Craton is given by Anand and Paine (2002).

The type of geochemical sampling used in this laterite sampling program targeted the important ferruginous upper part, the lateritic residuum. This comprises lateritic duricrust, and loose lateritic gravel composed of ferruginous nodules and pisoliths. The lateritic residuum forms a useful sample medium for detecting dispersion haloes in the regolith emanating from Au, base metal and rare metal deposits (Smith et al., 1992; Anand et al., 1993; Anand, 2001). The target and associated pathfinder elements are closely associated with the secondary Fe oxides and oxyhydroxides that are the main components of the lateritic residuum.

Ferruginous pisoliths and nodules are not only found on lateritic residuum, but can also form a lag on eroded, saprolite-dominated areas (Anand, 1998a) or become a part of colluvium and alluvium in depositional terrains. In these non-residual environments, the relationship between the ferruginous materials and the underlying bedrock and weathering profile is less direct than in a residual setting in which the regolith profile and the lateritic residuum are preserved. However, on the broad spacing and scale of this geochemical survey, some lateral movement of the nodules and pisoliths (for up to 1 km), is acceptable and even desirable. In contrast, lateritic duricrust might be more representative of the local bedrock and is generally more suitable for follow-up sampling.

Some depositional terrains contain small lenses of ferruginous material exposed in the colluvium by the erosion from small streams, or as a lag developed on degraded rabbit warrens. Gravely material is concentrated where current velocities were locally high or a small pocket has developed in the stream bed. The degraded warrens are very slight rises (100–200 mm) on flat, sandy depositional plains. The lateritic material is quite variable (mixed nodules and pisoliths), the cutans are severely

worn, the nodules small and chipped and the material is scarce, requiring much patience to collect. Samples seldom weigh more than a few hundred grams at the most from such sites.

Pisoliths and nodules might also have formed in sediment, and this material might be difficult to distinguish from lateritic residuum in the field. A gravel of authigenic pisoliths developed in sediments will have little or no genetic relationship with the underlying or nearby bedrock (Anand and Paine, 2002) and therefore is not deliberately targeted as a sample medium.

Sampling

Terminology and classification of sample materials

The optimum sample medium for the laterite geochemical database is lateritic gravel, which consists of nodules and pisoliths that form the upper part of the lateritic residuum. These contributed 84% of the samples in the western Yilgarn Craton. Where this material is too scarce or absent, lag formed from this gravel is the next best option (10.4% of samples). In the absence of gravel, ferruginous duricrust was collected (2% of samples); these samples generally comprise nodules released from the duricrust and fragments of duricrust. Sample material was collected over an area of about 50 × 50 m. In depositional terrain, particularly colluvium, pisoliths and nodules were collected from around the roots of fallen trees, at the bases of trees, or from the surface. These samples are marked as 'colluvium' in the database and comprise 4% of all samples.

Lateritic gravel generally comprises pisoliths and nodules varying from approximately 5 to 30 mm diameter. The gravel shows a wide variation in colour from light brown through yellow and dark red to black. Its composition ranges from maghemite- or hematite- to goethite-rich. Those with very low Fe and Al contents are mainly composed of quartz grains and kaolinite. These are incipient nodules that are common in the central part of the South West Terrane and were described in more detail by Shu et al. (1998). Other samples have very high Fe contents (99th percentile: 62% Fe_2O_3) and might have formed from Fe-rich bedrock (such as a mafic dyke), or they might be authigenic. The majority, however, have Fe_2O_3 abundances between 11 and 39% (10–90th percentiles). Alumina abundances range from 14 to 36% (10–90th percentiles), with a strong positive correlation between annual rainfall and the Al content in ferruginous gravel in the western part of the Yilgarn Craton.

At a 9-km sample spacing (i.e. an area of influence of approximately 70 km^2) it is critical to collect a representative sample. To interpret the data and assess the significance of subtle geochemical signatures, it is important to consider the setting of the sample (if it was from lateritic residuum, from lag or from colluvium). Lag derived from lateritic residuum generally has been dispersed and mixed, and is more suitable for a regional survey than residual lateritic duricrust and its gravel.

There are many other types of ferruginous materials on the Yilgarn Craton (Anand, 1998a; Anand and Paine, 2002) that have different chemical characteristics to those of lateritic residuum and the gravel formed from it. Iron-cemented gravel (ferricrete) formed on or within sediments would be expected to show no genetic relationship with the underlying mottled and saprolitic clays of the basement (Anand and Paine, 2002). Care was taken to avoid sampling ferricrete by understanding the regolith materials in their local landform setting. However, authigenic or partly authigenic pisoliths (nodules with an authigenic coating) might have been sampled inadvertently. A few samples in this dataset have high Ti and V abundances potentially indicating detrital enrichment of ilmenite, and possibly are derived from ferricrete rather than from lateritic residuum (Anand and Paine, 2002). However, for the purpose of this release, the analyses have been retained and the sample medium marked as 'Ferruginous gravel?' or LQ100 (see the standardized code of fig. 9.1 in Anand et al., 2002).

Care was taken to ensure that uniform and compatible sample media were collected and appropriately coded following the terminology and classification of Anand and Paine (2002) and Anand et al. (2002). However, more than ten samplers have contributed to this dataset, including the CSIRO–AGE and Astro Yilgarn Regolith collections, and minor inconsistencies in selection and classification of materials are inevitable.

Sample collection

Samples were sourced from two pre-existing collections of lateritic materials, but the majority of samples were collected during the course of the current program. Lateritic residuum from the CSIRO–AGE and the CRC LEME–Astro Yilgarn regolith collections were reanalysed in preference to collecting new samples, in order to reduce costs. The sample locations from collections were checked against a theoretical 9 km-spaced triangular grid and those samples within a radius of up to 4 km from the grid nodes were included for reanalysis, provided that the minimum weight of the available sample was greater than 400 g of unprepared sample or greater than 100 g of pulp. Where total sample and pulp were both available, a small sample of the original material was taken as a reference and approximately 100 g of the pulp was taken for geochemical analysis. The CSIRO–AGE collection yielded 616 samples and the Astro Yilgarn Regolith collection yielded 509 samples (together making up 36% of the total samples analysed).

A total of 2017 new samples were collected by fieldwork specifically for this project (Fig. 4). Some sites were excised due to access problems (e.g. mine sites, disease-risk areas, private property, or difficult terrain). Standardized sample and landform descriptions are available for all new sites, but not for some from the CSIRO–AGE and Astro collections.

All proposed new sample locations were plotted on GSWA 1:250 000 geological maps, with sites

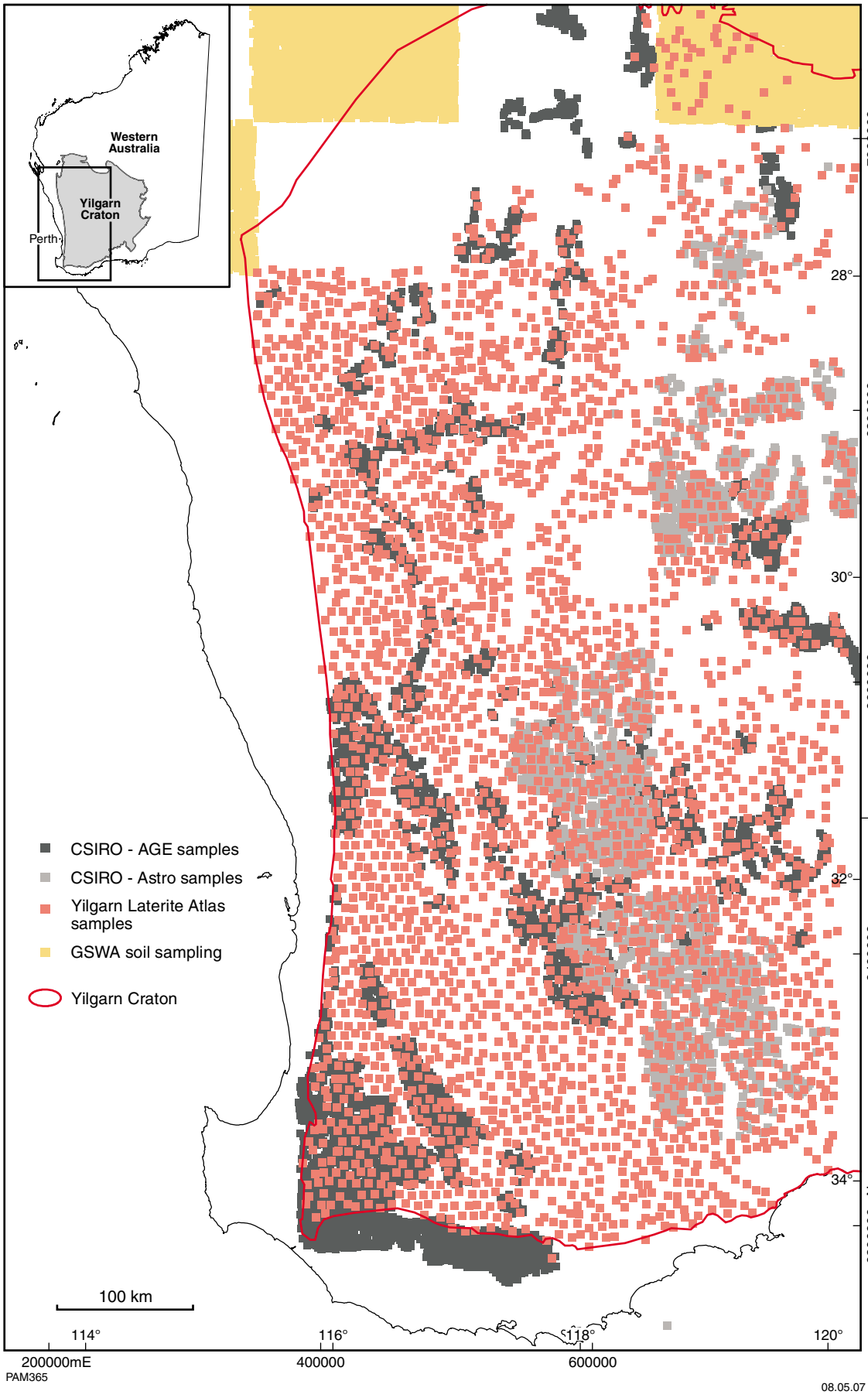

Figure 4. Location of field sample sites and samples from pre-existing sample collections

preferentially located in areas of lateritic residuum (*Czl*) or sandplain (*Czs*). Outside the Wheat Belt, Thematic Mapper TM imagery was found to be invaluable in identifying likely sample sites. The imagery was processed using methods established by Tapley and Gozzard (1992) using ratios of bands 5/7:4/7:4/2 as R:G:B.

Sample locations in areas with extensive overburden or erosion were moved to the nearest suitable site within a radius of approximately 4 km. Sample teams were given some discretion to move the sample site slightly from areas of largely transported cover (generally in areas of broad drainage) or from areas that were clearly inaccessible, in order to maintain the sample spacing. In about 25% of all cases, no suitable sample material was available or access by vehicle was too difficult.

At the majority of new sites, two samples (each about 1 kg) were collected, one as a reference and the other for geochemical analysis. At about 2% of sites, an additional third sample was collected for analysis (i.e. field duplicate) to test within-site variability. Sampling strategies for regional laterite sampling are given in Cornelius et al. (2001).

In agricultural areas, sampling was mainly along public road reserves and tracks, to minimize the need to contact landowners. Care was taken to avoid areas of disturbance and contamination. Access to private property was sought where necessary. On pastoral or Crown land, samples were collected along roads, tracks, fences and grid lines. Permits were obtained to access all CALM-controlled land in the southwest Yilgarn Craton and permission was sought from the local CALM officer to enter specific nature reserves.

In the field, regolith–landform information was gathered at each sample site, together with representative digital photographs (Appendix 4 on DVDs at the back of this Record) to illustrate the landform and the disposition of the sampled material. Sample information was recorded on a standard form and subsequently entered into an Access database and linked to the analytical data. Extracts of this information are given in the database on the CD at the back of this Record.

Parts of the northwest Yilgarn Craton are covered with dense native bush and scrub, mainly north and northeast of the agricultural zone. Here, vehicle access was difficult and, in places, impossible. Some sites were reached on foot, but the time taken meant this approach was largely impractical, except over short distances (<1 km). For such inaccessible areas, sampling by helicopter is an alternative approach, but funding restrictions prevented this.

On weathered granite and gneissic terrain, the residual profile is covered by yellow sandplain soils and silts. These are gently inclined plains with abundant shardy quartz, generally with a low breakaway at one margin and a backslope leading to depositional tracts. Beneath the sandplain lies a layer of ferruginous pisoliths in sand, forming lateritic gravel, the optimal sample medium. This layer is readily masked by sandplain sands and it is generally necessary to sample the lateritic gravel from the bevelled edge of the sandplain (Fig. 5a). Options within the sandplain are pisoliths and nodules caught up in the roots of uprooted trees (tree throw), pisolitic material excavated by rabbit warrens (Fig. 5b) and by fence-post augers (Fig. 5c) where the sand is thin. Road-gravel pits are important, particularly in the agricultural areas.

Breakaways, where lateritic duricrust is exposed, also offer the opportunity for sampling, but material from some of these locations tends to be a nodular lag from the eroded duricrust rather than gravely lateritic residuum. If these breakaways are excessively eroded, only saprolite and the mottled zone are exposed. The adjoining lower edge of the sandplain or small 'nests' or accumulations of relict pisoliths, retained in pockets on the breakaway surface (Fig. 5d), might yield acceptable material.

Where weathered greenstones form hills, a thick weathered mantle is commonly absent, probably due to stripping, leaving only saprolite and saprock, but where the topography is muted, deposits of lateritic gravel might be developed. Careful search of extensive areas of lag on colluvial plains within or adjoining greenstone belts might provide sparse, worn pisoliths, giving a colluvial sample. A caution is that this might contain some authigenic pisoliths.

Pisolith petrography

External appearance

The external appearances of the nodules and pisoliths vary significantly from site to site (see Appendix 1). Colour is generally determined by the relative contents of clay (white) to Fe oxide (red, brown), the species of Fe oxides and oxyhydroxides (brown or yellow — goethite; red — hematite), the degree of preservation of cutans (cutans are generally lighter), and the occurrence of Mn minerals (black).

Cutans

Where an argillan is developed, the surfaces are smooth. Others are rough, where the cutan contains coarse quartz or the cutan is largely absent. Where cutans are largely absent, the pisolith is said to be 'worn', implying some transport. However, in places, pisoliths are scattered on the land surface with rough or 'rasp' surfaces and little or no cutans (Fig. 6a). Adjacent to these, pisoliths with well-developed, smooth cutans are found just below the surface (Fig. 6b). In addition to abrasion, solution might also play a part in the removal of cutans, especially where the pisolith reaches the surface due to downwasting. Here, the cutan that was stable within the soil profile, where it has developed, becomes unstable. The 'rasp' surface consists of sharp, protruding crystals, generally of shardy quartz of the pisolith core, giving the pisolith the appearance of a 'Ferrero Rocher ™' chocolate confectionary (Figs 7a,b).

Most cutans are thin and add only a few percent to the radius of the core (Fig. 8a). A few are thick, making up 20% or more of the pisolith diameter (Fig. 8b). Most cutans are discontinuous (Fig. 8a) in that the core is exposed on some of the pisolith surface. Internally, well-structured cutans show distinct layers of goethite-

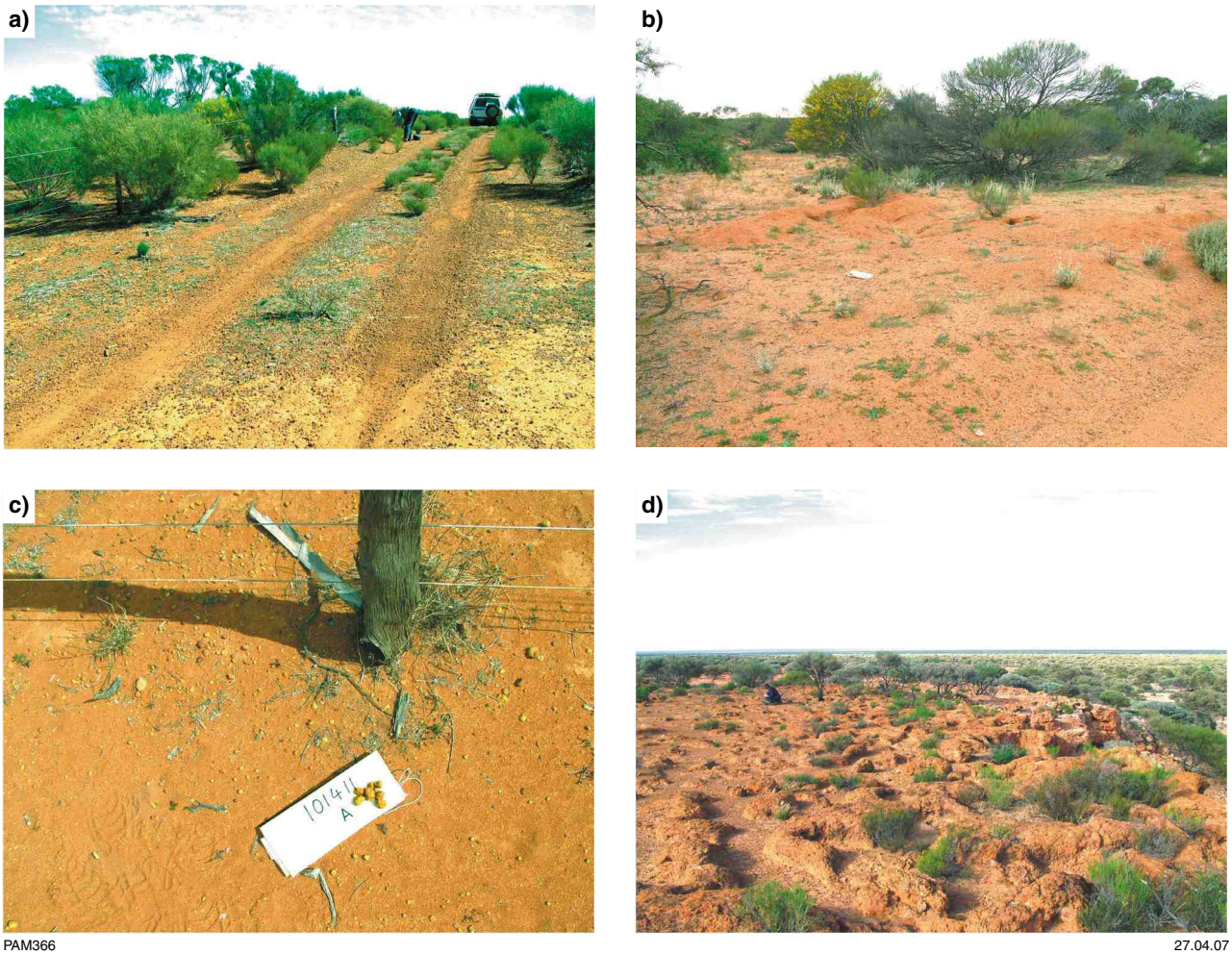

Figure 5. Field photos: a) bevelled edge of sandplain exposing lateritic gravel; b) rabbit warren exposing lateritic gravel; c) fence post with lateritic gravel exposed by auger; and d) pockets in upper surface of breakaway with nests of gravel

impregnated clay and very fine quartz, though small disconformities are developed within them. Other cutans are poorly structured, where the material is only very roughly layered. In these cases, the cutan materials are coarser and it can be difficult to distinguish cutan from core.

Cores

The cores are wholly or partly exposed where cutans are worn or dissolved away. Generally the cores are quartz-rich if derived from granitic rocks, or rich in ferruginous clay if derived from an array of greenstones (not necessarily mafic).

Pisoliths from residual profiles (LT)

The cores of pisoliths and nodules from residual profiles can be monomictic, although a few show slight variations indicating minor lateral movement and mixing. The sources of the materials are various layers within the upper regolith (lateritic residuum to mottled zone, with some retaining saprolitic fabrics).

Pisoliths developed on granitic rocks

The cores of these are rich in shardy quartz (2–4 mm; Fig. 8c). A few rather immature profiles contain, in addition to the shardy quartz, a few remnants of deeply weathered perthitic microcline. These clasts are all closely to moderately closely packed, with clay glaebules*, clay fragments, ferruginous granules, and books and expanded stacks of mica (in a few) in goethite-stained clay.

For some pisoliths, part of the clay matrix has been replaced with banded aluminosilicate cement, which also lines small voids. Many have rims in which the clays are stained yellow by goethite and this grades inwards

* Glaebule: a three-dimensional compound unit within the matrix of a soil material, or occurring as a discrete physical fabric element, generally approximately equant or prolate in shape, and with a sharp boundary (Brewer and Sleeman, 1988).

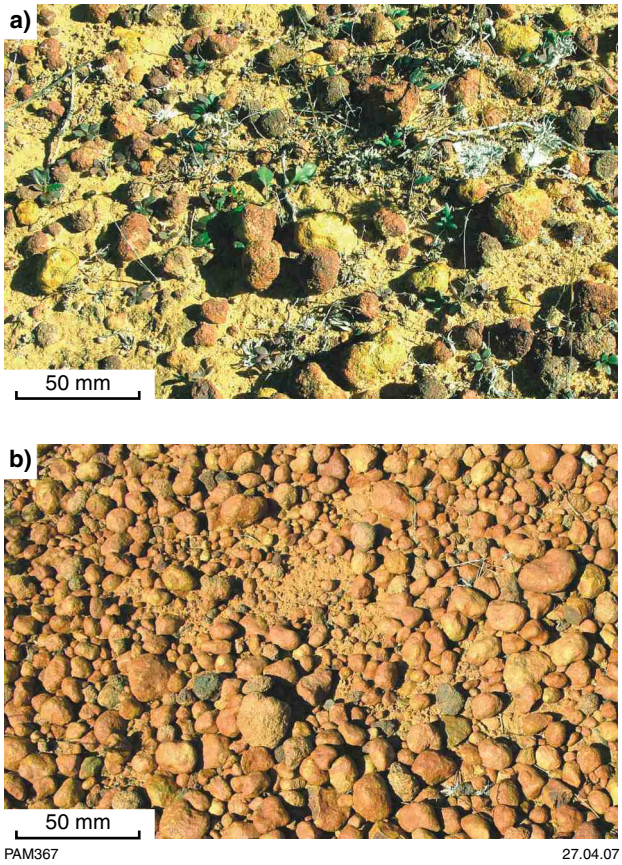

Figure 6. Rough and smooth pisoliths: a) rough surface of pisoliths on the surface, near Mount Gibson; and b) smooth surfaces of pisoliths exposed in small costean, adjacent to those shown on Figure 6a

to brown hematite staining, implying hydration from the outside.

A few nodules, 30–50 mm in size, are shaped like a cup or jar. These are typical of the upper mottled zone rather than of lateritic duricrust. They are filled with pale-yellow, angular, quartz sand (Fig. 9a) and a few clay glaebules, all cemented by a pale, weakly banded aluminosilicate material. Many are loose at the surface in places, although some are seen within the mottled zone on some breakaways. These cup-shaped nodules are suspected to be related to insect activity. Tilley et al. (1997) described broadly similar structures in the Weipa bauxite, where they are called 'mother pisolites' or 'rattlers'. Lea (1925) noted similar but calcareous structures along 500 km of coast in South Australia and reaching up to 60 km inland. They are thought to be pupal chambers, the walls of which have been hardened since by calcification, bauxitization, or (in this case) ferruginization.

Pisoliths developed on greenstones

The cores of these pisoliths consist largely of ferruginous clay (yellow mottled with red) with some fretted quartz. Some contain goethite with fingerprint fabrics after saprolitic clays (kaolinite(–smectite); Fig. 9d), and some cracked and fragmented hematite. These are surrounded by goethite. Voids in the clay are lined or filled with weakly banded light-brown, aluminosilicate cement (Fig. 8d) or with layered goethite and hematite. The cutans are generally thin, delicately banded goethite-stained argillans (Fig. 9b).

Pisoliths from colluvial profiles (CV)

Some depositional terrains contain small lenses of lateritic material exposed in the colluvium by the action of small streams or as a lag developed on degraded rabbit warrens.

Pisoliths largely from granitic terrains

These are generally rich in Mn and are developed at the base of the colluvium as a concentration of black pisoliths, many of which are broken. The cores consist of close-packed shards of quartz and microcline, with some clay glaebules in a minimum of Fe-stained clay and aluminosilicate cement. A Mn mineral, probably hollandite (minor Ba and K), has permeated and hardened the clay matrix.

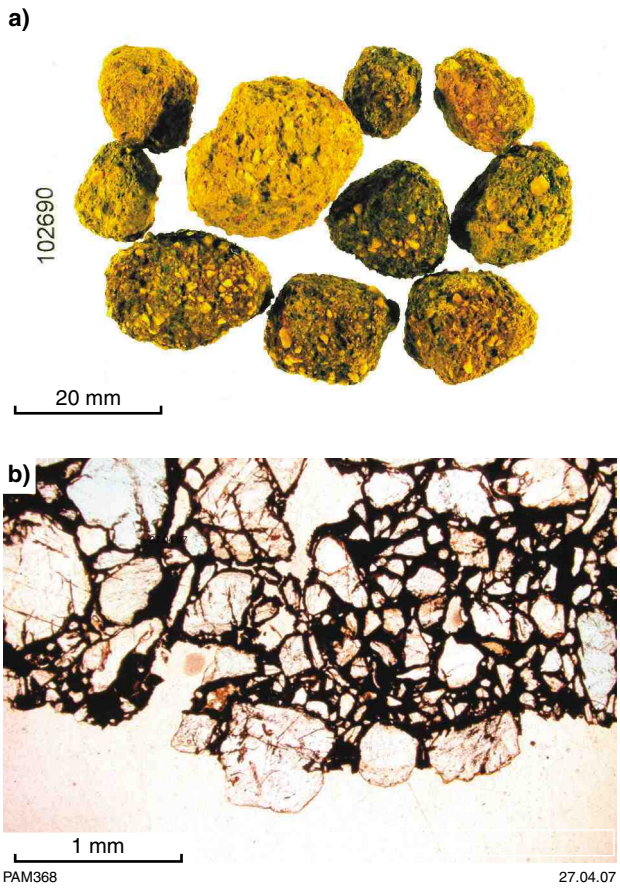

Figure 7. Pisoliths with rasp surfaces: a) nodules with exposed cores and rasp or 'Ferrero Rocher' surface texture (specimen 102690); b) protruding quartz grains of rasp surface texture (specimen 102690)

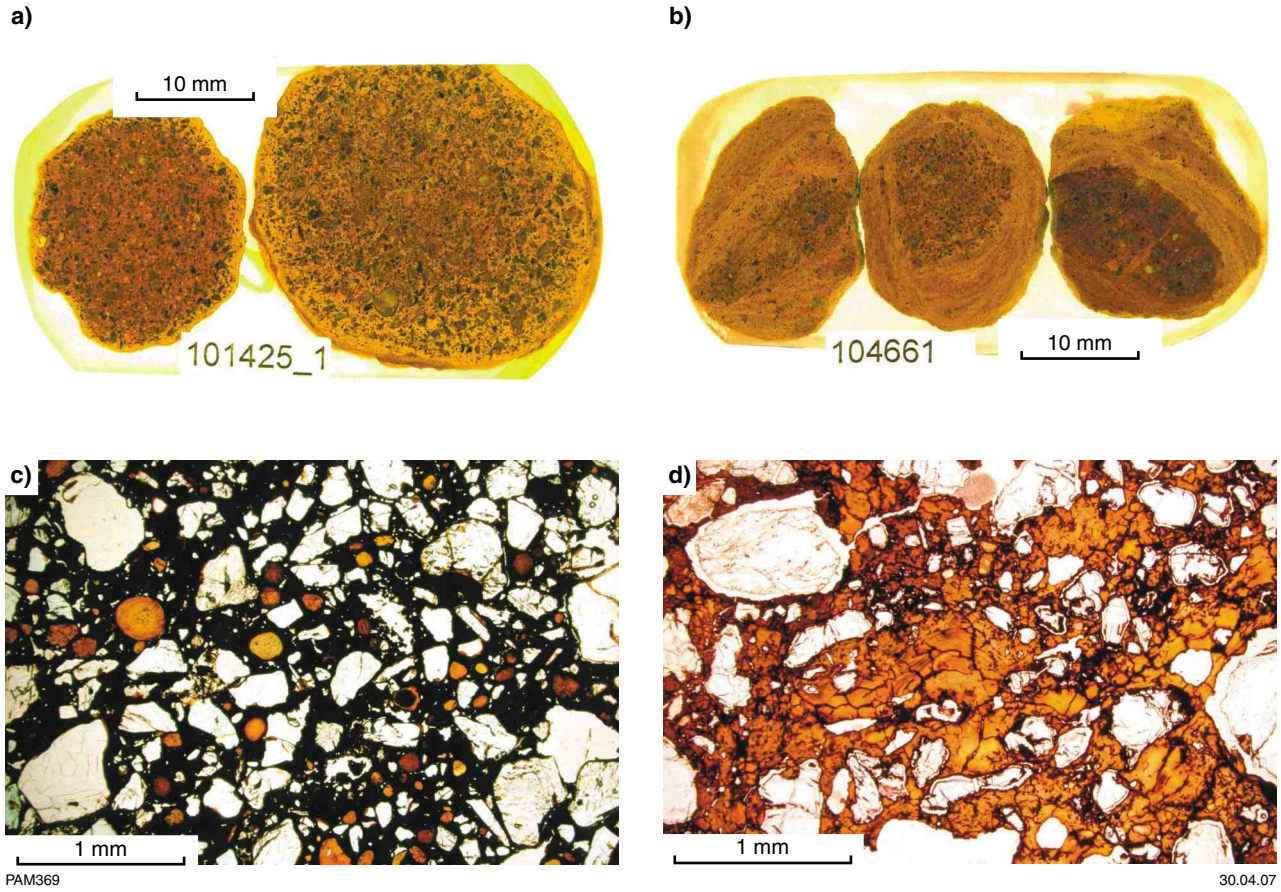

Figure 8. **Petrography of cutans and cores: a) a thin, discontinuous ferruginous argillan on a core of shardy quartz in ferruginous clay. Core margin is goethite rich and grades to hematite rich (specimen 101425); b) pisoliths with thick, discontinuous cutans containing disconformities; c) shardy, angular quartz and clay glaebules packed in ferruginous clay (specimen 102351); and d) fretted angular quartz cemented by banded, brown aluminosilicate (specimen 102862)**

Pisoliths largely from greenstones

These pisoliths are worn and chipped, leaving minimal argillaceous cutans. The cores consist of mottled red-brown to yellow-brown ferruginous clay containing fretted quartz. Some show fingerprint fabrics (Fig. 9d) with books and stacks of phyllosilicates (mica, kaolinite, and smectite). In others, the ferruginous clay forms spherical structures (ooliths; Fig. 9c), which are, in turn, set in a later generation of ferruginous clay. Some ooliths contain smaller ooliths, indicating a multi-cyclic process of formation.

Sample preparation and analysis

Introduction

Samples were prepared and analysed by Ultra Trace Laboratories, Canning Vale, Western Australia, following a public tender. The analyte suite, digestions, methods and lower detection limits are listed in Table 1. The details of the digestions are given below from www.ultratrace.com.au/services/index.php (Ruane D., Ultra Trace Laboratories, 2006, personal comm.).

For all new samples, approximately 1 kg of reference material was retained. For most samples from the Astro Yilgarn Regolith and CSIRO–AGE collections, a small reference sample (0.1 – 0.4 kg) was kept, apart from approximately 260 samples from the Astro Yilgarn Regolith collection, where only pulp was available.

Sample preparation

For each of the newly collected samples, a 1–1.5 kg sample was milled to less than 75 µm in a robotic low-Cr steel ring mill. Some samples required crushing to reduce the particle size prior to milling. Crushing equipment and the ring mill were cleaned with compressed air and a barren quartz wash between each sample.

Samples previously analysed for the CSIRO–AGE project had been prepared at CSIRO using an agate mill. Samples from the Astro Yilgarn Regolith project were prepared at CSIRO using a low-Cr (K1045) case-hardened ring mill with a barren quartz wash between samples

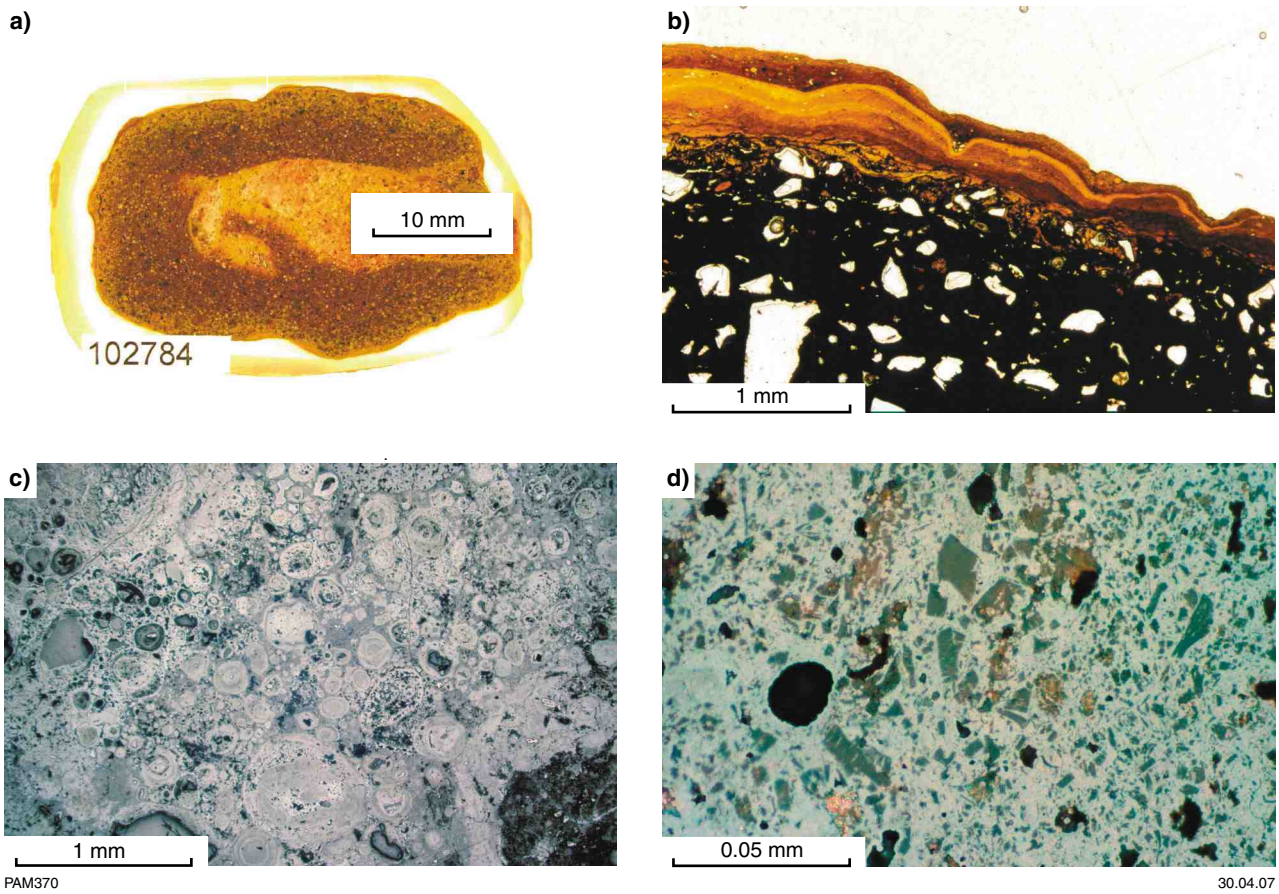

Figure 9. Petrography of pisoliths: a) a mottled-zone nodule with a cup form. The central void is now filled with cemented sandy material (specimen 102784); b) core of fretted quartz grains loosely packed in ferruginous clay coated by thin, well-structured, delicately banded argillan (specimen 101862-1); c) complex ooliths of ferruginous clay set in a later generation of ferruginous clay (specimen 101862); and d) fingerprint structure with remnants of phyllosilicates (specimen 102062)

(Robertson et al., 1996). Ignition loss was determined for all samples at 1000ºC using thermal gravimetric analysis.

Dissolution and analysis

A suite of 53 elements, including Au, was analysed variously by X-ray fluorescence (XRF), inductively coupled plasma optical emission spectrometry (ICP-OES), and inductively coupled plasma mass spectrometry (ICP-MS). For cost reasons, instrumental neutron activation analysis (INAA) was not used in this project, although approximately 300 samples had been analysed previously by INAA (Becquerel Laboratories) and XRF (CSIRO) for the Astro Yilgarn Regolith Project. These INAA analyses (Cornelius et al., 2005a) can be used for comparison. The following sample preparation and analytical procedures were used.

Sodium peroxide fusion

A 0.25 g aliquot of the sample was fused at 700ºC in alumina crucibles with sodium peroxide. The fused material was dissolved in concentrated hydrochloric acid, diluted to 500 ml with water, and analysed by ICP-OES or ICP-MS.

Four-acid digest

A 0.3 g aliquot of the sample was taken up in nitric, perchloric, hydrochloric, and hydrofluoric acids. The digest temperature was raised steadily to dryness. The remaining solids were dissolved to a final volume of 50 ml in 10% hydrochloric acid and analysed by ICP-OES and ICP-MS. Although many silicates are destroyed by hot hydrofluoric acid, data from this multi-acid digest (MAD) must be interpreted with care. Cassiterite, rutile, monazite, ilmenite, garnet, wolframite, spinels, titanite, beryl, zircon, tourmaline and excess barite are resistant (Hall, 1999). They are also resistant to regolith processes. Thus, a few critical elements were also analysed after fusion (Ta, Sn) in case any of these minerals were present. However, fusion entails a degraded detection limit, as the sample must be diluted significantly before spectrometric analysis.

Aqua regia

A 40 g sample was digested in concentrated mixed nitric and hydrochloric acids in plastic bottles. The digest was diluted and mixed. Analysis was by ICP-MS for Au, Hg and Cd (and semi-quantitatively for Pt). The plastic bottles were discarded after use, thus ensuring no cross contamination.

Table 1. Analytical methods and lower limits of detection

Analyte	*Digest*	*Method*	*Lower detection limit*
		Percentage	
SiO_2	fusion disc	XRF	0.01
TiO_2	fusion disc	XRF	0.001
Al_2O_3	fusion disc	XRF	0.01
Fe_2O_3	fusion disc	XRF	0.01
MnO	fusion disc	XRF	0.01
MgO	fusion disc	XRF	0.01
CaO	fusion disc	XRF	0.01
Na_2O	fusion disc	XRF	0.01
K_2O	fusion disc	XRF	0.01
P_2O_5	fusion disc	XRF	0.001
		Parts per million (unless otherwise indicated)	
Ag	4 acid	ICP-MS	0.5
As	4 acid	ICP-MS	0.5
Au (ppb)	aqua regia	ICP-MS	0.2
Ba	sodium peroxide fusion	ICP-MS	10
Be	4 acid	ICP-MS	0.1
Bi	4 acid	ICP-MS	0.1
Cd	aqua regia	ICP-MS	0.05
Ce	4 acid	ICP-MS	0.05
Cl	fusion disc	XRF	20
Co	4 acid	ICP-MS+AES	1+2
Cr	fusion disc	XRF	10
Cs	4 acid	ICP-MS	0.1
Cu	4 acid	ICP-AES	1
Eu	4 acid	ICP-MS	0.02
Ga	4 acid	ICP-MS	0.2
Hg (ppb)	aqua regia	ICP-MS	10
In	4 acid	ICP-MS	0.02
Ir (ppb)	Ni_fire assay	ICP-MS	0.2-1
La	4 acid	ICP-MS	0.05
Lu	4 acid	ICP-MS	0.02
Mo	4 acid	ICP-MS	0.2
Nb	sodium peroxide fusion	ICP-MS	1
Ni	4 acid	ICP-AES	1
Os (ppb)	Ni_fire assay	ICP-MS	0.2–1
Pb	4 acid	ICP-MS	1
Pd (ppb)	Ni_fire assay	ICP-MS	0.2–1
Pt (ppb)	Ni_fire assay	ICP-MS	0.2–1
Rb	sodium peroxide fusion	ICP-MS	0.2
Rh (ppb)	Ni_fire assay	ICP-MS	0.2–1
Ru (ppb)	Ni_fire assay	ICP-MS	0.2–1
S	fusion disc	XRF	10
Sb	4 acid	ICP-MS	0.1
Sc	4 acid	ICP-AES	1
Se	4 acid	ICP-MS	1
Sm	4 acid	ICP-MS	0.05
Sn	4 acid	ICP-MS	1
Sn_fus	sodium peroxide fusion	ICP-MS	10
Sr	4 acid	ICP-MS	0.1
Ta	4 acid	ICP-MS	0.05
Ta_fus	sodium peroxide fusion	ICP-MS	0.5
Te	4 acid	ICP-MS	0.2
Th	sodium peroxide fusion	ICP-MS	0.5
Tl	4 acid	ICP-MS	0.1
Tm	4 acid	ICP-MS	0.02
U	4 acid	ICP-MS	0.05
V	fusion disc	XRF	10
W	sodium peroxide fusion	ICP-MS	5
Y	sodium peroxide fusion	ICP-MS	0.1
Yb	4 acid	ICP-MS	0.05
Zn	4 acid	ICP-AES	1
Zr	fusion disc	XRF	5

Fusion disc

Fused discs for X-ray fluorescence analysis were made on a Labtec Essa robotic fused-bead system using 1.5 g sample and 10.5 g of Li borate flux (12 parts lithium metaborate and 22 parts lithium tetraborate) that were fused at 1050ºC. Analysis was by Philips PW2404/2440 X-ray spectrometer using a 4 kW end window Rh X-ray tube.

Ni fire assay

A 25 g sample was mixed with a Ni-carbonate–sulfur-based flux and fused. The resultant Ni-sulfide button was pulverized and a portion was digested to remove the Ni-sulfide base. Recovery of the platinoids was undertaken in a reducing environment coupled with Te coprecipitation. The insoluble platinoid sulfides were separated by filtration, digested and the resulting solution was analysed by ICP-MS for Pt, Pd, Rh, Ru, Os and Ir, with a detection limit of less than 1 ppb.

Quality control

Quality control was maintained throughout the program by analysing recognized standards (5% of total analyses), duplicates (5% of total analyses), and blanks (5% of total analyses) provided by the analytical laboratory. Thus, in any batch of forty analyses, 34 samples were unknowns, two were a recognized standard, two were duplicates of unknowns, and two were blanks. In addition to field and sample duplicates, two specifically prepared laterite reference materials were submitted with each batch as unknowns. Approximately 300 samples that were previously analysed for the Astro Yilgarn Regolith program by INAA and XRF (Cornelius et al., 2005a) are available for comparison with ICP-MS and XRF (Ultra Trace Laboratory) analyses. A systematic discrepancy exists between Zr results by XRF (CSIRO) compared with Zr by XRF (Ultra Trace Laboratories) for concentrations ranging from 50 to 500 ppm. Measurements by Ultra Trace were, on average, about 10% higher than those by CSIRO (Fig. 10). This is due to differing calibrations. No correction was applied to Zr results as all samples, including the former Astro ones, were re-analysed by Ultra Trace. There were no significant differences for other analytes.

Approximately 150 samples from the CSIRO–AGE collection were analysed by Ultra Trace Laboratories as part of a preliminary survey in early 2002, prior to the commencement of the main sampling and analytical program for this project. To integrate these analyses into the main dataset with confidence, approximately 10% of the analyses were repeated as part of this analytical program, and deemed acceptable using the above criteria for duplicates.

Accuracy

Independent verification of the data was provided by repeat analyses of two specially prepared regolith samples

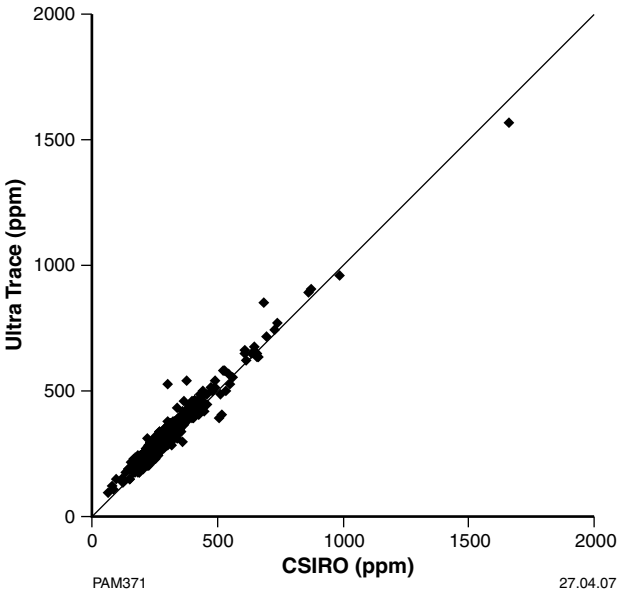

Figure 10. Comparison of CSIRO XRF Zr data with that by Ultra Trace by XRF

and six international standards. Two 100 kg amounts of lateritic nodules and pisoliths from the western Yilgarn Craton were crushed and pulped to less than 75 μm and homogenized by Gannett Holdings, Perth (New Norcia NEWN305 and Gidgeganup GG305). NEWN305 has elevated PGE and base metal abundances, whereas GG305 has the composition of lateritic residuum developed on granite–gneiss of the Darling Range. Analyses for all analytes were obtained from six international and national laboratories and consensus elemental abundances calculated. In general, analyses of recognized standards provided by Ultra Trace Laboratories and of the two CSIRO reference materials were accepted if the analysed elemental abundance and the consensus abundance agreed to within 20%, providing the analyte abundance is at least ten times the lower limit of detection.

Insufficient accuracy was recorded for the measurement of Nb in fusion discs by XRF and these measurements were repeated using a sodium-peroxide fusion digest with ICP-MS finish.

Precision

For all analytes, the precision should be better than 20% [(2×standard deviation/mean) × 100] at 10 times the lower limit of detection. Duplicate analyses were acceptable if the half relative difference (HRD; ((assay #1-assay#2)/(assay #1 + assay#2)) × 100) is less than 10, provided the analyte abundance is greater than 10 times the lower limit of detection. Blank results were acceptable if they were less than three times the lower limit of detection.

Copper and Zn showed insufficient precision in two batches and these were reanalysed for these elements by the same method with a satisfactory result.

Analytical results

Data presentation

All analytical results are listed in Appendix 2 (see CD in back pocket) in tab-delimited .txt and in MS-Access file formats. The file also contains information on the sample type and material. Reference material analyses and original laboratory reports are included in Appendix 2. Comparisons may be made between statistics of the total data set, those over granitic rocks, and those over greenstone belts in Appendix 2.

Summary statistics for all analytes are listed in Tables 2–4 and Appendix 2. Results for all analytes and two cumulative indices, the CHI6* (Smith et al., 1989) and the PEG4* index (Smith et al., 1987), are shown as bubble plots with the size of the bubbles proportional to the element abundance superimposed on contoured images, thus combining a summary of regional trends with objectivity of raw data. Contour plots are not shown due to a majority of the results being less than the lower limit of detection. The normalized element abundances were imaged using indicator kriging* (based on 90th percentiles, subjectively chosen based on the best visual presentation of regional trends) in ArcGIS 8.2 to highlight regional trends ranging from red-orange indicating high abundances to blue indicating low abundances (see Appendix 3). Single high points are downgraded by the smoothing effect of kriging, but can be identified on the bubble plot. In places, there are single points with high elemental abundances surrounded by generally low abundances. Statistically, these are 'nuggetty' and are referred to as 'isolated concentrations'. In other places, groups of samples with generally high abundances are clustered together. These are referred to as 'regional concentrations'. Typicality indices have been used to distinguish samples with an affinity towards alkaline ultramafic rocks and high-Mg basalts and ultramafic rocks.

Non-metals

Phosphorus

The distribution of P shows two regional features. A large regional P concentration in the northern part coincides with high Ba and Cs and a second regional P concentration extends along the west margin of the Yilgarn Craton and east to a line extending from Moora to Jerramungup. Between the northern and the southwest regional concentrations is a 50–250 km-wide zone with predominantly low-P abundances, isolated concentrations, and small clusters of high-P abundances.

Sulfur

On a broad scale, the distribution of S resembles that of P, with several regional S concentrations in the north and

* Indicator kriging better accounts for the continuity of high and low values and is particularly appropriate if the data are skewed. It is robust to extreme values and it gives a better approximation of the conditional expectation than ordinary kriging. Local probability distributions reflect the local data and not just the geometry of the values (Mueller, U., written comm., 2007).

Table 2. Summary statistics — lateritic residuum

	5th	*10th*	*25th*	*50th*	*75th*	*90th*	*95th*	*97th*	*98th*	*99th*	*Mean*	*Std dev.*	*Min.*	*Max.*	*Count*
							Percentage								
SiO_2	13.22	19.30	34.20	46.50	53.90	60.57	63.80	66.18	68.17	70.14	43.11	15.25	2.53	85.10	2 464
TiO_2	0.34	0.39	0.48	0.65	1.02	1.51	1.93	2.27	2.51	3.15	0.84	0.60	0.10	6.72	2 464
Al_2O_3	12.12	14.10	17.10	20.45	24.60	31.67	40.46	45.21	49.00	52.24	22.05	8.33	5.14	60.60	2 464
Fe_2O_3	9.47	11.50	15.40	20.60	30.80	42.10	50.37	55.90	60.10	63.92	24.23	12.72	2.42	84.10	2 464
MnO	0.005	0.005	0.005	0.005	0.010	0.030	0.040	0.060	0.080	0.147	0.018	0.095	0.005	3.800	2 464
MgO	0.02	0.03	0.04	0.06	0.08	0.12	0.14	0.15	0.17	0.20	0.07	0.06	0.01	1.85	2 464
CaO	0.005	0.005	0.010	0.020	0.030	0.050	0.070	0.080	0.100	0.140	0.030	0.064	0.005	2.480	2 464
Na_2O	0.005	0.005	0.005	0.020	0.040	0.070	0.110	0.140	0.167	0.220	0.033	0.061	0.000	1.200	2 464
K_2O	0.01	0.02	0.03	0.06	0.13	0.31	0.49	0.65	0.81	1.46	0.14	0.32	0.01	5.55	2 464
P_2O_5	0.011	0.013	0.018	0.026	0.036	0.050	0.060	0.069	0.076	0.091	0.029	0.018	0.004	0.282	2 464
							Parts per million (unless otherwise indicated)								
Ag	0.25	0.25	0.25	0.25	0.25	0.25	0.25	0.25	0.25	0.25	0.25	0.05	0.25	1.00	2 464
As	7.5	9.5	14.0	20.0	28.5	37.4	45.5	56.6	73.3	129.0	26.0	45.2	2.0	1 140.0	2 464
Au ARL1 (ppb)	0.10	0.10	0.10	0.20	0.60	1.00	1.60	2.20	4.00	14.32	1.70	31.45	0.10	1 460.00	2 464
Au ARL2 (ppb)	0.10	0.10	0.40	0.80	2.55	25.56	62.91	81.46	139.22	276.88	19.88	120.99	0.10	1 450.00	158
Au ARL3 (ppb)	0.10	0.10	0.40	1.00	2.40	12.38	30.55	46.27	57.73	67.53	5.35	13.54	0.10	97.40	172
Ba	10	20	30	40	90	267	618	1 072	1 599	2 738	1 419	25 489	5	517 099	2 464
Be	0.3	0.4	0.6	0.8	1.2	1.6	1.9	2.2	2.4	2.8	0.9	0.6	0.1	10.1	2 464
Bi	0.05	0.1	0.2	0.3	0.5	0.8	1.3	1.7	2.4	4	0.5	1.7	0.05	65.9	2 464
Cd	0.025	0.025	0.025	0.025	0.025	0.025	0.025	0.025	0.025	0.025	0.025	0.005	0.025	0.150	2 464
Ce	6	8	14	26	49	87	127	155	179	275	44	86	2	2 640	2 464
Cl	10	40	60	80	120	200	300	380	455	660	114	146	10	2 660	2 464
Co	2	2	3	5	7	11	15	21	24	38	7	10	1	259	2 464
Cr	90	120	170	250	380	610	908	1 382	2 042	5 702	437	1 116	5	22 200	2 464
Cs	0.05	0.1	0.2	0.4	0.7	1.1	1.4	1.6	1.8	2.2	0.5	0.6	0.05	23.4	2 464
Cu	3	3	6	10	19	43	76	105	125	209	21	39	1	767	2 464
Eu	0.06	0.08	0.12	0.18	0.32	0.48	0.64	0.8	0.9	1.1074	0.3	0.2	0.02	3.52	2 464
Ga	23	27	34	45	55	68	81	90	97	106	47	19	7	307	2 464
Hg (ppb)	5	5	5	10	30	70	110	140	180	250	30	55	5	860	2 464
In	0.08	0.08	0.1	0.14	0.18	0.22	0.26	0.28	0.3	0.36	0.1	0.1	0.01	0.56	2 464
La	1.75	2.20	3.45	5.58	9.35	15.37	21.69	29.27	35.10	49.83	8.10	9.14	0.80	121.00	2 464
Lu	0.01	0.04	0.04	0.06	0.1	0.14	0.18	0.2	0.22	0.28	0.1	0.1	0.01	0.62	2 464
Mo	2.2	2.8	3.8	5.0	6.6	8.4	10.2	11.8	14.0	18.6	5.5	3.5	0.4	72.2	2 464
Nb	6	7	9	13	18	25	30	34	36	41	15	9	1	221	2 464
Ni	11	14	20	29	42	59	79	99	137	266	40	83	1	2 130	2 464
Pb	16	20	28	37	48	64	76	89	101	124	41	24	2	332	2 464
Rb	1.2	1.8	3.0	5.2	10.0	18.4	27.2	37.0	46.5	65.1	9.2	15.4	0.1	305.0	2 464
S	100	130	210	320	450	610	740	830	927	1061	354	220	5	2 220	2 464
Sb	0.2	0.2	0.3	0.6	0.8	1.1	1.5	1.8	2.4	4.7	1.2	19.4	0.1	960.0	2 464
Sc	6	7	11	16	26	46	66	80	90	116	23	22	1	295	2 464
Se	0.5	0.5	0.5	2.0	4.0	5.0	6.0	7.0	7.0	8.0	2.4	2.0	0.5	12.0	2 464
Sm	0.35	0.4	0.6	0.95	1.55	2.3	3.15	3.8055	4.45	6.0185	1.3	1.2	0.15	18.1	2 464
Sn	0.5	1.0	2.0	2.0	3.0	4.0	5.0	6.0	6.0	8.0	2.4	2.3	0.5	88.0	2 464
Sn_FUS	5	5	5	5	5	5	5	5	5	10	5	2	5	110	2 464
Sr	2	3	4	6	10	16	23	31	38	51	9	13	1	349	2 464
Ta_MAD	0.35	0.40	0.55	0.75	1.10	1.60	1.99	2.35	2.75	3.37	0.94	0.78	0.05	21.10	2 464
Ta_FUS	0.25	0.50	0.50	1.00	1.50	2.00	2.50	3.00	3.50	4.50	1.11	1.26	0.25	34.00	1 987
Te	0.1	0.1	0.1	0.1	0.1	0.2	0.2	0.4	0.4	0.4	0.1	0.1	0.1	1.6	2 464
Th	18	24	43	76	127	194	243	286	326	406	97	83	1	1 010	2 464
Tl	0.05	0.05	0.05	0.05	0.05	0.10	0.20	0.30	0.50	0.90	0.09	0.26	0.05	8.90	2 464
Tm	0.01	0.02	0.04	0.06	0.10	0.14	0.18	0.20	0.24	0.30	0.08	0.06	0.01	0.68	2 464
U	1.75	2.15	2.95	4.5	6.95	10.5	13.3	15.911	17.6	21.5	5.7	4.4	0.5	51.7	2 464
V	160	200	280	390	550	810	990	1 141	1 285	1 397	461	285	40	4 540	2 464
W	2.5	2.5	2.5	2.5	2.5	2.5	2.5	5.0	10.0	15.0	3.0	4.6	2.5	135.0	2 464
Y	2.4	2.9	4.1	6.0	8.8	12.9	16.5	19.4	23.2	30.4	7.4	6.1	0.1	116.0	2 464
Yb	0.2	0.2	0.3	0.5	0.7	1.0	1.3	1.5	1.7	2.1	0.6	0.4	0.1	4.5	2 464
Zn	4	5	7	10	15	23	31	38	44	60	13	14	1	391	2 464
Zr	195	220	270	335	455	600	704	800	872	999	384	193	55	3 790	2 464
LOI1000	5.16	6.07	7.54	8.93	10.26	11.61	12.87	13.77	14.86	16.42	8.96	2.44	0.00	23.51	1 824
PEG4	8	9	11	14	18	23	28	31	36	46	16	29	3	1 363	2 464
CHI6	93	111	130	153	183	225	266	312	358	510	171	142	58	4 457	2 464

NOTES: ARL1–3 are original and Au repeat analyses
FUS fusion
MAD Mixed-acid digest
LOI Ignition loss at 1000°C

Table 3. Summary statistics — lag after lateritic residuum

	5th	10th	25th	50th	75th	90th	95th	97th	98th	99th	Mean	Std dev.	Min.	Max.	Count
							Percentage								
SiO_2	10.28	15.85	26.50	46.25	55.30	61.75	67.05	69.74	71.48	74.75	42.26	17.58	2.63	79.80	456
TiO_2	0.37	0.42	0.50	0.68	0.96	1.42	2.01	2.73	3.23	3.50	0.87	0.68	0.05	6.34	456
Al_2O_3	8.70	11.15	14.90	18.65	21.90	27.30	34.95	38.09	41.60	45.15	19.13	7.36	3.36	49.20	456
Fe_2O_3	8.90	11.35	15.48	22.00	38.70	57.05	65.28	70.67	71.88	74.27	28.60	17.78	4.88	84.20	456
MnO	0.005	0.005	0.005	0.010	0.020	0.040	0.080	0.120	0.166	0.294	0.025	0.076	0.005	1.140	456
MgO	0.02	0.03	0.04	0.06	0.08	0.12	0.15	0.19	0.23	0.33	0.07	0.07	0.01	0.83	456
CaO	0.005	0.010	0.020	0.030	0.040	0.070	0.100	0.120	0.180	0.215	0.039	0.052	0.005	0.800	456
Na_2O	0.005	0.005	0.005	0.010	0.030	0.060	0.100	0.130	0.178	0.314	0.030	0.062	0.005	0.780	456
K_2O	0.01	0.01	0.02	0.05	0.11	0.30	0.68	1.51	2.13	2.41	0.18	0.47	0.01	4.04	456
P_2O_5	0.014	0.017	0.022	0.030	0.047	0.076	0.098	0.123	0.141	0.193	0.042	0.047	0.009	0.511	456
							Parts per million (unless otherwise indicated)								
Ag	0.25	0.25	0.25	0.25	0.25	0.25	0.25	0.25	0.25	0.50	0.25	0.03	0.25	0.50	456
As	6.4	8.0	12.5	19.5	28.5	40.5	57.4	74.9	102.3	176.4	30.6	98.4	2.0	1 910.0	456
Au ARL1 (ppb)	0.10	0.10	0.10	0.20	0.60	1.20	3.25	6.34	10.34	32.34	1.86	16.19	0.10	323.00	456
Au ARL2 (ppb)	0.10	0.10	0.40	1.00	7.20	33.64	71.44	142.14	206.56	279.28	19.70	62.08	0.10	352.00	37
Au ARL3 (ppb)	0.10	0.20	0.40	1.20	4.20	23.04	41.48	70.89	96.99	209.40	12.57	47.12	0.10	329.00	53
Ba	10	20	30	40	130	480	935	1 709	2 048	3 188	246	832	5	10 800	456
Be	0.3	0.4	0.5	0.7	1.0	1.5	1.7	1.9	2.2	2.8	0.8	0.6	0.2	9.6	456
Bi	0.05	0.10	0.20	0.30	0.60	1.25	2.00	2.34	3.05	5.88	0.63	1.36	0.05	19.10	456
Cd	0.025	0.025	0.025	0.025	0.025	0.025	0.050	0.100	0.100	0.150	0.030	0.026	0.025	0.350	456
Ce	5	6	13	24	47	75	113	146	181	228	37	47	3	580	456
Cl	10	10	40	80	140	260	385	507	652	769	126	148	10	1 140	456
Co	2	2	3	5	7	11	22	39	61	87	8	16	1	198	456
Cr	90	110	160	280	513	1 080	2 675	5 388	7 225	8 803	718	1 649	20	14 500	456
Cs	0.05	0.05	0.20	0.30	0.60	0.90	1.43	1.80	2.09	2.89	0.49	0.56	0.05	5.50	456
Cu	3	4	6	13	32	91	135	154	180	272	39	128	2	2 080	456
Eu	0.08	0.08	0.12	0.18	0.30	0.48	0.70	0.83	1.17	1.28	0.26	0.24	0.02	1.98	456
Ga	19	23	32	44	56	67	71	80	86	90	45	18	9	149	456
Hg (ppb)	5	5	5	10	30	60	80	100	119	150	24	35	5	310	456
In	0.06	0.08	0.10	0.14	0.18	0.24	0.28	0.32	0.34	0.36	0.15	0.07	0.02	0.42	456
La	1.70	2.20	3.05	5.33	9.26	16.45	26.48	35.59	43.65	58.37	8.41	10.12	0.75	85.70	456
Lu	0.02	0.04	0.04	0.06	0.10	0.16	0.21	0.26	0.30	0.36	0.08	0.06	0.01	0.46	456
Mo	1.4	2.0	3.4	4.8	6.2	8.5	10.9	12.5	13.8	19.8	5.4	4.7	0.6	78.4	456
Nb	4	6	9	14	19	25	33	37	42	50	15	9	1	59	456
Ni	11	14	20	29	45	77	147	210	321	610	57	149	3	2 150	456
Pb	15	19	27	36	49	67	77	87	94	107	41	26	5	367	456
Rb	1.0	1.4	2.6	4.6	9.4	17.4	31.7	63.9	96.5	123.8	10.8	25.1	0.1	273.0	456
S	140	170	230	320	460	660	790	940	1 057	1 204	389	286	50	3 570	456
Sb	0.2	0.2	0.3	0.6	1.0	1.6	2.7	4.7	6.8	10.0	1.2	4.7	0.1	79.8	456
Sc	6	7	11	18	32	67	84	105	114	131	29	36	4	476	456
Se	0.5	0.5	0.5	2.0	3.0	5.0	6.0	6.0	6.9	8.0	2.2	1.9	0.5	12.0	456
Sm	0.35	0.40	0.55	0.95	1.55	2.55	3.28	4.25	5.17	6.59	1.29	1.16	0.20	9.00	456
Sn	0.5	1.0	2.0	2.0	3.0	4.0	5.0	5.0	6.0	7.0	2.3	1.6	0.5	20.0	456
Sn_FUS	5	5	5	5	5	5	5	5	5	10	5	1	5	20	456
Sr	2.2	2.5	3.7	6.0	9.7	18.6	29.5	45.7	58.9	73.1	10.3	17.7	1.3	225.0	456
Ta_MAD	0.29	0.35	0.55	0.80	1.10	1.55	1.91	2.20	2.40	3.10	0.91	0.66	0.05	7.40	456
Ta_FUS	0.25	0.25	0.50	1.00	1.50	2.00	2.50	3.00	3.00	5.30	1.15	1.14	0.25	16.00	381
Te	0.1	0.1	0.1	0.1	0.1	0.2	0.4	0.4	0.4	0.4	0.1	0.1	0.1	1.0	456
Th	11	18	37	75	122	173	224	244	281	364	89	74	0	586	456
Tl	0.05	0.05	0.05	0.05	0.05	0.10	0.30	0.50	0.70	0.99	0.10	0.19	0.05	2.30	456
Tm	0.02	0.04	0.04	0.06	0.10	0.16	0.20	0.26	0.28	0.37	0.08	0.06	0.01	0.48	456
U	1.55	1.88	2.65	4.08	6.36	9.43	11.65	13.80	17.26	19.57	5.13	3.96	0.70	34.30	456
V	158	190	280	400	620	980	1 173	1 374	1 400	1 799	508	349	40	2 280	456
W	2.5	2.5	2.5	2.5	2.5	2.5	5.0	10.0	10.0	20.0	3.1	3.5	2.5	50.0	456
Y	2.4	3.0	4.0	5.9	9.0	13.8	20.6	23.3	26.0	29.5	7.7	6.9	0.1	87.4	456
Yb	0.2	0.3	0.4	0.5	0.7	1.1	1.4	1.8	2.1	2.3	0.6	0.4	0.1	3.2	456
Zn	5	6	8	13	21	33	47	64	83	184	20	32	2	408	456
Zr	149	185	265	335	470	640	775	988	1 119	1 199	392	219	60	1 530	456
LOI1000	3.38	4.63	6.83	8.50	9.88	11.38	11.99	12.71	13.64	15.62	8.30	2.67	1.18	17.60	243
PEG4	6	8	11	15	19	25	30	35	42	48	17	15	3	247	456
CHI6	84	99	124	154	187	237	295	356	427	587	173	131	62	2 163	456

NOTES: ARL1–3 are original and Au repeat analyses
FUS fusion
MAD Mixed-acid digest
LOI Ignition loss at 1000°C

Table 4. Summary statistics — colluvium (nodules and pisoliths)

	5th	*10th*	*25th*	*50th*	*75th*	*90th*	*95th*	*97th*	*98th*	*99th*	*Mean*	*Std dev.*	*Min.*	*Max.*	*Count*
							Percentage								
SiO_2	15.00	19.30	34.20	47.70	56.00	61.50	65.90	68.90	71.30	74.10	44.33	16.29	6.08	83.20	201
TiO_2	0.37	0.41	0.49	0.65	0.98	1.74	2.16	2.26	2.76	4.19	0.89	0.72	0.01	5.63	201
Al_2O_3	8.53	10.60	13.90	17.30	21.50	24.90	28.40	41.30	41.40	44.50	18.12	7.84	0.43	62.60	201
Fe_2O_3	10.10	11.70	17.40	23.40	36.30	51.30	58.30	61.80	63.50	71.10	28.09	15.33	6.58	73.70	201
MnO	0.005	0.005	0.005	0.010	0.030	0.070	0.170	0.480	0.930	1.420	0.070	0.302	0.005	3.420	201
MgO	0.03	0.04	0.06	0.09	0.12	0.17	0.19	0.22	0.27	0.32	0.10	0.07	0.01	0.69	201
CaO	0.005	0.010	0.020	0.030	0.050	0.100	0.180	0.220	0.240	0.520	0.060	0.114	0.005	1.200	201
Na_2O	0.005	0.005	0.010	0.040	0.070	0.110	0.200	0.250	0.390	0.450	0.060	0.092	0.005	0.830	201
K_2O	0.02	0.02	0.05	0.09	0.24	0.68	1.48	2.06	2.42	2.65	0.30	0.56	0.01	3.81	201
P_2O_5	0.013	0.016	0.026	0.038	0.058	0.081	0.098	0.108	0.121	0.127	0.045	0.028	0.008	0.192	201
							Parts per million (unless otherwise indicated)								
Ag	0.25	0.25	0.25	0.25	0.25	0.25	0.25	0.50	0.50	0.50	0.26	0.07	0.25	1.00	201
As	6.5	7.5	12.0	22.0	30.5	41.5	64.5	113.0	218.0	408.0	34.6	78.7	2.0	885.0	201
Au ARL1 (ppb)	0.10	0.10	0.10	0.10	0.40	0.80	2.20	11.60	36.20	697.00	17.38	128.45	0.10	1 460.00	201
Au ARL2 (ppb)	0.10	0.10	0.35	0.50	5.50	28.70	598.55	931.12	1 104.08	1 277.04	93.08	321.92	0.10	1 450.00	24
Au ARL3 (ppb)	0.31	0.52	0.80	1.40	3.00	7.40	10.40	11.60	12.20	12.80	3.21	4.63	0.10	13.40	7
Ba	20	20	40	80	300	900	1 350	1 930	2 510	2 760	325	631	5	4 910	201
Be	0.4	0.4	0.6	0.8	1.2	1.6	2.3	2.6	2.8	3.8	1.0	0.6	0.1	4.2	201
Bi	0.05	0.05	0.20	0.40	0.60	1.50	2.20	2.80	3.90	61.00	1.70	9.24	0.05	86.80	201
Cd	0.025	0.025	0.025	0.025	0.025	0.025	0.050	0.100	0.100	0.150	0.032	0.043	0.025	0.550	201
Ce	6	9	13	24	40	89	155	421	525	544	57	152	3	1 700	201
Cl	40	40	60	100	180	280	380	400	440	480	142	113	10	820	201
Co	2	2	3	5	9	15	23	35	38	58	9	14	1	141	201
Cr	70	110	170	250	390	610	1 230	1 780	2 070	2 820	423	859	30	10 100	201
Cs	0.05	0.10	0.20	0.40	0.70	1.20	1.80	2.50	2.90	3.20	0.59	0.64	0.05	3.70	201
Cu	3	5	7	15	33	91	135	160	165	185	33	47	2	324	201
Eu	0.10	0.12	0.16	0.26	0.40	0.62	0.90	1.30	1.38	1.54	0.34	0.33	0.04	2.98	201
Ga	19	21	29	41	51	65	77	83	88	97	43	19	2	135	201
Hg (ppb)	5	5	5	10	30	50	80	100	130	140	23	29	5	180	201
In	0.06	0.08	0.10	0.12	0.18	0.22	0.26	0.36	0.60	10.20	0.32	1.51	0.02	13.90	201
La	2.10	2.65	4.10	6.40	11.30	21.70	30.80	38.90	44.20	59.50	10.31	11.93	1.05	103.00	201
Lu	0.04	0.04	0.06	0.08	0.12	0.18	0.22	0.26	0.32	0.34	0.09	0.07	0.01	0.50	201
Mo	2.2	2.8	4.0	5.4	7.0	10.2	11.6	12.2	14.6	15.4	6.1	3.7	1.0	38.4	201
Nb	6	7	10	13	19	25	33	40	44	49	15	9	1	62	201
Ni	13	16	20	28	40	67	93	112	128	148	36	30	6	231	201
Pb	17	22	32	43	56	81	98	123	161	167	49	33	5	242	201
Rb	1.4	1.8	3.4	6.6	14.2	36.4	75.8	111.0	137.0	170.0	17.7	35.6	0.1	329.0	201
S	90	120	200	300	430	550	620	740	780	860	330	181	5	1 140	201
Sb	0.1	0.2	0.3	0.7	1.0	1.5	4.4	5.8	17.1	33.3	1.7	5.4	0.1	50.7	201
Sc	5	7	10	15	23	47	64	85	88	133	23	23	2	160	201
Se	0.5	0.5	0.5	2.0	4.0	4.0	6.0	7.0	7.0	8.0	2.4	1.9	0.5	11.0	201
Sm	0.40	0.55	0.75	1.20	1.75	2.80	4.85	5.65	7.20	8.35	1.63	1.73	0.25	15.60	201
Sn	0.5	1.0	2.0	2.0	3.0	4.0	5.0	5.0	7.0	22.0	2.8	5.2	0.5	67.0	201
Sn_FUS	5	5	5	5	5	5	5	5	10	60	6	11	5	130	201
Sr	3.0	3.6	5.1	9.1	15.9	29.1	42.1	54.5	57.3	65.4	13.6	14.1	1.6	97.1	201
Ta_MAD	0.25	0.35	0.50	0.70	1.20	1.75	2.50	3.00	3.70	4.25	0.97	0.82	0.03	6.10	201
Ta_FUS	0.25	0.50	0.50	1.00	1.50	2.50	3.00	4.00	4.67	5.92	1.32	1.17	0.25	8.00	184
Te	0.1	0.1	0.1	0.1	0.2	0.2	0.4	0.4	0.4	0.4	0.1	0.1	0.1	1.2	201
Th	16	21	36	65	110	154	200	235	247	296	82	71	2	650	201
Tl	0.05	0.05	0.05	0.05	0.10	0.30	0.70	1.50	3.10	3.70	0.24	0.76	0.05	7.80	201
Tm	0.04	0.04	0.04	0.08	0.12	0.18	0.24	0.28	0.32	0.36	0.10	0.07	0.01	0.56	201
U	1.55	1.90	2.90	4.15	5.80	8.40	10.30	11.50	12.30	15.90	4.73	2.99	0.15	22.70	201
V	170	200	300	420	600	880	1 160	1 260	1 370	1 400	508	357	60	3 510	201
W	2.5	2.5	2.5	2.5	2.5	5.0	5.0	10.0	10.0	15.0	3.1	2.3	2.5	25.0	201
Y	2.7	3.6	4.7	7.3	10.2	16.9	24.1	27.0	29.2	32.7	9.0	6.6	1.8	38.4	201
Yb	0.3	0.3	0.4	0.6	0.8	1.2	1.6	1.8	2.1	2.2	0.7	0.5	0.2	3.5	201
Zn	5	6	10	15	24	41	54	58	63	68	20	16	3	116	201
Zr	160	220	250	315	390	555	680	695	770	870	351	178	35	1 780	201
LOI1000	3.39	5.13	6.28	7.72	9.26	10.30	10.60	11.42	11.53	11.55	7.59	2.27	1.07	14.63	112
PEG4	7	9	11	14	19	27	36	43	88	105	18	17	3	155	201
CHI6	79	101	125	158	191	255	314	346	426	2204	207	314	64	3 287	201

NOTES: ARL1–3 are original and Au repeat analyses
FUS fusion
MAD Mixed-acid digest
LOI Ignition loss at 1000°C

a distinct S regional concentration along the southwest margin of the Yilgarn Craton. Sulfur abundances are high on granitic bedrock as well as on greenstone sequences; however, the 90th percentile of S abundances on greenstone (780 ppm) is 25% greater than on granite (620 ppm).

High-S abundances in the northern part of the survey area appear to reflect more greenstone compared with the southern Yilgarn Craton. However, S abundances over greenstone in the Southern Cross region do not show equally elevated concentrations. Environmental factors (e.g. bushfires) therefore appear equally possible. Derivation of S from sea spray is considered unlikely, due to the limited extent of high-S abundances in the southwest Yilgarn Craton and the long distance from the coast in the case of high-S abundances in the northern Yilgarn Craton. Barite ($BaSO_4$) is developed in red-brown hardpan (Mahizhnan, 2004); hardpans are common north of the Menzies line, in the north part of the survey area. Barite and gypsum contribute to a late regolith cement affecting all upper parts of the regolith profile; residual or depositional parts alike.

Selenium

The distribution of Se shows a number of patchy regional concentrations extending along a line from approximately Mullewa in the northwest to Southern Cross in the southeast. South of this line (i.e. throughout most of the Wheat Belt), Se abundances are generally low. Likewise, Se abundances in the northeast of the survey area are less than along the northwest regional trend. Most concentrations of high Se (90th percentile is 5 ppm) are within granitic terrains, with few high abundances coincident with greenstone sequences. Given the chalcophile affinity of Se, this might indicate widespread finely distributed bedrock sulfides in parts of the granitic terrains, possibly hosted by mafic inliers or melanocratic gneiss. Two distinct concentrations of high Se within the general trend are centred on an area south of Mullewa and northeast of Southern Cross, with abundances of 5–15 ppm Se.

Rare earth elements

The rare earth elements (REE) La, Ce, Eu, Sm, Yb, and Lu are, in general, more abundant in lateritic residuum on granitic rocks (90th percentile for La is 16.3 ppm) than on greenstone sequences (90th percentile for La is 9.95 ppm). Abundances are also high over pegmatite dykes (e.g. around Bridgetown–Greenbushes) and alkaline ultramafic rocks such as in an area northeast of Mukinbudin (Cornelius et al., 2005b), with some REE concentrations above the respective 99th percentiles. The regional distribution varies between light REE (La and Ce), medium REE (Sm and Eu), and heavy REE (Yb and Lu). The light REE are elevated in all granitic domains of the survey area. Cerium is more enriched in the central part, whereas La is equally enriched in the southern and northern parts of the survey area. The medium REE show a similar distribution to that of the light REE, but the clusters of high abundances are more confined. Along the south margin of the Yilgarn Craton, north of the Proterozoic rocks, medium REE abundances are high, corresponding with high Na, K, Mg, and Sr abundances. The distribution of high-Yb and -Lu abundances resembles that of Sm, but is less extensive. The heavy REE show concentrations in the northern part (south of Meekatharra) and the eastern part (east of Lake Barlee) of the survey area that are more distinct than the corresponding abundances for light REE and medium REE. These regional differences in REE abundances and interelement ratios might indicate different bedrock suites within the felsic terrain.

Thorium

The 90th percentiles vary significantly between granite terrain (194 ppm) and greenstone terrain (86 ppm). There are several patchy regional concentrations of Th in granite gneiss terrain in the central part of the survey area. The most prominent ones are west-southwest and northwest of Merredin, with abundances of 400–850 ppm. Although Th abundances in the northern survey area are generally less than in the south, a large cluster of high-Th abundances is centred on Paynes Find (200–700 ppm), possibly indicating a Th-rich granite intrusion. Thorium is also commonly associated with goethite.

Uranium

The regional distribution of U shows three distinct domains. Generally low abundances are in the northern part of the survey area, with a few scattered single-point concentrations (including the maximum U abundance of 51.7 ppm southwest of Paynes Find). There are a number of regional concentrations of high U in the central part, and generally low abundances in the southeast part. The conspicuous absence of concentrations of high U in the northern part of the survey area coincides with the presence of valley calcretes anomalous in U (Butt et al., 1984; Cameron, 1984; French and Allen, 1984). The high-U domain in the central Yilgarn Craton and the low-U domain in the northern Yilgarn Craton are separated, broadly, along the Menzies line. It remains open whether environmental factors such as summer rainfall associated with cyclonic depressions or primary U abundances in bedrock (i.e. different granite types) control the distribution of U in lateritic residuum. Where there has been an antithetical relationship between Th and U in granite areas, this might indicate different granite types. In the north Yilgarn, it would appear that U has been leached from the regolith, concentrated in the trunk drainages, and is consequently depleted in the upper residual regolith.

Alkalis

Sodium

Strong leaching during weathering depletes the alkalis in lateritic residuum. The 90th percentile for Na (as $\%Na_2O$) in granitic terrains is 0.08%, and in greenstone terrains

is 0.06%. The main feature of the Na distribution in the Yilgarn Craton is a regional concentration of Na in the southern part of the survey area, extending approximately 370 × 80 km and trending east from Bridgetown to Ravensthorpe. The position of the regional concentration, approximately 50 km inland from the coast, does not appear to be related to eolian derivation of Na from the Southern Ocean. Instead, incomplete decomposition of feldspar has resulted in remnant feldspar particles in lateritic residuum and this is confirmed by petrographic examination. In the northern part of the survey area, there are small clusters of increased Na abundances within the granitic terrain, possibly related to very coarse grained bedrock.

Potassium

The dominant regional K trend is a concentration in the southern part of the survey area, approximately 270 × 90 km, trending east-northeast along the Proterozoic rocks overlying and adjacent to the Yilgarn Craton. Petrographic work reveals small quantities of weathered microcline perthite in the lateritic residuum of this region (compare with Na).

North of the regional concentration, K (as $\%K_2O$) forms several clusters of relatively high-K abundance such as a 20 × 40 km cluster approximately 35 km southeast of the Saddleback greenstone belt. The irregular distribution of K abundances in the northern part of the survey area makes it more likely that differences in the K content of the bedrock and differences in the completeness of weathering are the causes of the variation in K abundance in the regolith.

Rubidium

The Rb distribution shows several clusters within granitic terrain (90th percentile 19.8 ppm), whereas abundances in greenstone terrain are generally low (90th percentile 9.9 ppm); there are no significant craton-scale trends. Regional clusters of elevated Rb abundances might be related to specific granite types as well as the presence of Proterozoic rocks along the margin of Archean rocks. There is a noteworthy regional enrichment of Rb east of Lake Barlee in granites adjacent to greenstone, where a cluster of Rb abundances ranging from 35 to 45 ppm might indicate a particular granite intrusion or regional alteration. Other elements enriched in this area are Be, Cs and REE.

Caesium

The Cs distribution is very similar to that of Rb. It shows several regional concentrations of high Cs in the northern part of the survey area, along the southern margin of the Yilgarn Craton within Proterozoic rocks overlying the Yilgarn Craton. As with Rb, Cs abundances generally are greater in granitic terrain (90th percentile 1.1 ppm) compared with greenstone terrain (90th percentile 0.8 ppm).

Alkaline earths

Beryllium

Although naturally associated with fluid-rich rocks such as pegmatites, greisens and skarns, Be abundances are similar in granitic and greenstone terrains (90th percentiles 1.6 and 1.4 ppm respectively). There are a few clusters of elevated Be abundances in the northern part of the survey area (such as east of Lake Barlee, with a maximum abundance of 3.7 ppm) that might correspond to regional hydrothermal alteration.

Magnesium and calcium

Both Mg (as %MgO) and Ca (as %CaO) are strongly depleted in lateritic residuum compared with their respective abundances in bedrock, and comprise only a minor part of the oxides (90th percentiles 0.12 and 0.13% respectively). However, secondary carbonate introduced to lateritic residuum by hydromorphic processes can significantly increase both the Mg and, particularly, the Ca contents. On a craton scale, Mg abundances are high north of the Albany–Fraser Orogen, extending for approximately 300 km in an east–west and 75 km in a north–south direction. The origin of this concentration might indicate a less intensely weathered regolith and, potentially, the presence of mica.

Samples with Ca (as %CaO) at greater than 2% have been excluded from the dataset, as they probably represent calcrete rather than lateritic residuum. A distinct Ca concentration in the northern part of the survey area is due to the introduction of calcite to the colluvium and calcite impregnation of ferruginous materials. Other Ca concentrations are located within or close to greenstone sequences and might reflect incomplete weathering of calcic feldspar and amphibole in the bedrock.

Strontium

There is little difference between Sr abundances on granitic and greenstone terrains (90th percentiles 18 and 17 ppm respectively). Regionally, there are two areas of elevated Sr in laterite, one north of the Albany–Fraser Orogen (230 × 100 km) and the other in the northern part of the survey area (to the west of Mount Magnet) of approximately 160 km in diameter. There are several isolated concentrations and small clusters throughout the survey area. In lateritic residuum, Sr abundances appear to reflect differences in bedrock composition. Where samples are dominantly from colluvium, such as west of Mount Magnet, Sr strongly correlates with Ca, indicating hydromorphic carbonate enrichment. There is a correlation with Na, particularly in the north and south, which probably reflects incomplete feldspar weathering.

Barium

There is a major difference between the Ba distribution in the north and south of the survey area that is significantly stronger than that between granitic and greenstone terrains

(90th percentiles 360 and 315 ppm respectively). The boundary between the two groups approximately follows the so-called Menzies line, an environmental divide based on a number of factors including soil and climate (Anand et al., in press). To the south of the boundary, tall eucalypt open woodlands dominate, whereas north of it acacia trees and shrub dominate. Barite ($BaSO_4$) is developed in red-brown hardpan (Mahizhnan, 2004); hardpans are common north of the Menzies Line, in the north part of the survey area. Barite contributes to a late regolith cement and affects all upper parts of the regolith profile; residual or depositional parts alike.

Transition metals

Scandium

Scandium is associated with Fe- and Mg-rich rocks, hence its greater abundance in laterite developed on greenstones and greenstone remnants of the western Yilgarn Craton (90th percentile 114 ppm) compared to granitic rocks (90th percentile is 39 ppm). It is concentrated in some residual rocks and is abundant in some pegmatites.

There are two major Sc trends outside known greenstone belts. The first is approximately 130 km long, extending southeast along the Saddleback greenstone belt and extending 40 km south of the greenstone sequence. A second trend extends approximately 400 km south-southeast along the western margin of the Yilgarn Craton from Toodyay to Mullewa. Both trends might indicate the presence of mafic remnants within these regions.

Vanadium

Vanadium is mainly associated with mafic rocks in the Yilgarn Craton and hence its far greater abundance in greenstone sequences (90th percentile 1370 ppm) than in the granite–gneiss terrains (90th percentile 780 ppm). Two noticeable exceptions are an association of high V and Ti in parts of the southwest Yilgarn Craton (see **Titanium**) and in the Jimperding metamorphic belt, and a distinct regional V concentration (approximately 70 km across) also associated with Sc in an area south of Mullewa near the western boundary of the Yilgarn Craton. On a craton-scale, the abundance of V is greater in the northern Yilgarn Craton where elevated V in laterite over some greenstone belts could indicate a higher proportion of mafic rocks, such as at Diemals – Mount Jackson, Rothsay – Golden Grove, and Windimurra.

Titanium

Although the Ti abundance (as $\%TiO_2$) over greenstones exceeds that over granitic rocks (90th percentiles 2.3 and 1.5% respectively), high-Ti abundances are developed in the southwest Yilgarn Craton over an area bounded by the Darling escarpment in the west and a line from Perenjori in the north to Bremer Bay in the south. Titanium concentrations in this area are generally 1–3% (maximum 12.9%), and probably reflect the relatively high proportion of mafic dykes (Fig. 11). In the northern Yilgarn Craton, high Ti is associated with the Windimurra and Narndee intrusions.

Manganese

On a craton scale, there are increased Mn abundances (as %MnO) on greenstone sequences (90th percentile 0.08 compared to 0.03% in granitic terrain), with some localized Mn concentrations due to secondary Mn enrichment in hardpanized colluvium with Mn up to 3.9%. Black staining on the outside of ferruginous gravel is an indication of highly anomalous Mn. This type of Mn-rich gravel, which generally occurs at the base of the colluvium, was avoided during sampling and was only collected where no other material was available. All elements closely associated with Mn oxides and hydroxides (e.g. Co, Tl, Cd, and Zn) must be treated with caution in manganiferous samples.

Iron

The regional distribution of Fe (as $\%Fe_2O_3$) is a good proxy for the abundance of mafic rocks and banded iron-formation in the bedrock; lateritic residuum on greenstone sequences generally has more Fe (90th percentile 66.5%) than that on granitic terrain (90th percentile 40.9%). Thus, Fe abundances are, overall, greater in the north and northeast of the survey area than in the south, reflecting abundant greenstones and intrusive complexes.

Cobalt

In bedrock, Co is strongly associated with sulfides, whereas in the regolith there is a strong association between Ni and Co (such as in nickel laterites) and Co and Mn in the case of secondary Mn coatings and infusions. The regional distribution of high Co is primarily controlled by the presence of mafic–ultramafic volcanic and intrusive rocks. Beyond greenstone successions, isolated high-Co abundances are commonly associated with secondary Mn in colluvium and lag such as west of Mount Magnet and around Meekatharra. A regional high-Co concentration (10–45 ppm) outside known greenstone belts is located over an area of approximately 130 × 70 km, 100 km north-northeast of Albany. Some of these Co concentrations appear to coincide with the intersections of northwest faults (e.g. Dumbleyung Fault) and east-southeast dykes.

Chromium

Chromium is a reliable indicator of mafic–ultramafic rocks in the regolith, due to the weathering resistance of chromite. High-Cr abundances not only outline the extent of greenstone belts (90th percentile 6380 ppm), but also show remnants of greenstones, sills, and layered intrusions within areas of granite–gneiss (90th percentile 550 ppm). The Cr distribution (Fig. 12) clearly outlines the main greenstone belts in the western Yilgarn Craton as well as mafic–ultramafic intrusions such as at Narndee and Windimurra. Concentrations of chromium also indicate greenstone remnants near Lake Grace, and scattered mafic

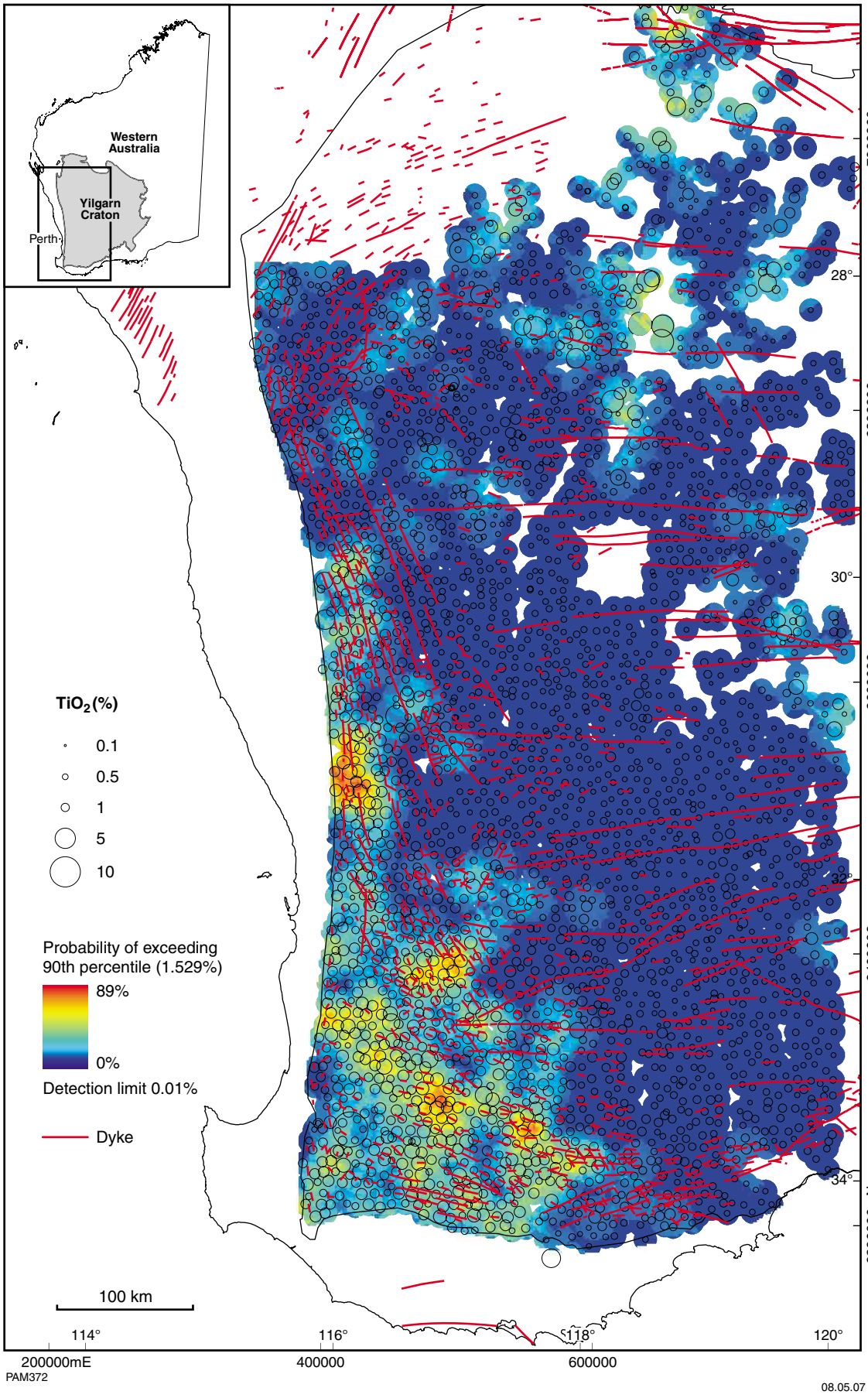

Figure 11. Kriged image and bubble plot of Ti (as TiO_2) and abundances of mafic dykes

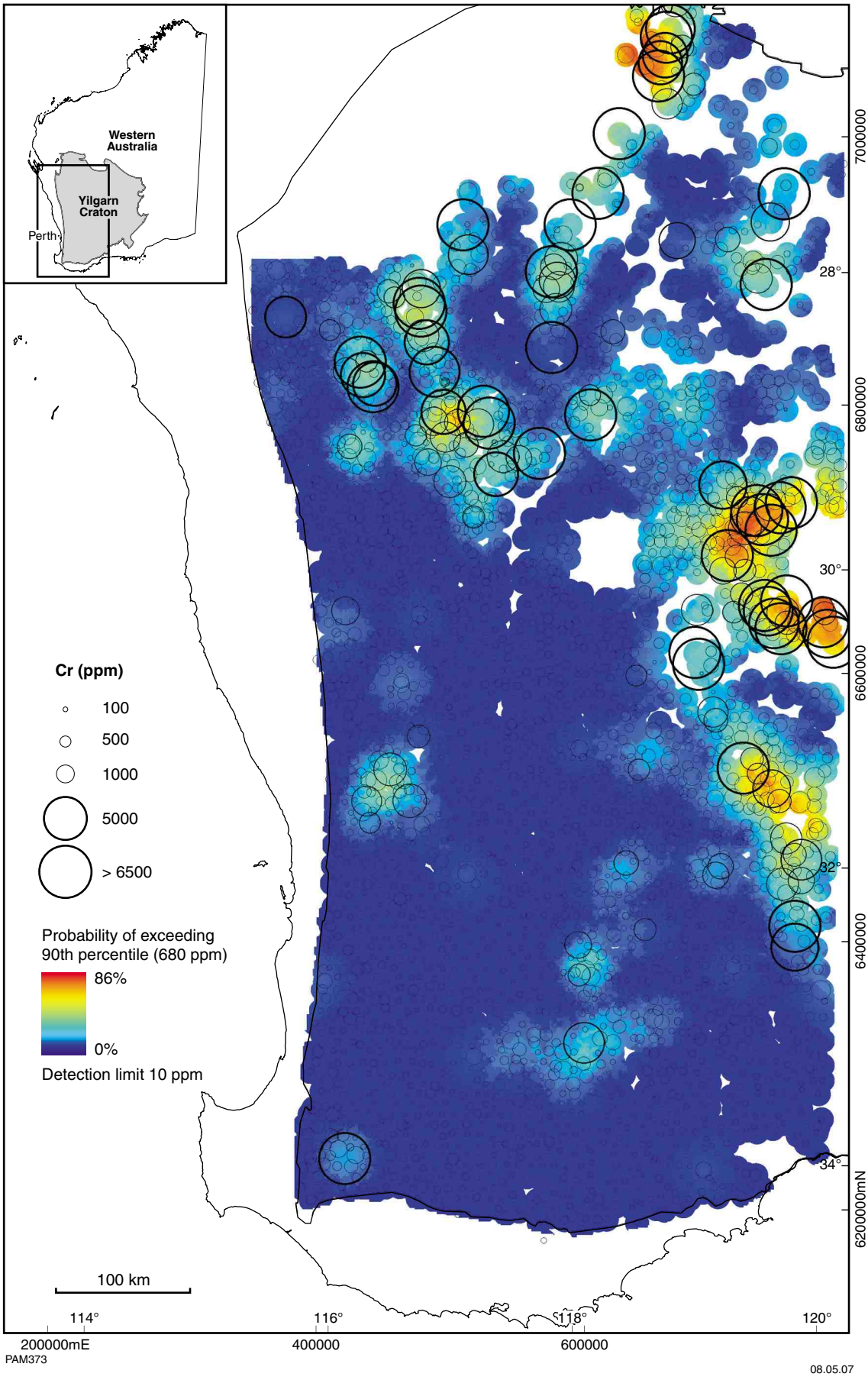

Figure 12. Kriged image and bubble plot of Cr abundances

or ultramafic rocks in the southwest Yilgarn Craton such as near Bridgetown, and in the Jimperding metamorphic belt northeast of Perth.

Nickel

In Archean bedrock, Ni is concentrated in ultramafic rocks. Accordingly, Ni abundances are greater in greenstone belts (90th percentile 303 ppm) than in felsic-dominated terrains (90th percentile 55 ppm).

Outside known greenstone belts (Fig. 13), there is a Ni concentration in the Jimperding metamorphic belt south of Wongan Hills, with a maximum of 270 ppm Ni in sample 103191. Greater Ni (and Cr) abundances confirm the presence of mafic and ultramafic rocks within the Jimperding metamorphic belt, such as the Coates Gabbro. Some isolated high-Ni abundances throughout the western Yilgarn Craton, both within and beyond known greenstone belts, might be due to secondary enrichment of Ni, but could also indicate small ultramafic remnants. A peak Ni abundance of 2150 ppm (sample 101655) is related to a mafic–ultramafic complex south of the Windimurra Complex.

Copper

On a regional scale, Cu abundances are significantly greater in greenstone belts (90th percentile 180 ppm) than in granite–gneiss terrains (90th percentile 38 ppm), with a few noticeable exceptions. Regional concentrations of high Cu in the southwest of the craton (Fig. 14), along strike from the Saddleback greenstone belt, extend from approximately 20 km south of the Saddleback greenstone belt to the southern edge of the craton, a distance of approximately 120 km. A series of high-Cu concentrations, south of the Wongan Hills greenstone belt in the Jimperding metamorphic belt, trend approximately 300 km northwest and extend approximately 300 km towards Mullewa. This trend might reflect abundant mafic rocks in this part of the metamorphic belt, with a small amount of associated base metal sulfide such as at Yarawindah Brook, southeast of New Norcia. A sample near the Yarawindah Brook mafic–ultramafic body has a Cu abundance of 140 ppm. Localized high-Cu concentrations around Bridgetown might be associated with mafic–ultramafic intrusive rocks.

The Mount Gibson – Golden Grove, Diemals – Mount Jackson, and Meekatharra greenstone belts all show high-Cu abundances, with one sample reaching 2080 ppm approximately 40 km southeast of Golden Grove. In the Mount Gibson belt, several Cu-rich Au deposits and the Golden Grove Cu–Zn–Au deposits are evidence of this trend. In the Diemals – Mount Jackson greenstone belt, high Cu in lateritic residuum might indicate the presence of more widespread base metal sulfides.

Zinc

At a regional scale, Zn abundances in greenstone belts (90th percentile 56 ppm) exceed those in granitic terrain (90th percentile 24 ppm) due to the Zn content of contained base metal sulfides, black shales, and minor sulfides in mafic igneous rocks. Outside greenstone belts, most concentrations of Zn are associated with secondary Mn oxides and hydroxides. In the southwest of the Yilgarn Craton, high-Zn abundances are associated with the Jimperding metamorphic belt, and small greenstone remnants near Griffins Find. A peak of 408 ppm Zn (sample 100970) lies northeast of the Mullewa greenstone belt and is unexplained.

Yttrium

In the granitic and greenstone terrains of the northwest Yilgarn Craton (90th percentiles 13.3 and 13.2 ppm respectively), high-Y abundances form several small clusters. In the southwest Yilgarn Craton, elevated Y forms a broad, regional trend along the Darling Range, extending inland to Corrigin, with a cluster of very high abundances (52–116 ppm) near Bridgetown and Greenbushes. As Y is associated with rare earth elements (e.g. in pegmatite and carbonatite), these concentrations might indicate further pegmatite in the area. Another regional Y trend, extending east-northeast and parallel to the Albany–Fraser Orogen, is also associated with elevated REE and alkali elements. A base metal concentration east of Lake Barlee also is associated with high Y.

Zirconium

Zirconium is more abundant in felsic rocks and hence abundances in the granite–gneiss terrains (90th percentile 614 ppm) significantly exceed those in greenstone terrains (90th percentile 390 ppm). The regional distribution shows a group of high-Zr samples south of Mullewa covering an area of approximately 100 × 90 km, with Zr abundances ranging between 500 and 1700 ppm. Other high-Zr samples are scattered throughout granitic rocks of the western Yilgarn Craton and might characterize specific granite populations, although some may have been incorporated from eolian materials.

Niobium

As with Zr, Nb is mostly associated with felsic rocks (90th percentile in granitic terrain is 25 ppm; in greenstone terrain it is 16 ppm), with the exception of alkaline ultramafic rocks. The distribution pattern shows several regional concentrations of high Nb, particularly in the western half of the survey area. Abundances are generally low over greenstones. Several clusters of anomalous Nb abundances are developed within the regional concentrations and the areas of low abundances. The source of such enrichment might be either a large granitic body with high-Nb content, pegmatite dykes, or alkaline rocks (see sample 102689 and Cornelius et al., 2006). One sample southeast of Meekatharra contains 221 ppm Nb and is probably related to pegmatites.

Molybdenum

There are clusters and isolated high-Mo abundances throughout the survey area. Most are in granitic

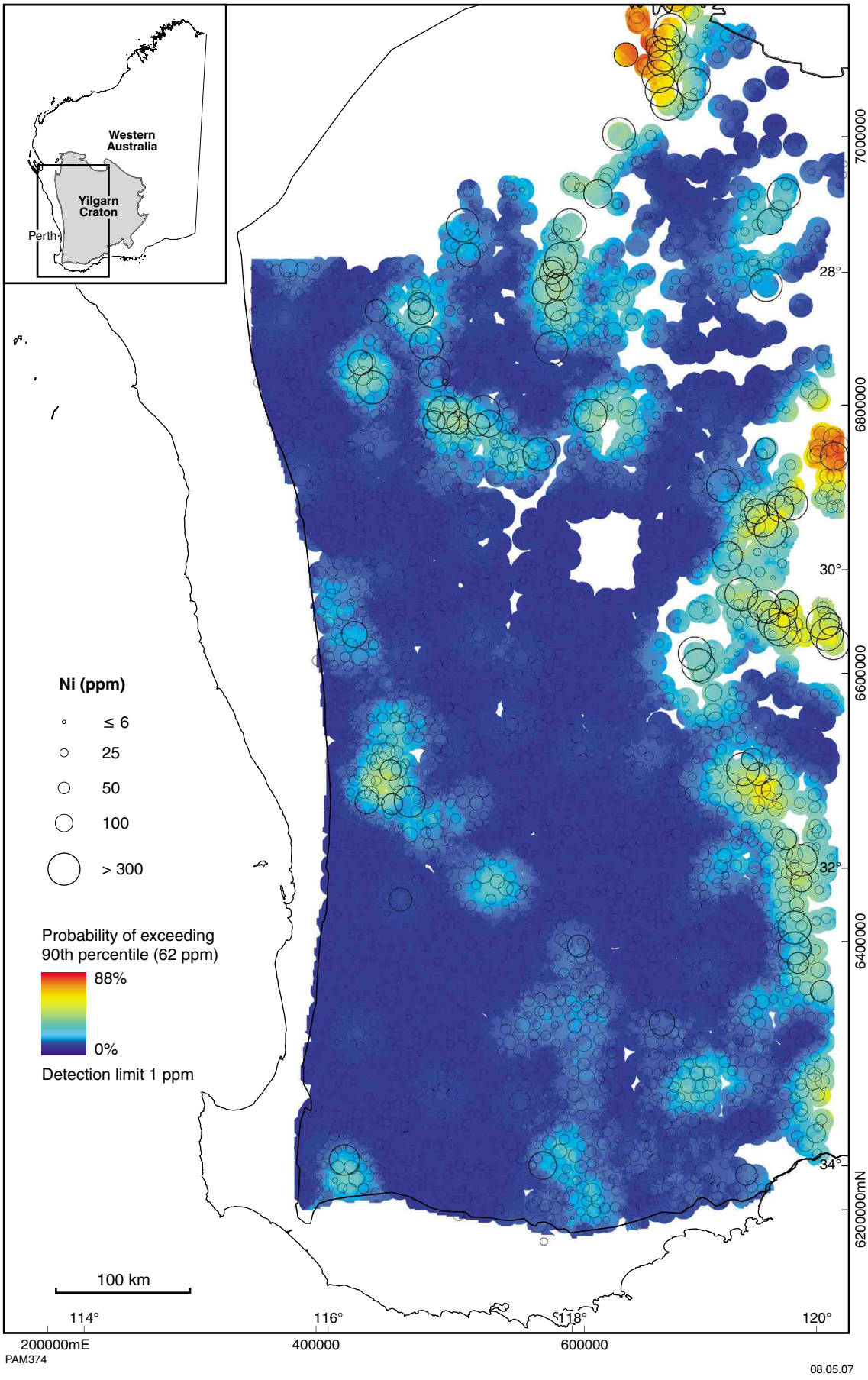

Figure 13. Kriged image and bubble plot of Ni abundances

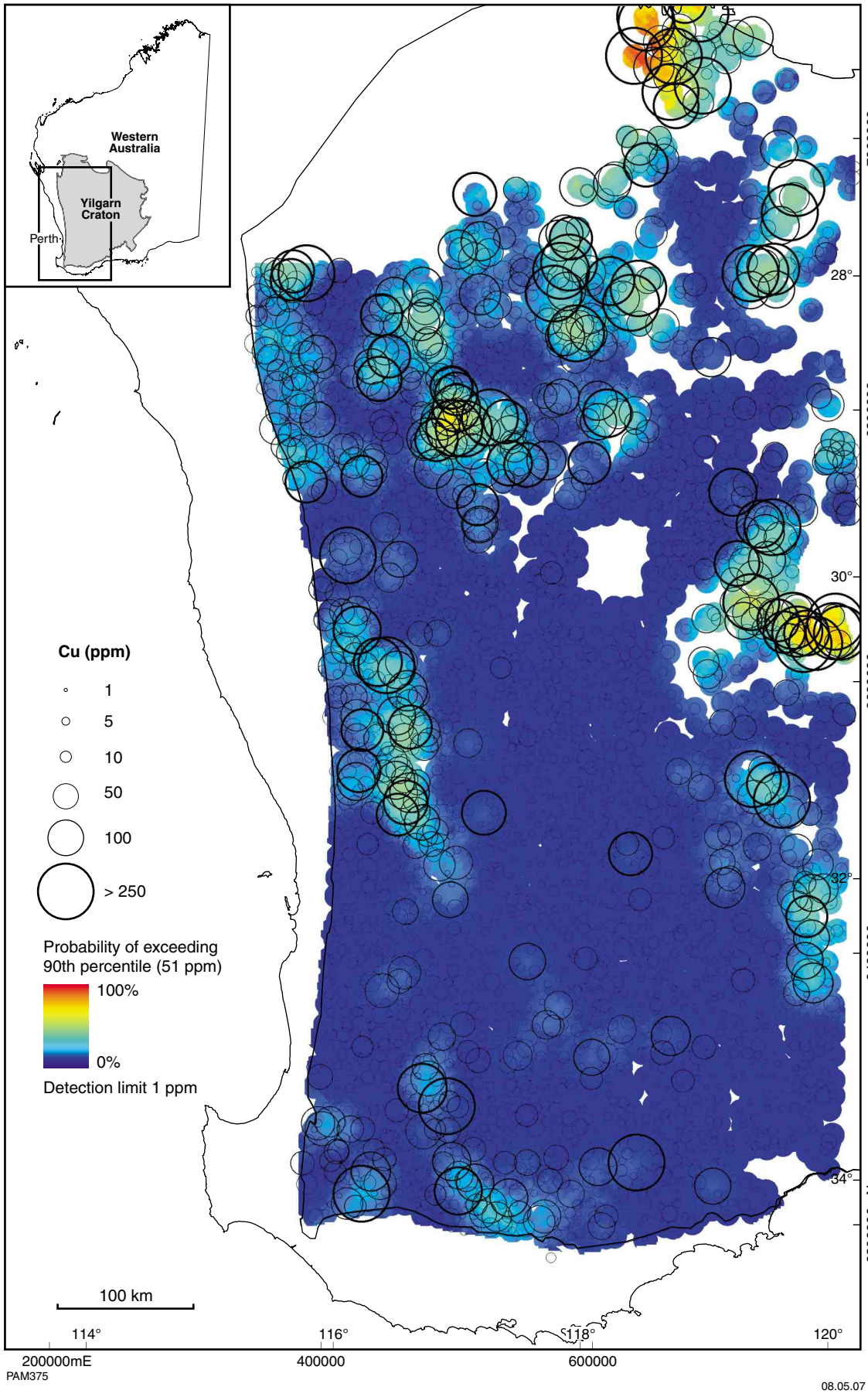

Figure 14. Kriged image and bubble plot of Cu abundances

terrain, generally proximal to greenstone sequences or metamorphic belts such as the Jimperding and Chittering belts. Molybdenum abundances are slightly greater in granitic terrains (90th percentile 8.6 ppm) than in greenstone sequences (90th percentile 6.9 ppm). Whereas some Mo concentrations are associated with anomalous Au concentrations, most are not.

Platinum group elements (PGE)

The six platinum group elements Os, Ir, Ru, Rh, Pt, and Pd were included in the analytical suite following preliminary studies that showed many laterite samples with high-Cr, -Ni, and -Co abundances also have PGE concentrations above 1 ppb (i.e. at measurable levels). These concentrations can now be reliably and cost-effectively analysed using Ni fire assay techniques with a 0.1 – 1 ppb lower limit of detection. For cost reasons, only those samples with detectable Pt abundances in the aqua regia digestion were selected for Ni fire assay digestion and analysis for Os, Ir, Ru, Rh, Pt, and Pd.

A total of 449 samples were analysed for PGE at Ultra Trace Laboratories. Results show combined PGE abundances of up to 186 ppb in regional laterite samples and a 95th percentile for combined PGE of 68 ppb.

Regions with an overall higher abundance of total PGE in the laterite are, naturally, all greenstone belts, but particularly include the Diemals – Mount Jackson and the Mount Gibson – Yalgoo greenstone belts. Platinum and Pd, however, are also anomalous in many gneissic terrains throughout the western Yilgarn Craton and the metamorphic belts near the western margin of the craton. A typical example of such enrichment is the Yarawindah Brook PGE prospect near New Norcia in the northern Jimperding metamorphic belt (not sampled as part of the Laterite Database program).

In contrast to the widespread Pt and Pd enrichment, Ru, Os, Ir, and Rh are generally more closely associated with greenstone sequences and are indicative of the presence of mafic–ultramafic bedrock and associated Ni-sulfide mineralization.

Silver

Most Ag analyses (>98.9%) are less than the detection limit of 0.5 ppb. Results one to two times the lower limit of detection form several clusters in the northern half of the survey area, particularly in the Mount Gibson – Golden Grove – Yalgoo area. It is unclear whether these results have much significance, as even these abundances are close to the limit of detection. However, the close spatial relationship of high Ag with known mineralization might indicate a subtle mineralization signature.

Cadmium

All high-Cd abundances are located in the northern part of the survey area. Cadmium shows a very strong affinity with Mn oxides, and all Cd abundances greater than 0.1 ppm are in weakly to moderately manganiferous samples. Thus, Cd abundances in such samples probably have little relevance to bedrock Cd abundances.

Tantalum

Tantalum abundances are generally greater in granitic (90th percentile 2 ppm by fusion digest) than in greenstone terrains (90th percentile 1.5 ppm by fusion digest) and show several high regional and single point concentrations. In the northeast, several clusters of high-Ta abundance are located in granitic terrains between greenstone sequences; however, sampling is incomplete. The Greenbushes area, host to the world-class Greenbushes Sn–Ta mine, demonstrates the limitations of this 9 km-spaced survey. There is a strong regional Ta signature in the southwest part of the Yilgarn Craton that extends over 280 km from Toodyay in the north to Bridgetown in the south, and from the Darling escarpment in the west to approximately 70 km inland. However, on a local scale, the 9-km sampling does not show a Ta dispersion halo around the Greenbushes mineral deposit due to a small area with background-level Ta near the mine that was coincidentally sampled by this survey. An additional sample, taken within one kilometre of the mine, contained 21 ppm Ta (four-acid digest).

In the northern half of the survey area, a 30 × 30 km area of relatively high Ta (max. 8 ppm Ta by fusion) is located approximately 70 km west of Mount Magnet. Isolated high abundances southeast of Meekatharra show a maximum of 34 ppm (fusion digest). Limited follow-up sampling by Astro Mining Ltd with a focus on pegmatite or Ta-rich granite did not find any significant anomalies (Astro Mining Ltd, 2001, personal comm.).

Tungsten

The most prominent features on a regional scale in the north are a series of north-northwesterly trending high-W concentrations from Mount Gibson to Yalgoo, and a northeasterly trending belt from Paynes Find to Mount Magnet, which together form an annular structure with a diameter of approximately 200 km around a region of low-W abundance. Other prominent but patchy concentrations of high W are in the southwest, centred on the Greenbushes Sn–Ta deposit, and a regional northwest trend in the Jimperding metamorphic belt near Coates and in the Saddleback greenstone belt. The diameter of the W halo in lateritic residuum around the Greenbushes Sn–Ta mineralization is 10–20 km and reaches 15 ppm.

The maximum W abundance is 135 ppm in the Marvel Loch area, south of Southern Cross. Abundances of W in greenstone (90th percentile 5 ppm) generally exceed those in granitic terrain (90th percentile 2.5 ppm) and may reflect hydrothermal alteration.

Gold

Gold abundances in greenstone (90th percentile 10.6 ppb) exceed those in granitic terrain (90th percentile 0.8 ppb). Most Au concentrations correspond, on a broad scale,

with areas of known Au mineralization (Fig. 15) around Meekatharra, Mount Magnet, Sandstone, Yalgoo, Mount Gibson, Gullewa, Golden Grove, Westonia, Southern Cross, the Mount Dimer greenstone belt, Bullock Pool, and Griffins Find (36 ppb approximately 20 km northwest of Griffins Find). A high value of 1460 ppb at Golden Grove is from over the orebody (sample 101504_3). In the Jimperding metamorphic belt, a cluster of samples (max. 17 ppb Au) is located approximately 30 km north of the Wundowie Au deposit. The Boddington Au mine, the largest Au deposit in the southwest Yilgarn Craton, only shows a very weak Au signature (4.4 ppb), due to the intense leaching of Au from the nodular–pisolitic gravel at the surface (Anand, 1998b).

In the high rainfall areas, it is imperative to include chalcophile elements as well as Au in regional Au exploration using lateritic nodules and pisoliths (Anand, 1998b, 2001). The significance of several single-point high-Au concentrations throughout the southwest Yilgarn Craton needs to be established by close-spaced follow-up sampling of lateritic residuum and other sample media.

Mercury

Mercury displays one of the most distinct craton-scale trends unrelated to greenstone sequences (Fig. 16). High-Hg abundances extend for over 500 km from northwest of Wongan Hills to Jerramungup in the south. There, the trend continues to the northeast along the Archean–Proterozoic boundary. Mercury abundances range between 100 and 500 ppb, with a maximum abundance of 820 ppb approximately 30 km east of Wongan Hills. The origin and significance of this spatially massive Hg trend remains unclear, but it appears broadly aligned with the southeasterly trending gneiss–migmatite zone along the eastern boundary of the South West Terrane. There is also a spatial relationship with sites of seismic activity (Fig. 17), as shown on the Geoscience Australia website (www.ga.gov.au/urban/projects/nrap/perth_earthquake.jsp), broadly parallel to regional southeast faults in the southwest Yilgarn Craton (Fig. 17). To our knowledge, this is the first time this regional Hg trend has been revealed. There is an absence of any high-Hg abundances in the northern part of the survey area except for the northwest continuation of the major trend towards the western margin of the Yilgarn Craton west of Perenjori. This is also shown by the generally greater Hg abundances in granitic terrain (90th percentile 70 ppb) compared with greenstone sequences (90th percentile 40 ppb).

Other metals

Aluminium and gallium

Areas of high-Al abundance (as $\%Al_2O_3$) in lateritic gravel in the southern part of the west margin of the Yilgarn Craton (Fig. 18) show a very close correlation with areas of high rainfall (Fig. 1). Leaching of alkalis, alkaline earths, Si and Fe has left a lateritic residuum that is very rich in residual Al. The development of bauxitic regolith profiles in the Darling Range is discussed in detail by Anand (1998b). In the southwest Yilgarn Craton, the regional distribution of Ga closely resembles that of Al due to substitution of Ga for Al in Al–Fe oxides and oxyhydroxides.

Indium

Relatively high In is developed both in greenstone (90th percentile 0.26 ppm) and in granitic terrains (90th percentile 0.22 ppm). Of the three clusters of relatively high concentrations, one is located in the southwest corner of the Yilgarn Craton centred on Bridgetown (0.2–0.5 ppm In), and the second is in the Chittering and Jimperding metamorphic belts (0.2–0.4 ppm In). The third coincides with the Golden Grove sequence. The maximum concentration of 13.9 ppm In is near Gossan Hill (Golden Grove) and is associated with volcanic-hosted massive sulfide mineralization. Other isolated high-In concentrations up to 0.6 ppm are developed throughout the western Yilgarn Craton.

Tin

On a craton scale, most of the high Sn is concentrated within 90–100 km of the southwest margin of the Yilgarn Craton, with a 90th percentile for Sn in granitic terrain of 4 ppm and 3 ppm in greenstone terrains (mixed acid digest). The maximum Sn is 130 ppm (fusion) in lateritic gravel near Gossan Hill, Golden Grove. There is 110 ppm Sn (fusion) in lateritic residuum from the Wongan Hills greenstone belt. A cluster of high-Sn abundances (7–20 ppm Sn by fusion) is located northwest of the Saddleback greenstone belt. One location (100258) southeast of Meekatharra has a Sn concentration of 40 ppm (fusion). Seventy kilometres northwest of Mount Magnet, high-Sn abundances of 10–20 ppm (fusion) are associated with high As (55 ppm).

Thallium

Most Tl enrichments in ferruginous gravel are associated with secondary Mn oxides (Fig. 19), and therefore have limited significance for bedrock interpretation. Non-manganiferous material such as 100263, 101494 and 103281 (see red circle in Figure 19), with Tl abundances of 1.5 ppm, might indicate primary Tl-rich bedrock, possibly Cu–Pb–Zn sulfides or black shale.

Lead

Lead (Fig. 20) abundances are very similar across felsic and mafic–ultramafic terrains in the Yilgarn Craton (90th percentile in granitic terrain 67 ppm compared with 51 ppm in greenstone sequences).

High-Pb abundances, particularly in the northern half of the Yilgarn Craton, are generally associated with Mn-rich colluvial samples. It is likely that soluble Pb was scavenged by Mn oxides and hydroxides, in a similar fashion to Cd. In general, high Pb in the southern Yilgarn Craton is not associated with high Mn. High Pb inland from Bremer Bay is associated with high REE and Na.

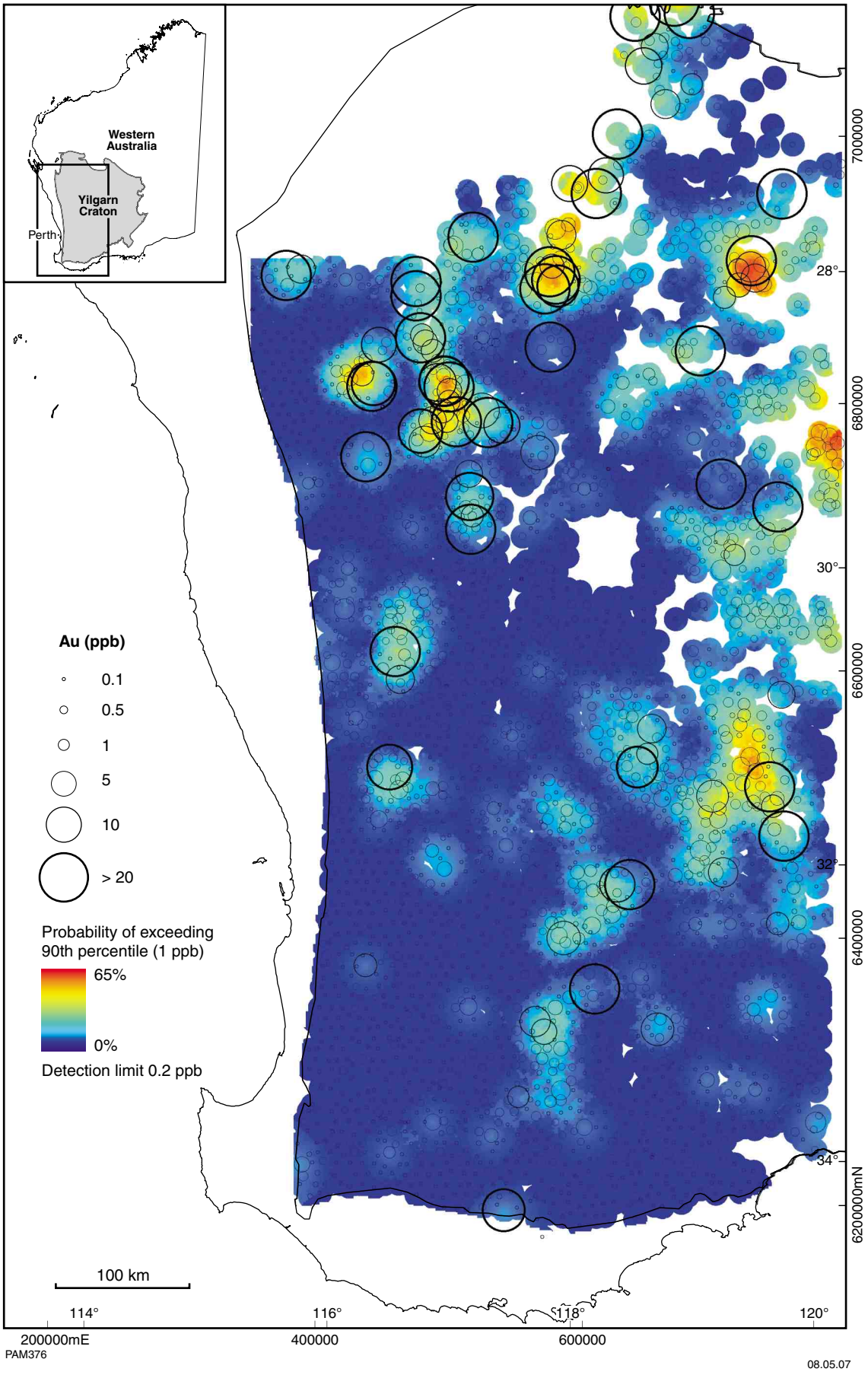

Figure 15. Kriged image and bubble plot of Au abundances

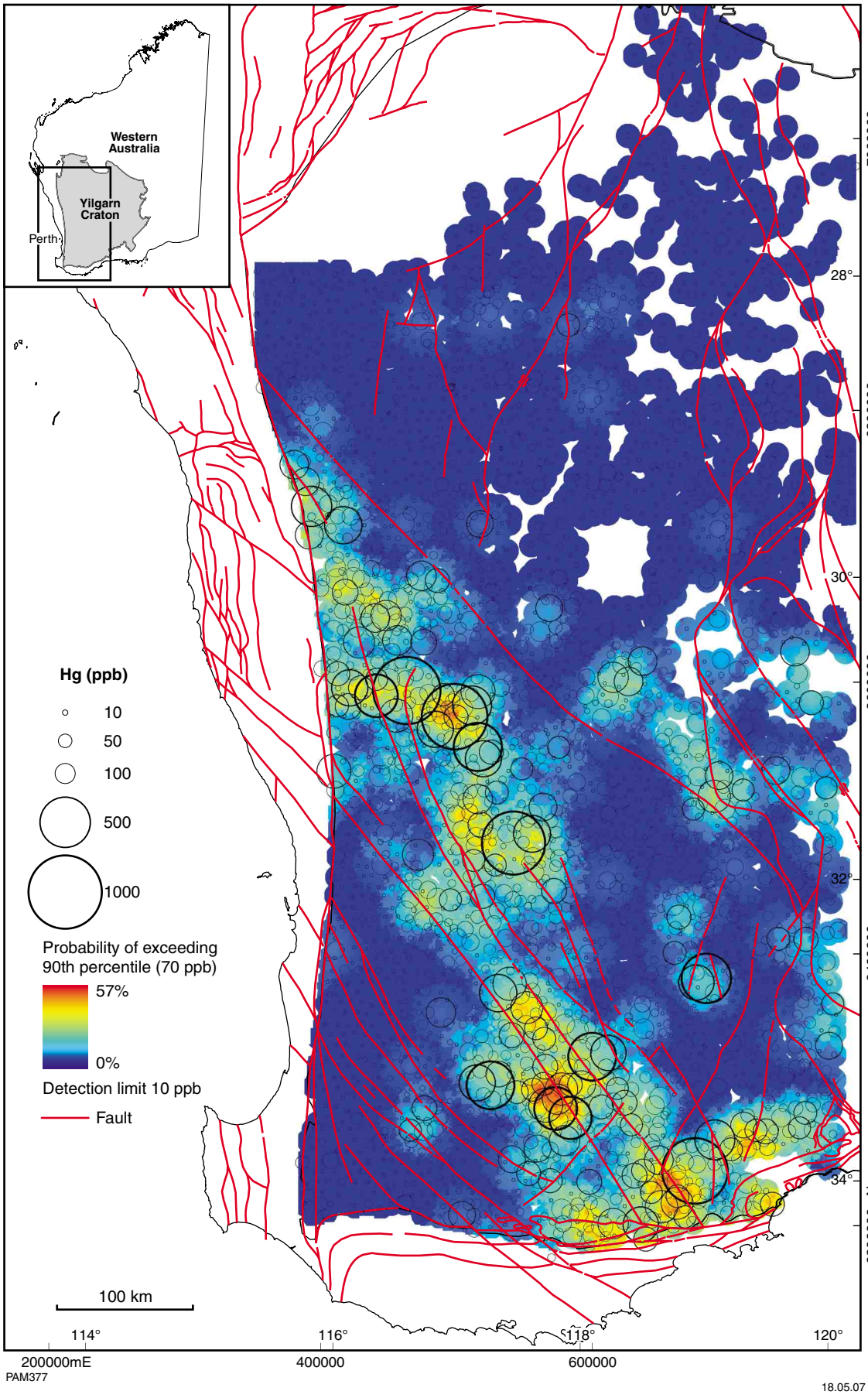

Figure 16. Kriged image and bubble plot of Hg abundances and fault distribution in the western Yilgarn Craton (after Myers and Hocking, 1998)

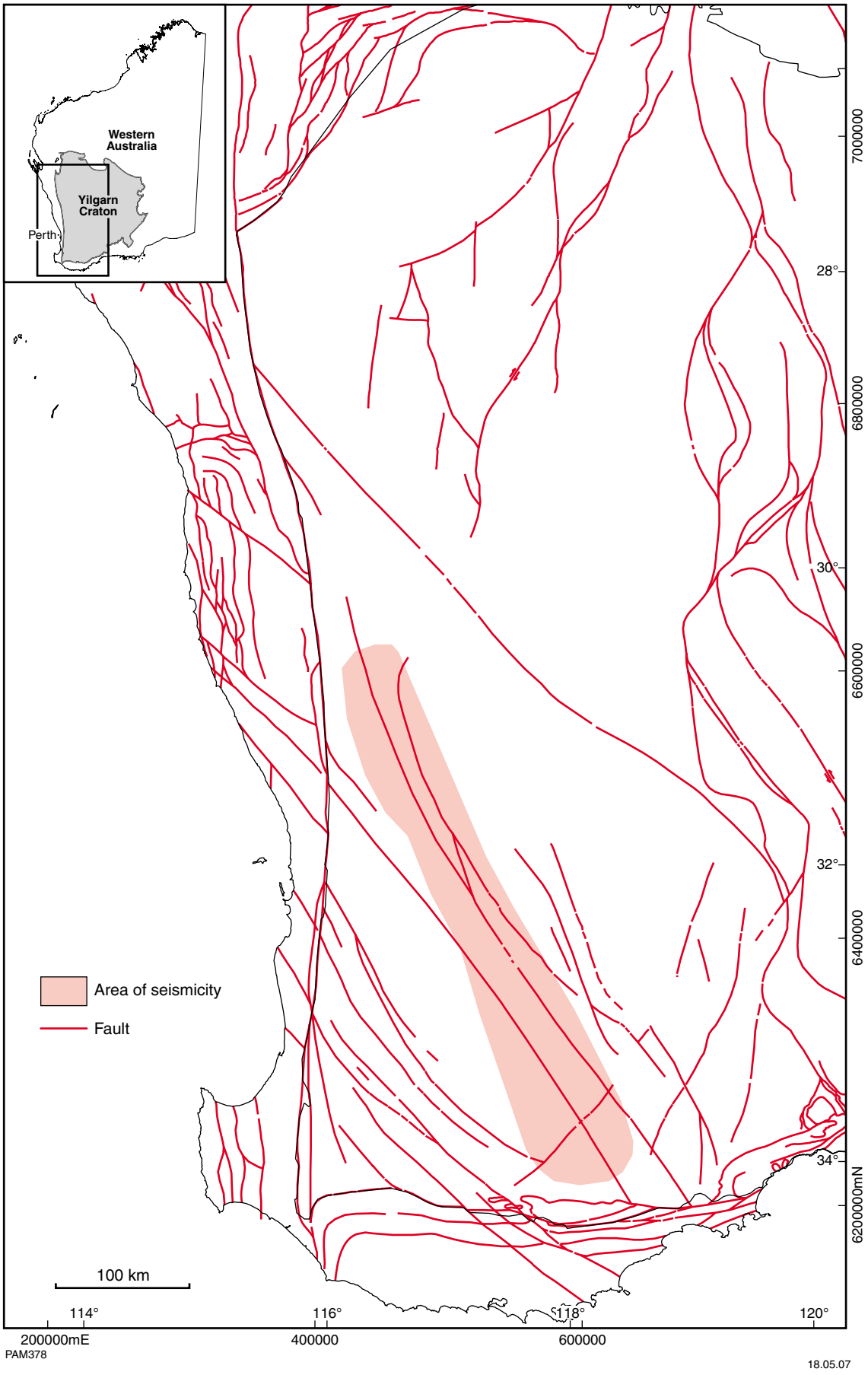

Figure 17. Fault distribution in the western Yilgarn Craton (after Myers and Hocking, 1998) and areas with the most intense seismic activity (after Geoscience Australia website)

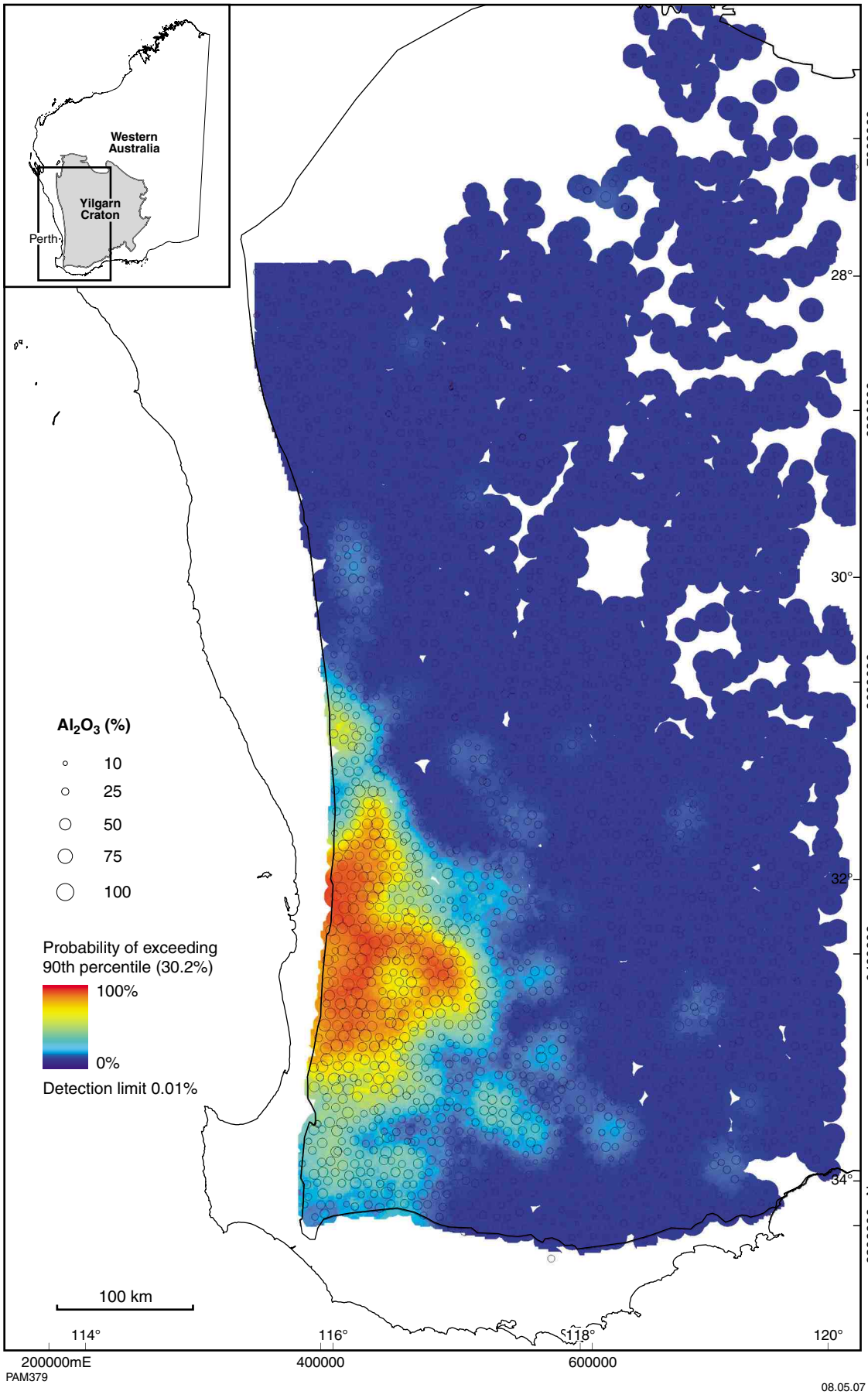

Figure 18. Kriged image and bubble plot of Al (as Al_2O_3) abundances

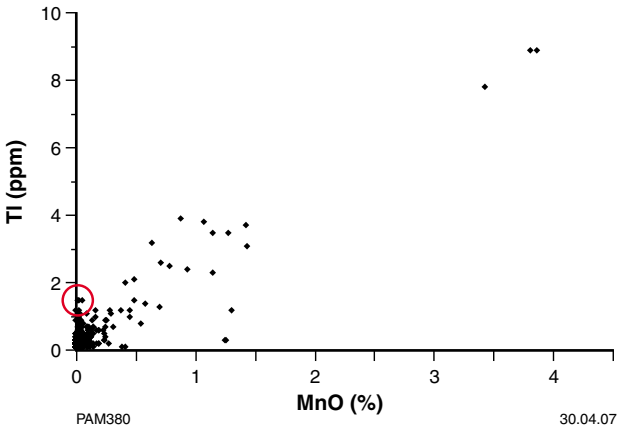

Figure 19. Scattergram of Tl and Mn (red circle indicates non-manganiferous samples)

Bismuth

Bismuth abundances are greater in the northeast of the survey area than in the southwest, and appear spatially associated with greenstone belts (90th percentile 1.3 ppm compared with the 90th percentile of 0.9 ppm in granitic terrain). There are four significant regional clusters of concentrated Bi. These are east of the Gullewa greenstone belt (maximum 9.1 ppm Bi) and around the Golden Grove base metal district (maximum 86.8 ppm; Smith and Perdrix, 1983); the southern part of the Kirkalocka greenstone belt (maximum 11.2 ppm Bi); southeast of Meekatharra (maximum 65.9 ppm Bi — the highest concentration outside the Golden Grove base metal district); and along the Southern Cross greenstone belt (maximum 19.1 ppm Bi). In the southwest Yilgarn Craton, Bi concentrations reach 8–9 ppm in the Jimperding metamorphic belt and the Wongan Hills greenstone belt, but are low elsewhere.

Metalloids

Silica

There is a distinct region of low Si in the southwest part of the Yilgarn Craton (west of a line from Moora to Albany) that corresponds with an enrichment in Al and reflects leaching of silica in areas of high rainfall. East of the Moora to Albany line, Si abundances (as $\%SiO_2$) are relatively high, with notable areas east of the Wongan Hill greenstone belt (150 km across) and north of the Proterozoic Albany–Fraser Orogen. The northeast part of the survey area shows local clusters of high Si. High Si in lateritic residuum could indicate coarse-grained granitic rocks with large quartz crystals that resist weathering, or silicification of the regolith.

Arsenic

Arsenic is one of the most important pathfinder elements for gold and base metal mineralization and shows wide dispersion, due to its mobility in the regolith (Fig. 21). In the survey area, there are three main patterns. There is a region of concentrated As in the northeast (associated with the more abundant greenstone sequences; 90th percentile 119 ppm) and relatively low craton-scale As in the southwest associated with dominantly granitic terrain (90th percentile 36 ppm). Another area of high As extends along the southern boundary of the Yilgarn Craton with the Proterozoic rocks, and in the Bridgetown–Yornup region.

In the southwest, a series of high-As abundances are located around Bridgetown–Greenbushes–Yornup. These trend southeast for approximately 60 km and extend northeast for about 20–25 km. They were earlier recognized by Smith et al. (1989). There are probably multiple sources of the As. Pegmatite at Greenbushes has anomalous As concentrations that yield a large As anomaly in lateritic residuum (Smith et al., 1987). Massive sulfide has been encountered 25 km southwest of Bridgetown, and the Yornup ultramafic–mafic intrusion might host sulfides. Another prominent As trend is located along the southern margin of the Yilgarn Craton, north of the Albany–Fraser Orogen, and extends for approximately 160 km east-northeast from Albany to Bremer Bay. There are small clusters of high-As concentrations in the Jimperding and Chittering metamorphic belts, the Wongan Hill greenstone belt, and near mafic–ultramafic remnants in the Bullock Pool – Griffins Find areas.

In the northeast of the survey area, there are three prominent areas of high As within the broader trends. One extends approximately 120 km south-southeast from Southern Cross, enveloping many known Au and Ni mining centres in the Southern Cross greenstone belt. A second area is located southwest of Lake Barlee and includes (one reaching 1910 ppm), but is not limited to, the Diemals greenstone belt. Here, many high As concentrations cover an area approximately 80 km in diameter in granitic terrain and its source is unknown. Due to the residual nature of the laterite, mechanical or hydromorphic transport from the nearest greenstone sequence (approximately 30 km away) seems unlikely.

A third area of high As, originally recognized by Smith et al. (1989) is centred on the Golden Grove – Mount Gibson greenstone belt, covering both greenstone sequences and adjoining granitic terrain. It is approximately 80 km in diameter. On an even broader scale, there is a high-As trend that extends from the Tallering Peak sequence in the northwest to the Mount Gibson mine in the southeast, a distance of approximately 230 km. This trend includes part of the Gullewa greenstone belt and the granite between this belt and the Golden Grove sequence. The trend also appears to continue to the northeast towards the Dalgaranga area. Smaller, high-As clusters are associated with the Mount Magnet, Sandstone and Meekatharra mining districts, where the sample pattern is incomplete and their true extent cannot be assessed.

Antimony

The regional distribution of Sb broadly resembles that of As, with a marked increase in the background abundance from the southwest to the northeast. There are two areas

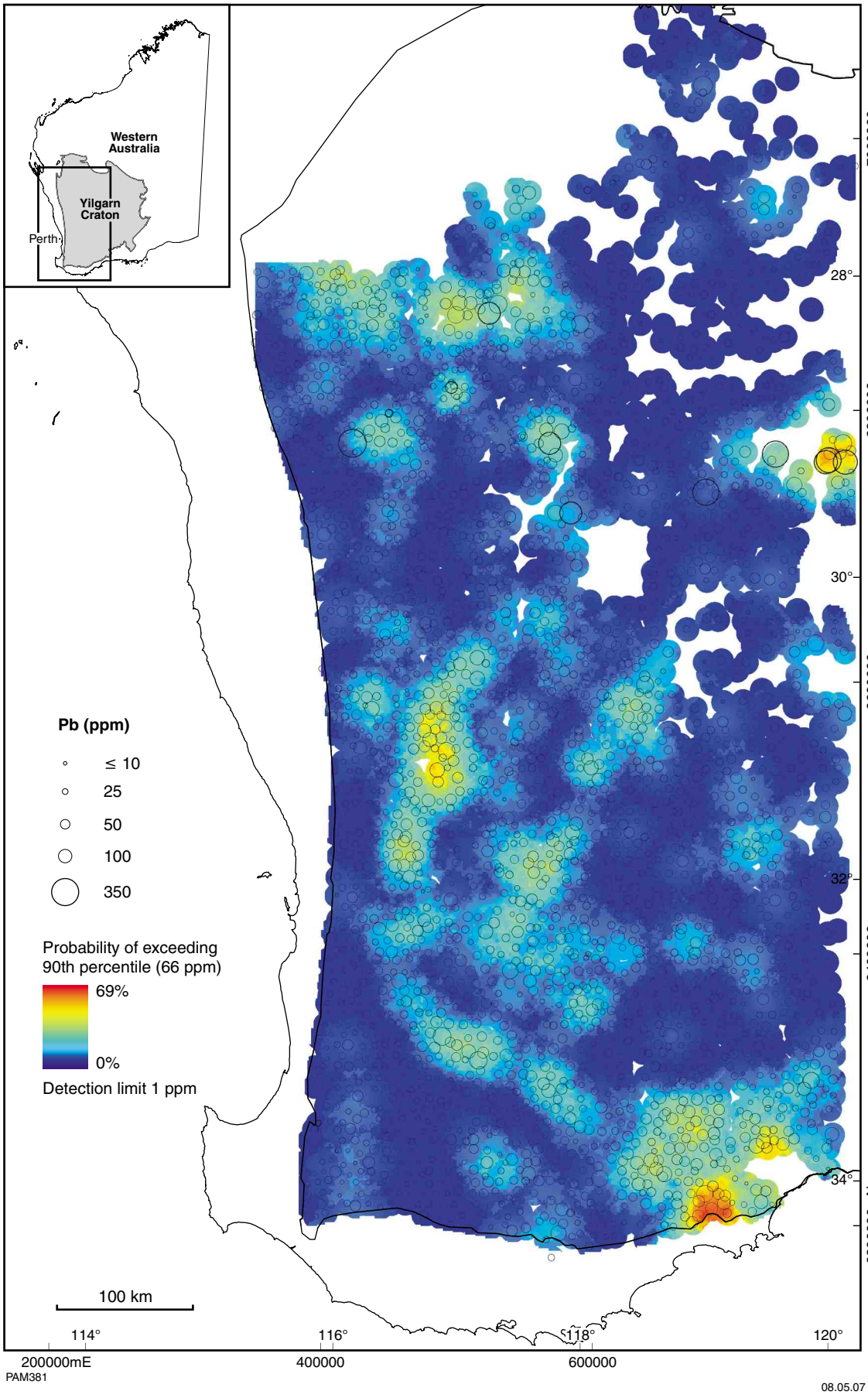

Figure 20. Kriged image and bubble plot of Pb abundances

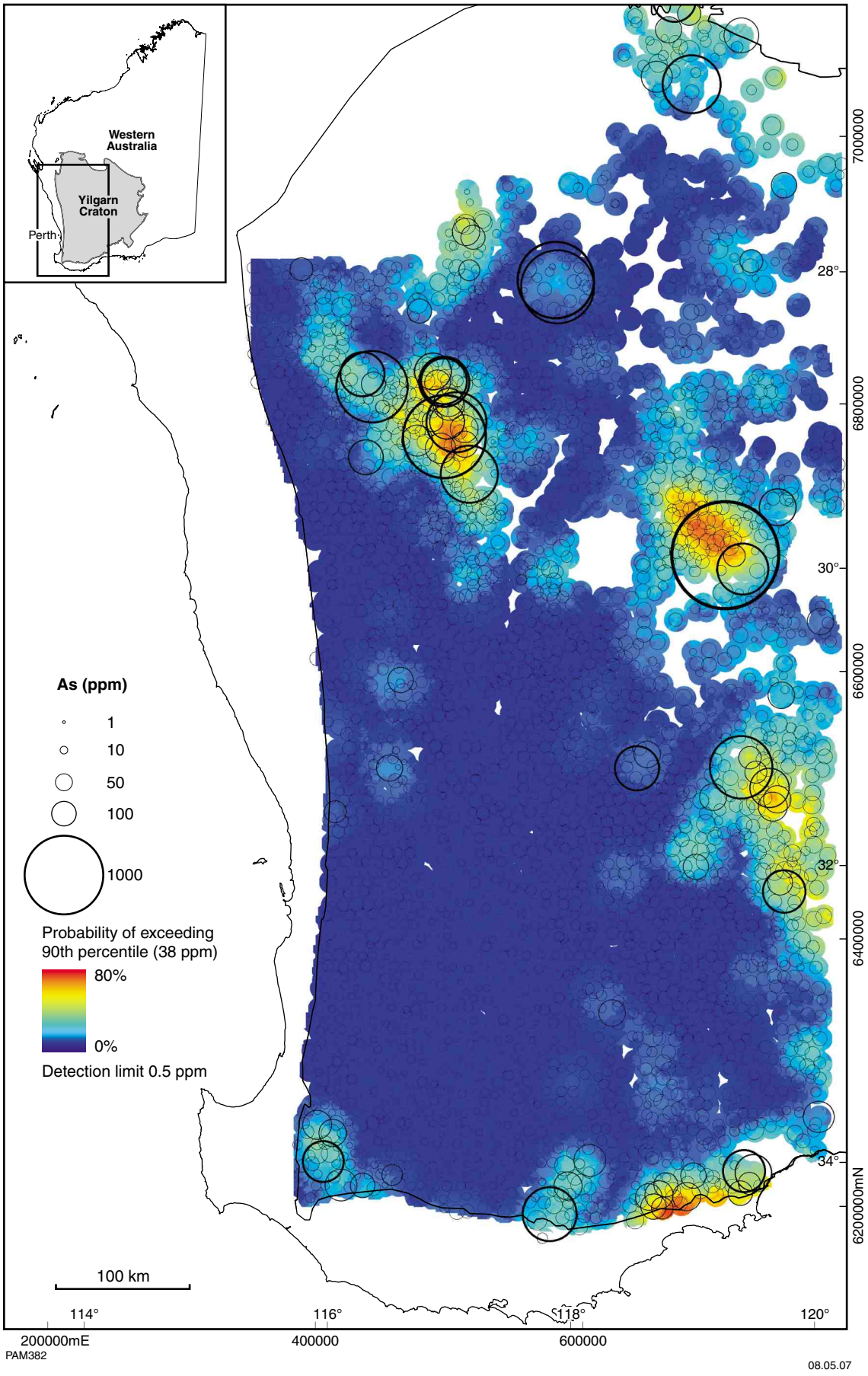

Figure 21. Kriged image and bubble plot of As abundances

of elevated Sb. One is southwest of Lake Barlee, broadly coincident with high As, and the other is a distinct trend from Yalgoo in the northwest to Mount Gibson in the southeast, and includes parts of the Gullewa greenstone belt over a distance of approximately 180 km. One sample reached 960 ppm Sb at the Brandy Hill Au mine. Again, there is similarity between this and the As trend; however, Sb abundances in greenstone sequences (90th percentile 6.6 ppm) are significantly greater than those in granitic terrains (90th percentile 1.1 ppm). Small clusters of high-Sb concentrations characterize the other Au-mining centres. In the southwest of the survey area, Sb is locally high near Bridgetown, north of the Boddington gold mine, in the Jimperding and Chittering metamorphic belts, at Wongan Hills, and along the southern margin of the Yilgarn Craton.

Tellurium

In a similar fashion to As and Sb, Te shows a craton-scale general increase from the southwest to the northeast of the western Yilgarn Craton. However, regional trends are less well defined than for As and Sb. There is a weak (0.2 – 0.4 ppm) trend southwest of Lake Barlee that coincides with high As and Sb. Elsewhere, single-point Te concentrations are scattered and show less spatial relationship with known mining centres than high As and Sb. The Te 90th percentiles for both granitic and greenstone terrains are 0.2 ppm.

CHI6* (or chalcophile) index

The CHI6* index (As+3.56Sb+10Bi+3Mo+30Ag+30Sn+10W+3.5Se), first introduced by Smith and Perdrix (1983), provides a useful summary and highlights areas with anomalous concentrations of one or many of the eight chalcophile elements that make up the index. It is a weighted sum of critical pathfinder elements (which overcomes the bias towards abundant elements that a simple sum would provide) and allows neighbouring high abundances in different elements to reinforce one another. However, as with the related PEG4* index discussed below, extreme concentrations of a single element can bias the index and caution is required with interpretation.

The most significant feature of the kriged and contoured CHI6* (Fig. 22) data is a cluster of anomalous scores in the Southern Cross greenstone belt, an area of known Au deposits. Most significant contributors to the high CHI6* scores are As and Sb, followed by Bi, Mo, Se, Sn, and W.

There are smaller, less anomalous clusters around Bridgetown–Yornup in the southwest (As, Bi, Sb, Sn and W), in the Westonia region west of Southern Cross (As, Bi, and Sb) and within and along strike of Proterozoic rocks overlying the southernmost part of the craton (As and Sb). The clusters in the southwest Yilgarn Craton broadly correlate with the 'chalcophile corridors' of Smith et al. (1989), but the present survey lacks resolution due to significantly wider sample spacing. However, the broader regional cover of this survey shows a weak concentration north of the Saddleback greenstone belt that had not been previously recognized. This geochemical signature (Sn, As, Mo, and Bi) extends into the Chittering and Jimperding metamorphic belts. Because some elements in the CHI6* index are shared with the PEG4* index (As, Sb, and Sn), the patterns here are similar.

PEG4* (or pegmatophile) index

The rare metals are of particular interest because of the world-class Sn–Ta ore body at Greenbushes in the southwest Yilgarn Craton. The PEG4* index, a sum of element abundances multiplied by empirical factors (0.09 As+1.33Sb+Sn+0.6Nb+Ta) was first introduced by Smith et al. (1987) to identify multi-element anomalies associated with the Sn–Ta pegmatite systems at Greenbushes. The index is used here to highlight regional rare-metal trends and to compare these to the earlier work mentioned above. Smith et al. (1987) showed PEG4* scores for lateritic gravel from the mineralized area at Greenbushes that reached up to 4300, with the 200 contour outlining the immediate mine area. Scores of greater than 45 delineate the broad footprint of the pegmatite system.

The data from this survey (Fig. 23) show a cluster of PEG4* scores greater than 46 (98th percentile) centred on the Bridgetown–Greenbushes area. However, there are two larger trends with similar PEG4* scores to the north, southwest, and northwest of the Saddleback greenstone belt. These trends appear to have a southeast–northwest orientation and the most significant concentration is located along strike of the Saddleback greenstone belt, with abundances of 19 ppm Sn, 6.6 ppm Ta, and 32 ppm Nb. This might indicate Sn–Ta pegmatites along strike of the Saddleback greenstone belt. Single anomalies and small clusters (groupings of 2–3 samples with PEG4* scores of greater than 33) are common throughout the southwest and might indicate less extensive swarms of pegmatite dykes.

The association of Au at the Boddington mine with As, Sb, and Sn (Anand, 1998b) suggests the pegmatophile signature northwest of Boddington might also have significance as a possible indicator of further Au mineralization along strike of the Saddleback greenstone belt, with one location (103881) showing 2.4 ppm Sb, 14 ppm As, and 40 ppm Mo.

The strength of these two additive indices is that the weighting factors and the element lists can be modified and thresholds (once established) could be subtracted (Robertson et al., 1994) to tailor them to particular commodities, ore types, or regions and this could be optimized by canonical analysis.

Potential for alkaline ultramafic rocks (kimberlite, lamproite, and lamprophyre)

The potential of the Astro Yilgarn Regolith data to show the geochemical signature of alkaline ultramafic rocks was evaluated using a typicality index (for explanation see Cornelius et al., 2005b). The results of multivariate

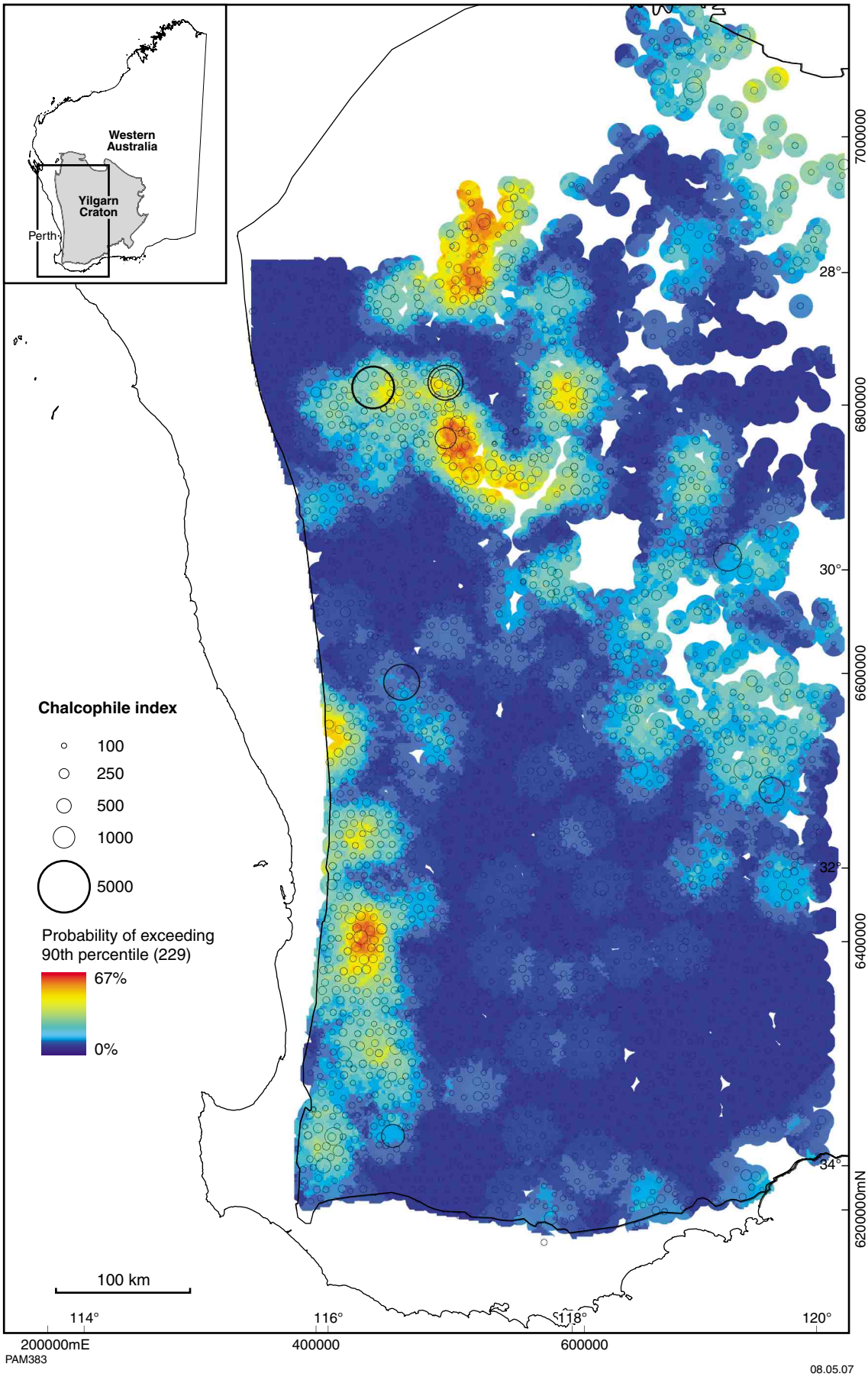

Figure 22. Kriged image and bubble plot of CHI6* scores

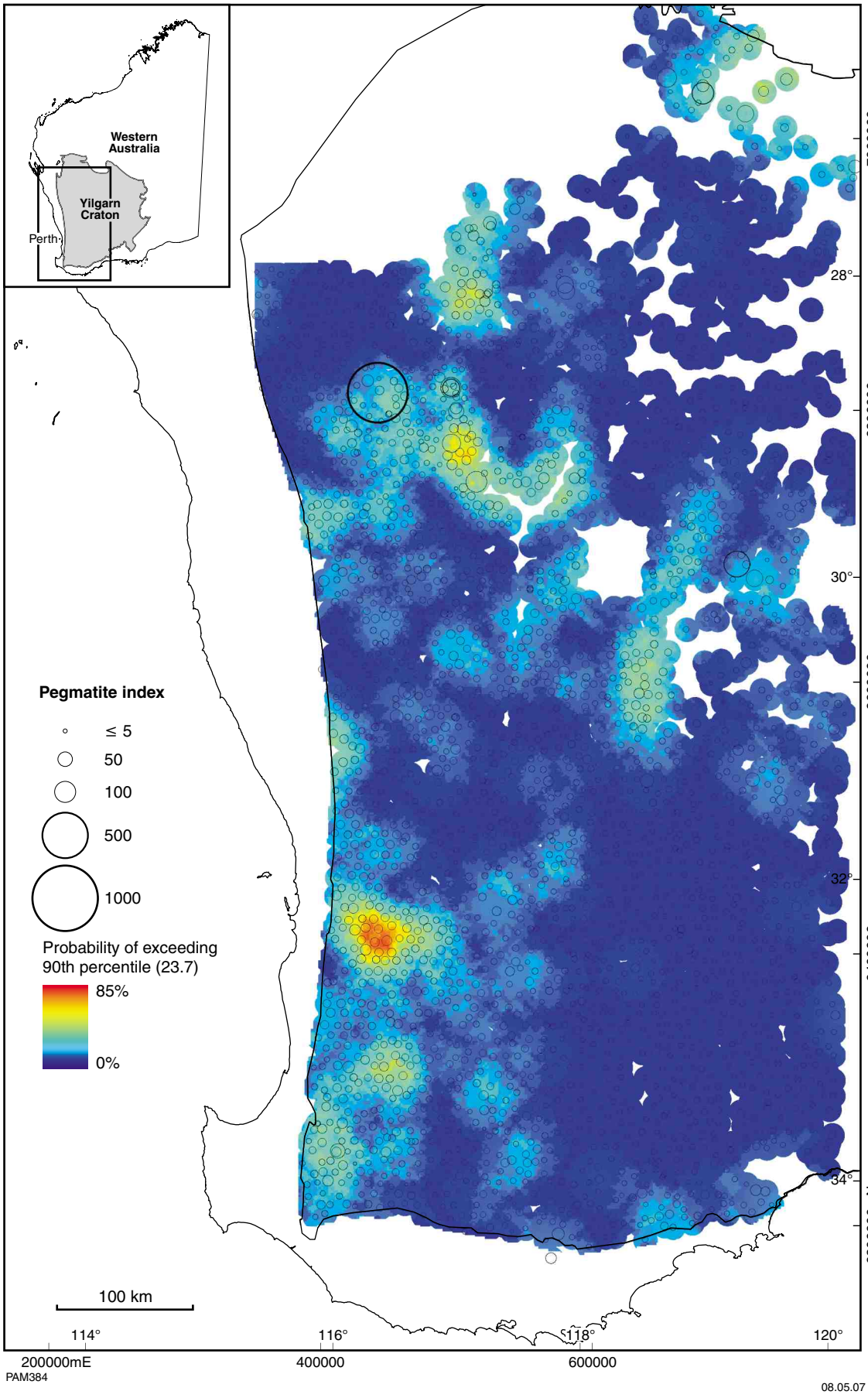

Figure 23. Kriged image and bubble plot of PEG4* scores

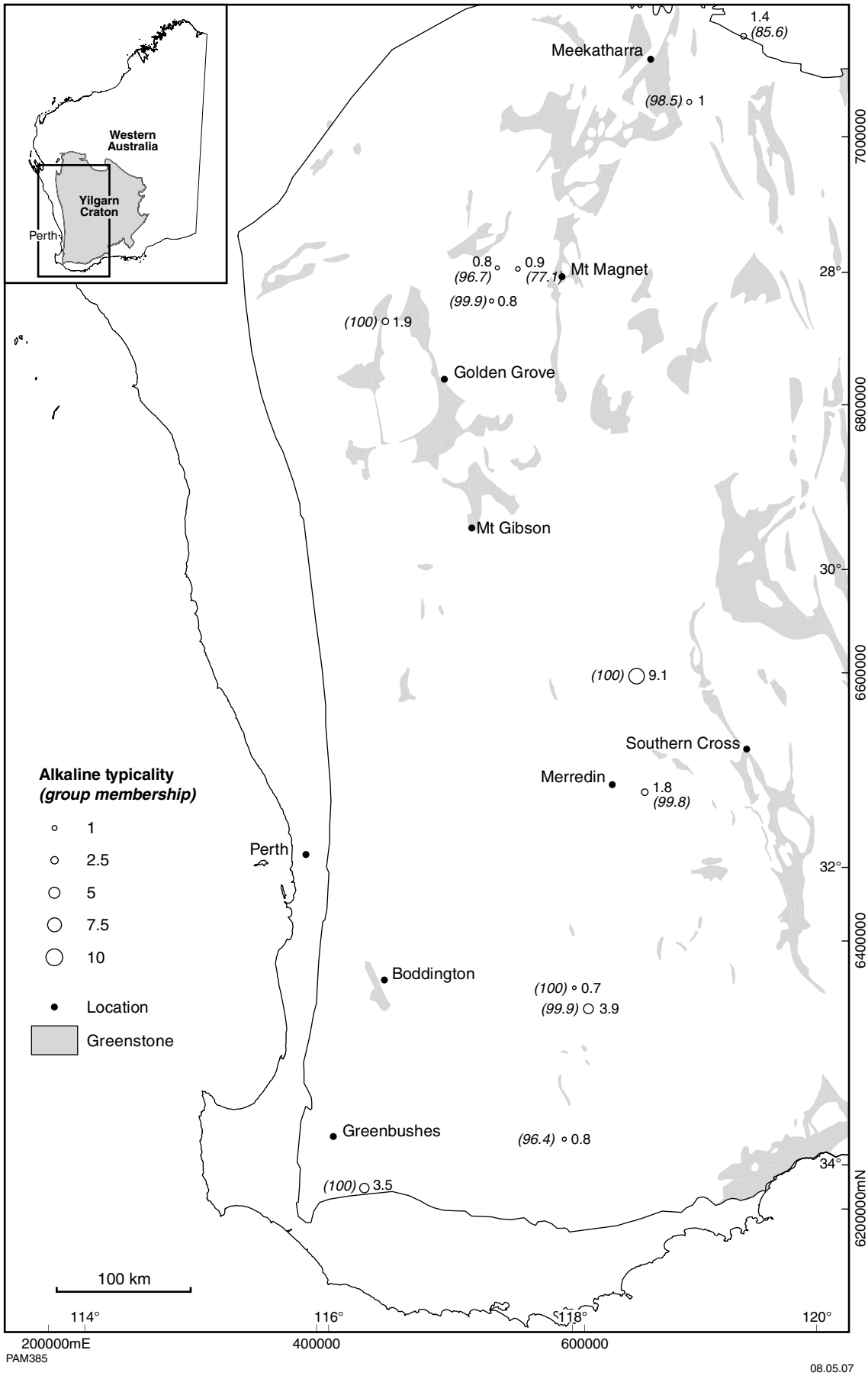

Figure 24. Map of typicality indices (in % next to sample point) based on a six-element allocation procedure for the southwest Yilgarn Craton

statistical analysis showed ferruginous gravel formed on or near small bodies of alkaline ultramafic rock at Nabberu, and near Errabiddy in the northeast Yilgarn Craton, have typicality scores of 10–30%.

Data from the samples newly acquired in this survey have been evaluated by the same multivariate statistical treatment using the same set of kimberlite target data and six elements (P, Nb, Co, Cr, La, and Sm), but a different granite-training dataset. In the southwestern Yilgarn Craton, the results (Fig. 24) show five anomalies (typicality score > 0.5%), with the highest score (9.1%) at 46 Gate Road, northeast of Mukinbudin, and a new anomaly (104123) approximately 30 km west-northwest of Lake Grace, with a typicality score of 3.9%. The anomalies occur along an approximately 350-km long north-northeast trend. With the exception of the 46 Gate Road locality, where the source of the anomaly appears to be lamprophyre as indicated by saprolite analyses, the source(s) of these low-priority anomalies remain unidentified. Another anomaly in this dataset, with a typicality score of 3.5%, is located 15 km east-northeast of Manjimup (locality 104800). The results show a small likelihood for further occurrences of alkaline ultramafic rocks in the southwest Yilgarn Craton and, based on the results of previous work, the source of the anomalous scores (>0.5%) is likely to be lamprophyre. In the northwestern Yilgarn Craton, five localities show a typicality greater than 0.5%. Locality 101225, approximately 18 km west of Yalgoo, has a score of 1.9%. Two localities 70 km east-northeast (100096) and 45 km southeast (100299) of Meekatharra have scores of 1.4 and 1% respectively. A group of three samples (100987, 100989, and 101136) approximately 50 km west of Mount Magnet show typicality scores of 0.8%, 0.9%, and 0.8% respectively. Some samples (101225 and 100299) are located in granitic terrain close to greenstone. Their scores are therefore unlikely to indicate nearby alkaline ultramafic source rocks and instead may result from mixing of greenstone and granitic signatures.

Conclusions

An evaluation of the laterite geochemical dataset for the western Yilgarn Craton reveals the following regional patterns:

- In the northeast part of the southwest Yilgarn Craton, the regional sampling shows clusters of elevated Au around greenstones and known Au occurrences. The size of these clusters appears larger than would be expected from lateral dispersion of detrital material from these occurrences alone. Therefore, there is potential for additional Au mineralization east-northeast and southeast of Merredin.
- The regional distribution of PGE shows a large number of as yet unexplained and generally untested PGE anomalies throughout the western Yilgarn, including the gneissic terrains along the western margin of the craton.
- Multivariate statistics can assist in detecting target-specific geochemical signatures in lateritic residuum in deeply weathered terrain (e.g. alkaline ultramafic rocks in the southwest Yilgarn). This has potential for kimberlite exploration and the detection of greenstone remnants and extensions covered beneath thick regolith.
- The westernmost part of the Yilgarn Craton contains elevated abundances of several elements. In the northern part, corresponding to the Jimperding metamorphic belt, south of the Wongan Hills greenstone belt, high regional-scale Cu concentrations are locally associated with anomalous As, Au, Bi, Hg, Mo, and Sb. Elevated Cr and Ni concentrations indicate the presence of mafic and ultramafic rocks within this metamorphic belt.
- A cluster of high CHI6* scores in the Bridgetown–Manjimup–Greenbushes area might be associated not only with Sn–Ta pegmatites at Greenbushes, but could also indicate massive sulfides due to anomalous As, In, and Bi.
- Northwest of the Saddleback greenstone belt, anomalous Sb, Sn, Ta, and Nb abundances might indicate pegmatites along strike of the greenstone sequence and, potentially, further Au mineralization.
- There are anomalous As, Bi, Mo, and Sb abundances in Proterozoic rocks along the southern margin of the Yilgarn Craton indicating potential for Au mineralization.
- In the Katanning–Lake Grace area, clusters of weakly anomalous Cr abundances indicate likely mafic remnants. Some of these contain anomalous Au.
- An as yet unexplained craton-scale southeast trend in Hg abundances, locally associated with anomalous Au, might indicate potential for Au mineralization at depth.

Acknowledgements

The project was financially supported by CSIRO EM, CRC LEME, GSWA, and MERIWA. CALM kindly granted access to nature reserves and other CALM-controlled land. Numerous private landowners and farmers granted access to their properties for sampling.

Ultra Trace Laboratories, Perth, provided all analytical data to exacting standards; Mr D. Ruane and Mr A. Christ provided analytical details and valuable discussions on analytical aspects. Mr A. Knowles of Gannett Holdings prepared two standards for the project.

Drs M. Pain, D. Hunter, F. Itzstein-Davy, and J. Cunneen, and Ms A. Riesz, Mrs J. Johnston and Mrs P. Foster, Ms M. Smith, Mr A. Riesz, Mr A. Hacket, and Mr C. Palmer assisted with the field sampling. Oxiana Ltd provided accommodation at their Golden Grove mine site. D. Wilkinson prepared sections of difficult regolith materials.

Drs R. E. Smith, C. R. M. Butt, R. R. Anand, S. Rogers, and D. J. Gray reviewed this report. All this support is acknowledged with appreciation.

References

ABEYSINGHE, P. B., and FLINT, D. J., in prep., Nickel and cobalt in Western Australia: commodity review for 2005: Western Australia Geological Survey, Record.

AHMAT, A. L., 1990, Windimurra Complex, *in* Geology and mineral resources of Western Australia: Western Australia Geological Survey, Memoir 3, p. 120–124.

ALLIBONE, A., WINDH, J., ETHERIDGE, M., BURTON, D., FANNING C. M., and WYSOCZANSKI, R., 1996, Structural and timing relationships of the Au–Cu mineralization at Boddington Gold Mine, Western Australia: Geological Society of Australia, 13th Australian Geological Convention, Canberra, Abstracts Series, no. 41, p. 13.

ANAND, R. R., 1994, Regolith–landform evolution and geochemical dispersion from the Boddington gold deposit, Western Australia: CSIRO Division of Exploration and Mining, Restricted Report 24R (reissued as CRC LEME, Open File Report 3).

ANAND, R. R., 1998a, Distribution, classification and evolution of ferruginous materials over greenstones on the Yilgarn Craton — implications for mineral exploration, *in* The State of the Regolith *edited by* R. A. EGGLETON: Proceedings of the Second Australian Conference on Landscape Evolution and Mineral Exploration, Conference Publications, Springwood, N.S.W., p. 175–193.

ANAND, R. R., 1998b, Regolith–landform evolution and geochemical dispersion from the Boddington gold deposit, Western Australia: CRC LEME, Open File Report, no. 3, 149p.

ANAND, R. R., 2001, Evolution, classification and use of ferruginous regolith materials in gold exploration, Yilgarn Craton, Western Australia: Geochemistry: Exploration, Environment, Analysis; v. 1, p. 221–236.

ANAND, R. R., CORNELIUS, M., and PHANG, C., in press, Use of biota and soils in mineral exploration in areas of transported cover, Yilgarn Craton, Western Australia: a contribution towards understanding mechanisms of anomaly formation: Geochemistry: Exploration, Environment, Analysis.

ANAND, R. R., and PAINE, M., 2002, Regolith geology of the Yilgarn Craton, Western Australia: implications for exploration: Australian Journal of Earth Sciences, v. 49, p. 3–162.

ANAND, R. R., PAINE, M. D., and SMITH, R. E., 2002, Genesis, classification and atlas of ferruginous materials, Yilgarn Craton: CRC LEME, Open File Report 73.

ANAND, R. R., SMITH, R. E., PHANG, C., WILDMAN, J. E., ROBERTSON, I. D. M., and MUNDAY, T. J., 1993, Geochemical exploration in complex lateritic environments of the Yilgarn Craton, Western Australia: CSIRO Division of Exploration and Mining, Restricted Report 442R (reissued as CRC LEME, Open File Report 58, 1998).

AUSTRALIAN NATIVE VEGETATION ASSESSMENT, 2001, Australian National Resources Atlas, National Land and Water Resources Audit: Land and Water Australia, Canberra, http://audit.ea.gov.au/ANRA/.

BREWER, R., and SLEEMAN, J. R., 1988. Soil structure and fabric: Adelaide, CSIRO, Division of Soils, 172p.

BUTT, C. R. M., 2005. Vegetation communities, *in* Regolith expression of Australian ore systems *edited by* C. R. M. BUTT, I. D. M. ROBERTSON, K. M. SCOTT, and M. CORNELIUS: Perth, CRC LEME, p. 49–51.

BUTT, C. R .M., MANN, A. W., and HORWITZ, R. C., 1984, Regional setting, distribution and genesis of surficial uranium deposits; calcretes and associated sediments in Western Australia, *in* Surficial uranium deposits: Vienna, International Atomic Energy Agency, IAEA-TECDOC-322, p. 165–170.

CAMERON, E., 1984, The Yeelerie calcrete uranium deposit, Western Australia: calcretes and associated sediments in Western Australia, *in* Surficial uranium deposits: Vienna, International Atomic Energy Agency, IAEA-TECDOC-322, p. 157–164.

CARTER, J. D., and LIPPLE, S. L., 1982, Moora, W.A.: Western Australia Geological Survey, 1:250 000 Geological Series Explanatory Notes.

CASSIDY, K. F., CHAMPION, D. C., and HUSTON, D. L., 2005, Crustal evolution constraints on the metallogeny of the Yilgarn Craton, *in* Mineral deposit research: meeting the global challenge *edited by* J. MAO and F. BIERELIN: Eighth Biennial SGA Meeting, Beijing, China, 2005, Proceedings: Berlin, Heidelberg, Springer, p. 901–904.

CASSIDY, K. F., CHAMPION, D. C., KRAPEZ, B., BARLEY, M. E., BROWN, S. J. A., BLEWETT, R. S., GROENEWALD, P. B., and TYLER, I. M., 2006, A revised geological framework for the Yilgarn Craton, Western Australia: Western Australia Geological Survey, Record 2006/8, 8p.

CASSIDY, K. F., CHAMPION, D. C., McNAUGHTON, N. J., FLETCHER, I. R., WHITAKER, A. J., BASTRAKOVA, I. V., and BUDD, A. R., 2002, Characterization and metallogenic significance of Archean granitoids of the Yilgarn Craton, Western Australia: Amira International Limited, AMIRA Project no. P482/MERIWA Project M281 (unpublished report).

CHEN, S. F., and WYCHE, S., 2003, Geology of the Bungalbin 1:100 000 sheet: Western Australia Geological Survey, 1:100 000 Geological Series Explanatory Notes, 27p.

CORNELIUS, A. J., CORNELIUS, M., SMITH, R. E., SINGH, B., and SHU, L., 2005a, Laterite geochemical database for the Central Yilgarn Craton, Western Australia: CRC LEME, Open File Report 188.

CORNELIUS, M., MORRIS, P. A., and CORNELIUS, A. J., 2006, Laterite geochemical database for the Southwest Yilgarn Craton, Western Australia: CRC LEME, Open File Report 201.

CORNELIUS, M., SINGH, B., MEYER, S., SMITH, R. E., and CORNELIUS, A. J., 2005b, Laterite geochemistry applied to diamond exploration in the Yilgarn Craton, Western Australia: Geochemistry: Exploration, Environment, Analysis, v. 5, p. 1–20.

CORNELIUS, M., SMITH, R. E., and COX, A., 2001, Laterite geochemistry for regional exploration surveys — a review and sampling strategies: Geochemistry, Exploration, Environment, Analysis, v. 1, p. 211–220.

CORNELIUS, M., STUMPFL, E. F., GEE, R. D., and PROCHASKA, W., 1987, Platinum group elements in mafic–ultramafic rocks of the Western Gneiss Terrain, Western Australia: Mineralogy and Petrology, v. 36, p. 247–265.

FLINT, D. J., and ABEYSINGHE, P. B., 2006, Overview of mineral exploration in Western Australia for 2005–06: Western Australia Geological Survey, Annual Review 2005–06, p. 7–20.

FLINT, D. J., ABEYSINGHE, P. B., GAO MAI, PAGEL, J., TOWNSEND, D. B., VANDERHOR, F., and JOCKEL, F., 2000, Geology and mineral resources of the Mid West Region: Western Australia Geological Survey, Record 2000/14, 142p.

FREEMAN, M. J., and DONALDSON, M. J., 2004, Major mineral deposits of southwestern Western Australia — a field guide. Western Australia Geological Survey, Record 2004/17, 38p.

FRENCH, R. R., and ALLEN, J. H., 1984, Lake Way uranium deposit, Wiluna, Western Australia; calcretes and associated sediments in

Western Australia, *in* Surficial uranium deposits: Vienna, International Atomic Energy Agency, IAEA-TECDOC-322, p. 149–156.

GEOLOGICAL SURVEY OF WESTERN AUSTRALIA, 1998, Laterite geochemistry of the Yilgarn Craton and Albany–Fraser Orogen: digital data from CSIRO–AGE: Western Australia Geological Survey, Record 1998/8, 13p.

GEOLOGICAL SURVEY OF WESTERN AUSTRALIA, 2005, Compilation of geochronology data, June 2005 update: Western Australia Geological Survey.

HALL, G. E. M., 1999, 'Near-total' acid digestions: Explore, v. 104, p. 15–18.

HARRISON, P. H., 1984, The mineral potential of layered igneous complexes within the Western Gneiss Terrain: Western Australia Geological Survey, Report 19, Professional Papers for 1984, p. 37–54.

HASSAN, L. Y., 1998, Mineral occurrences and exploration potential of southwest Western Australia: Western Australia Geological Survey, Report 65, 38p.

LEA, A. M., 1925, Notes on some calcareous insect puparia: Records of the South Australian Museum, 3 p. 35–36.

LIPPLE, S. L., 1982, Geology of the Wongan Hills: Western Australia Geological Survey, Record 1982/4.

MAHIZHNAN, A., 2004, Red-brown hardpan: distribution, origin and exploration implications for gold in the Yilgarn Craton of Western Australia: Perth, Curtin University of Technology, PhD thesis (unpublished).

MYERS, J. S., 1993, Precambrian history of the Western Australian craton and adjacent orogens: Annual Review of Earth and Planetary Sciences, v. 21, p. 453–485.

MYERS, J. S., and HOCKING, R. M. (compilers), 1998, Simplified geological map of Western Australia 1:2 500 000 (13th edition): Western Australia Geological Survey.

NEMCHIN, A. A., and PIDGEON, R. T., 1997, Evolution of the Darling Range Batholith, Yilgarn Craton, Western Australia: a SHRIMP zircon study: Journal of Petrology, v. 38, p. 625–649.

NEUENDORF, K. K. E., MEHL, J. P. Jr., and JACKSON, J. A., 2005, Glossary of Geology (5th edition): American Geological Institute, 779p.

PERRING, C. S., BARNES, S. J., and HILL, R. E. T., 1996, Geochemistry of komatiites from Forrestania, Southern Cross province, Western Australia: evidence for crustal contamination: Lithos, v. 37, p. 181–197.

PIDGEON, R. T., and HALLBERG, J. A., 2000, Age relationships in supracrustal sequences in the northern part of the Murchison Terrane, Archean Yilgarn Craton, Western Australia: a combined field and zircon U–Pb study: Australian Journal of Earth Sciences, v. 47, p. 153–165.

PIDGEON, R. T., and WILDE, S. A., 1985, Geochronology of granite and granite greenstone terrain — three years progress report to ARGS: Western Australian Institute of Technology, Department of Geology and Geophysics.

PIDGEON, R. T., and WILDE, S. A., 1986, Geochronology of the Wongan Hills greenstone belt, Western Gneiss Terrain, Yilgarn Block, Western Australia, *in* Earth Resources in Time and Space *edited by* D. I. GROVES et al.: Geological Society of Australia, 8th Australian Geological Convention, Adelaide, S.A., 1986, Abstracts Series, no. 15, p. 155–156.

RIGANTI, A., and CHEN, S. F., 2002, Geology of the Jackson 1:100 000 sheet: Western Australia Geological Survey, 1:100 000 Geological Series Explanatory Notes, 51p.

ROBERTSON, I. D. M., DYSON, M., HUDSON, E. G., CRABB, J. F., WILLING, M. J., and HART, M. K. W., 1996, A case-hardened, low contamination ring mill for multi-element geochemistry: Journal of Geochemical Exploration, v. 57, p. 153–158.

ROBERTSON, I. D. M., KING, J. D., ANAND, R. R., and BUTT, C. R. M., 1994, Regolith geology and geochemistry Mt Magnet District — Geochemical orientation studies, Stellar and Quasar deposits: CSIRO Exploration and Mining, Confidential Report 48C, 207p. (reissued as CRC LEME, Open File Report 92, 2001).

RUDDOCK, I., 1990, Narndee Complex, *in* Geology and mineral resources of Western Australia: Western Australia Geological Survey, Memoir 3, p. 124–126.

SHU, L., SINGH, B., and CORNELIUS, M., 1998, Regolith development and landscape evolution in the Merredin region, Western Australia: CRC LEME Restricted Report 93R / CSIRO Exploration and Mining Report 548R (reissued as CRC LEME, Open File Report 169, 2004).

SMITH, R. E., ANAND, R. R., CHURCHWARD, H. M., ROBERTSON, I. D. M., GRUNSKY, E. C., GRAY, D. J., WILDMAN, J. E., and PERDRIX, J. L., 1992, Laterite geochemistry for detecting concealed mineral deposits, Yilgarn Craton, Western Australia – Summary Report: CSIRO Division of Exploration Geoscience, Restricted Report 236R (reissued as CRC LEME, Open File Report 50, 1998).

SMITH, R. E., BIRRELL, R. D., and BRIGDEN, J. F., 1989, The implications to exploration of chalcophile corridors in the Archean Yilgarn Block, Western Australia, as revealed by laterite geochemistry: Journal of Geochemical Exploration, v. 32, p. 169–184.

SMITH, R. E., and PERDRIX, J. L., 1983. Pisolitic laterite geochemistry in the Golden Grove massive sulfide district, Western Australia: Journal of Geochemical Exploration, v. 18, p. 131–164.

SMITH, R. E., PERDRIX, J. L., and DAVIS, J. M., 1987, Dispersion into pisolitic laterite from the Greenbushes mineralized Sn–Ta pegmatite system, Western Australia, *in* Geochemical exploration 1985, Part I *edited by* R. G. GARRETT: Journal of Geochemical Exploration, v. 28, p. 251–265.

SYMONS, P. M., ANDERSON, G., BEARD, T. J., HAMILTON, L. M., REYNOLDS, G. D., ROBINSON, J. M., STALEY, R. W., and THOMPSON, C. M., 1990, Boddington gold deposit, *in* Geology of the mineral deposits of Australia and Papua New Guinea *edited by* F. E. HUGHES: Melbourne, The Australian Institute of Mining and Metallurgy, p. 165–169.

TAPLEY, I. J., and GOZZARD, J. R., 1992, Aerial photographic interpretation and Landsat Thematic Mapper image processing techniques for regolith–landform mapping: CSIRO Exploration Geoscience, Restricted Report 239R.

TILLEY, D. B., BARROWS, T. T., and ZIMMERMAN, E. C., 1997, Bauxitic insect pupal cases from northern Australia: Alcheringa, v. 21, p. 157–160.

TYLER, I. M., and HOCKING, R. M., 2001, A revision of the tectonic units of Western Australia. Western Australia Geological Survey, Annual Review 2000–01, p. 33–34.

WATKINS, K. P., 1990, Murchison Province, *in* Geology and mineral resources of Western Australia: Western Australia Geological Survey, Memoir 3, p. 32–60.

WATKINS, K. P., and HICKMAN, A. H., 1990, Geological evolution and mineralization of the Murchison Province, Western Australia: Western Australia Geological Survey, Bulletin 137, 267p.

WILDE, S. A., MIDDLETON, M. F., and EVANS, B. J., 1996, Terrane accretion in the southwestern Yilgarn Craton: evidence from a deep seismic crustal profile: Precambrian Research, v. 78, p. 179–196.

WYCHE, S., CHEN, S. F., GREENFIELD, J. E., and RIGANTI, A., 2001, Geology of the Johnston Range 1:100 000 sheet: Western Australia Geological Survey, 1:100 000 Geological Series Explanatory Notes, 31p.

WYCHE, S., NELSON, D. R., and RIGANTI, A., 2004, 4530–3130 Ma detrital zircons in the Southern Cross Granite–Greenstone Terrane, Western Australia: implications for the early evolution of the Yilgarn Craton: Australian Journal of Earth Sciences, v. 51, p. 31–45.

CORNELIUS et al.

Laterite geochemical database for the western Yilgarn Craton, Western Australia

RECORD 2007/9

This Record is published in digital format (PDF)and is available online at: www.doir.wa.gov.au/GSWA/publications. Laser-printed copies can be ordered from the Information Centre for the cost of printing and binding.

Further details of geological publications and maps produced by the Geological Survey of Western Australia can be obtained by contacting:

Information Centre
Department of Industry and Resources
100 Plain Street
East Perth WA 6004
Phone: (08) 9222 3459 Fax: (08) 9222 3444

www.doir.wa.gov.au/GSWA/publications

	All analyses												Granitic bedrock												Greenstone bedrock											
	Number of analyses	Minimum value	Maximum value	5th percentile	10th percentile	25th percentile	50th percentile	75th percentile	90th percentile	95th percentile	98th percentile	99th percentile	Number of analyses	Minimum value	Maximum value	5th percentile	10th percentile	25th percentile	50th percentile	75th percentile	90th percentile	95th percentile	98th percentile	99th percentile	Number of analyses	Minimum value	Maximum value	5th percentile	10th percentile	25th percentile	50th percentile	75th percentile	90th percentile	95th percentile	98th percentile	99th percentile
SiO2	3142	1.9	85.1	12.9	18.5	33.4	46.5	54.3	60.8	64.2	68.7	71.6	2907	2.5	85.1	14.8	20.9	36.0	47.4	54.8	61.3	64.7	68.9	71.8	235	1.9	69.5	7.4	10.0	15.2	21.2	36.1	51.9	56.5	61.5	63.9
TiO2	3142	0.01	12.94	0.35	0.40	0.49	0.65	1.01	1.53	1.96	2.64	3.40	2907	0.01	12.94	0.35	0.40	0.48	0.64	0.99	1.49	1.87	2.43	3.15	235	0.09	6.72	0.31	0.41	0.55	0.83	1.32	2.28	3.13	4.72	6.10
Al2O3	3142	0.4	62.6	11.0	13.1	16.5	20.0	23.8	30.2	39.3	47.7	51.9	2907	0.4	62.6	11.5	13.6	16.7	20.2	24.0	30.7	39.7	48.2	51.9	235	1.9	53.6	7.9	9.3	13.2	16.7	21.5	25.3	29.2	37.2	41.9
Fe2O3	3142	2.4	92.7	9.4	11.5	15.5	21.0	32.1	45.8	55.4	63.8	69.8	2907	2.4	84.2	9.2	11.2	15.2	20.2	29.5	40.8	48.3	58.9	65.2	235	10.0	92.7	16.4	19.7	34.2	48.0	58.2	66.5	71.3	75.0	79.3
MnO	3142	0.005	3.800	0.005	0.005	0.005	0.005	0.020	0.030	0.050	0.120	0.240	2907	0.005	3.800	0.005	0.005	0.005	0.005	0.020	0.030	0.040	0.090	0.230	235	0.005	0.540	0.005	0.005	0.005	0.020	0.040	0.080	0.113	0.192	0.343
MgO	3142	0.005	1.850	0.020	0.030	0.040	0.060	0.090	0.120	0.150	0.190	0.236	2907	0.005	1.850	0.020	0.030	0.040	0.060	0.090	0.120	0.150	0.180	0.220	235	0.005	0.810	0.010	0.020	0.040	0.060	0.095	0.130	0.180	0.266	0.353
CaO	3142	0.005	2.480	0.005	0.005	0.020	0.020	0.040	0.060	0.080	0.132	0.220	2907	0.005	2.480	0.005	0.005	0.010	0.020	0.040	0.060	0.080	0.120	0.209	235	0.005	1.200	0.005	0.010	0.020	0.030	0.050	0.080	0.123	0.260	0.310
Na2O	3142	0.005	1.260	0.005	0.005	0.005	0.020	0.040	0.090	0.160	0.270	0.340	2907	0.005	1.260	0.005	0.005	0.005	0.020	0.040	0.090	0.160	0.270	0.359	235	0.005	0.550	0.005	0.005	0.005	0.005	0.030	0.060	0.090	0.170	0.210
K2O	3142	0.005	5.550	0.010	0.020	0.030	0.060	0.130	0.340	0.560	1.185	2.142	2907	0.005	5.550	0.010	0.020	0.030	0.060	0.140	0.350	0.580	1.256	2.218	235	0.005	1.270	0.005	0.005	0.010	0.020	0.050	0.172	0.319	0.429	0.596
P2O5	3142	0.004	0.511	0.012	0.014	0.019	0.027	0.039	0.055	0.069	0.094	0.120	2907	0.004	0.511	0.012	0.014	0.018	0.026	0.038	0.052	0.066	0.091	0.112	235	0.007	0.456	0.011	0.016	0.023	0.038	0.053	0.074	0.094	0.137	0.171
Ag	3142	0.25	1.00	0.25	0.25	0.25	0.25	0.25	0.25	0.25	0.25	0.50	2907	0.25	1.00	0.25	0.25	0.25	0.25	0.25	0.25	0.25	0.25	0.25	235	0.25	1.00	0.25	0.25	0.25	0.25	0.25	0.25	0.50	1.00	1.00
As	3142	2	1910	8	9	14	20	29	38	49	96	157	2907	2	972	8	10	14	20	29	36	43	60	105	235	2	1910	7	8	13	23	52	119	225	560	777
Au	3142	0.1	1460.0	0.1	0.1	0.1	0.2	0.6	1.0	1.6	6.0	20.7	2907	0.1	1460.0	0.1	0.1	0.1	0.2	0.4	0.8	1.2	2.2	4.2	235	0.1	703.0	0.1	0.1	0.2	0.8	2.6	10.6	36.4	82.6	187.5
Au Rept1	221	0.1	1450.0	0.1	0.1	0.4	0.8	3.6	30.0	65.8	284.8	638.4	166	0.1	1450.0	0.1	0.1	0.2	0.4	1.4	11.3	32.9	307.4	961.2	55	0.1	352.0	0.7	1.0	1.6	6.6	29.4	64.4	147.9	181.3	261.3
Au Rept2	235	0.1	329.0	0.1	0.1	0.4	1.0	2.6	14.1	32.8	62.1	88.0	183	0.1	97.4	0.1	0.1	0.4	0.8	1.4	4.2	12.1	30.6	57.3	52	0.1	329.0	0.5	0.8	1.4	5.2	19.4	46.7	63.0	98.4	211.7
Ba	3142	4.5	11000	10	20	30	40	100	350	759	1689	2546	2907	4.5	11000	10	20	30	40	100	360	767	1780	2717	235	5	1500	5	20	20	50	120	318	601	963	1223
Be	3142	0.05	10	0.3	0.4	0.6	0.8	1.1	1.6	1.9	2.4	2.9	2907	0.05	10	0.3	0.4	0.6	0.8	1.2	1.6	1.9	2.5	2.9	235	0.05	10	0.3	0.4	0.4	0.7	1.0	1.4	1.7	2.1	2.4
Bi	3142	0.05	87	0.1	0.1	0.2	0.3	0.5	0.9	1.4	2.5	4.3	2907	0.05	79	0.1	0.1	0.2	0.3	0.5	0.9	1.3	2.4	3.9	235	0.05	87	0.1	0.1	0.2	0.4	0.7	1.3	2.7	6.4	12.2
Cd	3142	0.025	1	0.03	0.03	0.03	0.03	0.03	0.03	0.03	0.03	0.08	2907	0.025	1	0.03	0.03	0.03	0.03	0.03	0.03	0.03	0.03	0.05	235	0.025	0	0.03	0.03	0.03	0.03	0.03	0.03	0.03	0.10	0.10
Ce	3142	2.25	2640	6	8	14	26	48	86	127	184	281	2907	2.3	2640	6	9	15	27	50	89	129	193	286	235	2.25	236	4	5	7	13	21	31	42	68	148
Cl	3142	10	2660	10	40	60	80	140	220	320	480	692	2907	10	2660	10	20	60	80	140	220	340	480	720	235	10	520	10	40	40	80	120	200	280	366	413
Co	3142	0.5	259	2	2	3	5	7	11	16	29	52	2907	0.5	259	2	2	3	5	7	10	13	22	36	235	1	147	3	4	6	9	18	30	54	74	105
Cr	3142	5	22200	90	120	170	250	390	680	1050	2874	6554	2907	5	22200	90	110	160	240	360	550	727	1138	1827	235	40	19000	160	238	405	850	2090	6410	8520	9828	13216
Cs	3142	0.05	23	0.1	0.1	0.2	0.4	0.7	1.1	1.4	1.9	2.4	2907	0.05	23	0.1	0.1	0.2	0.4	0.7	1.1	1.4	2.0	2.5	235	0.05	3	0.1	0.1	0.1	0.2	0.4	0.8	1.0	1.5	1.9
Cu	3142	1	2080	3	4	6	10	22	51	93	148	250	2907	1	2080	3	3	6	10	18	38	64	111	150	235	2	1430	8	11	26	57	112	180	269	336	569
Eu	3142	0.02	5	0.08	0.08	0.12	0.20	0.32	0.48	0.66	0.96	1.23	2907	0.02	5	0.08	0.08	0.12	0.18	0.32	0.48	0.66	0.96	1.24	235	0.04	2	0.10	0.12	0.16	0.24	0.39	0.53	0.68	0.85	0.97
Ga	3142	1.6	307	21	25	34	44	55	68	79	95	105	2907	1.6	307	22	26	34	45	55	68	80	95	106	235	3.2	117	14	19	29	37	50	66	73	88	102
Hg	3142	5	860	5.0	5.0	5.0	10.0	30.0	70.0	100.0	161.8	235.9	2907	5	820	5.0	5.0	5.0	10.0	30.0	70.0	100.0	170.0	240.0	235	5	860	5.0	5.0	5.0	10.0	20.0	40.0	70.0	100.0	133.2
In	3142	0.01	14	0.1	0.1	0.1	0.1	0.2	0.2	0.3	0.3	0.4	2907	0.01	13	0.1	0.1	0.1	0.1	0.2	0.2	0.3	0.3	0.4	235	0.04	14	0.1	0.1	0.1	0.2	0.2	0.3	0.3	0.4	0.5
La	3142	0.75	121	1.8	2.2	3.4	5.7	9.6	15.9	22.8	38.9	52.0	2907	0.75	121	1.8	2.3	3.6	5.9	9.9	16.2	23.8	41.1	53.6	235	0.8	27	1.5	1.7	2.4	3.7	5.5	9.7	13.3	17.0	17.5
Lu	3142	0.01	1	0.02	0.04	0.04	0.06	0.10	0.14	0.18	0.24	0.32	2907	0.01	1	0.02	0.04	0.04	0.06	0.10	0.14	0.18	0.24	0.30	235	0.01	0	0.04	0.04	0.06	0.08	0.14	0.20	0.24	0.33	0.36
Mo	3142	0.4	78	2.0	2.6	3.8	5.0	6.6	8.4	10.6	14.0	18.6	2907	0.6	78	2.4	3.0	3.8	5.0	6.6	8.6	10.6	14.2	18.6	235	0.4	35	0.8	1.0	1.6	2.8	4.5	6.9	8.0	11.7	14.5
Nb	3142	0.5	221	5	7	9	13	18	25	30	37	45	2907	0.5	221	6	7	10	13	19	25	30	37	46	235	0.5	42	2	3	5	8	11	16	20	24	33
Ni	3142	1	2150	11	14	20	29	42	62	87	159	300	2907	1	2150	11	14	19	28	40	55	70	97	134	235	6	2130	21	25	38	60	125	303	493	956	1302
Pb	3142	2	367	16	20	28	37	49	66	79	101	127	2907	2	367	18	22	29	38	50	67	80	102	129	235	5	148	9	12	17	26	39	51	58	69	78
Rb	3142	0.1	329	1	2	3	5	10	19	30	56	101	2907	0.1	329	1	2	3	6	11	20	31	63	107	235	0.1	54	1	1	1	2	4	10	14	25	33
S	3142	5	3570	100	140	210	320	450	620	750	940	1102	2907	5	3570	100	140	210	310	440	600	727	928	1119	235	50	1130	120	180	275	400	570	780	880	1006	1043
Sb	3142	0.05	960	0.2	0.2	0.3	0.6	0.9	1.2	1.6	3.5	7.0	2907	0.05	36	0.1	0.2	0.3	0.6	0.8	1.1	1.3	1.7	2.6	235	0.05	960	0.3	0.4	0.6	1.1	2.6	6.6	10.6	48.5	71.4
Sc	3142	1	476	6	7	11	17	26	49	71	97	120	2907	1	476	5	7	10	16	24	39	55	75	89	235	5	296	13	16	26	53	82	114	140	172	234
Se	3142	0.5	12	0.5	0.5	0.5	2.0	4.0	5.0	6.0	7.0	8.0	2907	0.5	12	0.5	0.5	0.5	2.0	4.0	5.0	6.0	7.0	8.0	235	0.5	8	0.5	0.5	0.5	2.0	3.0	5.0	5.0	6.0	7.0
Sm	3142	0.15	18	0.4	0.4	0.6	1.0	1.6	2.4	3.3	4.9	6.5	2907	0.15	18	0.4	0.4	0.6	1.0	1.6	2.5	3.4	5.1	6.7	235	0.15	5	0.4	0.5	0.7	1.0	1.4	2.1	2.6	3.0	3.2
Sn_MAD	3142	0.5	88	0.5	1.0	2.0	2.0	3.0	4.0	5.0	6.0	8.0	2907	0.5	67	0.5	1.0	2.0	2.0	3.0	4.0	5.0	6.0	7.9	235	0.5	88	0.5	0.5	1.0	2.0	2.0	3.0	4.0	8.0	10.0
Sn_FUS	3142	5	130	5.0	5.0	5.0	5.0	5.0	5.0	5.0	5.0	10.0	2907	5	130	5.0	5.0	5.0	5.0	5.0	5.0	5.0	5.0	10.0	235	5	110	5.0	5.0	5.0	5.0	5.0	5.0	5.0	6.6	10.0
Sr	3142	0.9	349	2	3	4	6	10	18	26	45	64	2907	0.9	349	2	3	4	6	10	18	26	46	64	235	1.1	114	2	2	3	4	8	16	26	38	46
Ta_MAD	3142	0.025	21	0.3	0.4	0.6	0.8	1.1	1.6	2.0	2.8	3.5	2907	0.025	21	0.4	0.4	0.6	0.8	1.2	1.7	2.1	2.8	3.5	235	0.025	4	0.2	0.2	0.3	0.5	0.8	1.1	1.4	1.8	2.2
Ta_FUS	2568	0.25	34	0.3	0.3	0.5	1.0	1.5	2.0	2.5	3.5	5.0	2380	0.25	34	0.3	0.5	0.5	1.0	1.5	2.0	2.5	3.5	5.0	188	0.25	7	0.3	0.3	0.3	0.5	1.0	1.5	2.0	3.0	3.5
Te	3142	0.1	2	0.1	0.1	0.1	0.1	0.1	0.2	0.2	0.4	0.4	2907	0.1	2	0.1	0.1	0.1	0.1	0.1	0.2	0.2	0.4	0.4	235	0.1	1	0.1	0.1	0.1	0.1	0.1	0.2	0.4	0.4	0.6
Th	3142	0.25	1010	16	23	40	75	124	189	236	318	392	2907	0.25	1010	20	27	45	79	129	194	242	325	402	235	0.5	249	6	8	13	25	42	86	106	148	184
Tl	3142	0.05	9	0.1	0.1	0.1	0.1	0.1	0.2	0.3	0.6	1.1	2907	0.05	9	0.1	0.1	0.1	0.1	0.1	0.2	0.3	0.6	1.1	235	0.05	1	0.1	0.1	0.1	0.1	0.1	0.1	0.2	0.3	0.6
Tm	3142	0.01	1	0.02	0.02	0.04	0.06	0.10	0.14	0.18	0.26	0.32	2907	0.01	1	0.01	0.02	0.04	0.06	0.10	0.14	0.18	0.26	0.32	235	0.01	0	0.02	0.04	0.06	0.08	0.14	0.18	0.23	0.29	0.37
U	3142	0.15	52	1.7	2.1	2.9	4.4	6.8	10.2	12.8	17.4	21.0	2907	0.3	52	1.8	2.2	3.1	4.6	7.0	10.4	13.0	17.7	21.5	235	0.15	21	1.1	1.2	1.9	3.0	4.2	6.2	7.5	11.9	12.4
V	3142	40	4540	160	200	280	390	570	840	1040	1320	1456	2907	40	2720	160	198	280	380	540	780	950	1170	1359	235	60	4540	210	274	455	730	1060	1370	1693	2055	2498
W	3142	2.5	135	2.5	2.5	2.5	2.5	2.5	2.5	2.5	10.0	15.0	2907	2.5	125	2.5	2.5	2.5	2.5	2.5	2.5	2.5	10.0	10.0	235	2.5	135	2.5	2.5	2.5	2.5	2.5	5.0	10.0	25.0	28.3
Y	3142	0.05	116	2.4	3.0	4.1	6.1	9.0	13.2	17.6	25.2	31.1	2907	0.05	116	2.4	3.0	4.1	6.1	9.0	13.2	17.6	25.3	30.9	235	1.3	78	2.4	3.0	4.3	6.1	9.0	13.0	17.7	23.7	30.2
Yb	3142	0.1	8	0.2	0.3	0.3	0.5	0.7	1.0	1.3	1.8	2.2	2907	0.1	8	0.2	0.3	0.3	0.5	0.7	1.0	1.3	1.8	2.1	235	0.15	3	0.3	0.3	0.4	0.6	1.0	1.3	1.7	2.1	2.4
Zn	3142	1	408	4.0	5.0	7.0	10.0	16.0	26.0	35.9	54.0	82.4	2907	1	274	4.0	5.0	7.0	10.0	15.0	24.0	32.0	46.0	59.0	235	2	408	5.7	8.0	12.0	20.0	33.5	56.2	89.6	144.3	210.5
Zr	3142	35	3790	180	215	270	335	455	605	710	891	1098	2907	35	3790	205	230	275	340	460	615	725	914	1139	235	35	830	90	117	160	225	293	391	465	587	670
Pt	452	0.1	105.0	1.1	2.0	3.4	7.0	13.5	25.0	32.4	48.0	57.5																								
Pd	452	0.1	74.5	1.0	1.2	2.0	3.5	8.1	15.5	20.0	25.5	35.0																								
Ir	451	0.1	9.8	0.1	0.1	0.1	0.2	0.5	1.5	3.0	4.5	7.3																								
Os	452	0.1	7.2	0.2	0.2	0.5	0.9	1.6	2.2	3.0	4.2	5.8																								
Rh	452	0.1	7.7	0.1	0.1	0.2	0.4	1.3	2.9	3.5	4.8	6.4																								
Ru	452	0.1	53.0	0.3	0.4	0.6	1.1	2.0	7.0	13.9	24.7	25.8																								

PETROGRAPHY - DESCRIPTIONS AND PHOTOS

	Number	Mineralogy	Reason	Description
CV	101181	Ka,qz,fs	Typical 'black balls'in colluvium	Most of the pisoliths have a cutan, though some are broken, revealing the sandy core. The cores of the pisoliths consist of close-packed angular to shardy fragments of quartz and microcline, reaching 3 mm in size. The quartz is strained and some contains minute laths of green tourmaline. There are a few variably goethite-stained clay glaebules and some hematite granules in the core. These are set in a minimum of iron-stained kaolinite matrix. The cutan (5-10%) consists of similar, but more loosely packed, angular quartz and microcline with clay glaebules, set in a brown aluminosilicate cement that is banded with brown goethite and black hematite. GRANITE-DERIVED
CV	101184		Colluvium. Depositional sandplain with weak rise. High Mn.	The pisoliths are worn, exposing the sandy cores. The cores consist of loosely packed angular, strained quartz and minor microcline and ferruginous clay glaebules, set in several generations of goethite-stained clay matrix and aluminosilicate cement. This is permeated by patches of Mn minerals, probably hollandite (small Ba content). The cutans vary in thickness (20-30%), have a similar mineralogy but the Mn minerals form discontinuous layers. GRANITE DERIVED.
CV	101238	Ka,qz,gt,ru	Colluvium. Edge of depositional plain. High Mn	The pisoliths are worn. Partly exposing the sandy cores. The cores consist of angular, strained quartz and minor microcline and some clay glaebules. These are loosely packed in a matrix of goethite-stained clay. Voids have been filled with brown, slightly banded aluminosilicate cement and Mn minerals have penetrated the matrix. The cutans are minor (<5%), partly developed and consist of fine-grained angular quartz set in goethitic clay and banded with Mn minerals. GRANITE DERIVED
LTGS	101292		Windimurra. High Fe (70%) and Cr (1000) - greenstone	The pisoliths are round but slightly chipped with a yellow-brown cutan and deep red or black cores. The cores are complex, consisting of islands of cracked and fragmented hematite, surrounded by goethite. This has been, in turn, cracked and penetrated with grains of quartz and goethitic clay. This merges with the cutans (2%) that consist of delicately banded goethite and goethitic clay. GREENSTONE DERIVED
?	101425_1	Ka,qz,gt,hm	Edge of breakaway. 'Old' pisoliths, high position	The pisoliths are round, yellow-brown and partly worn, revealing their cores. The core consists of fragments of subangular quartz and numerous clay glaebules moderately closely packed in goethite-stained clay and permeated by very thin veinlets of hematite. The very thin (<2%) discontinuous cutans consist of weakly Fe oxide-stained clay and a few very fine, angular grains of quartz. FROM A DEEPLY WEATHERED TERRAIN
LTGS	101612		Yarndee. Greenstone-derived Cr 1100 ppm	These red-brown pisoliths are quite round, with largely intact cutans. The cores consist of hematitic clay, containing fragments of fretted quartz and hematite, and a few voids lined with delicately banded goethite and hematite. The cutan is thin (<2%) and consists of goethite-stained clay with a few included chips of hematite. and possibly some stained clay glaebules. PROBABLY MAFIC

LTGS	101768		Another example from greenstone	The pisoliths are yellow-brown and smooth, with intact but cracked cutans. The core consists of small lozenges and fragments of hematite, quartz and goethite, set loosely in a porous, goethite and hematite stained clay. This has cracked and is thinly veined with hematite. The clay matrix also contains fragments of brecciated clay. The hematite of the outer part of the clay pisolith has been hydrated to goethite. The cutan is thin (2%) and consists of layers of goethite clay with a few small chips of hematite. PROBABLY MAFIC.
CV	101862		CV below breakaway 70% Fe, 3% Ti Close to 101862_1	The pisoliths are round but many are worn and vary in colour from deep red-brown to yellow-brown. The cores are complex and consist of internally banded goethite ooliths and fragments of subround to fretted quartz, loosely packed in goethitic clay. Some ooliths contain internal ooliths, indicating a complex, multi-cyclic environment. Although cutans are largely absent, there are a few remnants of adhering patches of a young generation of goethitic clay and goethite. PROBABLY MAFIC
LT	101862_1		LT above breakaway 37% Fe and 0.4% Ti Close to 101862	The pisoliths are yellow, mottled with red and round. The core consists of shardy quartz loosely packed in goethitic clay. This has been veined with a second generation of goethitic clay. One pisolith is very goethite-rich and retains a fingerprint fabric indicating degraded kaolinitic saprolite. The cutan (2%) is a delicately banded ferruginous argillan. The saprolitic pisolith has no cutan. The mixture of saprolitic and pedolithic materials suggests a mixed provenance and some transport of the lateritic residuum. PROBABLY IN PART FELSIC
CVGS	102062	Ka, gt, hm, qz	Colluvium. Slight rise. Mt Gibson	The nodules are subround to subangular, are yellow-brown, mottled with red and show little development of cutans. Two of the three pisoliths have goethitic cores with fingerprint fabrics containing books and stacks of phyllosilicates (probably kaolinite and hydromuscovite). Both are spongy and the voids in one are infilled with crystalline carbonate. One has a very thin, discontinuous cutan of ferruginous clay; the other has adhering patches of ferruginous clay. PROBABLY MAFIC.
CVGS	102062_1		Colluvium – see photos. Mt Gibson	The pisoliths are round, yellow-brown mottled with red and have slightly chipped and cracked but well-developed cutans. The pisoliths are complex, containing internal pisoliths of hematite-stained spongy clay. Many have either thin cutans, or a gradational goethite-stained rim. Many of these small pisoliths, in turn, contain clay balls and glaebules. All these are set in ferruginous spongy clay, set with small clay granules and chips of quartz. The pisoliths have a discontinuous, thin (2%) cutan of unstructured ferruginous clay. One pisolith has a core of hematite- and goethite-stained clay with a remnant fingerprint fabric after saprolitic clays. GREENSTONE DERIVED BUT OF MIXED REGOLITH PROVENANCE.
LTGR	102103		LT. Fretting seems to be restricted to those pisoliths on surface. See photos.	There are two pisolith types: i) round, yellow-brown, smooth with cutans mottled with red and ii) dark brown, rough cores lacking cutans. The cores of both types are similar and consist of moderately closely packed angular to shardy quartz and a few clay glaebules set in a matrix of hematite-stained clay. Some voids are lined with a deep brown, banded aluminosilicate cement. The pisoliths have a gradationally goethite-stained rim. The cutan, where present, is a thin (1%), layered, goethite-stained argillan. GRANITIC TERRAIN

LTGR	102270	Ka,qz,gt,hm	LT. Layer below 0.7 m in sand. Nodule with hole	The pisoliths are yellow but the cutans are thin and partly worn. The core consists of subangular to fretted strained quartz, loosely packed in hematitic clay balls and deep-brown aluminosilicate cement. The pisoliths have a graded goethite-stained rim. The cutan is a very thin, delicately banded, goethitic argillan. GRANITIC TERRAIN
LTGR	102351	Ka,qz,gt,hm	LT. Gravel pit. Nodule with hole	The pisolith are round and yellow but the cutans are thin and discontinuous, revealing the sandy core. One has a hole in its core. The cores consist of loosely packed angular to shardy quartz and numerous clay balls and glaebules set in hematitic clay. The pisoliths have gradational rims of goethite-stained clay. The cutans are thin (<2%) goethite-stained argillans. GRANITIC TERRAIN
LTGR	102651	Ka,qz,gt	LT. Strange nodules ? ferricrete. 'Old' pisoliths	The pisoliths are yellow, slightly mottled with red, round and rough. They consist almost entirely of a core of angular to shardy quartz and a small number of clay glaebules, closely packed into hematitic clay. The pisoliths have a gradational rim of goethite staining in the matrix. There are traces of adhering less stained clay and fine quartz, possibly forming a remnant of a poorly structured cutan. Quartz grains project from the margin of the pisolith. One pisolith has a hole, partly filled with fine, angular quartz and cemented by relatively clear, weakly banded aluminosilicate. GRANITIC TERRAIN.
LTGR	102690		LT. Top of hill. Nodules in sand. 'Old' pisoliths.	The pisoliths are yellow-brown to deep yellow-brown and are round but very rough. Two of the larger pisoliths lack cutans; one smaller one has a thin cutan and a gradational goethite-stained rim. The cores of all consist of coarse quartz grains (up to 4 mm) of subangular, strained quartz packed tightly with smaller, shardy quartz grains in a hematitic clay matrix. The hematite in the matrix permeates from a network of very fine hematite veinlets. Quartz grains protrude from the edges of the larger pisoliths. The cutan on the smaller pisolith is a poorly structured, weakly goethite-stained argillan with chips and small grains of quartz. GRANITE
LTGR	102784	Ka,qz,gt,hm	LT. Upper slope of low hill on granite. Nodule with hole	The pisoliths are subround and yellow, with thin, partly worn cutans. The thin section gives a longitudinal view of a nodule with a hole in the centre. The core of the nodule consists of subangular to shardy quartz grains and numerous clay balls and oolitic glaebules. Many glaebules have a felted, relatively unstained clay core and an intensely stained, concentric argillan. All these are closely packed in a hematitic clay matrix. The outer rim of the nodule is gradationally goethite stained. The central cavity is packed with sandy, angular quartz grains and unstained oolitic clay glaebules, closely packed into an almost unstained clay matrix. The nodule has an extremely thin (<1%) and weakly goethite-stained argillan with minor quartz. GRANITE
LT	102862	Ka,qz,gt,hm	LT. Much ferruginous saprolite. Nodule with hole	The pisoliths are subround and yellow, mottled with brown with partly worn cutans. The cores consist of subangular to shardy quartz and a few matted clay fragments, loosely packed in a weakly goethite-stained clay matrix. Voids in the matrix have been completely filled with a weakly banded, light brown aluminosilicate cement showing brush extinction. The pisoliths are coated with an almost continuous but thin (2%), well-structured, banded, weakly goethite stained argillan. GNEISS OR METASED

LT	104183	Ka,qz,gt,hm	LT. Mature forrest near Collie. High S, Al, Darling Range	The pisoliths are rough, subround and are deep yellow-brown. There are three rather disparate pisoliths. Their cores consist of: i) Coarse (2 mm), fretted and fine, shardy quartz and irregular patches of massive clay stained from the rim by goethite. These lie loosely in a matrix of goethite-stained clay. ii) Coarse jig-saw quartz grains (4 mm) largely in optical continuity are set in a massive clay containing books and expanded stacks of muscovite and clay after remnant mica, variably stained by goethite. iii) Coarse, fretted quartz and a few small mica balls and glaebules set in a matrix of massive, goethite-stained clay. Only the first pisolith has a poorly structured discontinuous argillan, scattered with quartz grains. The others show quartz grains protruding from their margins. COMPLEX METAMORPHIC TERRAIN WITH QUARTZ VEINS AND LENSES
LTGR	104457		LT. On granite. Rasp cutan. 'Old' pisoliths from topo high.	The pisoliths are yellow-brown and rough, with cutan remnants. The pisoliths have cores of coarse, subangular polycrystalline strained quartz, packed tightly in fine, angular to shardy quartz and a minimum of goethite-stained clay. In places, the matrix has been removed and replaced by yellow-brown, weakly banded aluminosilicate. A poorly structured cutan of clay and quartz is discontinuously developed but, where it is absent, quartz grains protrude from the pisolith margins. GRANITE
LTGR	104481	Ka,qz,gt	LT. Quartz in nodules. 'Old' pisoliths from topo high. Dumbleyung.	The pisoliths are subround and yellow brown, most with a rough surface. The cores consist of subangular to shardy quartz grains, closely packed in a ferruginous clay matrix. Cutans are discontinuous but thick (10-15%) and consist of a poorly-structured open mesh of quartz in clay that is lightly stained with goethite. The clay matrix of some of the outer parts of the pisoliths has been replaced by a deep brown, partly banded aluminosilicate cement showing brush extinction. Where the cutans are absent, grains of quartz protrude from the margins. GRANITE
LT	104610	Qz,ru,hm	LT. High alkaline. North of Fitzgerald River	The pisoliths are subround, red-brown and rough, showing a few large quartz grains, and lack cutans. The cores consist of angular to shardy quartz grains, ferruginous granules and clay fragments, packed closely in a hematite-stained clay. The ferruginous granules consist of angular quartz very loosely packed in hematite. The hematite contains some weakly developed phyllosilicates remnants. There are no cutans. COMPLEX REGOLITH PROVENANCE
LT	104661	Qz,ka,ru,fs	LT. Gravel pit. High alkaline (Mg, Ca, Na) content.	The pisoliths are yellow-brown, subround and rough, some showing protruding quartz grains and have worn cutans. The cores consist of coarse, subround and fine, angular to shardy quartz grains fairly closely packed in a matrix of goethite-stained clay and banded, brown aluminosilicate cement. The cutans are thick (>20%), discontinuous and consist of poorly structured weakly goethite-stained clay and fine angular quartz.
LT	104663	Ka, qz	LT. Gravel pit. High alkaline.	The pisoliths are yellow-brown to brown, partly worn and round. The cores of the pisoliths consist of subround to angular quartz grains that are very loosely packed in yellow, goethite-stained clay. The cutans are thick (40%) and discontinuous, consisting of round to angular quartz grains tightly packed in a yellow goethite-stained clay. The cutans show a rough, semi-concentric banding related to Fe oxide staining and possibly some opaque QAZ cement.
				ka = Kaolinite: qz = qyartz: fs = Feldspar: gt = Goethite: ru = ruitle: hm= hematite


101181
2 cm


101184
2 cm


101238
2 cm


101292
2 cm


101425_1
2 cm


101612
2 cm


101768
2 cm


101862_1
2 cm


101862
2 cm


102062_1
2 cm

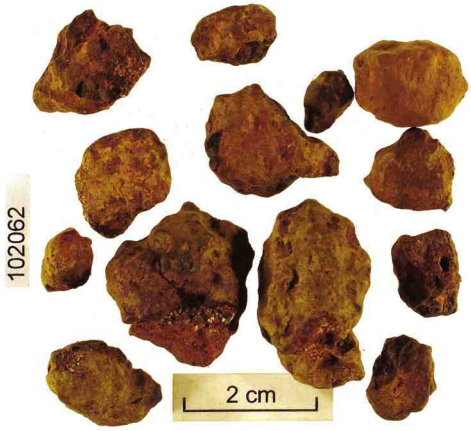
102062
2 cm


102103
2 cm


102270
2 cm


102351
2 cm


102651
2 cm


102690
2 cm


102784
2 cm


102862
2 cm


104183
2 cm

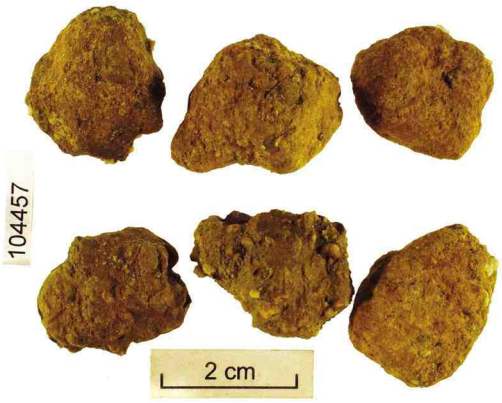
104457
2 cm


104481
2 cm


104610
2 cm


104661
2 cm


104663
2 cm

POLISHED BLOCKS


101184
10 mm


10 mm
101238


101181
10 mm

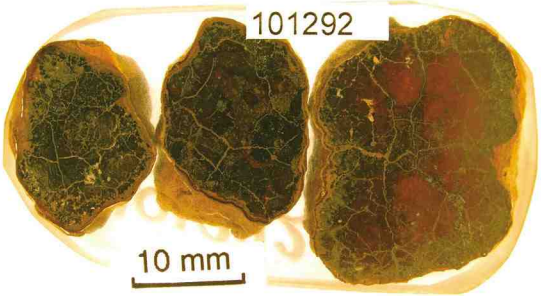
101292
10 mm

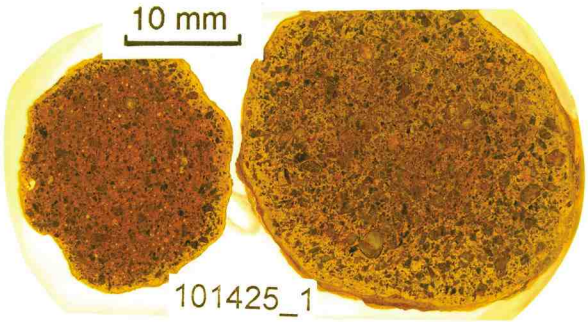
10 mm
101425_1


101612
10 mm


101768
10 mm

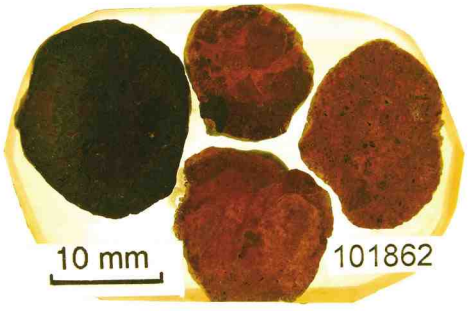
10 mm
101862

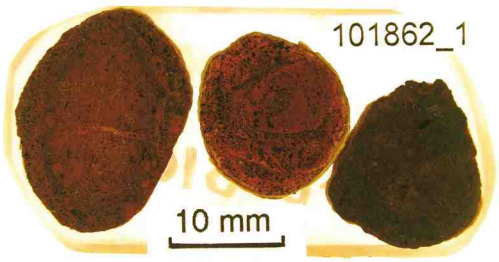
101862_1
10 mm


102062
10 mm


102062_1
10 mm


102103
10 mm

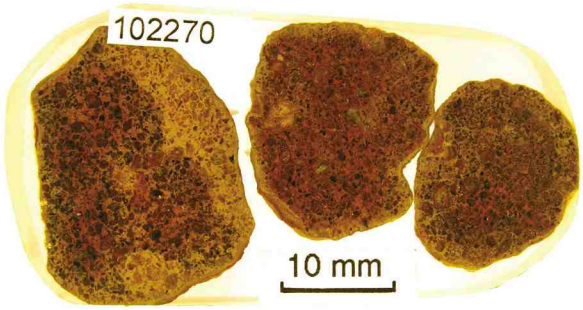
102270
10 mm


102351
10 mm


10 mm
102651


102690
10 mm

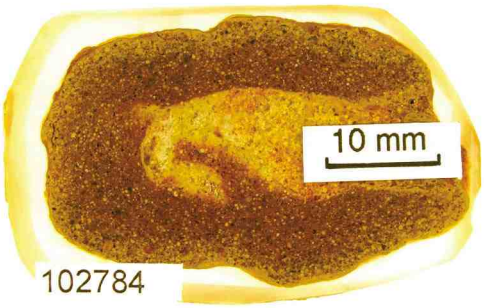
10 mm
102784


10 mm
102862


10 mm
104183

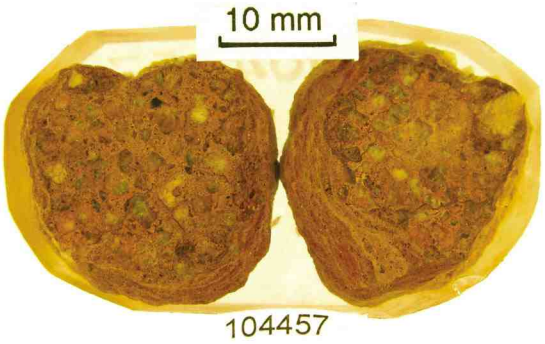
10 mm
104457


104481
10 mm


10 mm
104610


104661
10 mm


10 mm
104663

Thin and Polished Sections

Abbreviations:
txppl = Transmitted plain polarized light
nrf = Normally reflected light

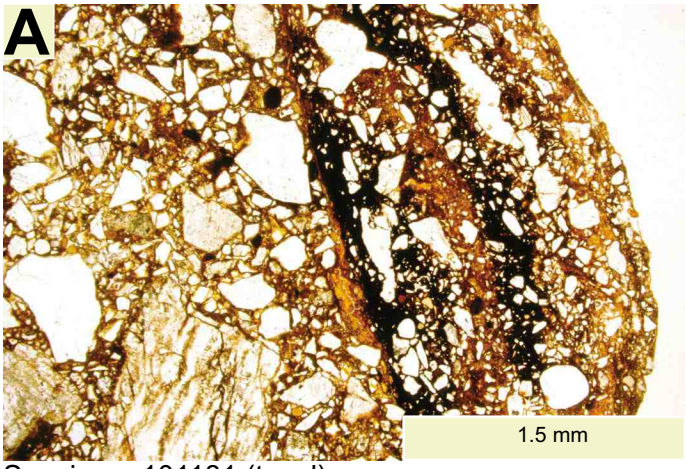

Specimen 101181 (txppl)

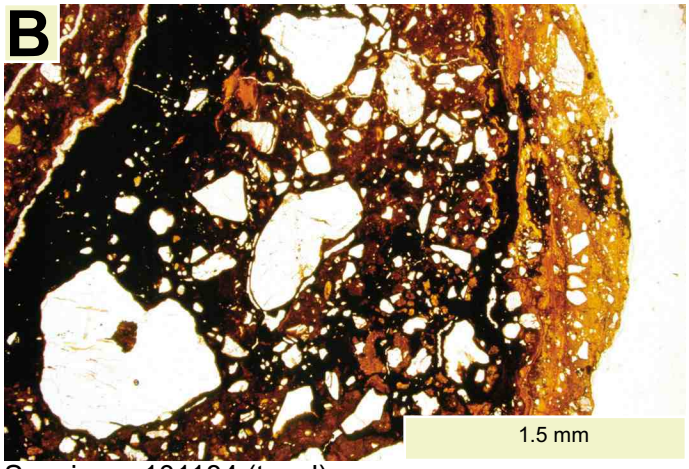

Specimen 101184 (txppl)

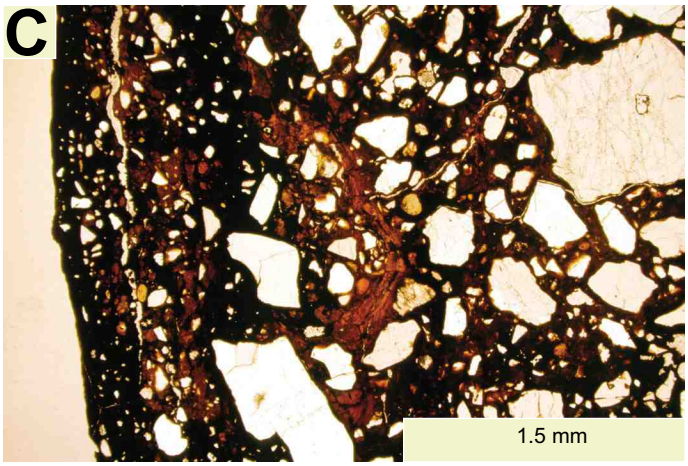

Specimen 101238 (txppl)

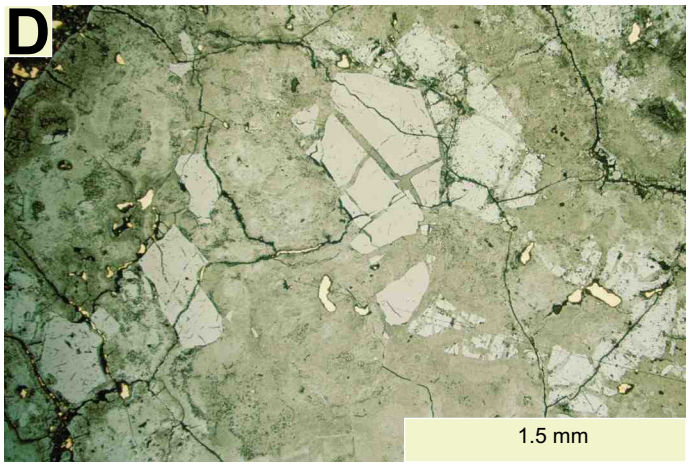

Specimen 101292 (nrf and txppl)

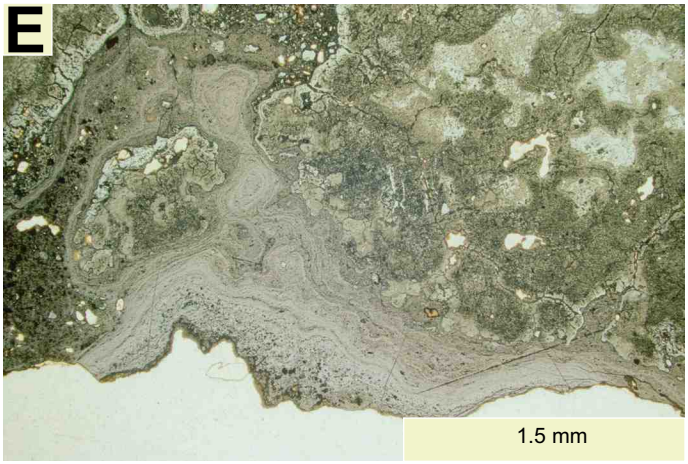

Specimen 101425_1 (nrf and txppl)

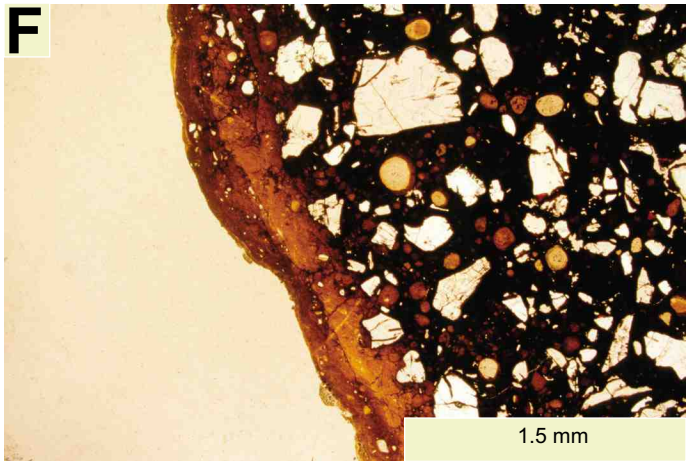

Specimen 101425_1 (txppl)

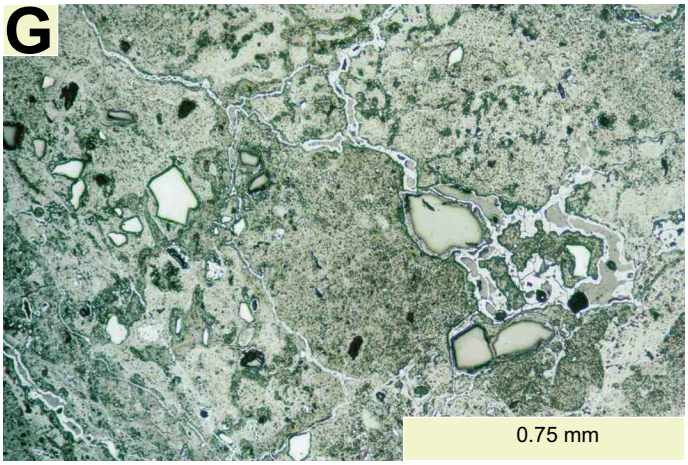

Specimen 101612 (nrf)

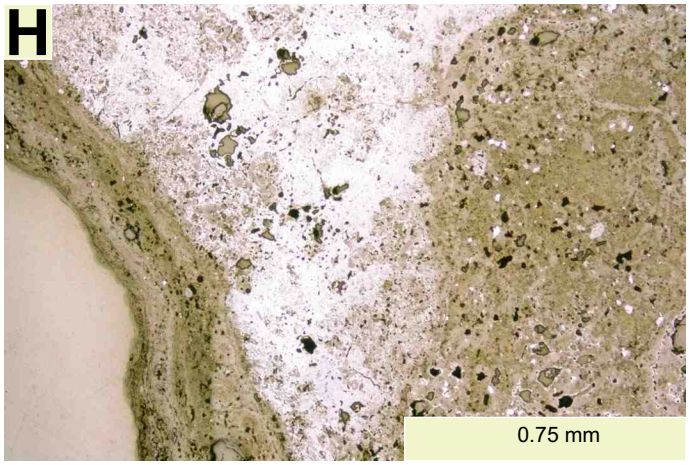

Specimen 101862_1 (nrf)

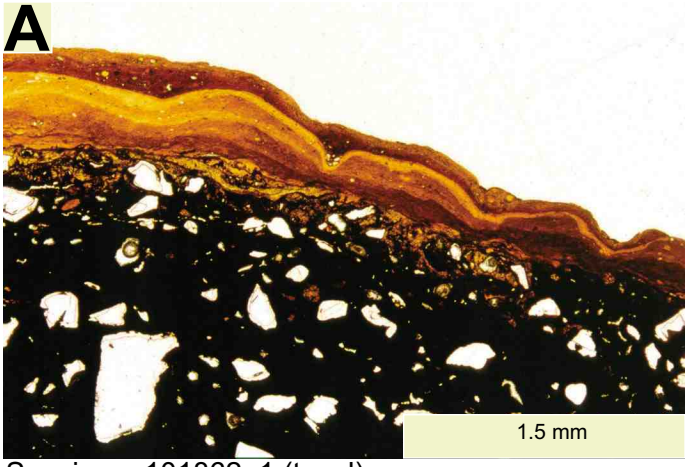

Specimen 101862_1 (txppl)

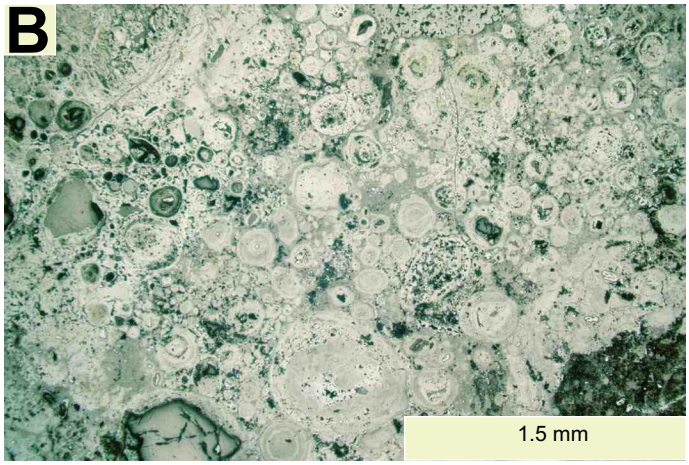

Specimen 101862 (nrl)

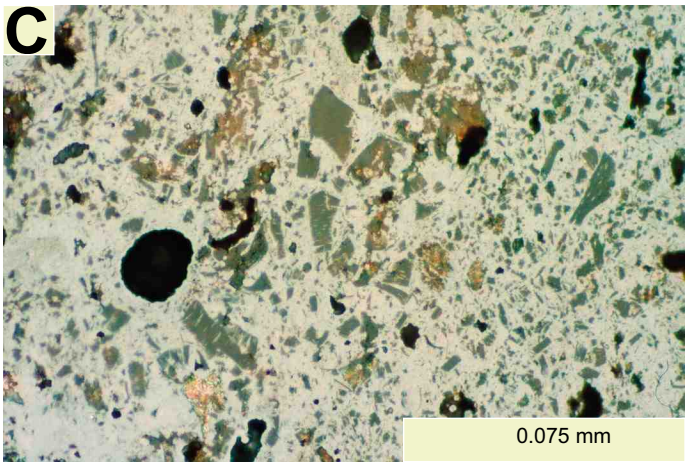

Specimen 102062 (nrl)

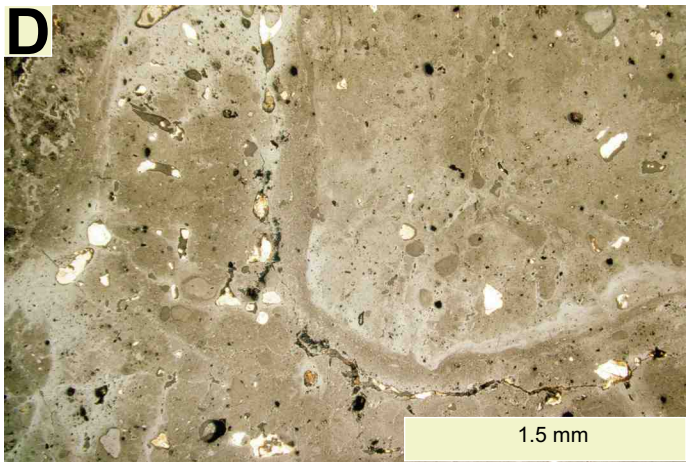

Specimen 102662_1 (nrl and txppl)

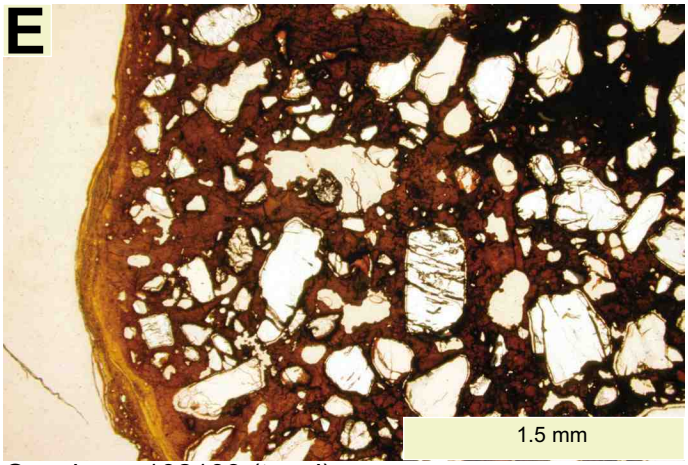

Specimen 102103 (txppl)

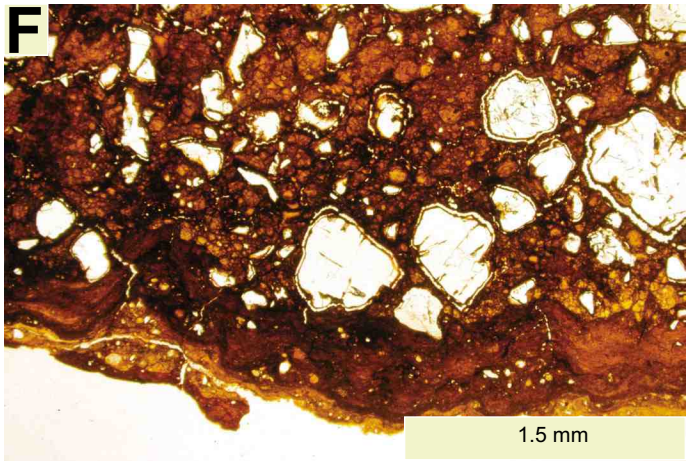

Specimen 102270 (txppl)

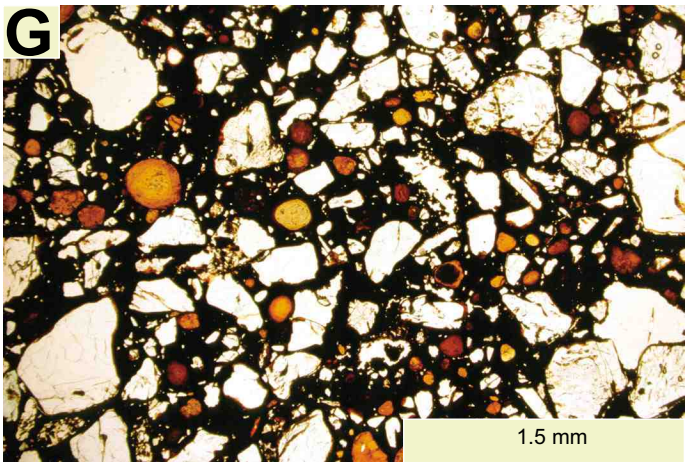

Specimen 102351 (txppl)

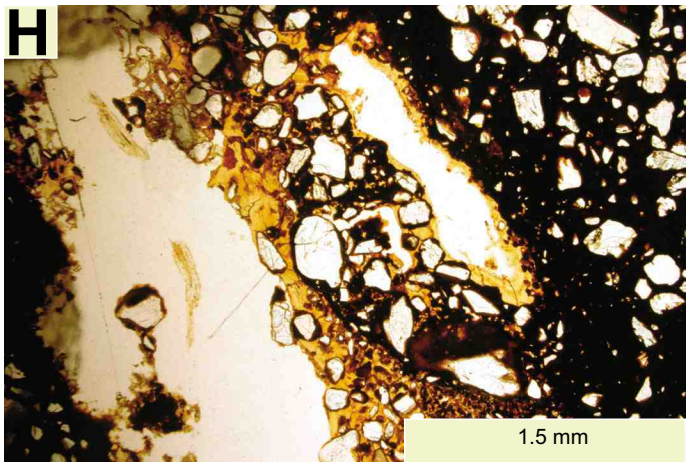

Specimen 102651 (txppl)

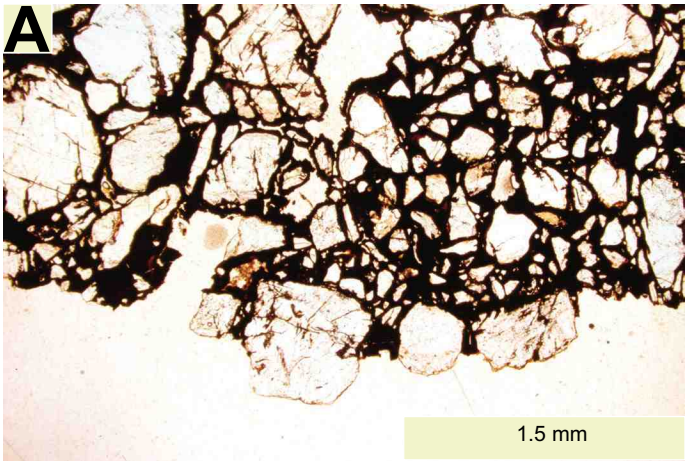

Specimen 102690 (txppl)

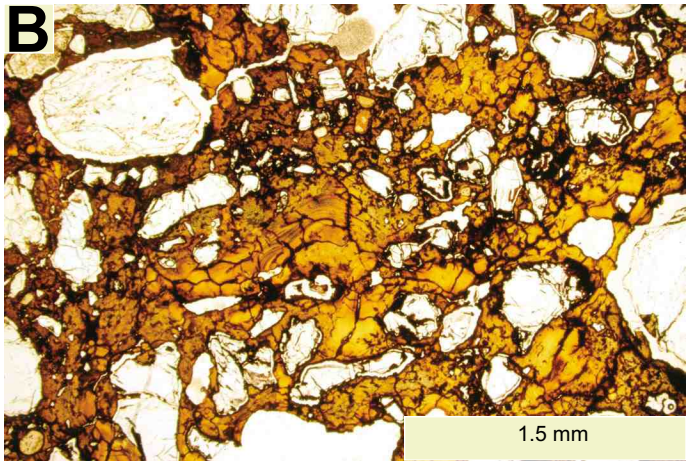

Specimen 102862 (txppl)

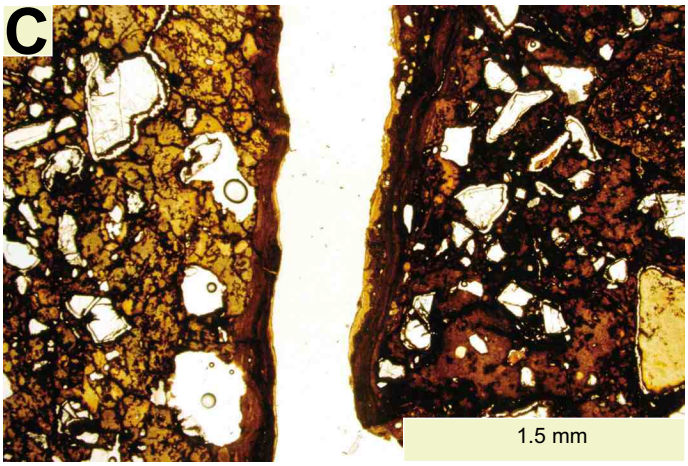

Specimen 102862 (txppl)

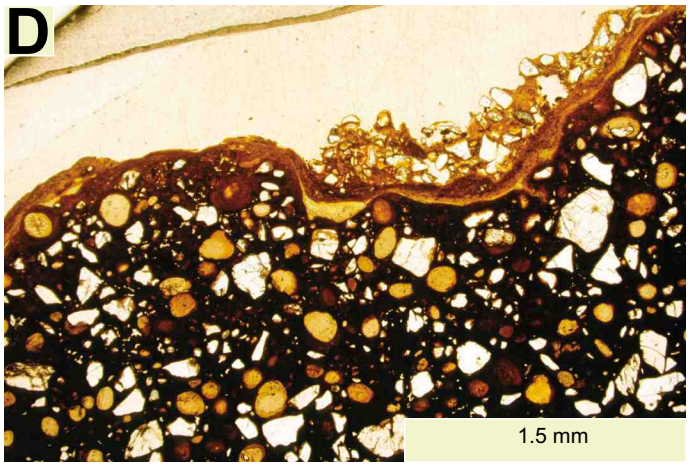

Specimen 102784 (txppl)

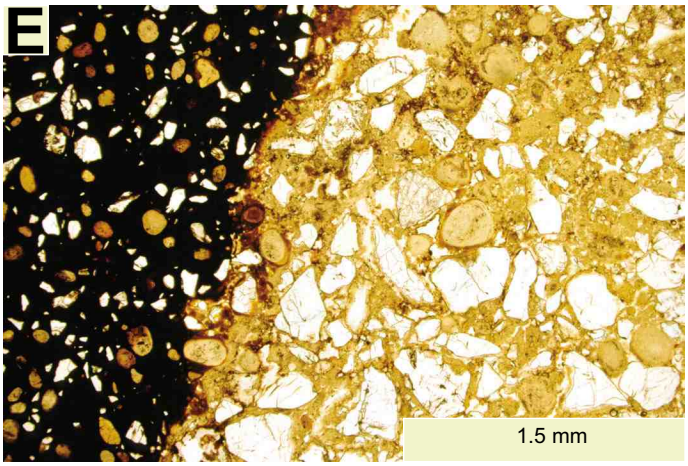

Specimen 102784 (txppl)

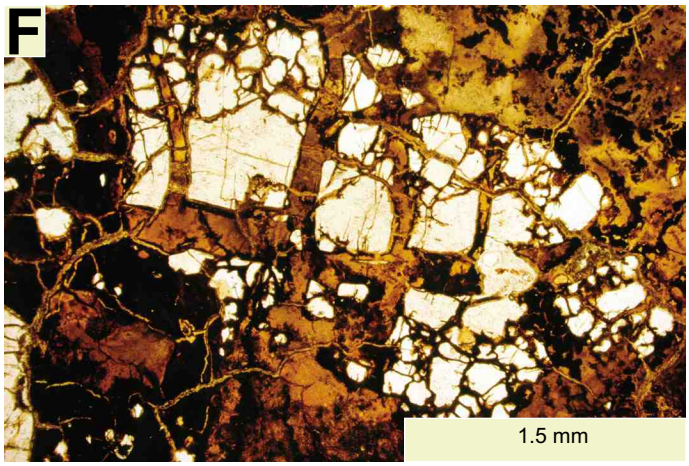

Specimen 104183 (txppl)

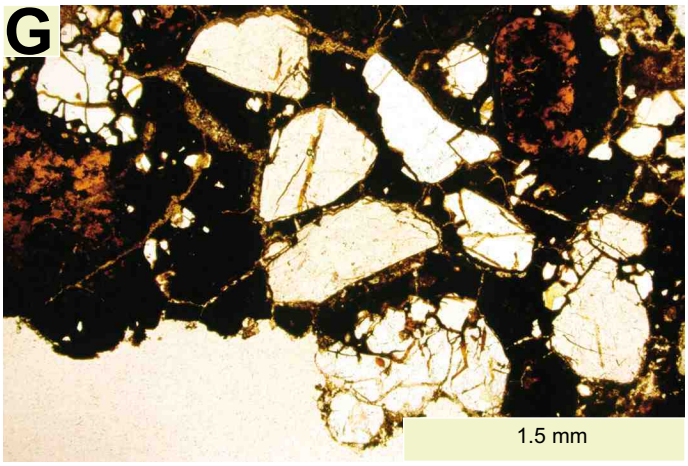

Specimen 104183 (txppl)

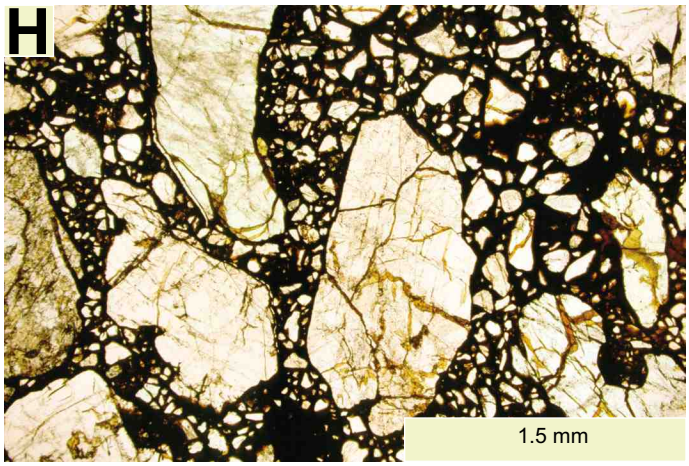

Specimen 104457 (txppl)

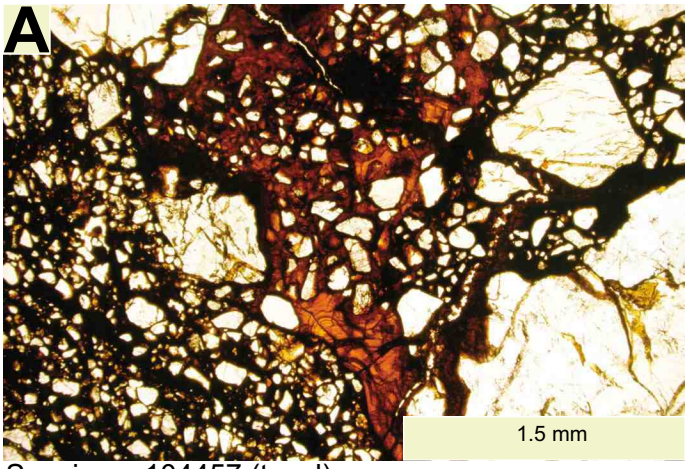

Specimen 104457 (txppl)

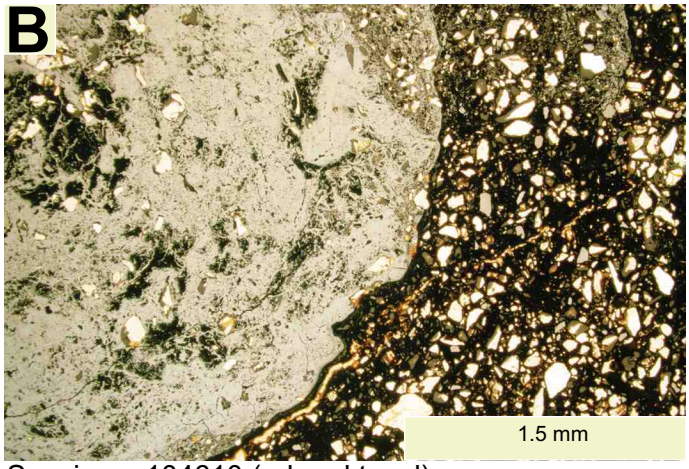

Specimen 104610 (nrl and txppl)

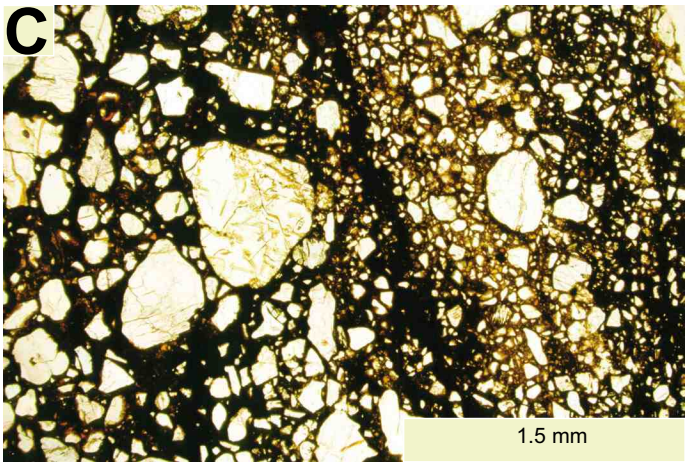

Specimen 104661 (txppl)

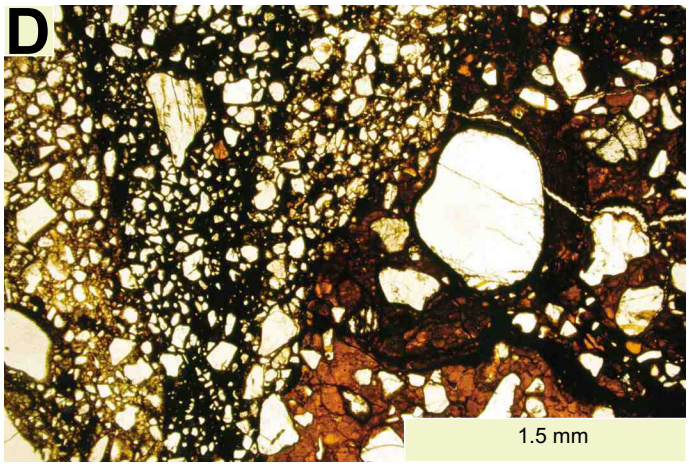

Specimen 104663 (txppl)

MAP APPENDIX

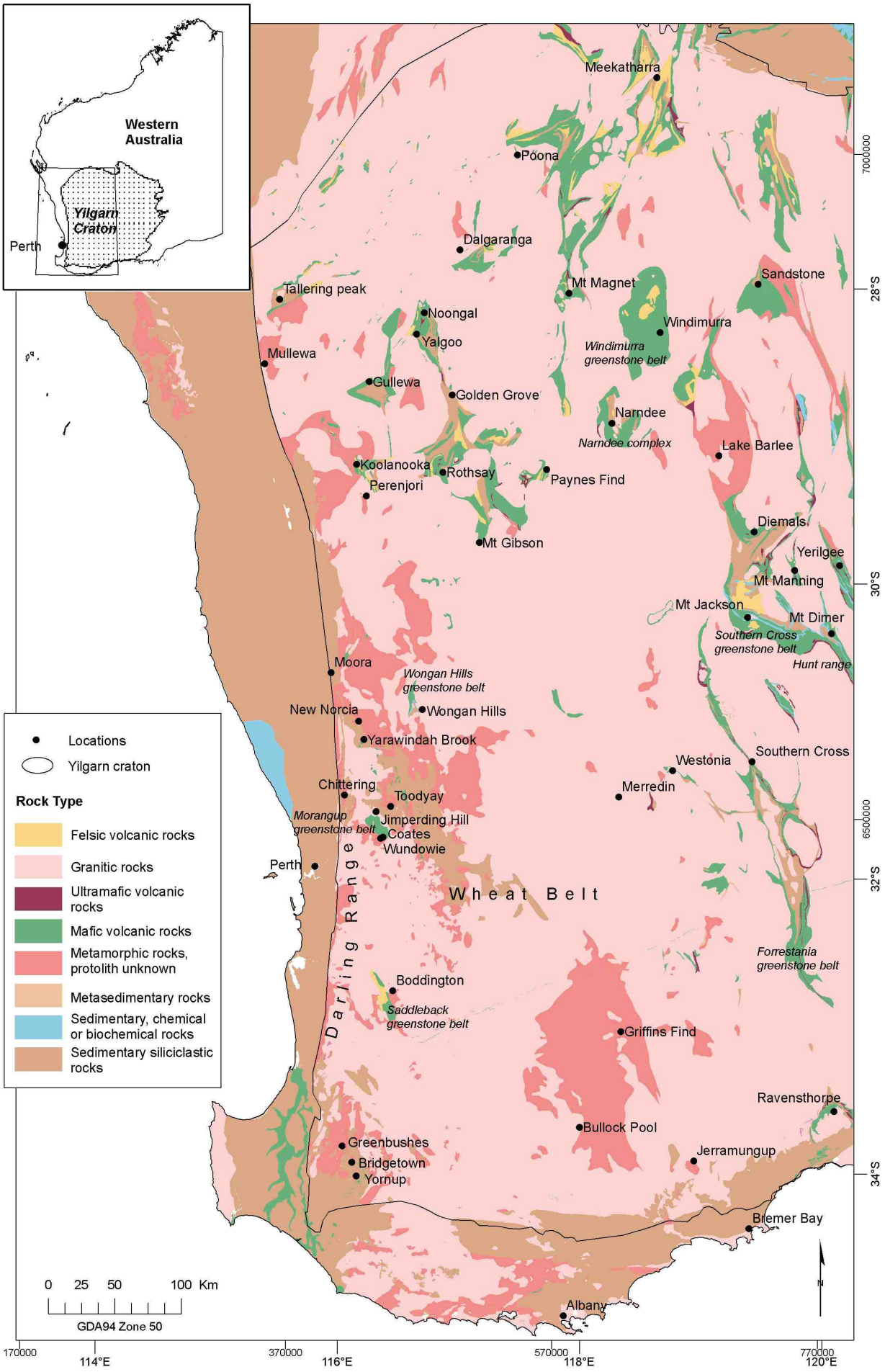
Western Australia
Yilgarn Craton
Perth
Meekatharra
Peona
Dalgaranga
Mt Magnet
Sandstone
Tallering peak
Noongal
Yalgoo
Windimurra
Windimurra greenstone belt
Mullewa
Gullewa
Golden Grove
Narndee
Narndee complex
Lake Barlee
Koolanooka
Rothsay
Paynes Find
Perenjori
Diemals
Mt Gibson
Yerilgee
Mt Manning
Mt Jackson
Mt Dimer
Southern Cross greenstone belt
Hunt range
Moora
Wongan Hills greenstone belt
New Norcia
Wongan Hills
Yarawindah Brook
Westonia
Southern Cross
Merredin
Chittering
Toodyay
Morangup greenstone belt
Jimperding Hill
Coates
Wundowie
Perth
Darling Range
Wheat Belt
Forrestania greenstone belt
Boddington
Saddleback greenstone belt
Griffins Find
Ravensthorpe
Bullock Pool
Greenbushes
Bridgetown
Yornup
Jerramungup
Bremer Bay
Albany
Locations
Yilgarn craton
Rock Type
Felsic volcanic rocks
Granitic rocks
Ultramafic volcanic rocks
Mafic volcanic rocks
Metamorphic rocks, protolith unknown
Metasedimentary rocks
Sedimentary, chemical or biochemical rocks
Sedimentary siliciclastic rocks
0 25 50 100 Km
GDA94 Zone 50
N
7000000
6500000
28°S
30°S
32°S
34°S
170000
370000
570000
770000
114°E
116°E
118°E
120°E

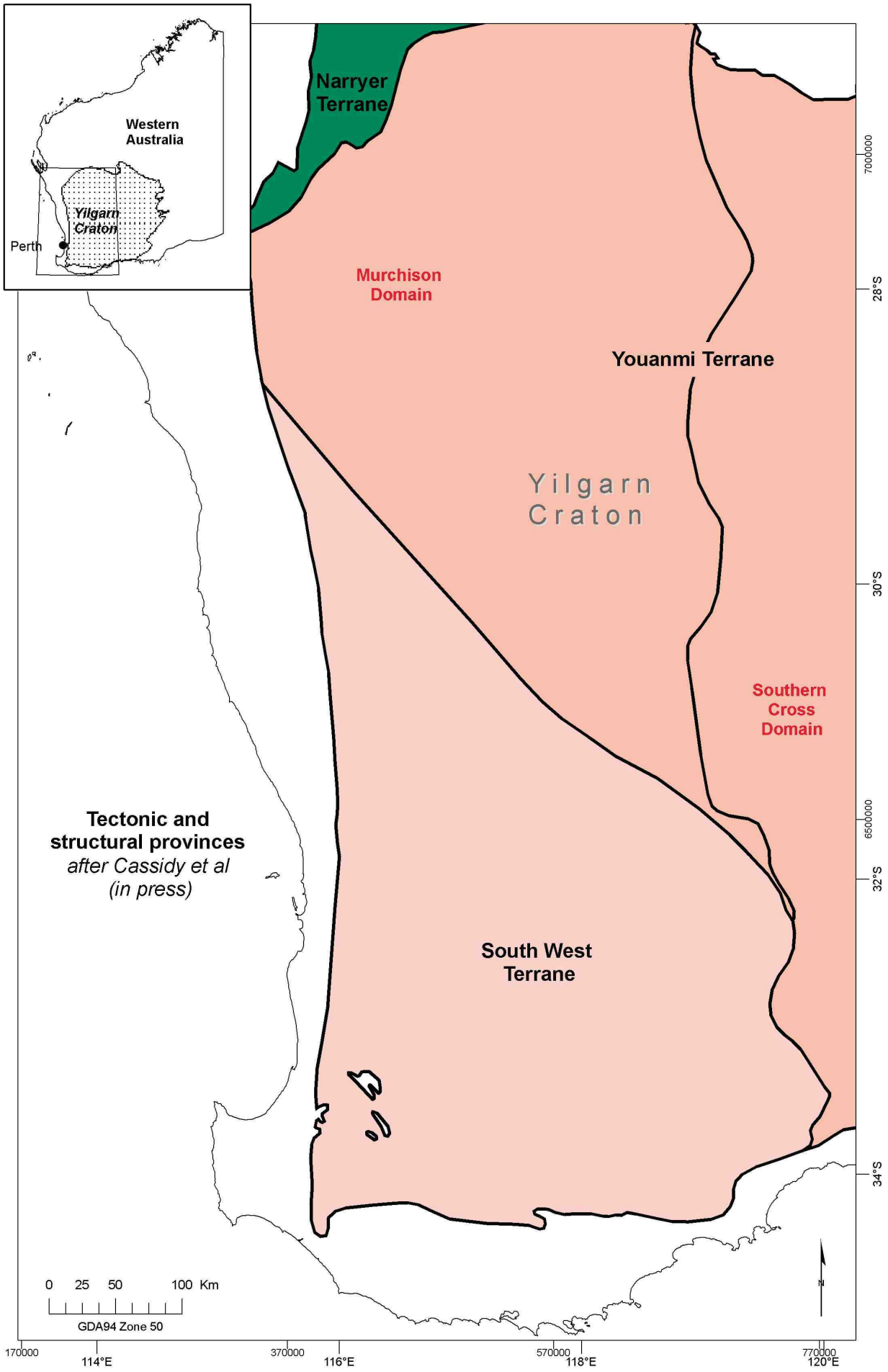
Western Australia
Yilgarn Craton
Perth
Narryer Terrane
Murchison Domain
Youanmi Terrane
Yilgarn Craton
Southern Cross Domain
South West Terrane
Tectonic and structural provinces
after Cassidy et al (in press)
0 25 50 100 Km
GDA94 Zone 50
N
7000000
28°S
30°S
6500000
32°S
34°S
170000
114°E
370000
116°E
570000
118°E
770000
120°E

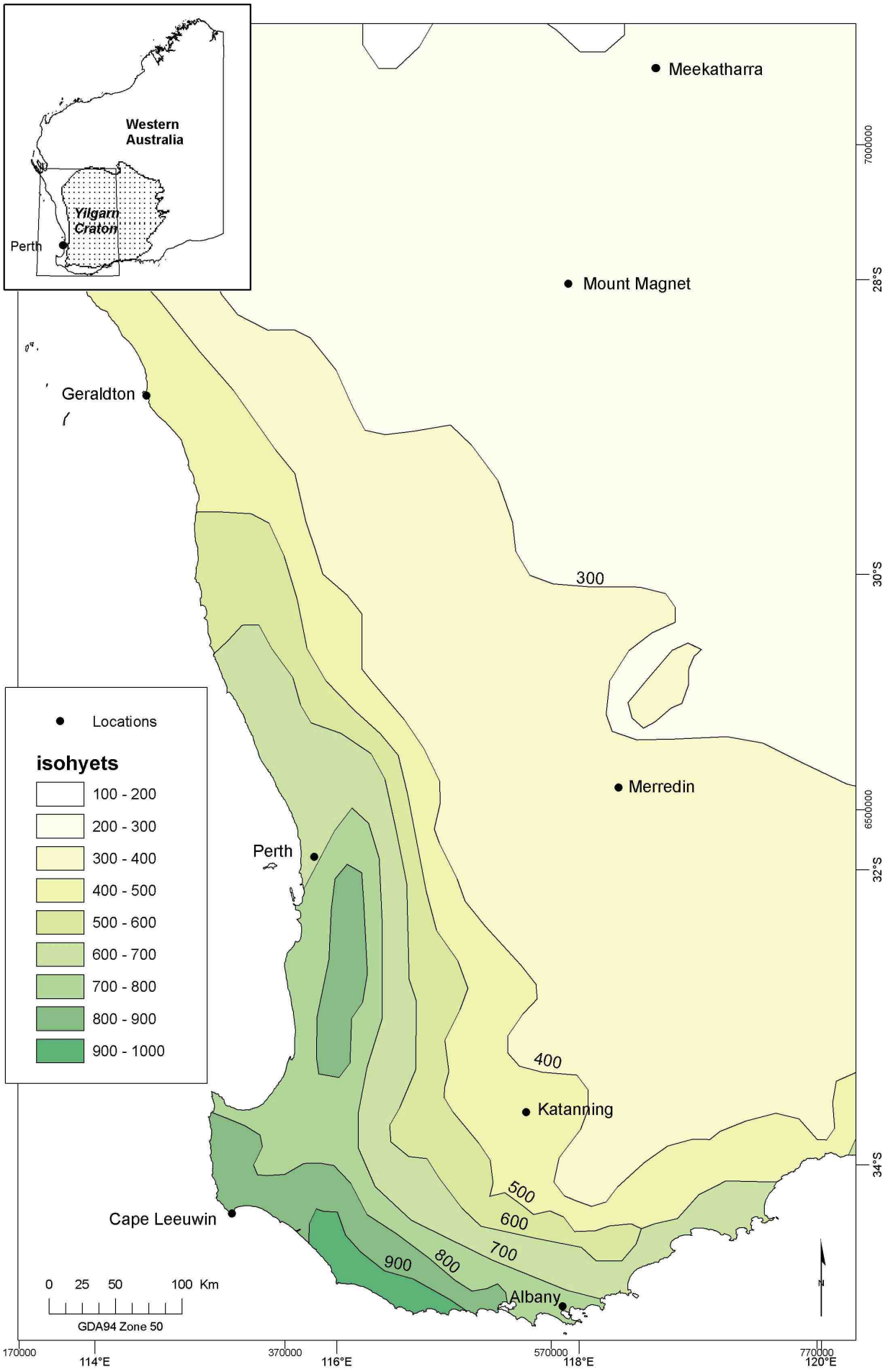
Western Australia
Yilgarn Craton
Perth
Meekatharra
Mount Magnet
Geraldton
Merredin
Perth
Katanning
Cape Leeuwin
Albany
300
400
500
600
700
800
900
Locations
isohyets
100 - 200
200 - 300
300 - 400
400 - 500
500 - 600
600 - 700
700 - 800
800 - 900
900 - 1000
0 25 50 100 Km
GDA94 Zone 50
7000000
28°S
30°S
6500000
32°S
34°S
170000
114°E
370000
116°E
570000
118°E
770000
120°E

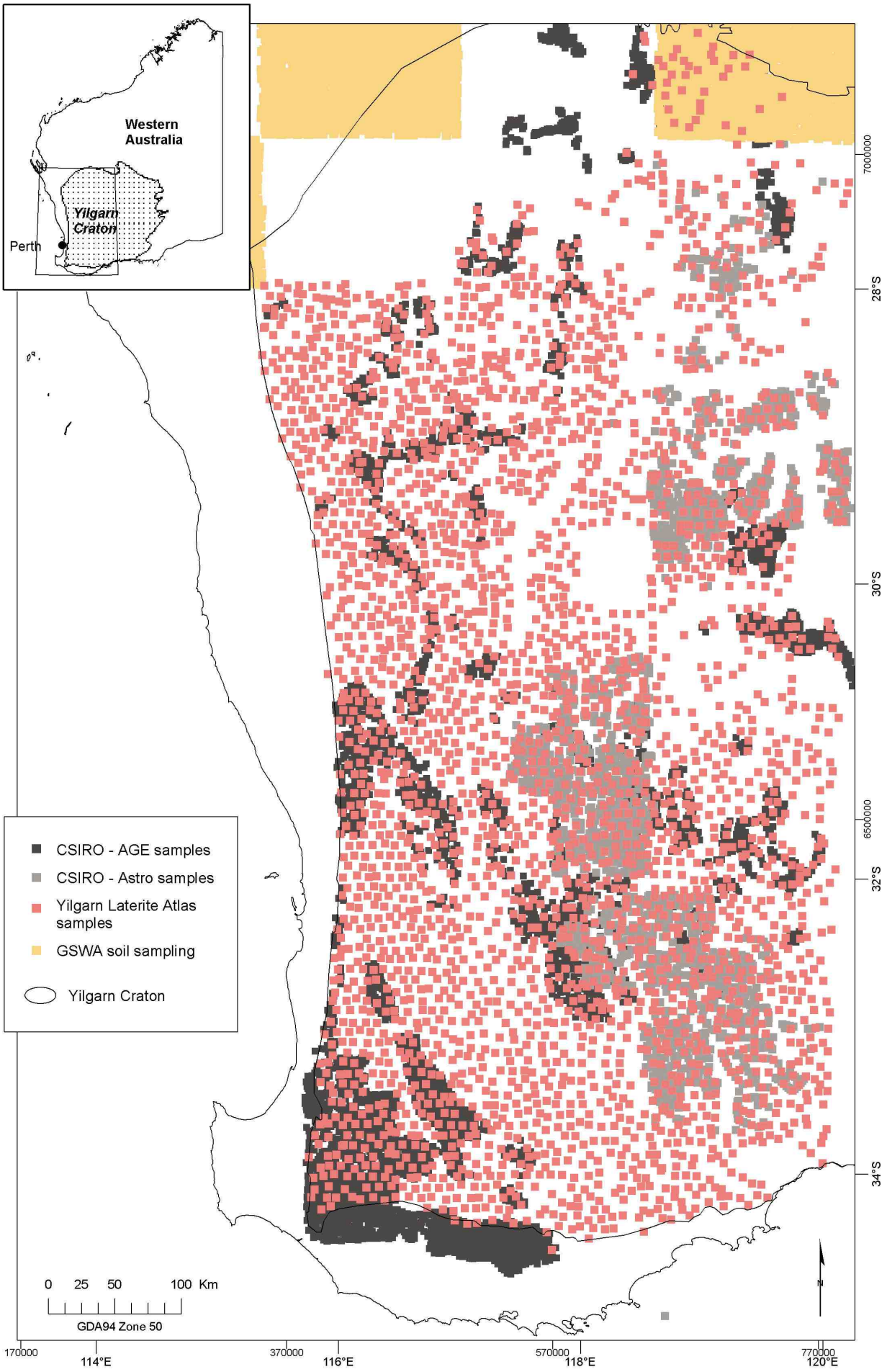
Western Australia
Yilgarn Craton
Perth
CSIRO - AGE samples
CSIRO - Astro samples
Yilgarn Laterite Atlas samples
GSWA soil sampling
Yilgarn Craton
0 25 50 100 Km
GDA94 Zone 50
N
7000000
28°S
30°S
6500000
32°S
34°S
170000
114°E
370000
116°E
570000
118°E
770000
120°E

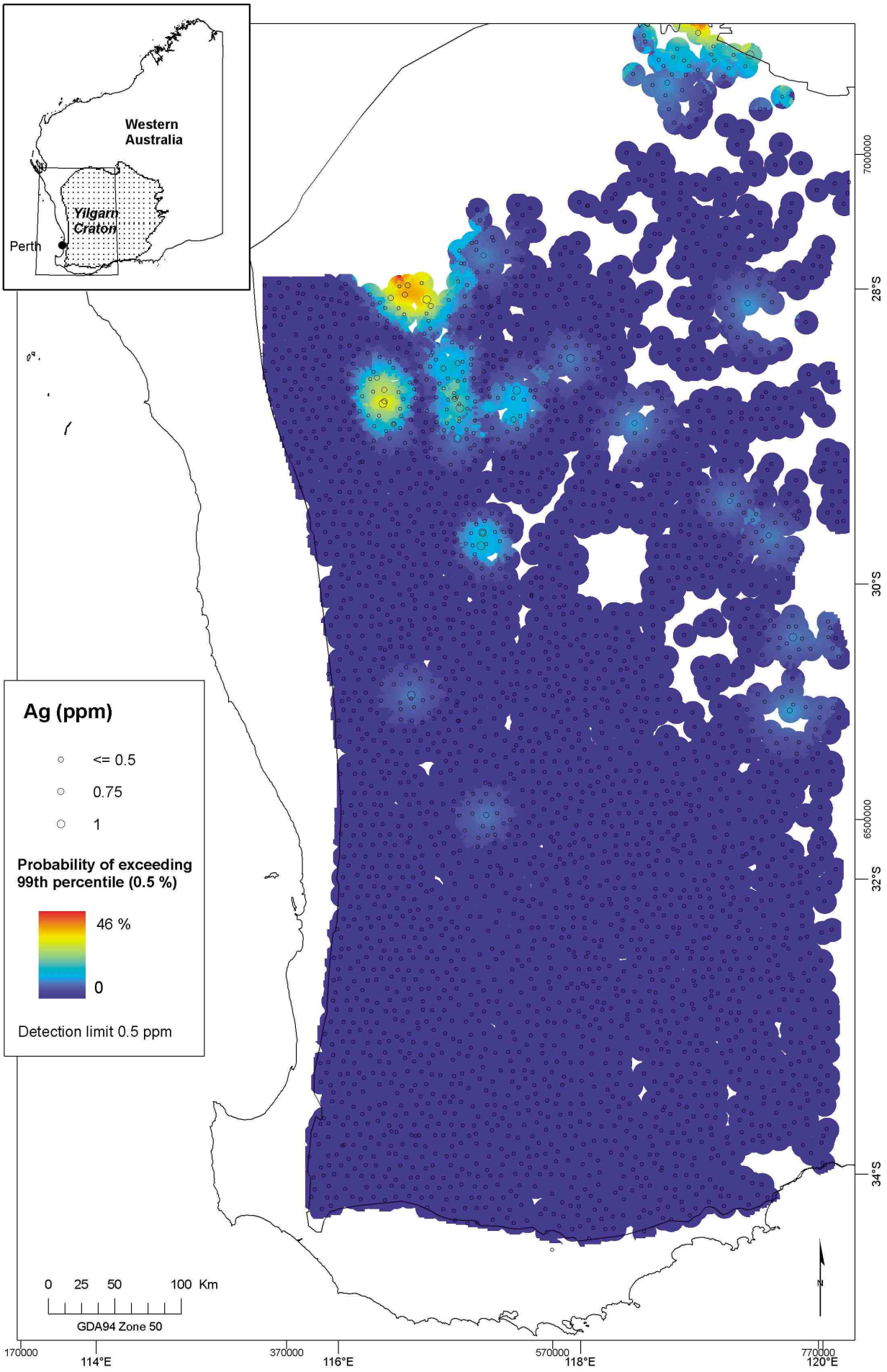
Western Australia
Yilgarn Craton
Perth
Ag (ppm)
<= 0.5
0.75
1
Probability of exceeding 99th percentile (0.5 %)
46 %
0
Detection limit 0.5 ppm
0 25 50 100 Km
GDA94 Zone 50
N
7000000
28°S
30°S
6500000
32°S
34°S
170000
114°E
370000
116°E
570000
118°E
770000
120°E

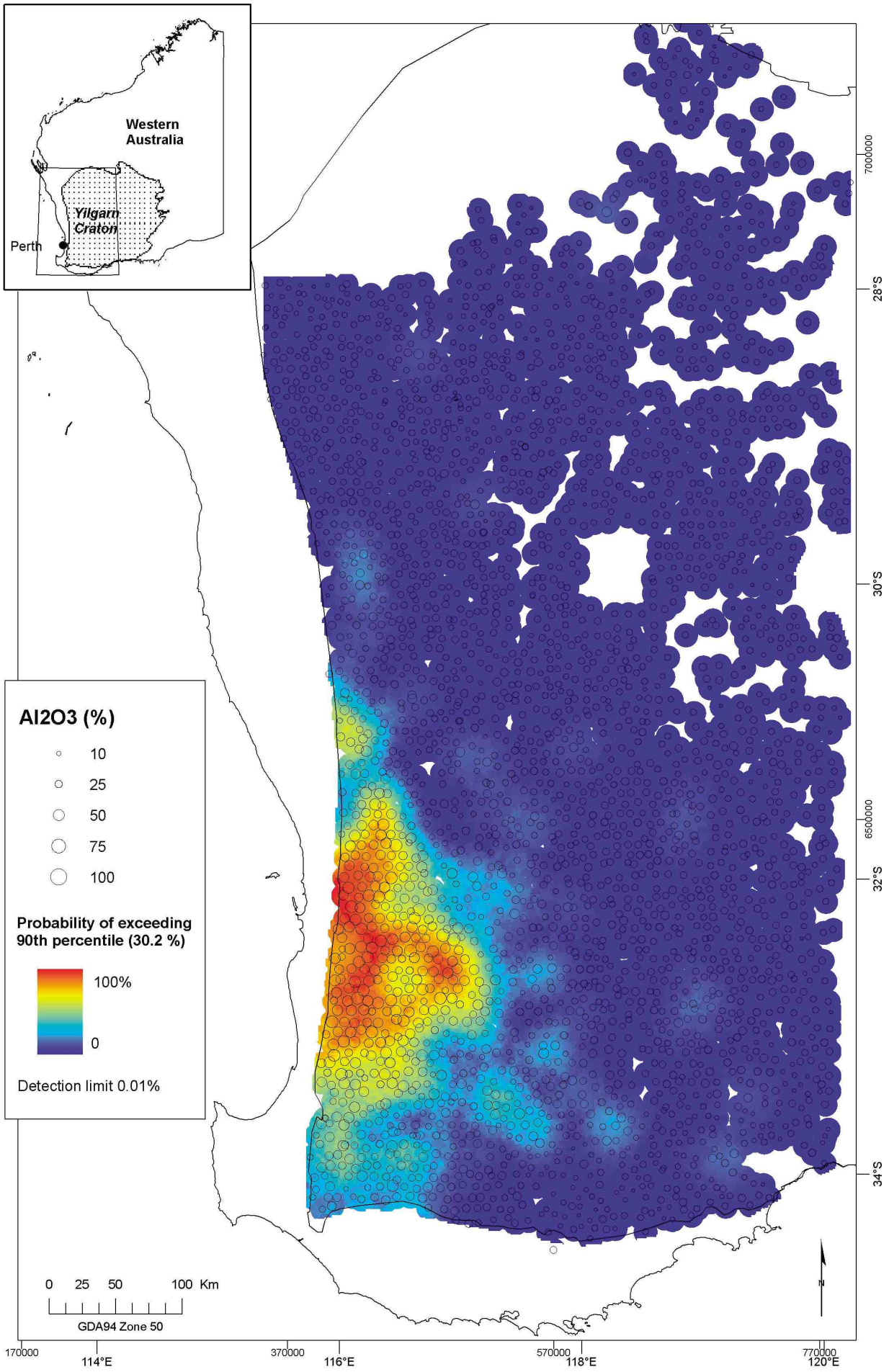
Western Australia
Yilgarn Craton
Perth
Al2O3 (%)
10
25
50
75
100
Probability of exceeding 90th percentile (30.2 %)
100%
0
Detection limit 0.01%
0 25 50 100 Km
GDA94 Zone 50
N
7000000
28°S
30°S
6500000
32°S
34°S
170000
114°E
370000
116°E
570000
118°E
770000
120°E

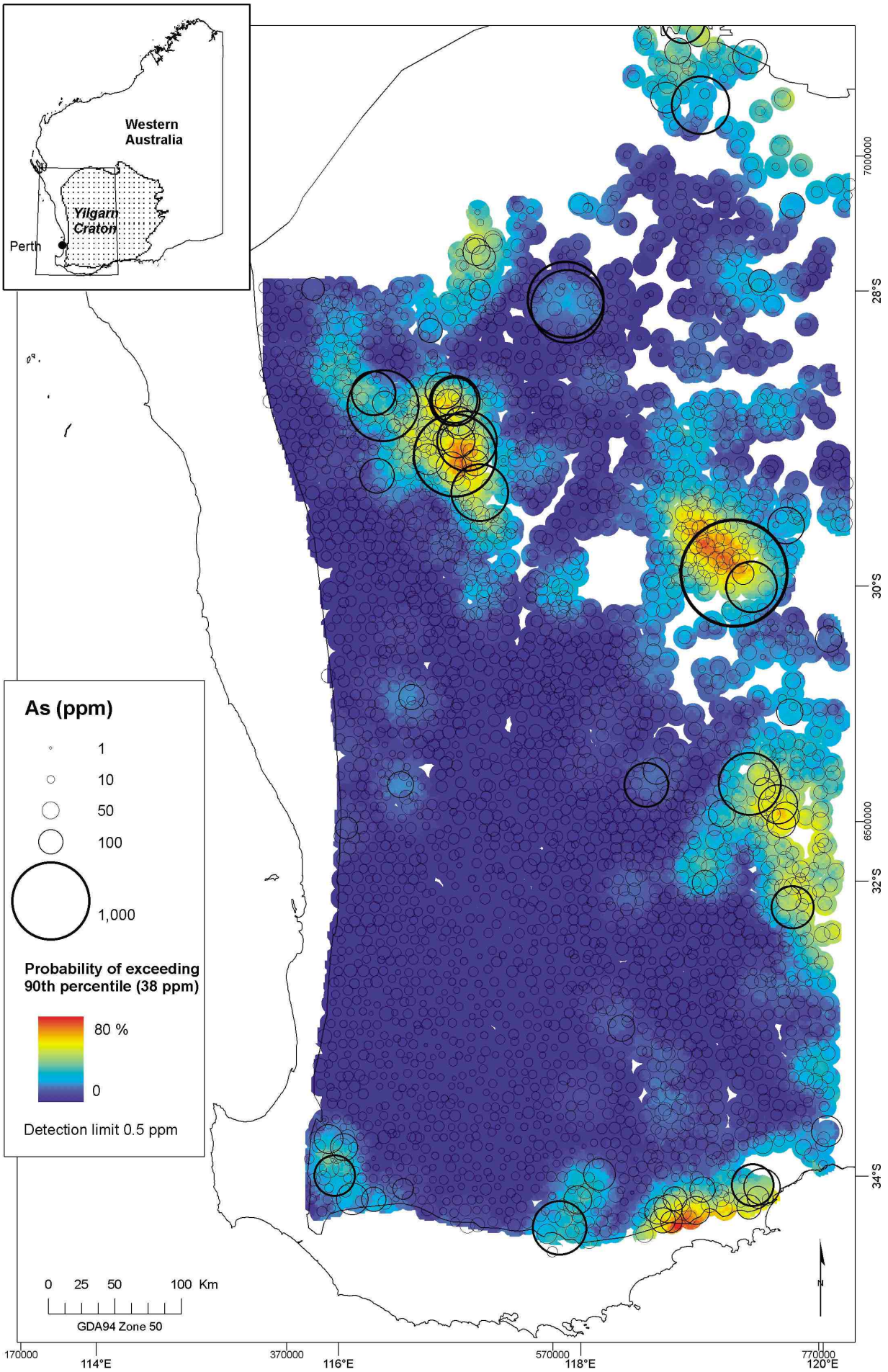
Western Australia
Yilgarn Craton
Perth
As (ppm)
1
10
50
100
1,000
Probability of exceeding 90th percentile (38 ppm)
80 %
0
Detection limit 0.5 ppm
0 25 50 100 Km
GDA94 Zone 50
N
170000
114°E
370000
116°E
570000
118°E
770000
120°E
7000000
28°S
6500000
30°S
32°S
34°S

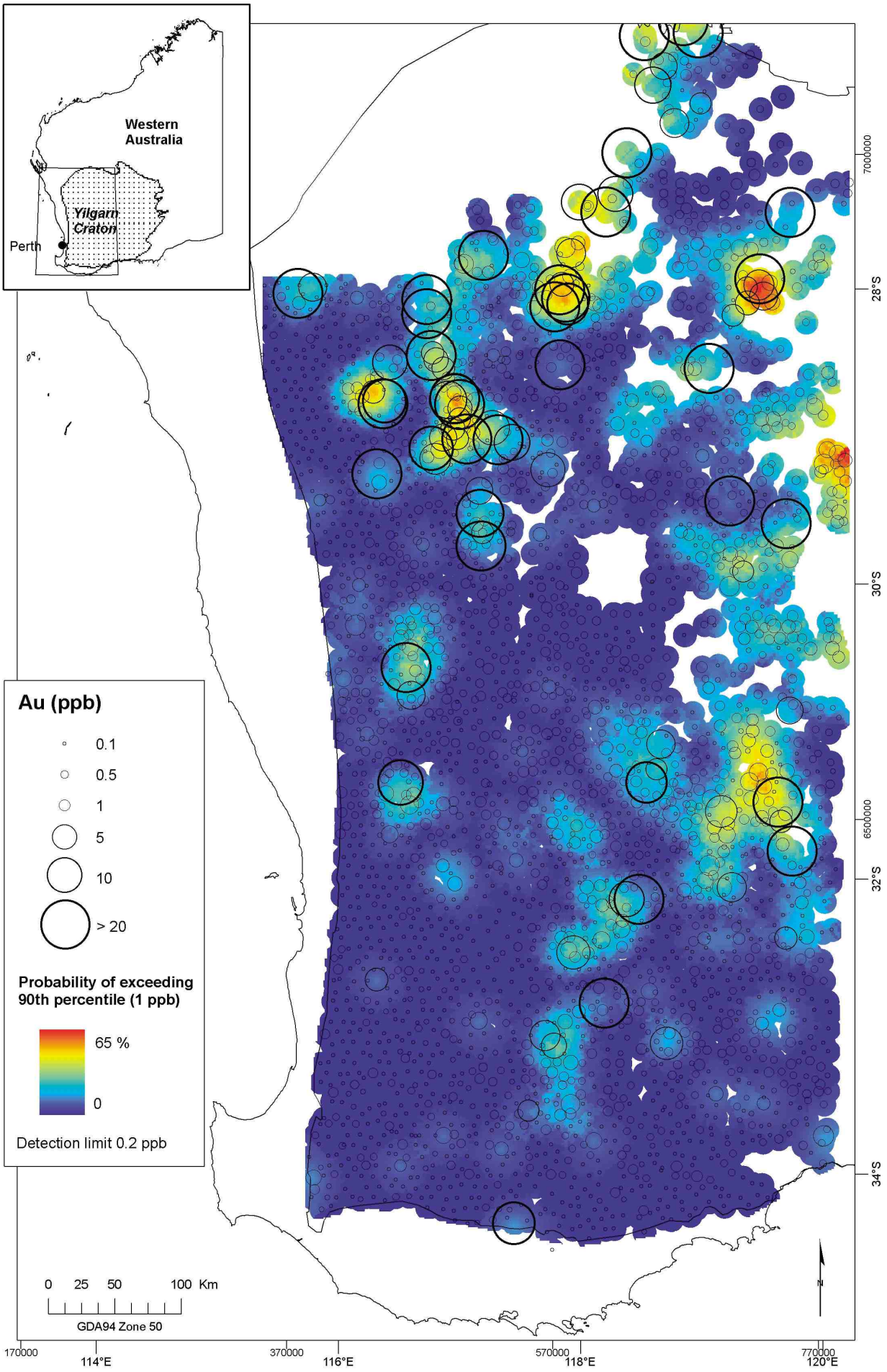
Western Australia
Yilgarn Craton
Perth
Au (ppb)
0.1
0.5
1
5
10
> 20
Probability of exceeding 90th percentile (1 ppb)
65 %
0
Detection limit 0.2 ppb
0 25 50 100 Km
GDA94 Zone 50
N
7000000
6500000
28°S
30°S
32°S
34°S
170000
370000
570000
770000
114°E
116°E
118°E
120°E

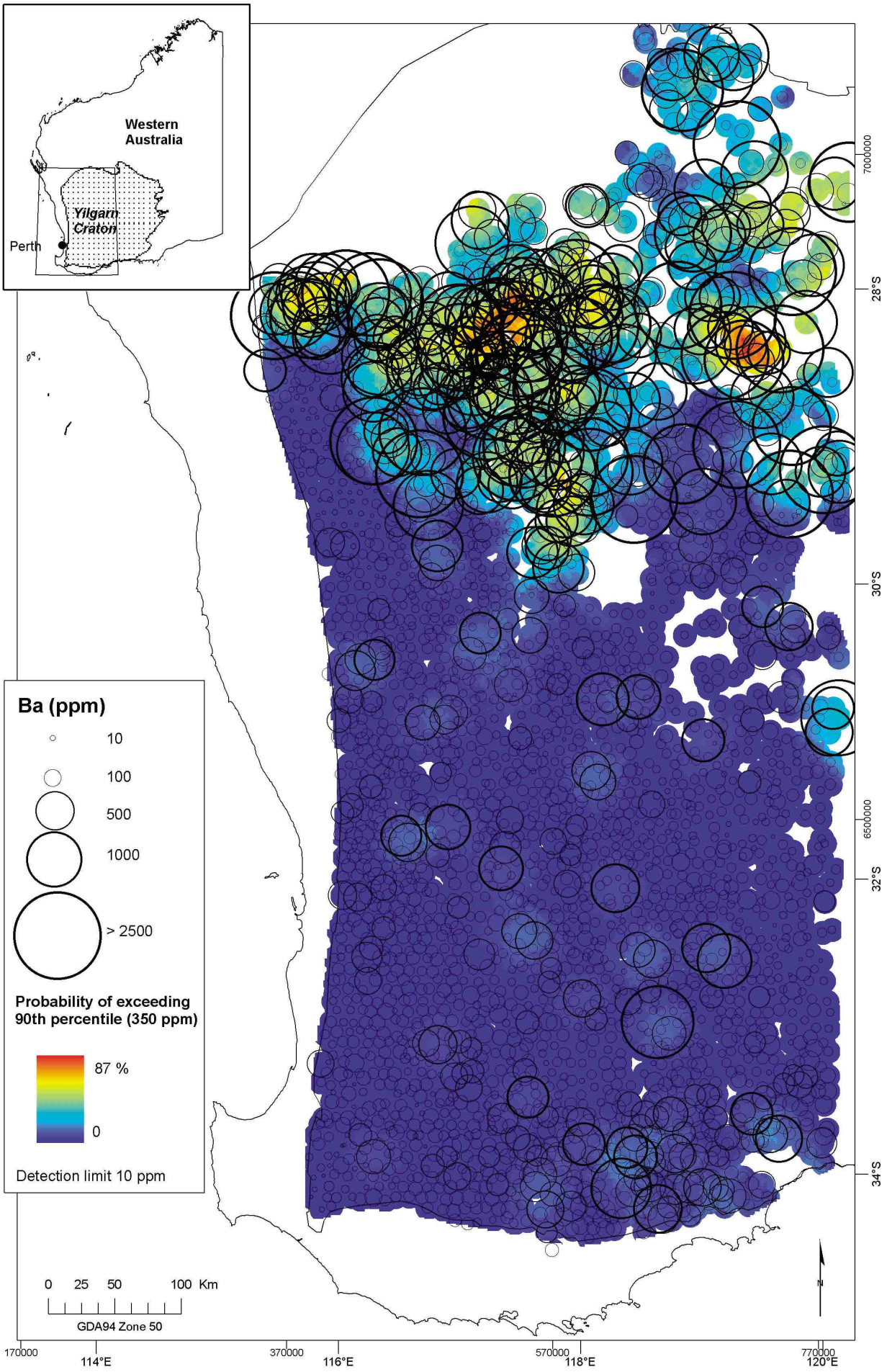
Western Australia
Yilgarn Craton
Perth
Ba (ppm)
10
100
500
1000
> 2500
Probability of exceeding 90th percentile (350 ppm)
87 %
0
Detection limit 10 ppm
0 25 50 100 Km
GDA94 Zone 50
7000000
28°S
30°S
6500000
32°S
34°S
170000
114°E
370000
116°E
570000
118°E
770000
120°E

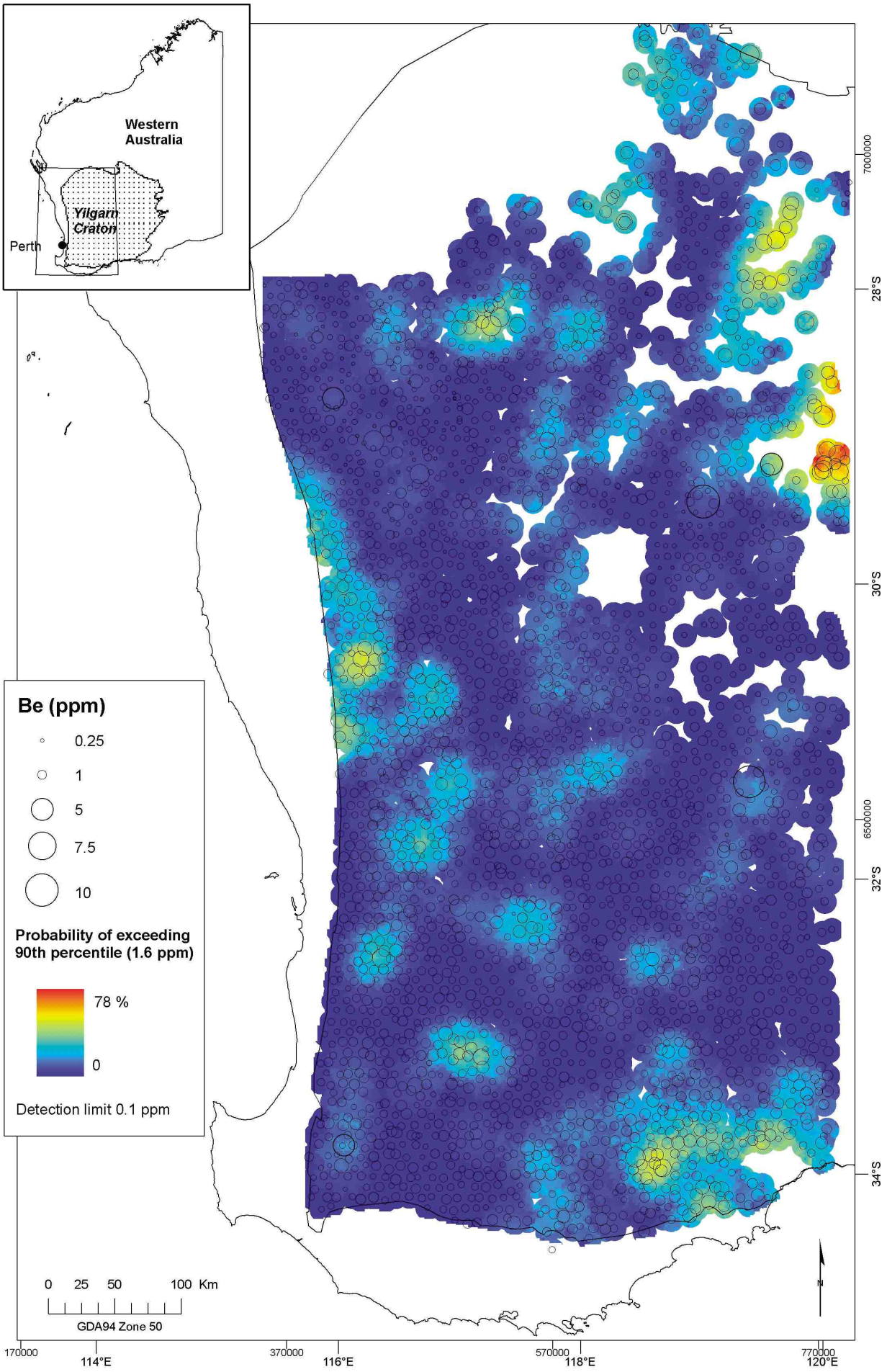
Western Australia
Yilgarn Craton
Perth
Be (ppm)
0.25
1
5
7.5
10
Probability of exceeding 90th percentile (1.6 ppm)
78 %
0
Detection limit 0.1 ppm
0 25 50 100 Km
GDA94 Zone 50
N
7000000
28°S
30°S
6500000
32°S
34°S
170000
114°E
370000
116°E
570000
118°E
770000
120°E

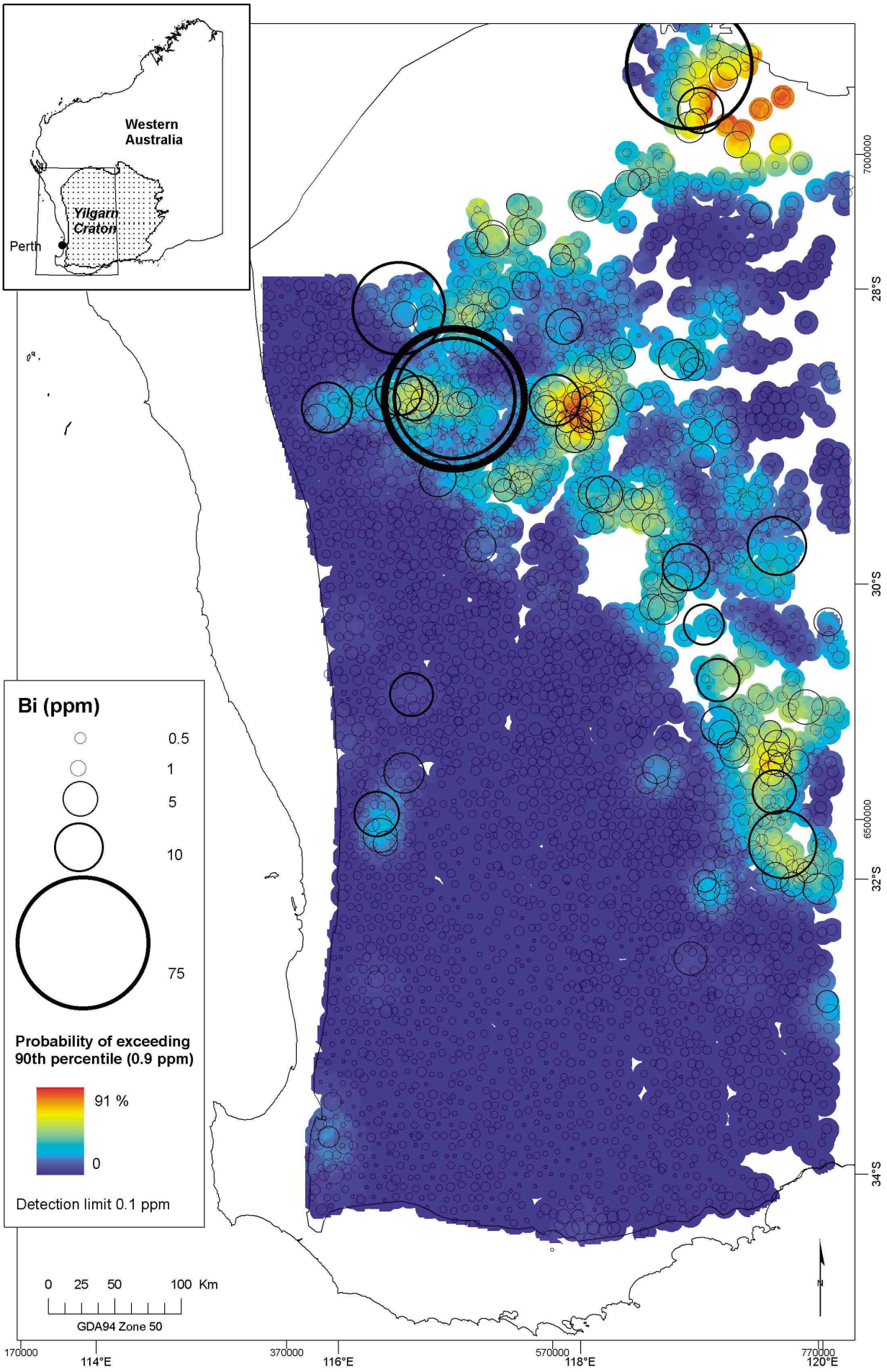
Western Australia
Yilgarn Craton
Perth
Bi (ppm)
0.5
1
5
10
75
Probability of exceeding 90th percentile (0.9 ppm)
91 %
0
Detection limit 0.1 ppm
0 25 50 100 Km
GDA94 Zone 50
N
7000000
6500000
28°S
30°S
32°S
34°S
170000
370000
570000
770000
114°E
116°E
118°E
120°E

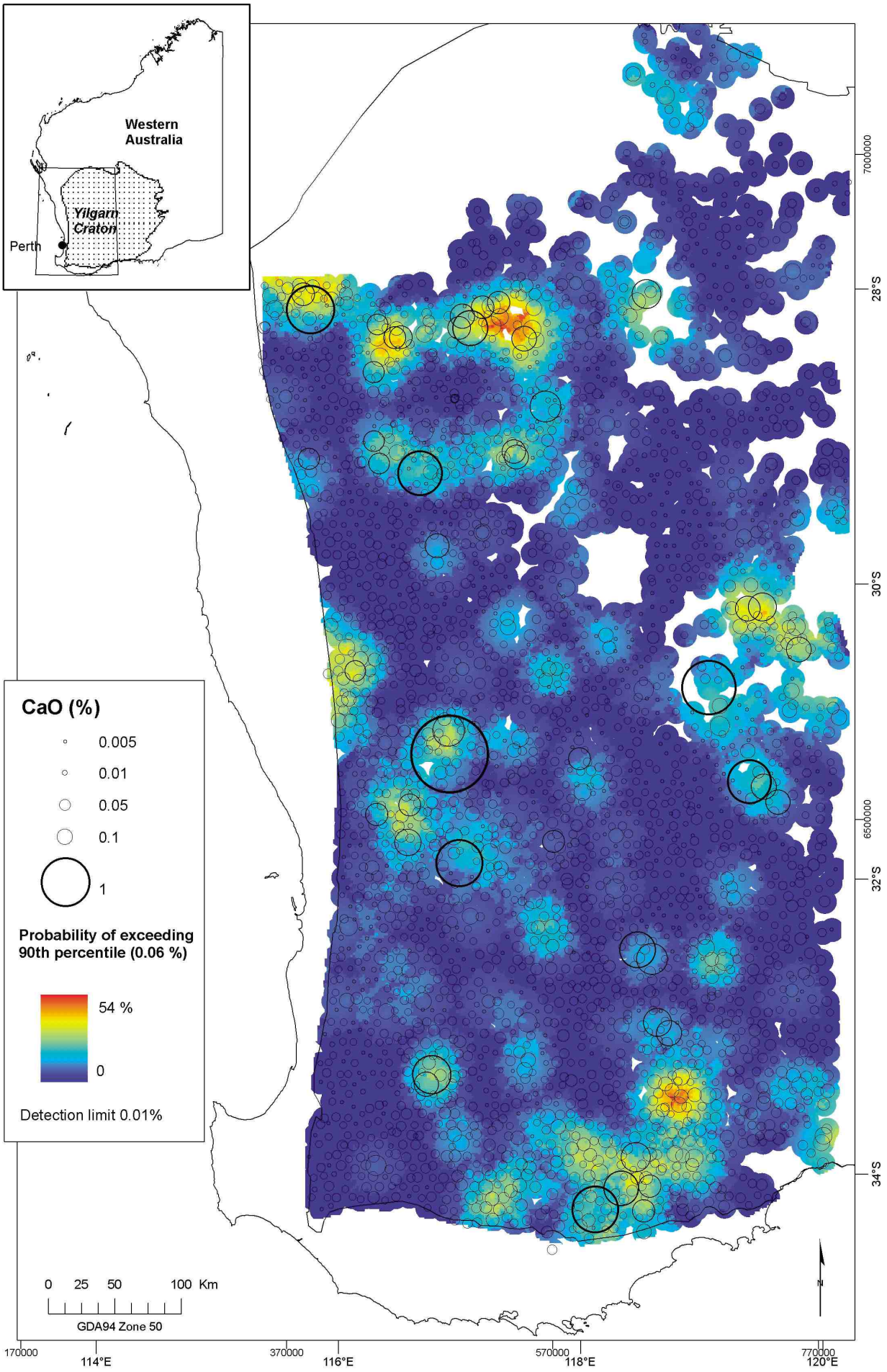
Western Australia
Yilgarn Craton
Perth
CaO (%)
0.005
0.01
0.05
0.1
1
Probability of exceeding 90th percentile (0.06 %)
54 %
0
Detection limit 0.01%
0 25 50 100 Km
GDA94 Zone 50
170000
114°E
370000
116°E
570000
118°E
770000
120°E
7000000
28°S
6500000
30°S
32°S
34°S
N

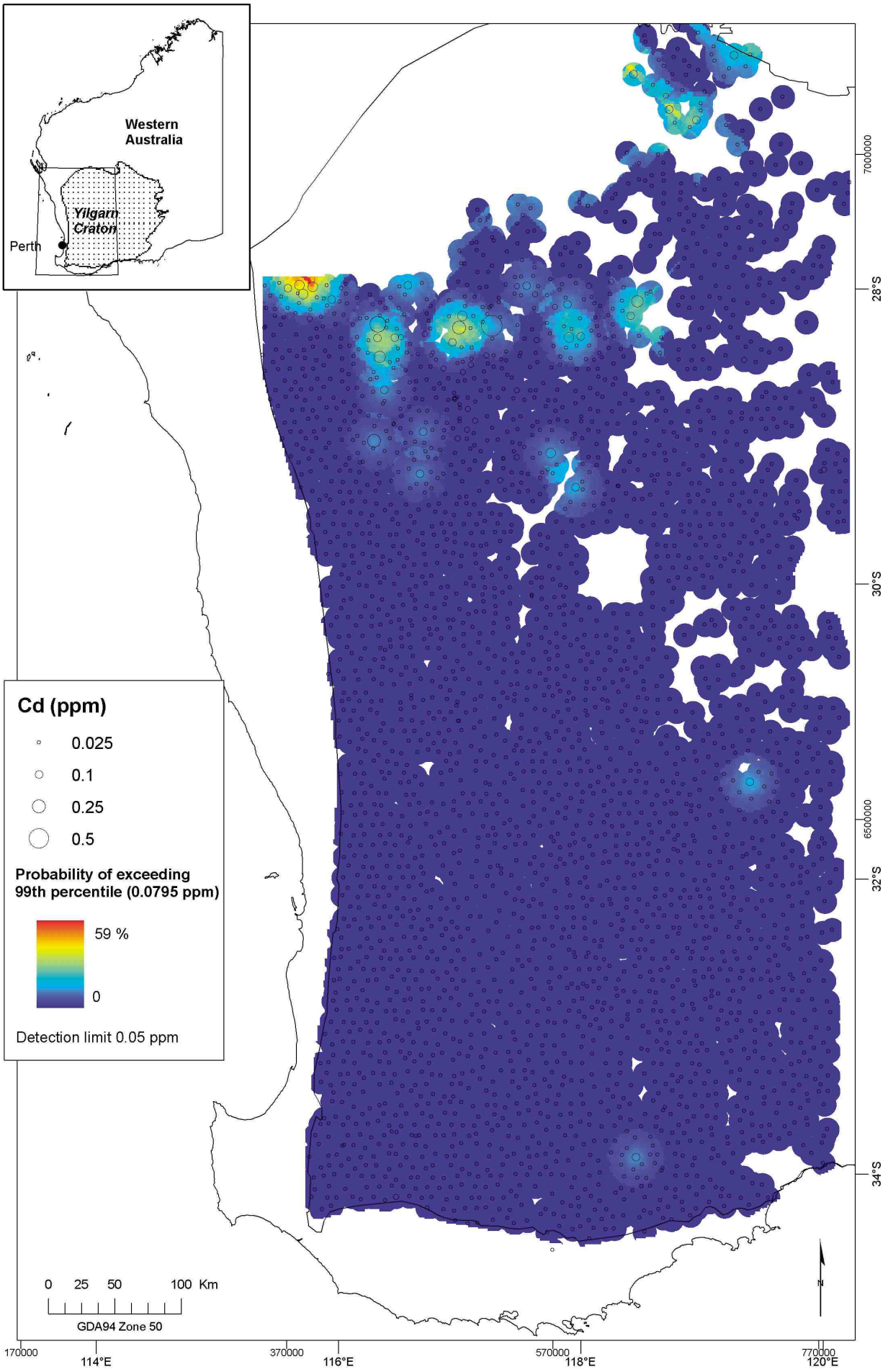
Western Australia
Yilgarn Craton
Perth
Cd (ppm)
0.025
0.1
0.25
0.5
Probability of exceeding 99th percentile (0.0795 ppm)
59 %
0
Detection limit 0.05 ppm
0 25 50 100 Km
GDA94 Zone 50
170000
114°E
370000
116°E
570000
118°E
770000
120°E
7000000
28°S
6500000
30°S
32°S
34°S
N

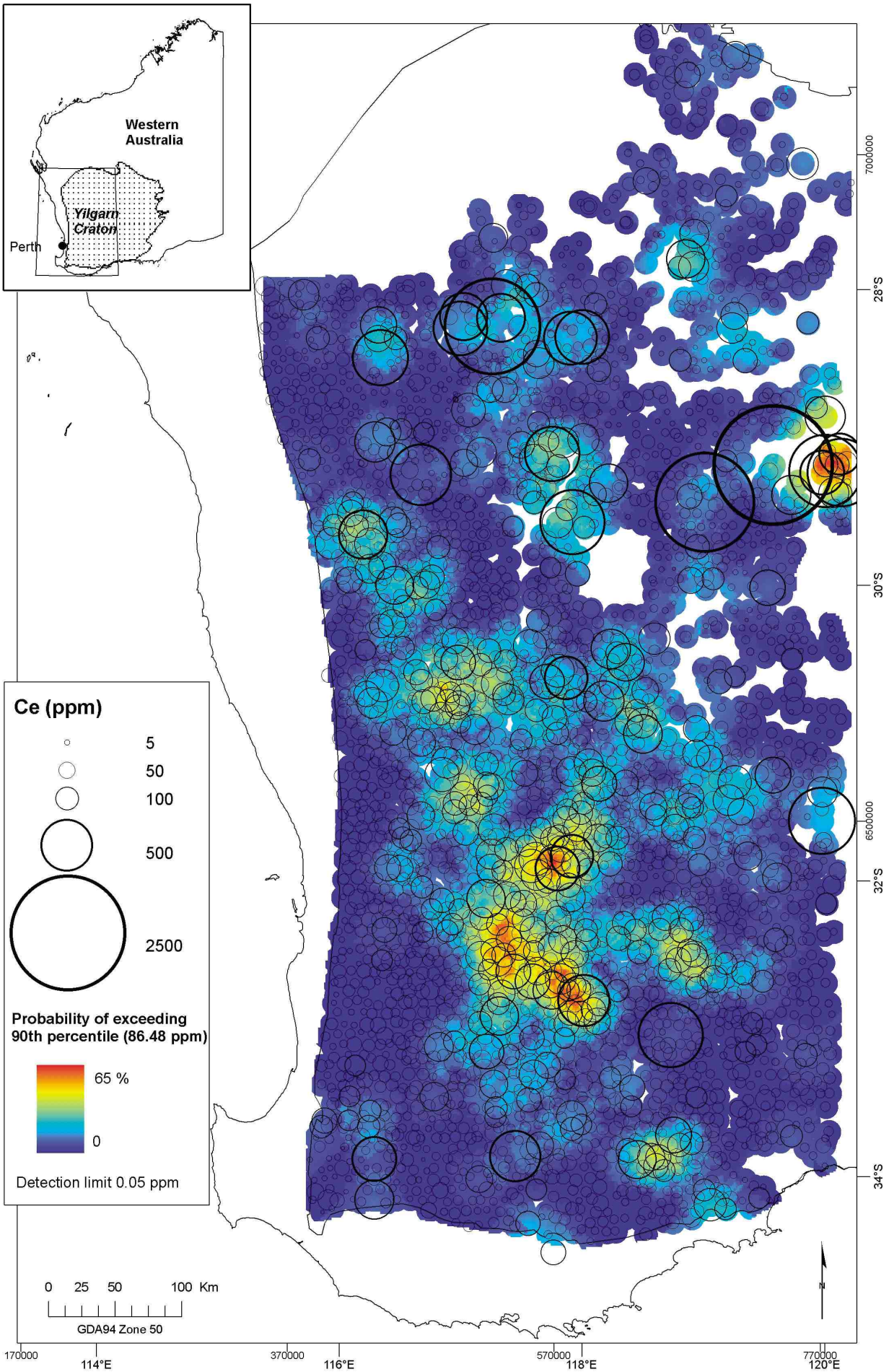
Western Australia
Yilgarn Craton
Perth
Ce (ppm)
5
50
100
500
2500
Probability of exceeding 90th percentile (86.48 ppm)
65 %
0
Detection limit 0.05 ppm
0 25 50 100 Km
GDA94 Zone 50
N
7000000
28°S
30°S
6500000
32°S
34°S
170000
114°E
370000
116°E
570000
118°E
770000
120°E

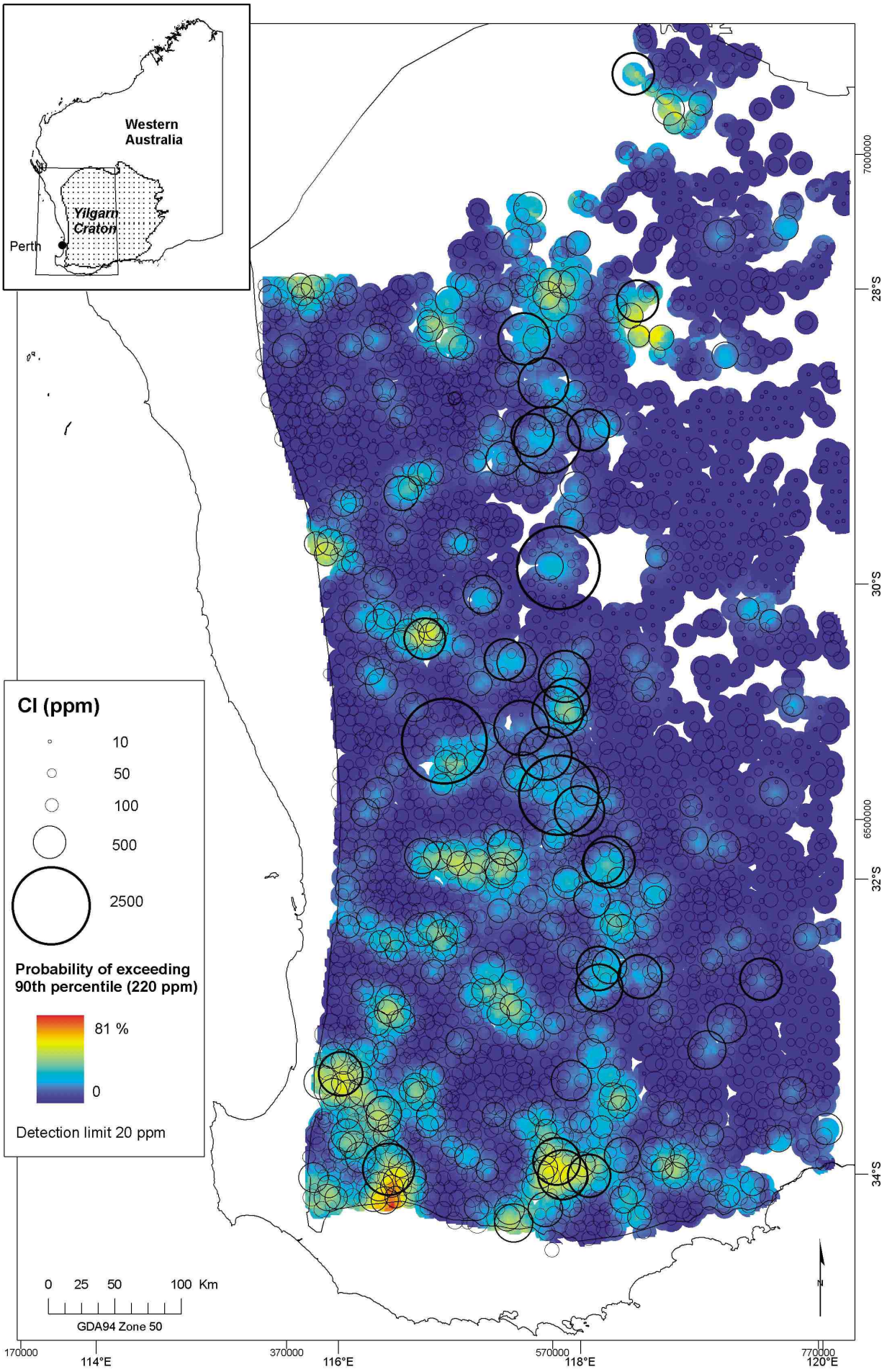
Western Australia
Yilgarn Craton
Perth
Cl (ppm)
10
50
100
500
2500
Probability of exceeding 90th percentile (220 ppm)
81 %
0
Detection limit 20 ppm
0 25 50 100 Km
GDA94 Zone 50
170000
114°E
370000
116°E
570000
118°E
770000
120°E
7000000
28°S
6500000
30°S
32°S
34°S
N

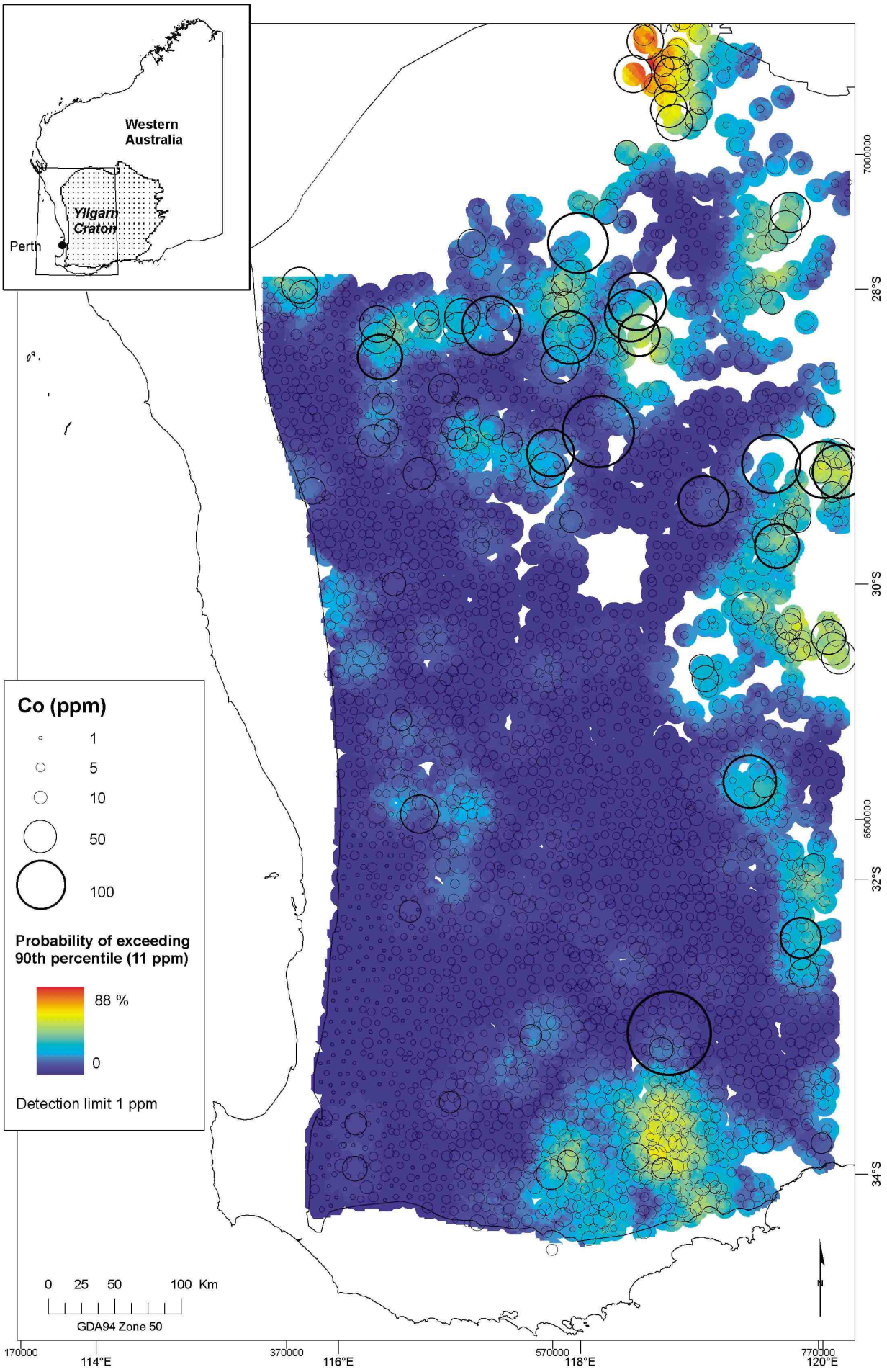
Western Australia
Yilgarn Craton
Perth
Co (ppm)
1
5
10
50
100
Probability of exceeding 90th percentile (11 ppm)
88 %
0
Detection limit 1 ppm
0 25 50 100 Km
GDA94 Zone 50
N
7000000
28°S
30°S
6500000
32°S
34°S
170000
114°E
370000
116°E
570000
118°E
770000
120°E

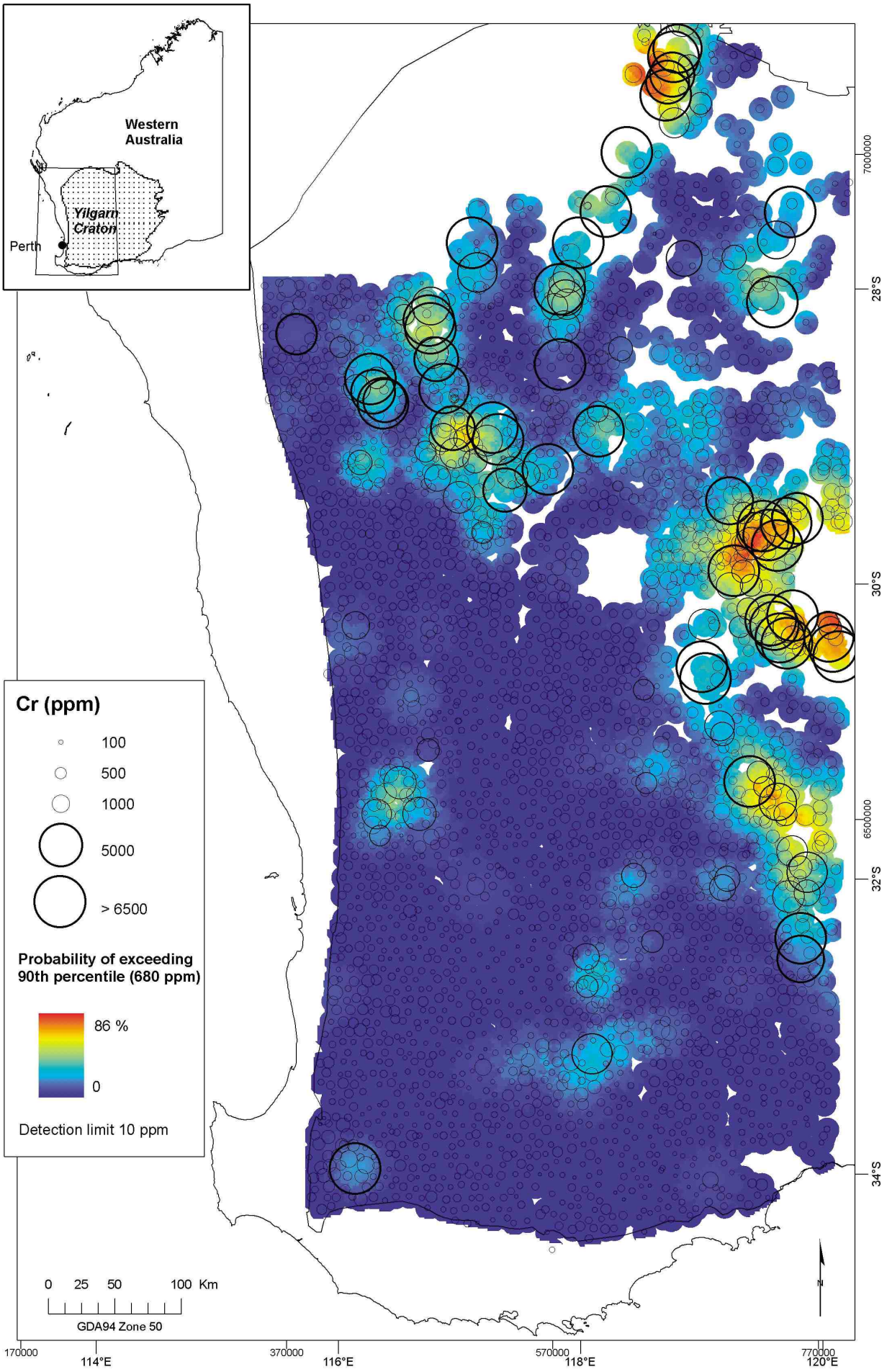
Western Australia
Yilgarn Craton
Perth
Cr (ppm)
100
500
1000
5000
> 6500
Probability of exceeding 90th percentile (680 ppm)
86 %
0
Detection limit 10 ppm
0 25 50 100 Km
GDA94 Zone 50
7000000
28°S
30°S
6500000
32°S
34°S
170000
114°E
370000
116°E
570000
118°E
770000
120°E

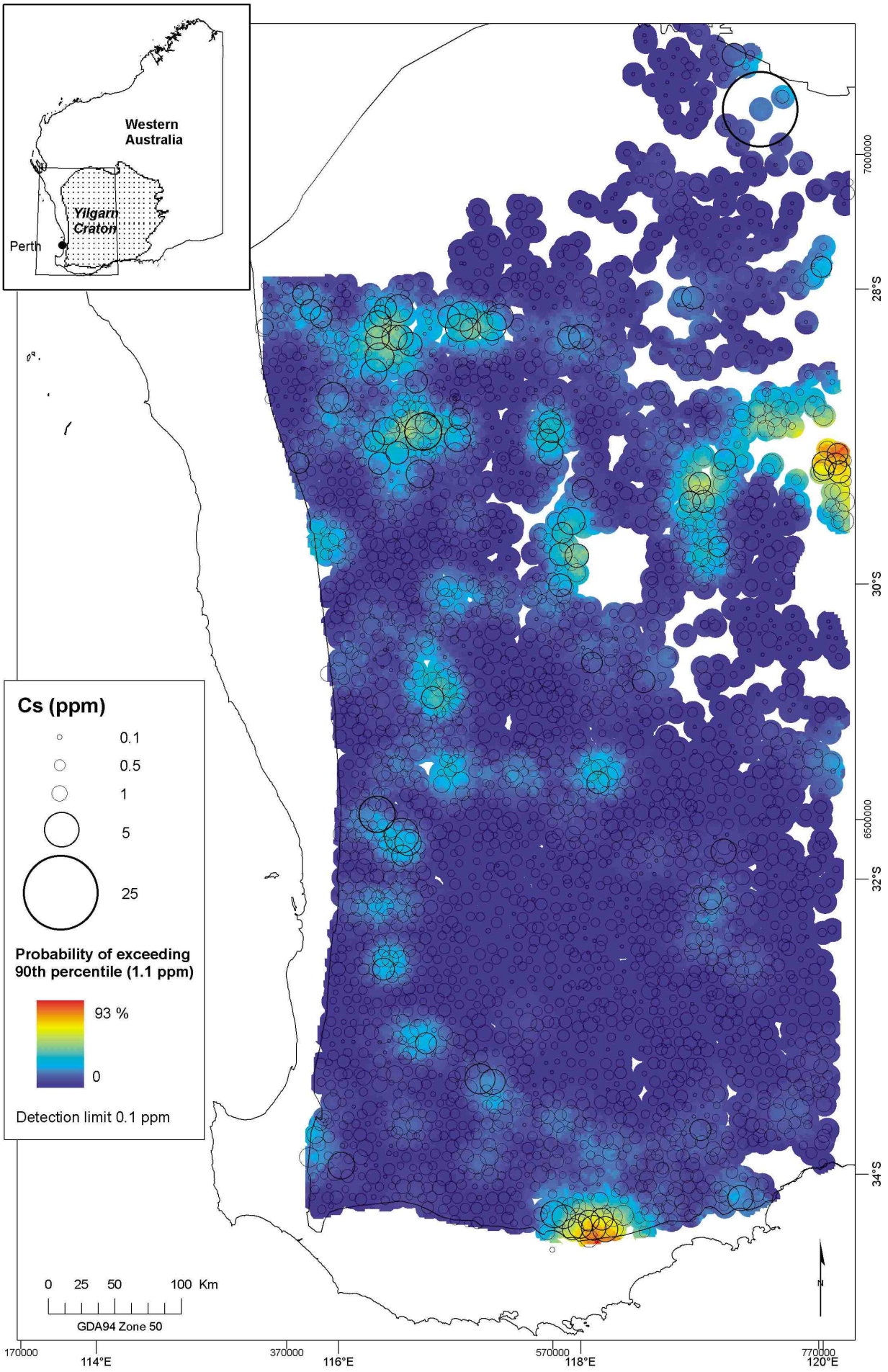
Western Australia
Yilgarn Craton
Perth
Cs (ppm)
0.1
0.5
1
5
25
Probability of exceeding 90th percentile (1.1 ppm)
93 %
0
Detection limit 0.1 ppm
0 25 50 100 Km
GDA94 Zone 50
N
170000
114°E
370000
116°E
570000
118°E
770000
120°E
7000000
28°S
6500000
30°S
32°S
34°S

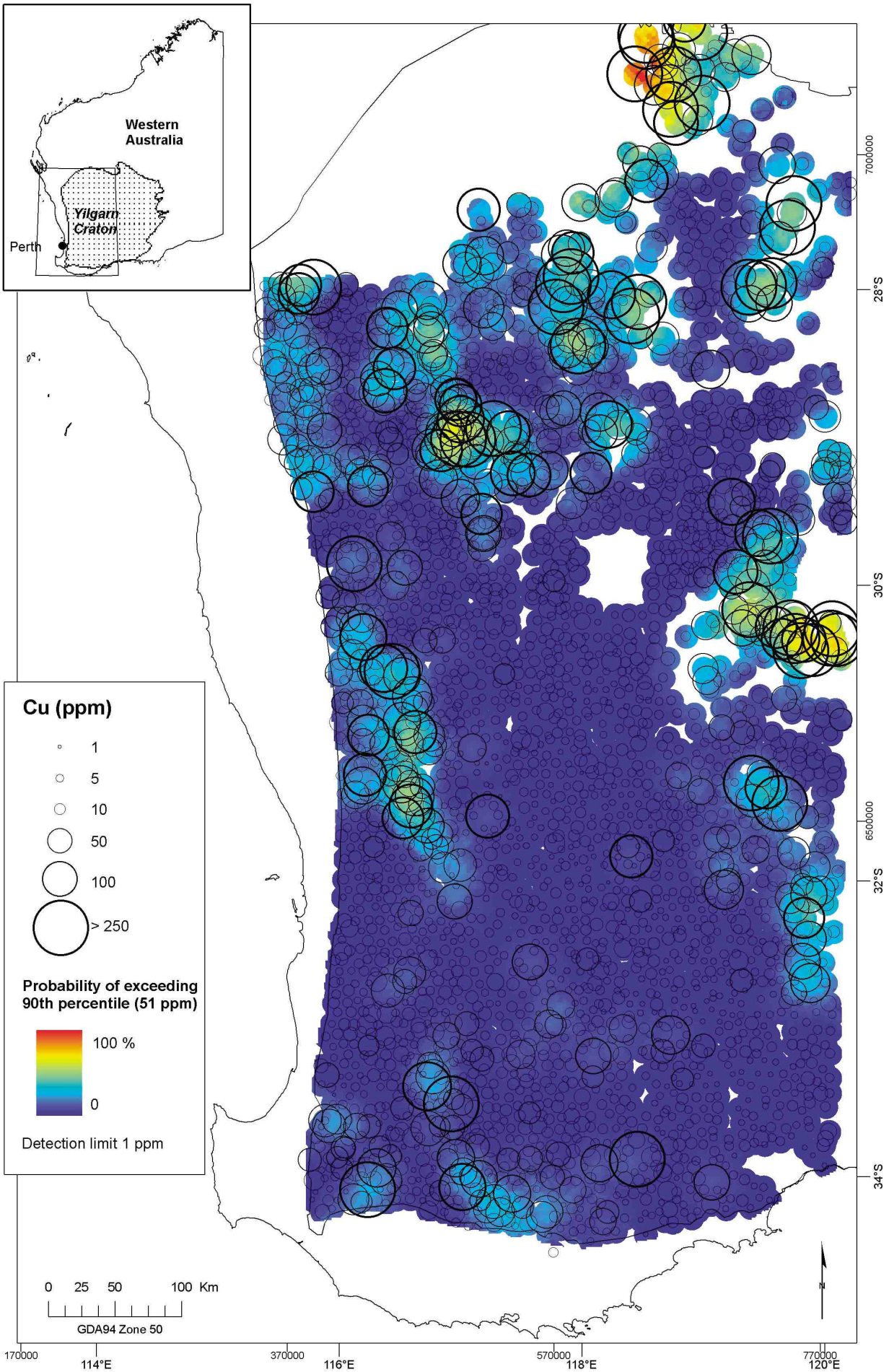
Western Australia
Yilgarn Craton
Perth
Cu (ppm)
1
5
10
50
100
> 250
Probability of exceeding 90th percentile (51 ppm)
100 %
0
Detection limit 1 ppm
0 25 50 100 Km
GDA94 Zone 50
N
7000000
28°S
30°S
6500000
32°S
34°S
170000
114°E
370000
116°E
570000
118°E
770000
120°E

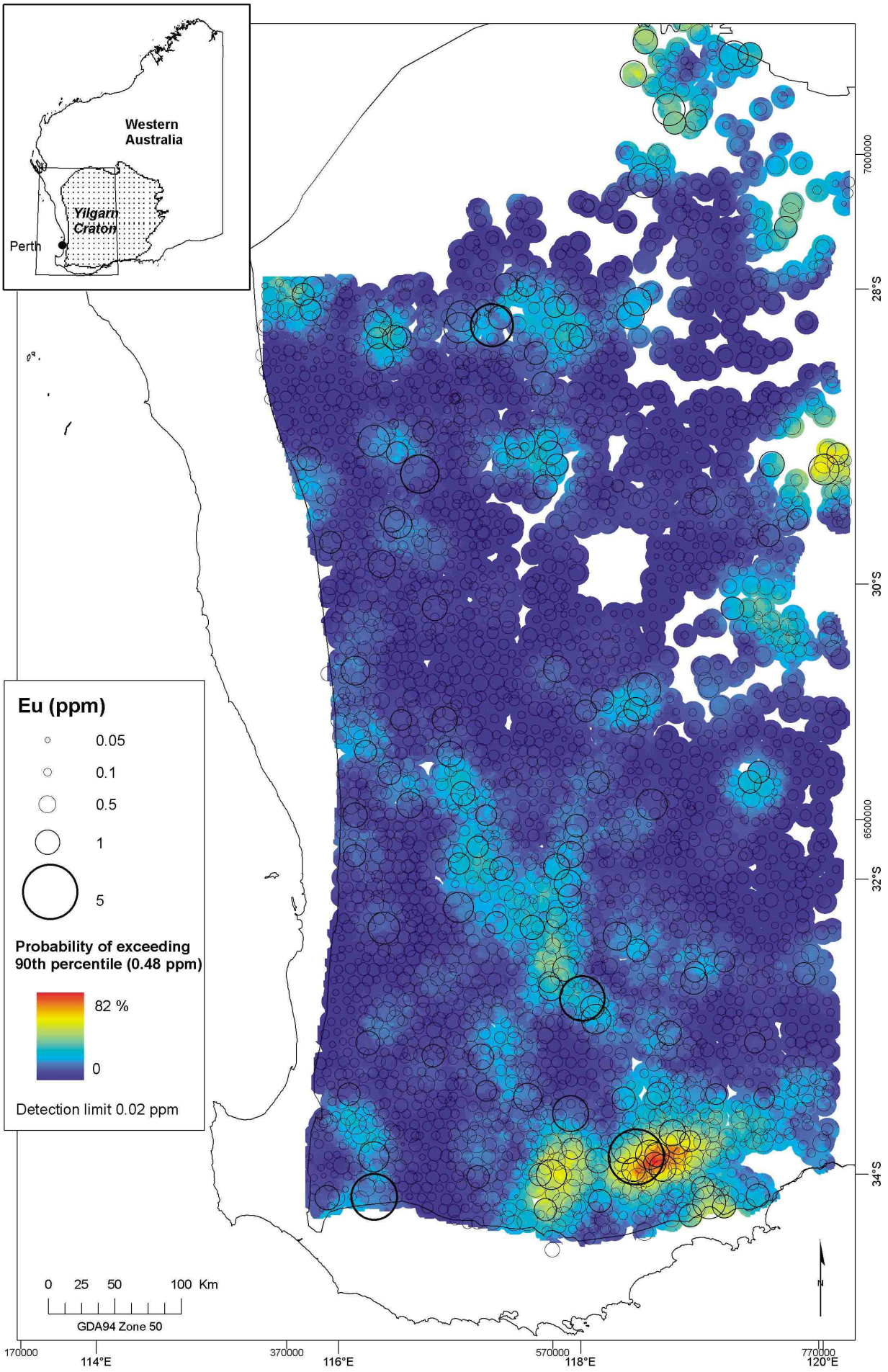
Western Australia
Yilgarn Craton
Perth
Eu (ppm)
0.05
0.1
0.5
1
5
Probability of exceeding 90th percentile (0.48 ppm)
82 %
0
Detection limit 0.02 ppm
0 25 50 100 Km
GDA94 Zone 50
7000000
28°S
30°S
6500000
32°S
34°S
170000
114°E
370000
116°E
570000
118°E
770000
120°E

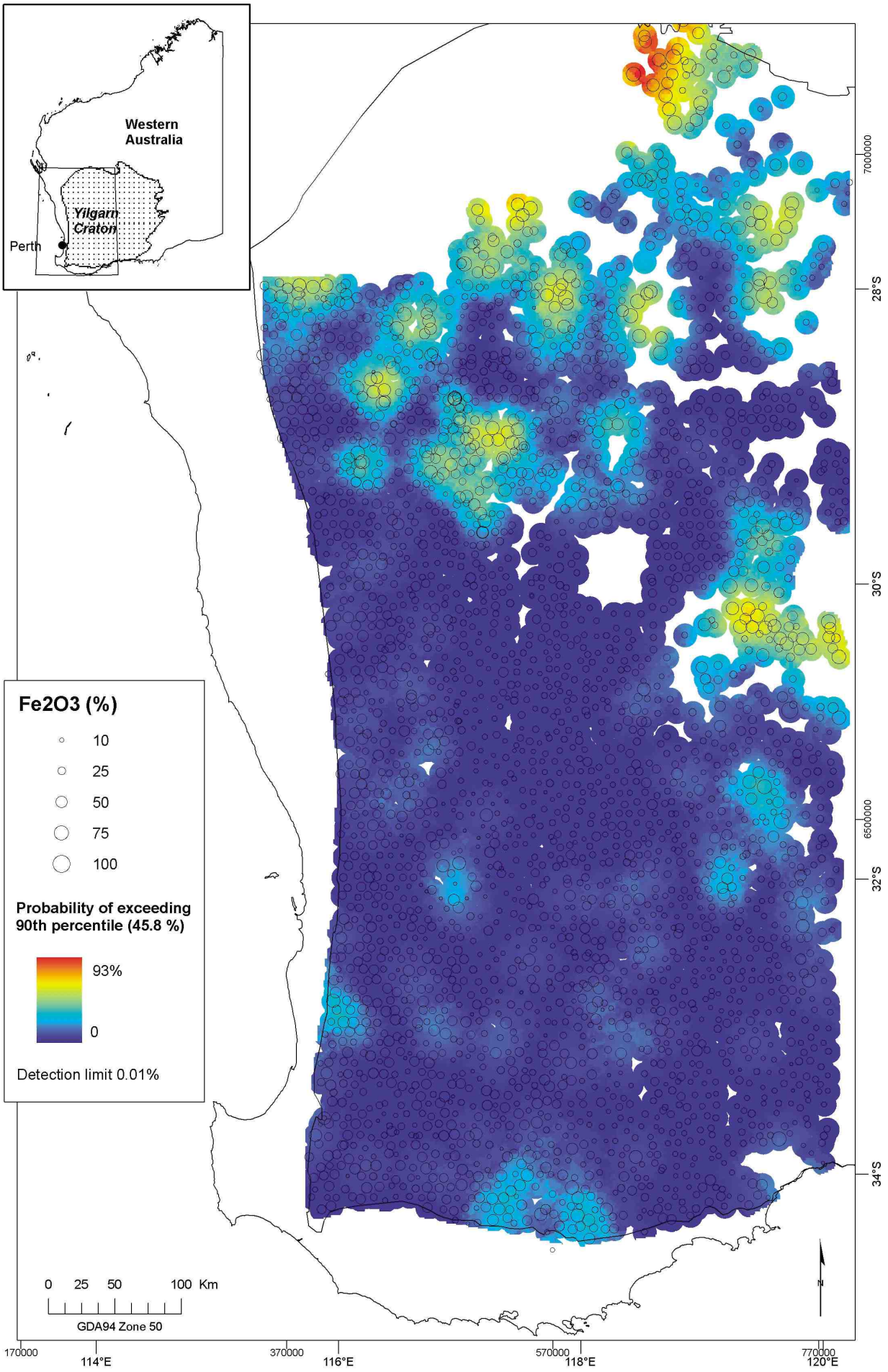
Western Australia
Yilgarn Craton
Perth
Fe2O3 (%)
10
25
50
75
100
Probability of exceeding 90th percentile (45.8 %)
93%
0
Detection limit 0.01%
0 25 50 100 Km
GDA94 Zone 50
N
7000000
28°S
30°S
6500000
32°S
34°S
170000
114°E
370000
116°E
570000
118°E
770000
120°E

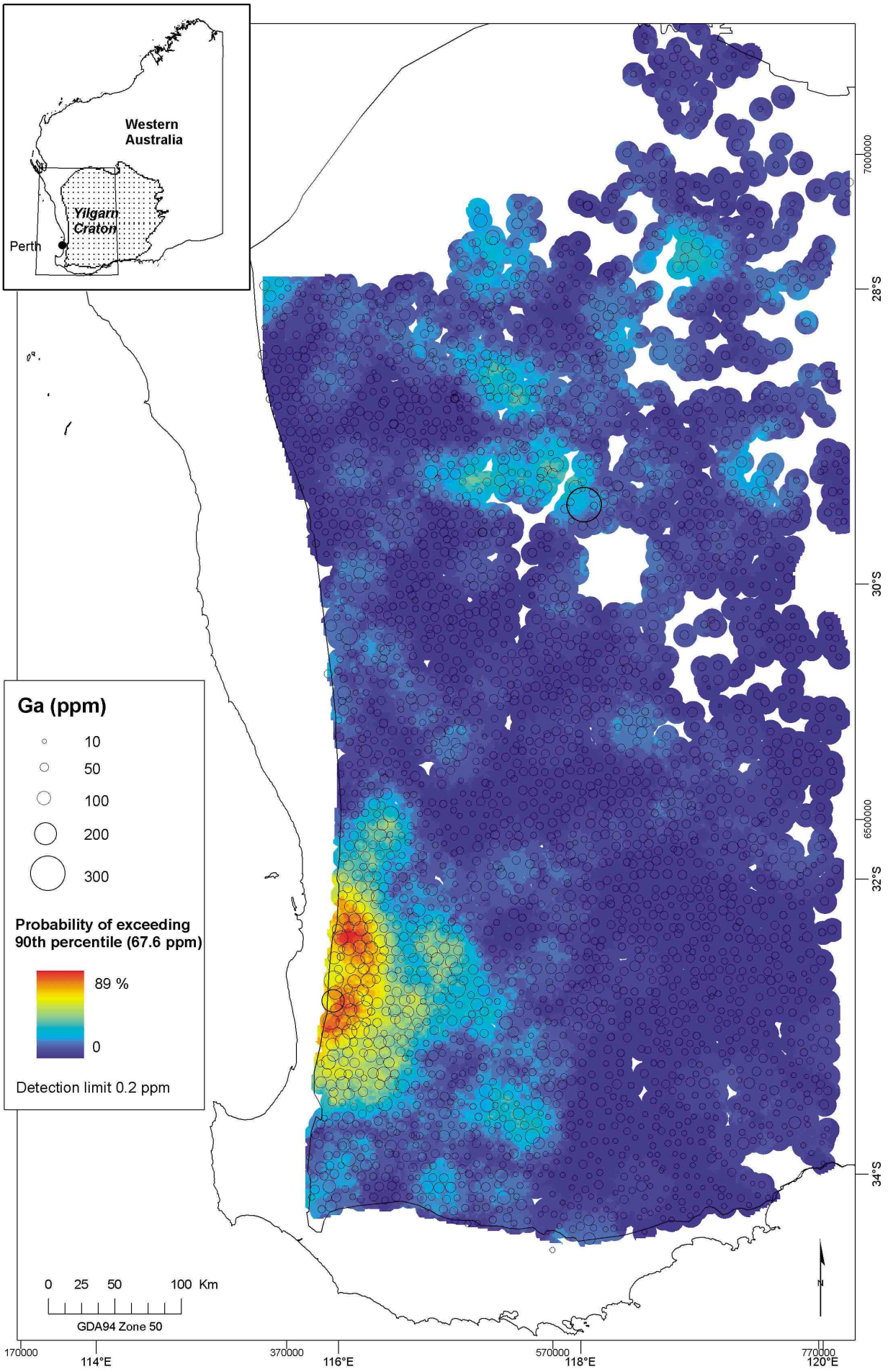
Western Australia
Yilgarn Craton
Perth
Ga (ppm)
10
50
100
200
300
Probability of exceeding 90th percentile (67.6 ppm)
89 %
0
Detection limit 0.2 ppm
0 25 50 100 Km
GDA94 Zone 50
N
7000000
28°S
30°S
6500000
32°S
34°S
170000
114°E
370000
116°E
570000
118°E
770000
120°E

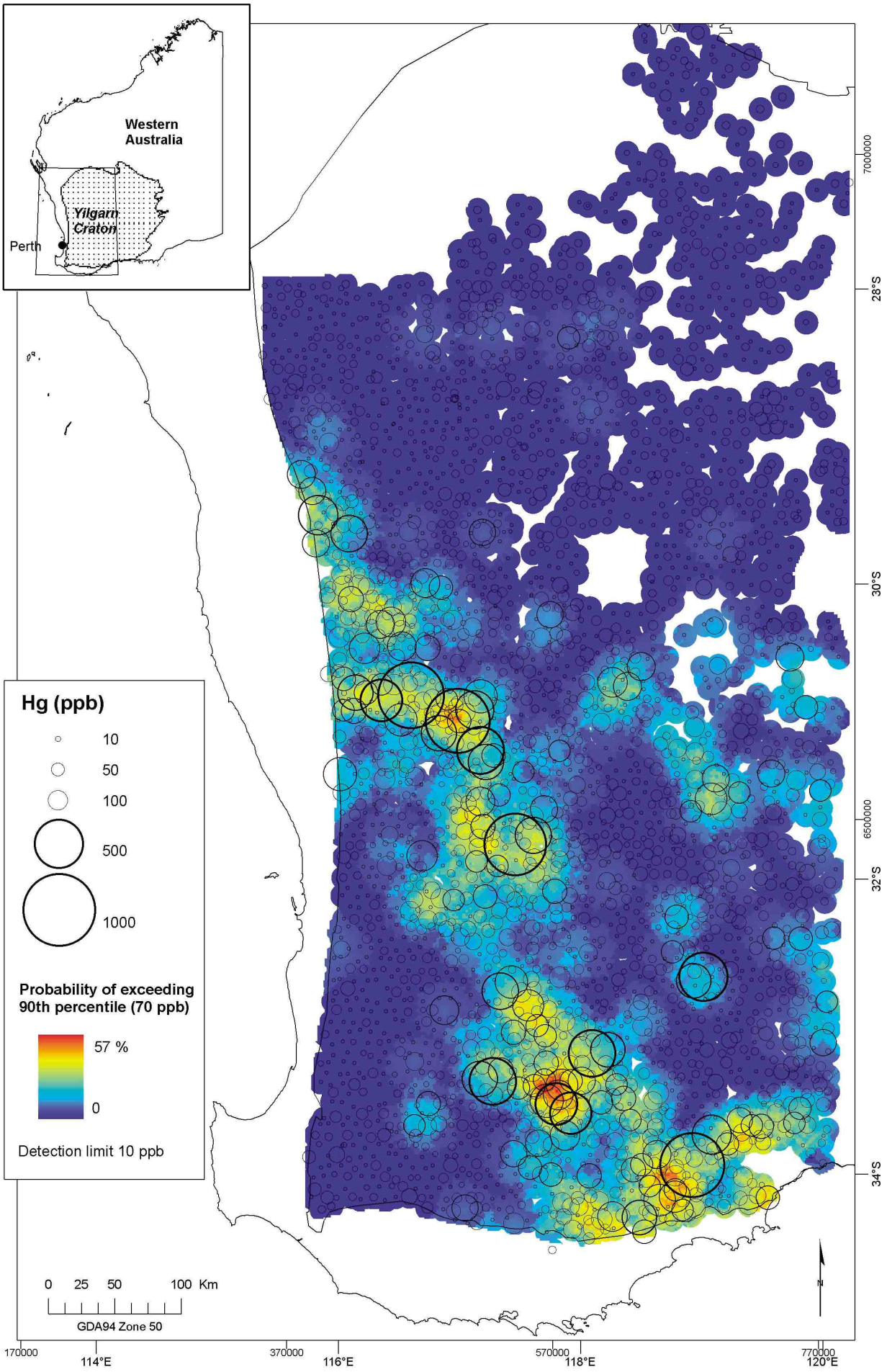
Western Australia
Yilgarn Craton
Perth
Hg (ppb)
10
50
100
500
1000
Probability of exceeding 90th percentile (70 ppb)
57 %
0
Detection limit 10 ppb
0 25 50 100 Km
GDA94 Zone 50
7000000
28°S
30°S
6500000
32°S
34°S
170000
114°E
370000
116°E
570000
118°E
770000
120°E

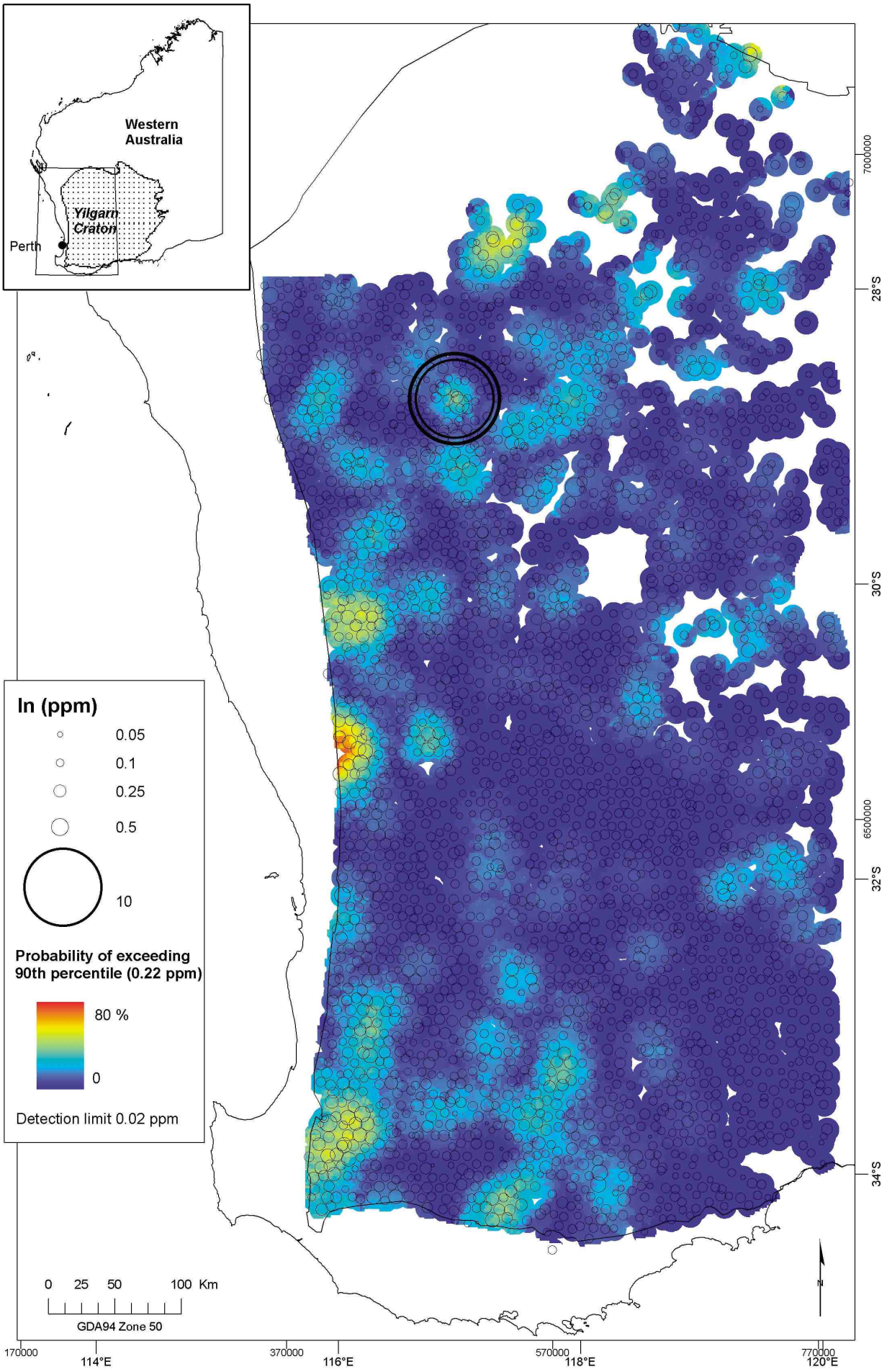
Western Australia
Yilgarn Craton
Perth
ln (ppm)
0.05
0.1
0.25
0.5
10
Probability of exceeding 90th percentile (0.22 ppm)
80 %
0
Detection limit 0.02 ppm
0 25 50 100 Km
GDA94 Zone 50
170000
114°E
370000
116°E
570000
118°E
770000
120°E
7000000
28°S
6500000
30°S
32°S
34°S
N

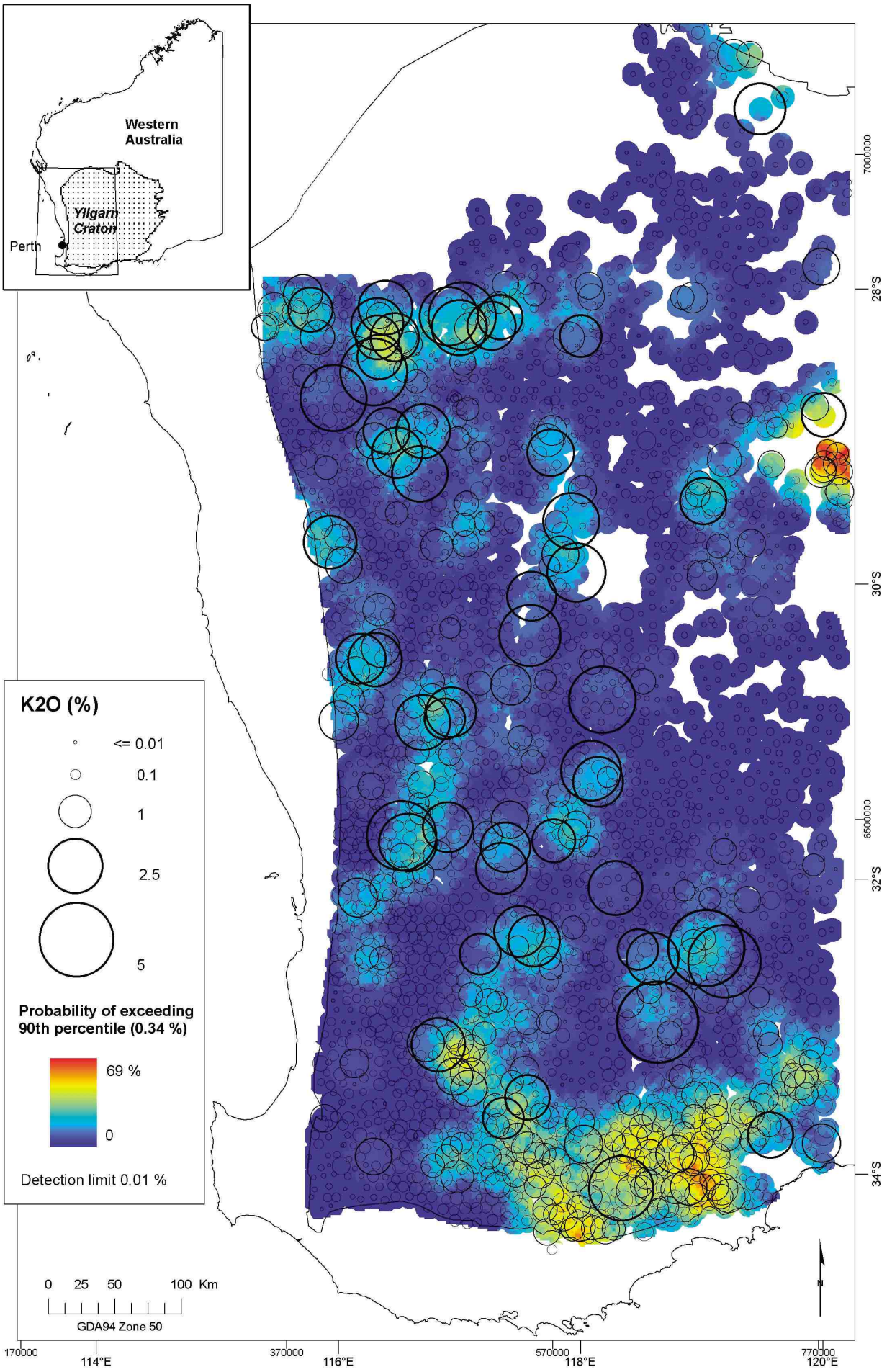
Western Australia
Yilgarn Craton
Perth
K2O (%)
<= 0.01
0.1
1
2.5
5
Probability of exceeding 90th percentile (0.34 %)
69 %
0
Detection limit 0.01 %
0 25 50 100 Km
GDA94 Zone 50
170000
114°E
370000
116°E
570000
118°E
770000
120°E
7000000
28°S
6500000
30°S
32°S
34°S
N

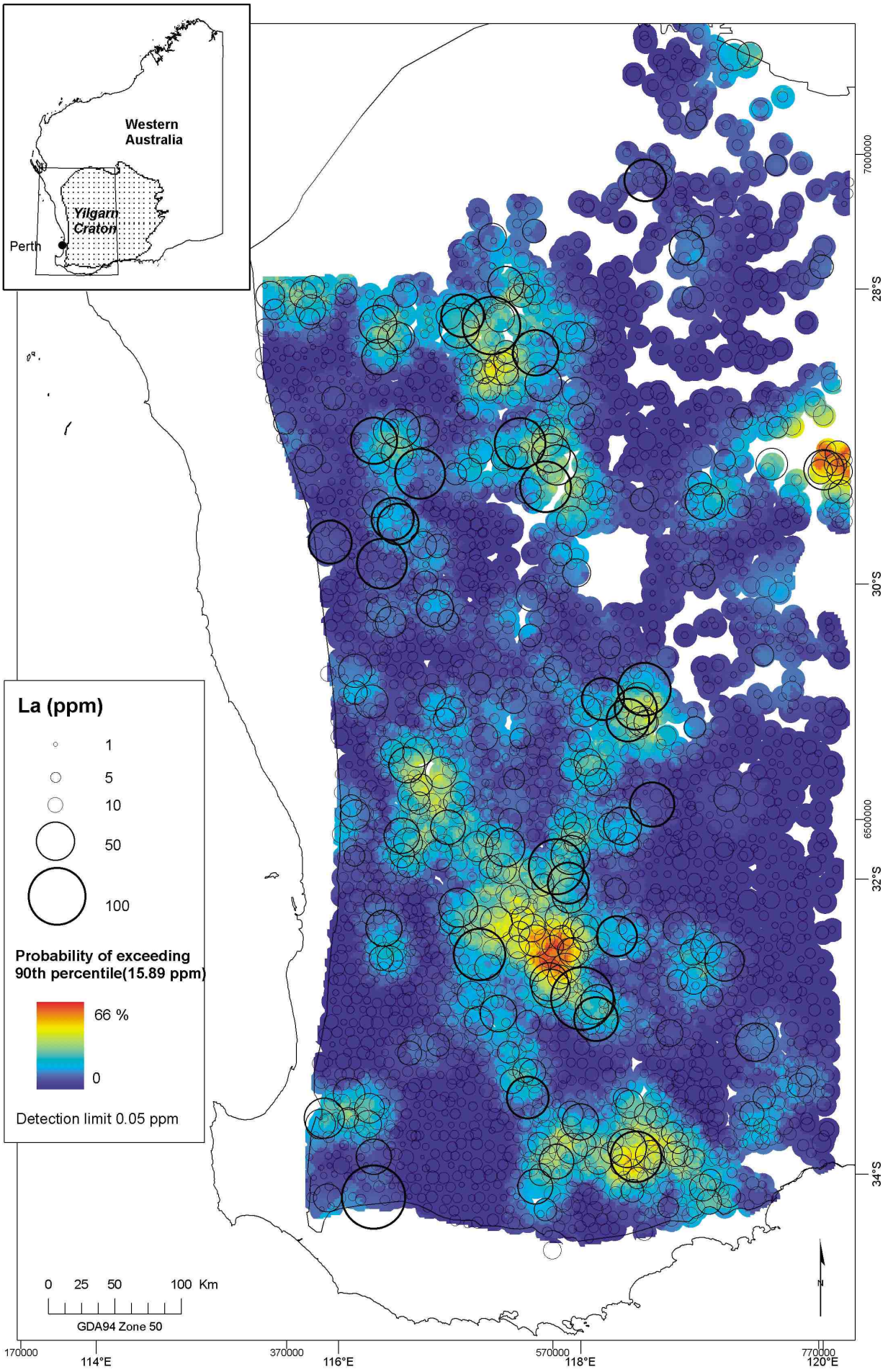
Western Australia
Yilgarn Craton
Perth
La (ppm)
1
5
10
50
100
Probability of exceeding 90th percentile(15.89 ppm)
66 %
0
Detection limit 0.05 ppm
0 25 50 100 Km
GDA94 Zone 50
N
7000000
28°S
30°S
6500000
32°S
34°S
170000
114°E
370000
116°E
570000
118°E
770000
120°E

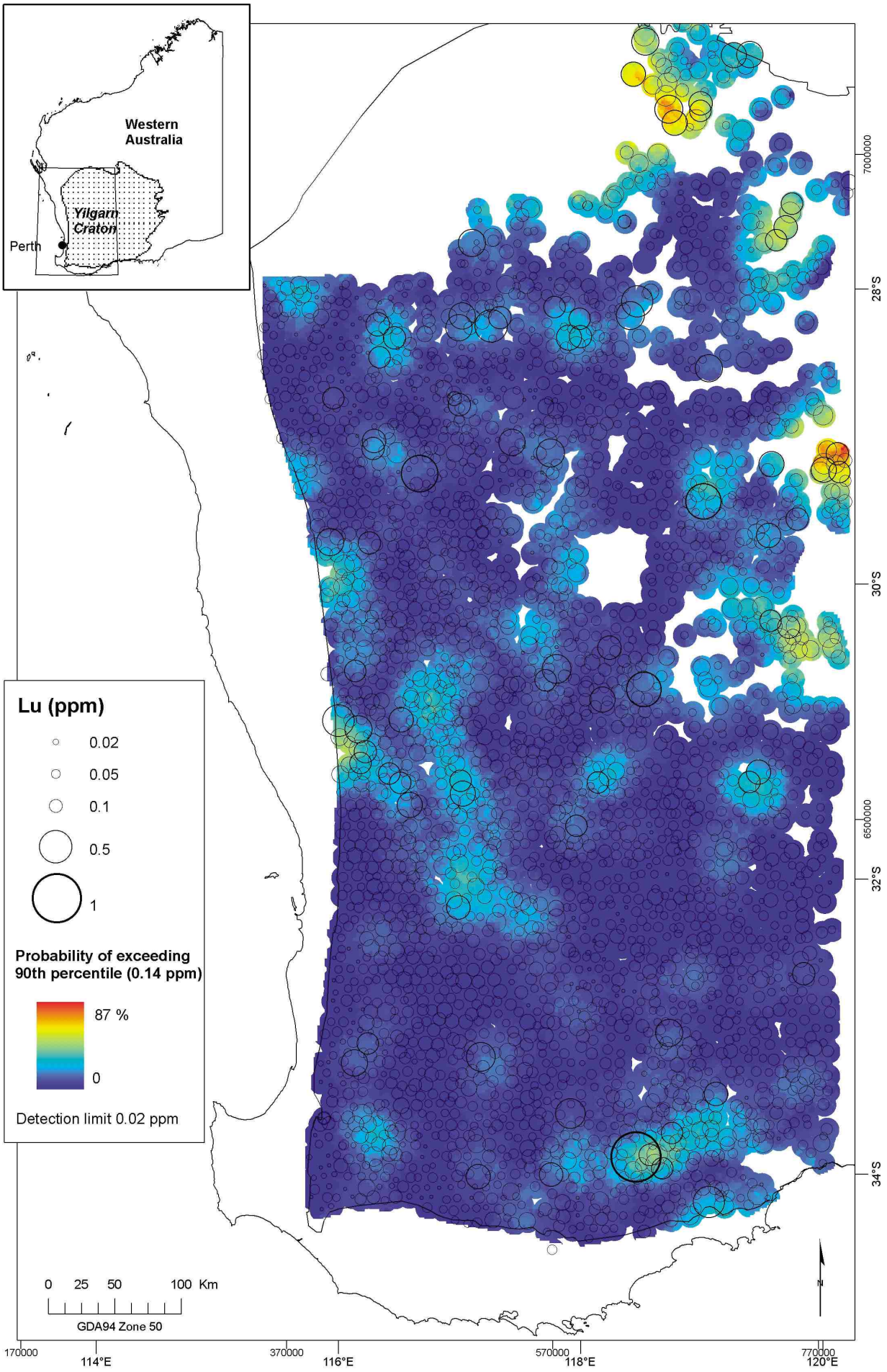
Western Australia
Yilgarn Craton
Perth
Lu (ppm)
0.02
0.05
0.1
0.5
1
Probability of exceeding 90th percentile (0.14 ppm)
87 %
0
Detection limit 0.02 ppm
0 25 50 100 Km
GDA94 Zone 50
170000
114°E
370000
116°E
570000
118°E
770000
120°E
7000000
28°S
6500000
30°S
32°S
34°S
N

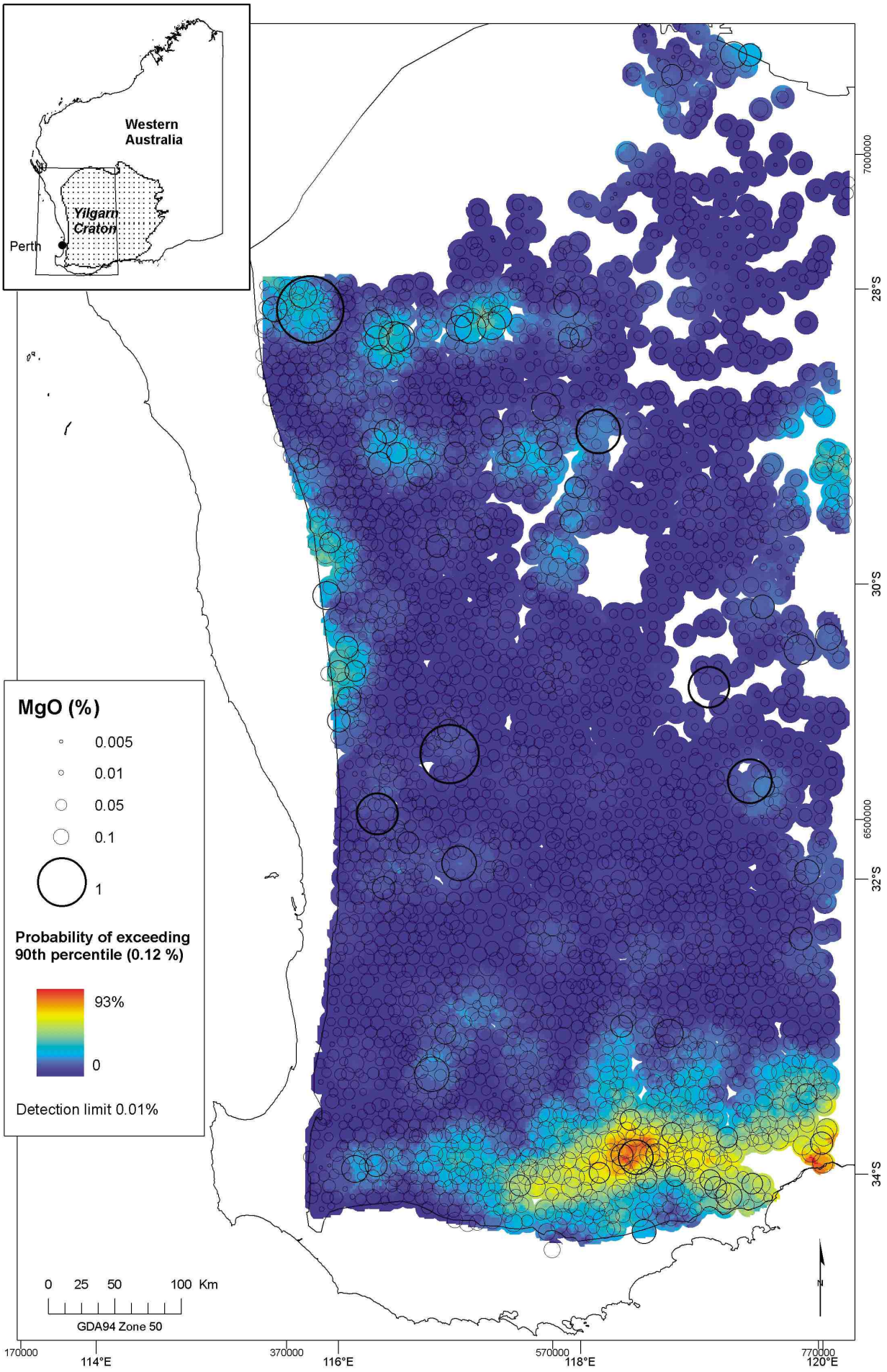
Western Australia
Yilgarn Craton
Perth
MgO (%)
0.005
0.01
0.05
0.1
1
Probability of exceeding 90th percentile (0.12 %)
93%
0
Detection limit 0.01%
0 25 50 100 Km
GDA94 Zone 50
170000
114°E
370000
116°E
570000
118°E
770000
120°E
7000000
28°S
6500000
30°S
32°S
34°S
N

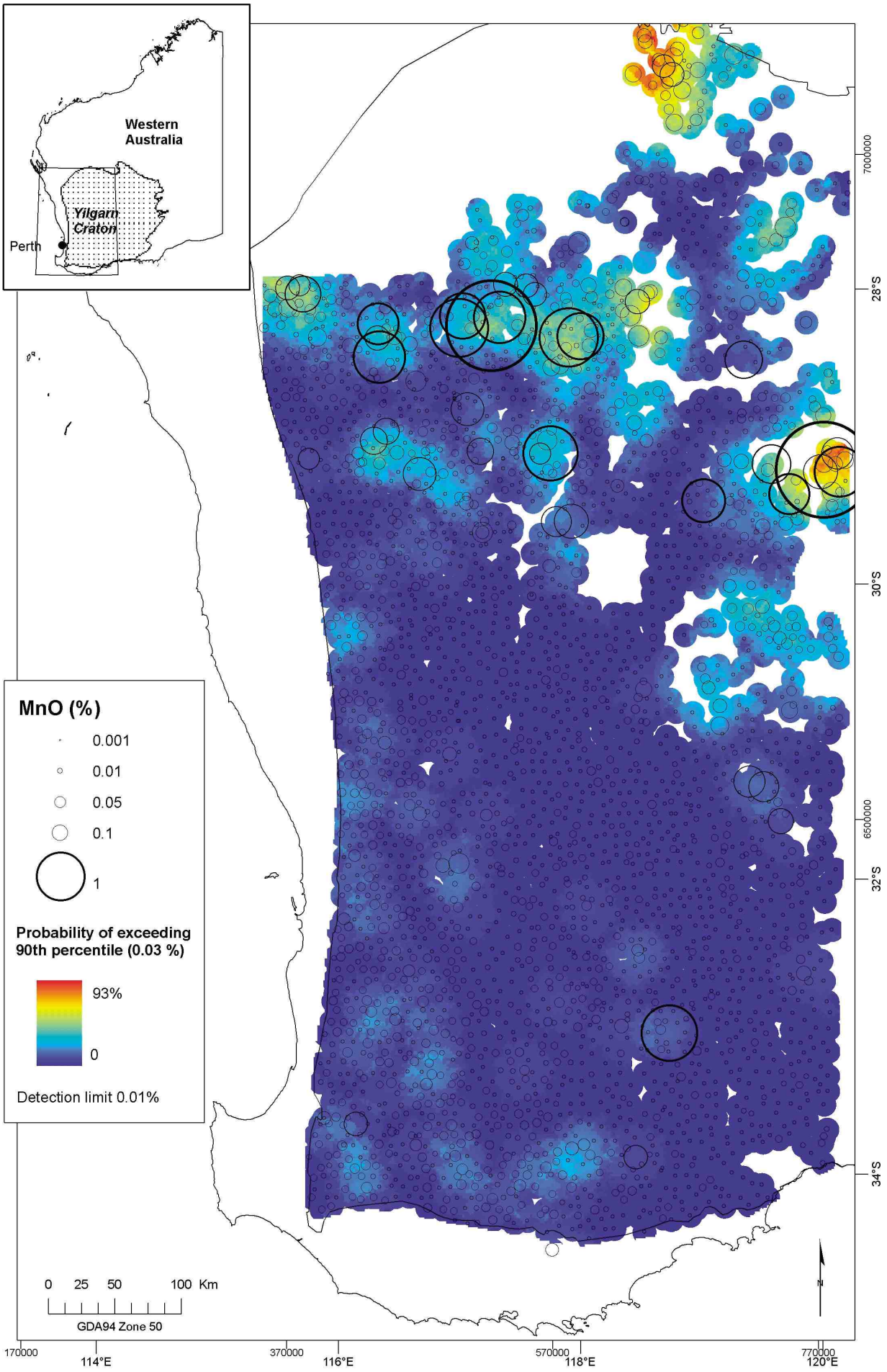
Western Australia
Yilgarn Craton
Perth
MnO (%)
0.001
0.01
0.05
0.1
1
Probability of exceeding 90th percentile (0.03 %)
93%
0
Detection limit 0.01%
0 25 50 100 Km
GDA94 Zone 50
170000
114°E
370000
116°E
570000
118°E
770000
120°E
7000000
28°S
6500000
30°S
32°S
34°S
N

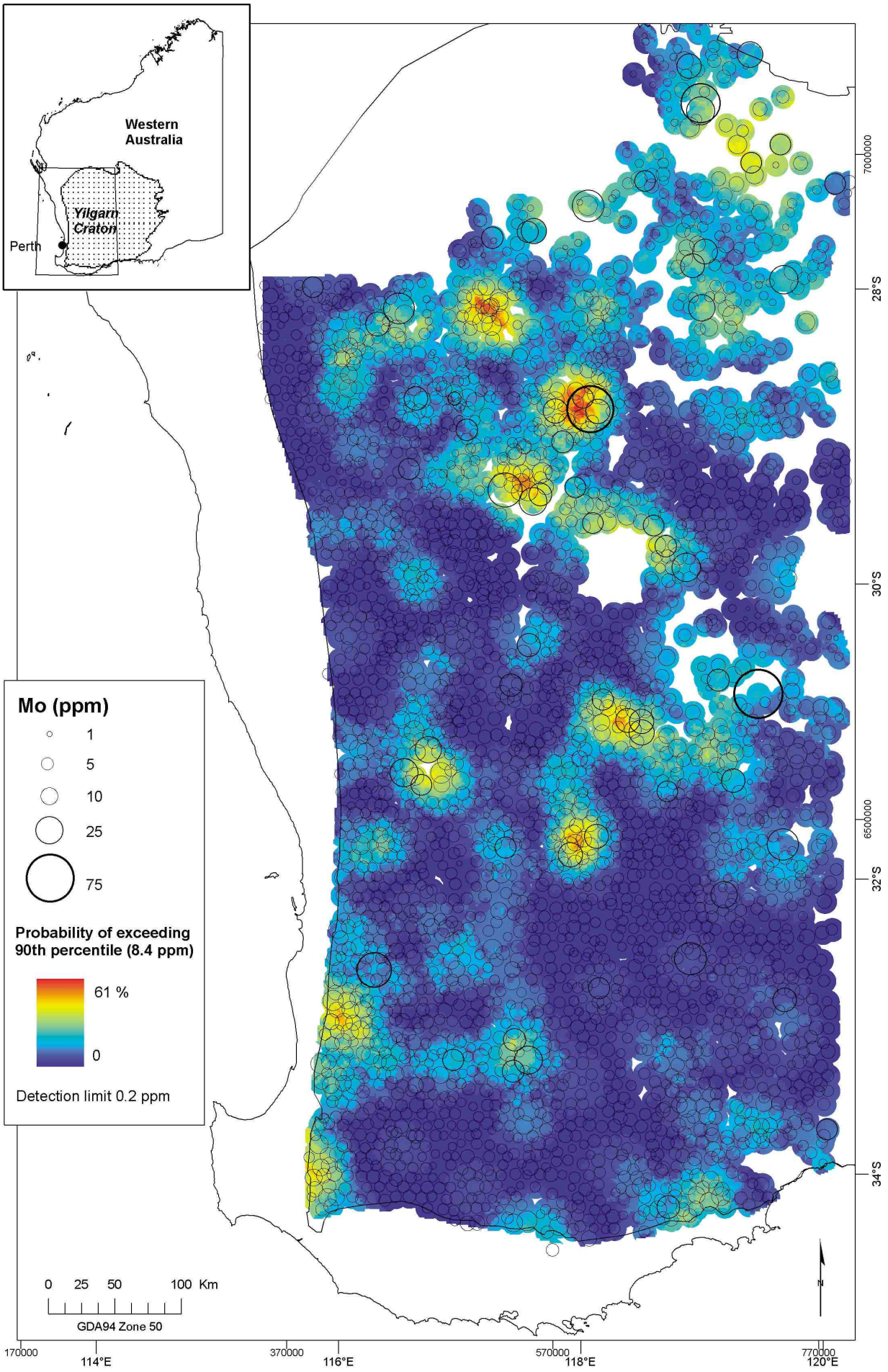
Western Australia
Yilgarn Craton
Perth
Mo (ppm)
1
5
10
25
75
Probability of exceeding 90th percentile (8.4 ppm)
61 %
0
Detection limit 0.2 ppm
0 25 50 100 Km
GDA94 Zone 50
N
7000000
28°S
30°S
6500000
32°S
34°S
170000
114°E
370000
116°E
570000
118°E
770000
120°E

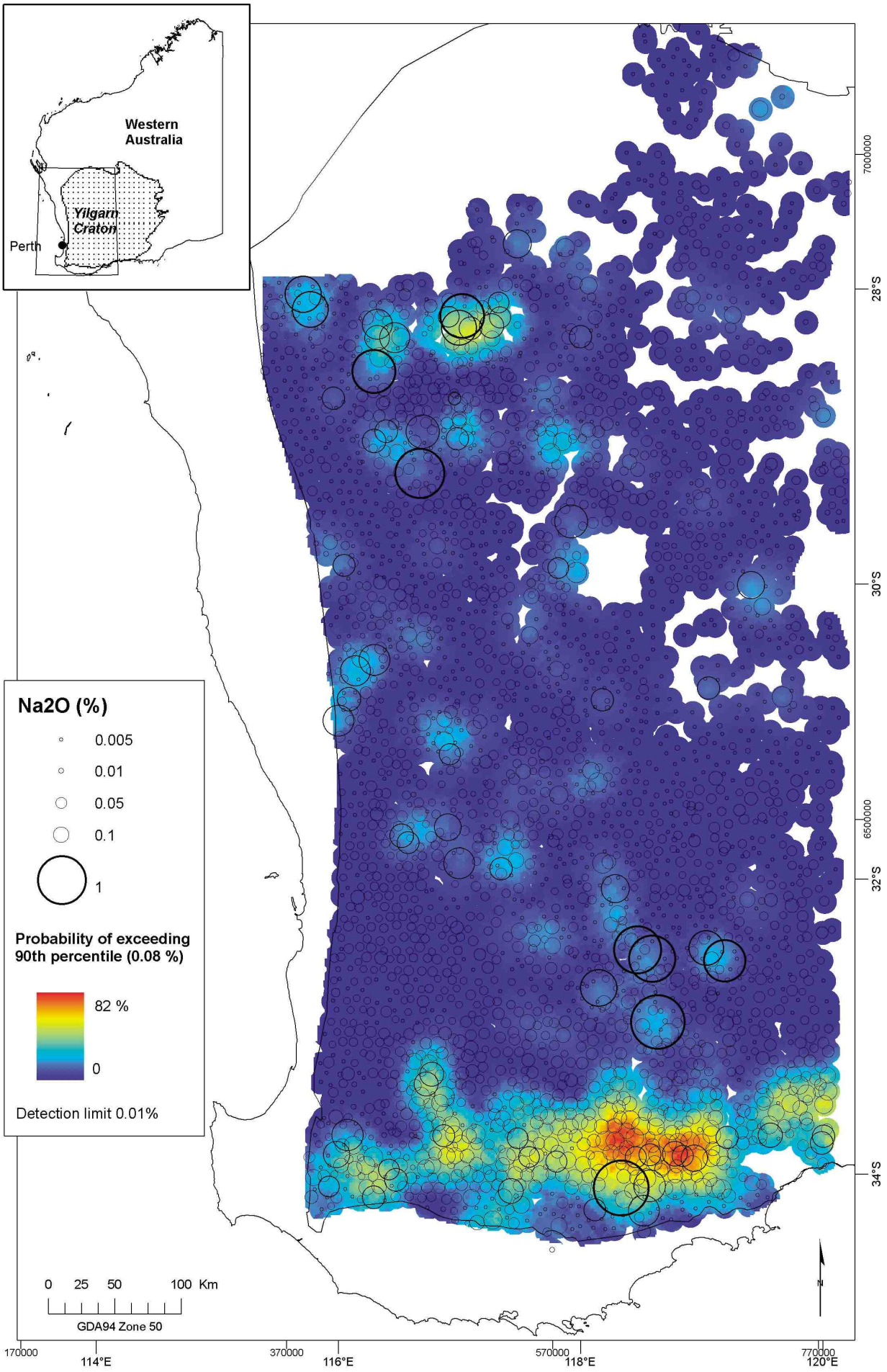
Western Australia
Yilgarn Craton
Perth
Na2O (%)
0.005
0.01
0.05
0.1
1
Probability of exceeding 90th percentile (0.08 %)
82 %
0
Detection limit 0.01%
0 25 50 100 Km
GDA94 Zone 50
170000
114°E
370000
116°E
570000
118°E
770000
120°E
7000000
28°S
6500000
30°S
32°S
34°S
N

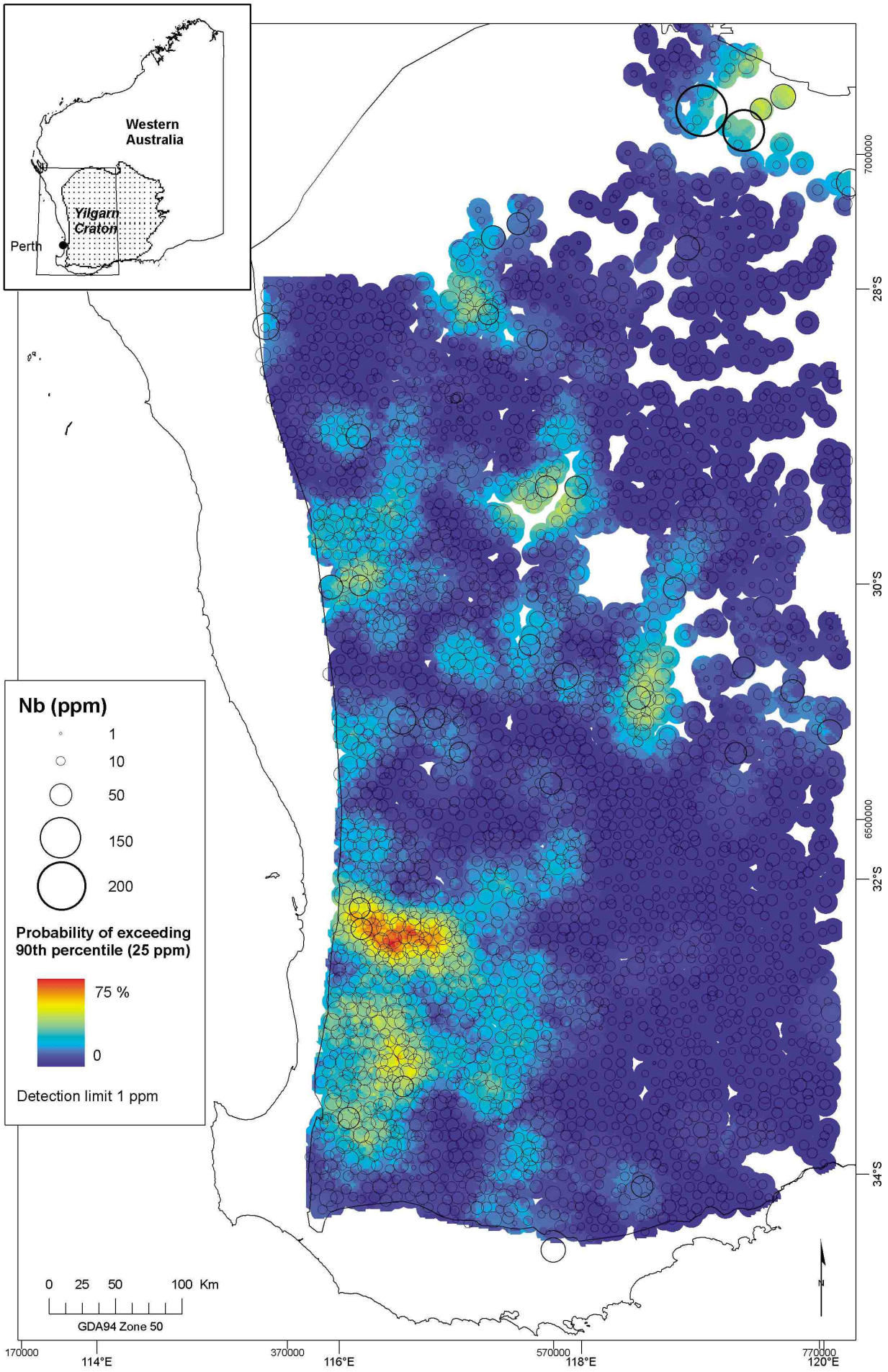
Western Australia
Yilgarn Craton
Perth
Nb (ppm)
1
10
50
150
200
Probability of exceeding 90th percentile (25 ppm)
75 %
0
Detection limit 1 ppm
0 25 50 100 Km
GDA94 Zone 50
170000
114°E
370000
116°E
570000
118°E
770000
120°E
7000000
28°S
6500000
30°S
32°S
34°S
N

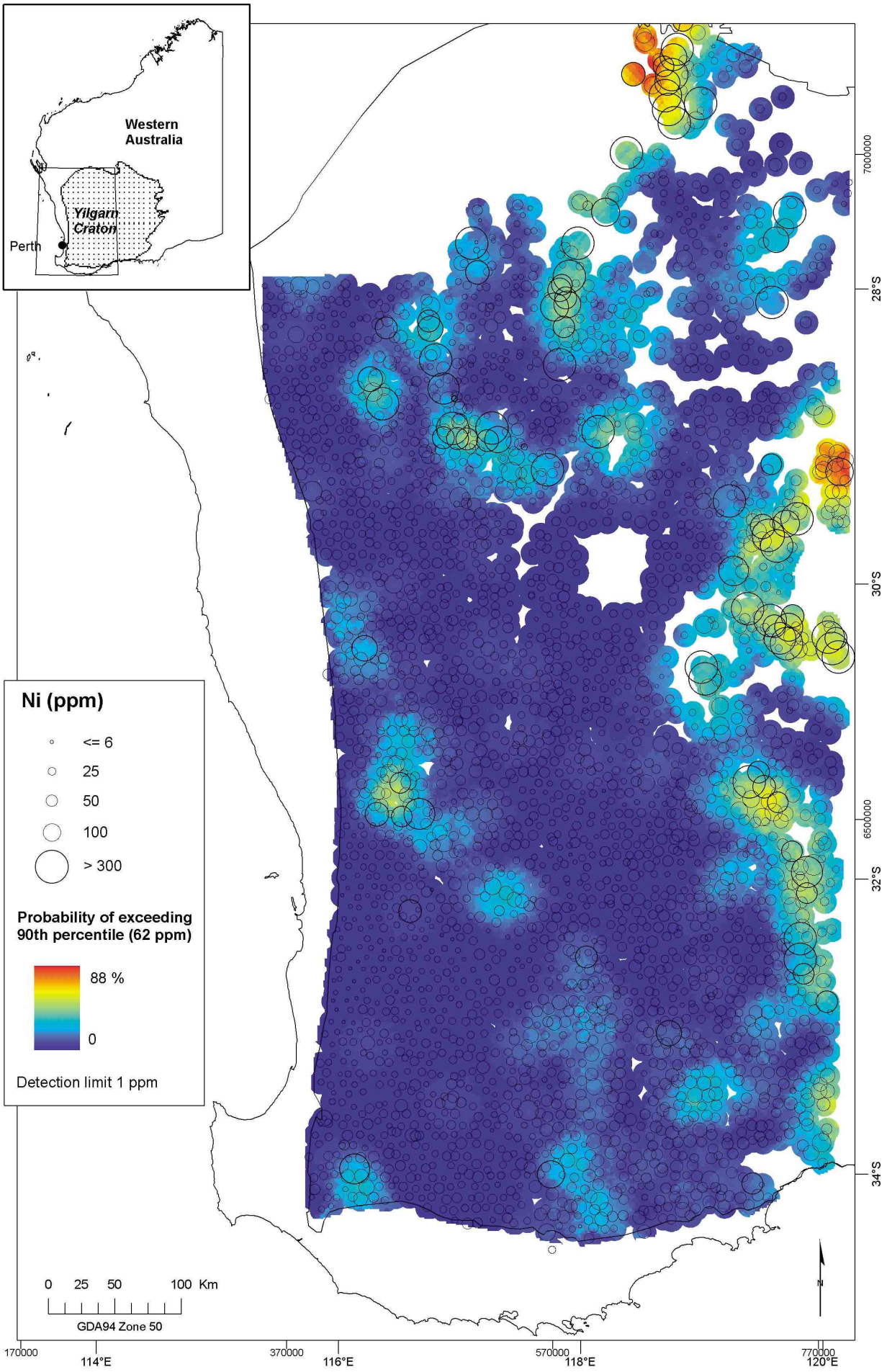
Western Australia
Yilgarn Craton
Perth
Ni (ppm)
<= 6
25
50
100
> 300
Probability of exceeding 90th percentile (62 ppm)
88 %
0
Detection limit 1 ppm
0 25 50 100 Km
GDA94 Zone 50
N
170000
114°E
370000
116°E
570000
118°E
770000
120°E
7000000
28°S
6500000
30°S
32°S
34°S

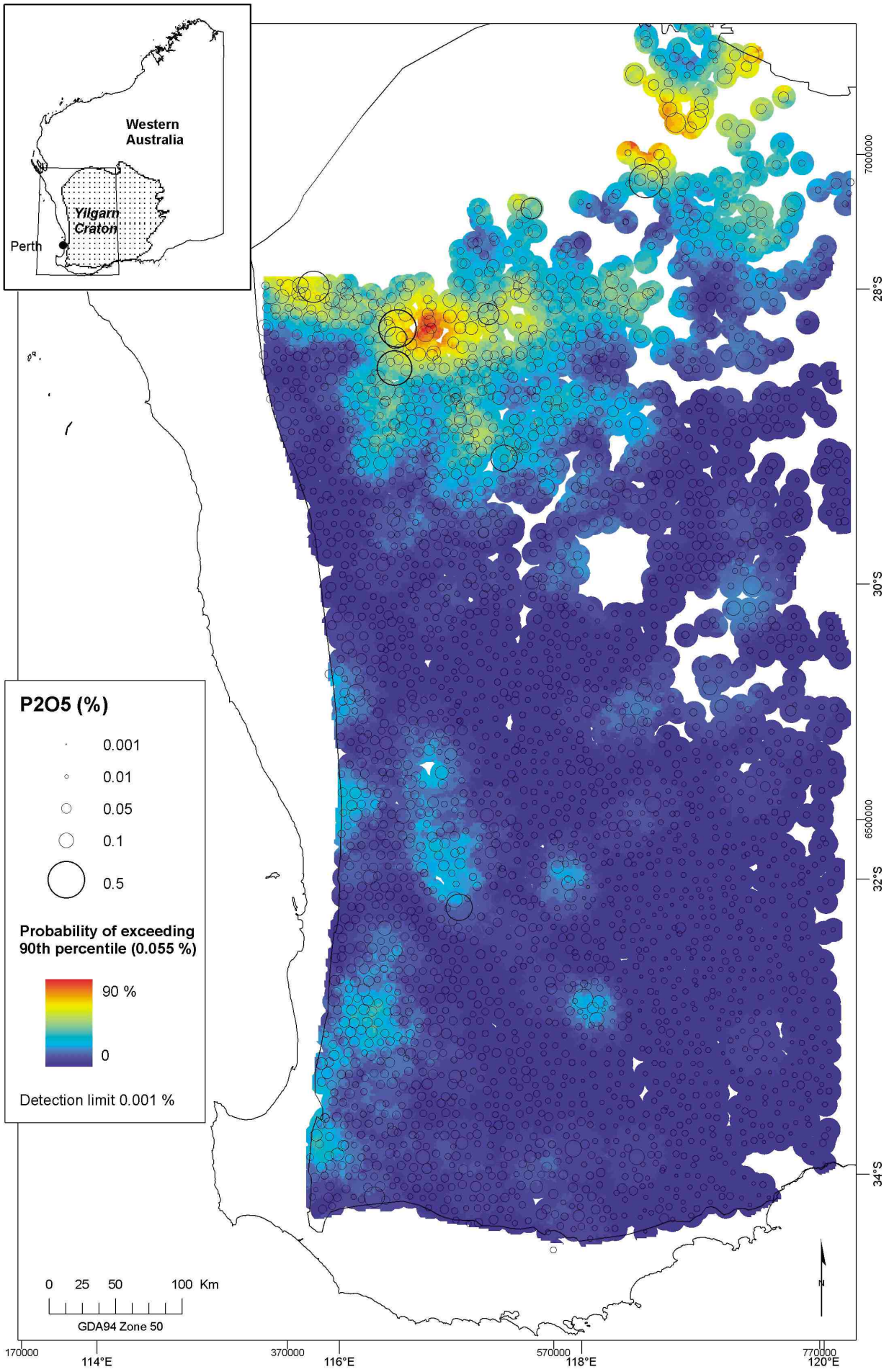
Western Australia
Yilgarn Craton
Perth
P2O5 (%)
0.001
0.01
0.05
0.1
0.5
Probability of exceeding 90th percentile (0.055 %)
90 %
0
Detection limit 0.001 %
0 25 50 100 Km
GDA94 Zone 50
170000
114°E
370000
116°E
570000
118°E
770000
120°E
7000000
28°S
6500000
30°S
32°S
34°S
N

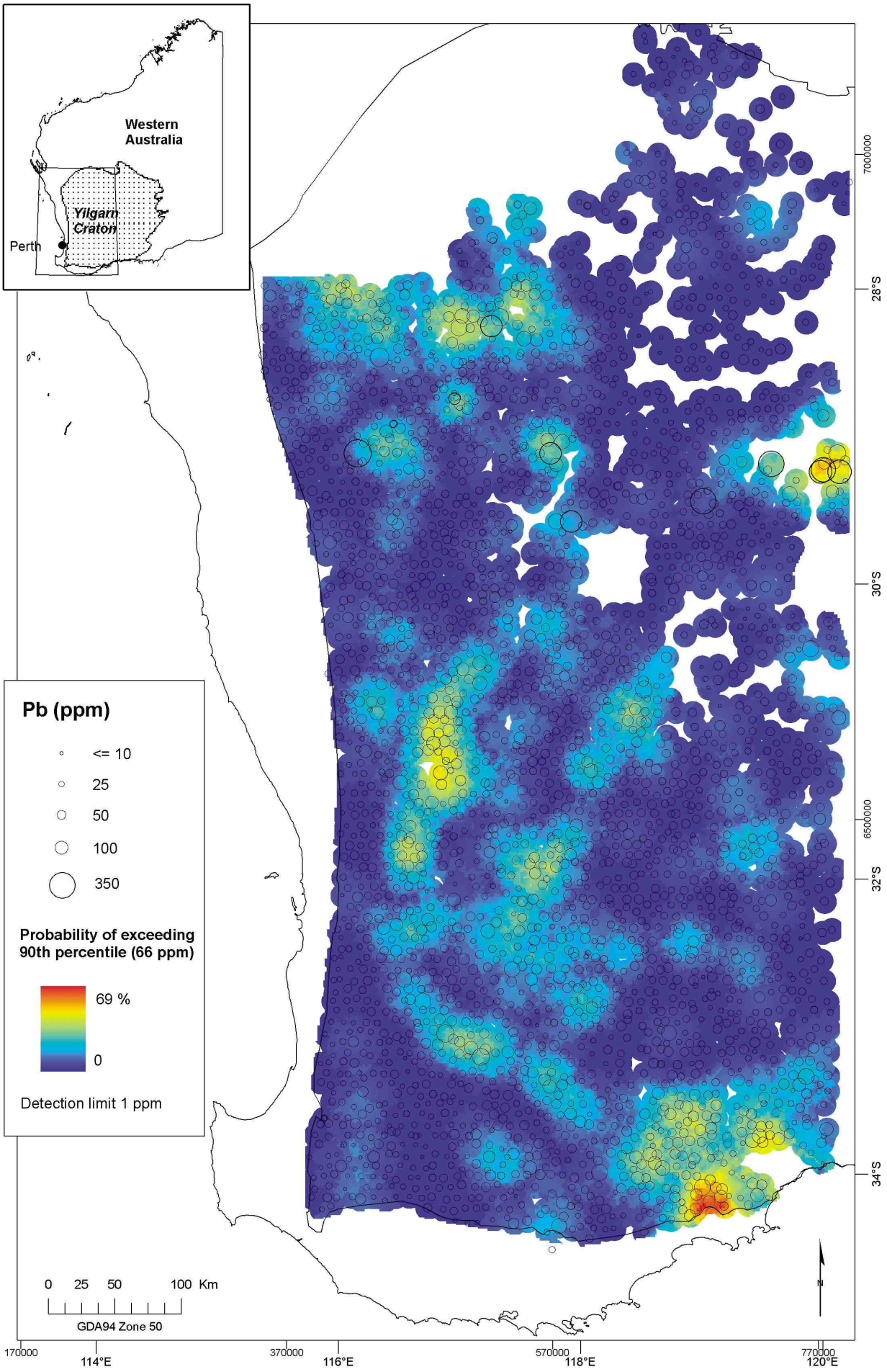
Western Australia
Yilgarn Craton
Perth
Pb (ppm)
<= 10
25
50
100
350
Probability of exceeding 90th percentile (66 ppm)
69 %
0
Detection limit 1 ppm
0 25 50 100 Km
GDA94 Zone 50
N
7000000
28°S
30°S
6500000
32°S
34°S
170000
114°E
370000
116°E
570000
118°E
770000
120°E

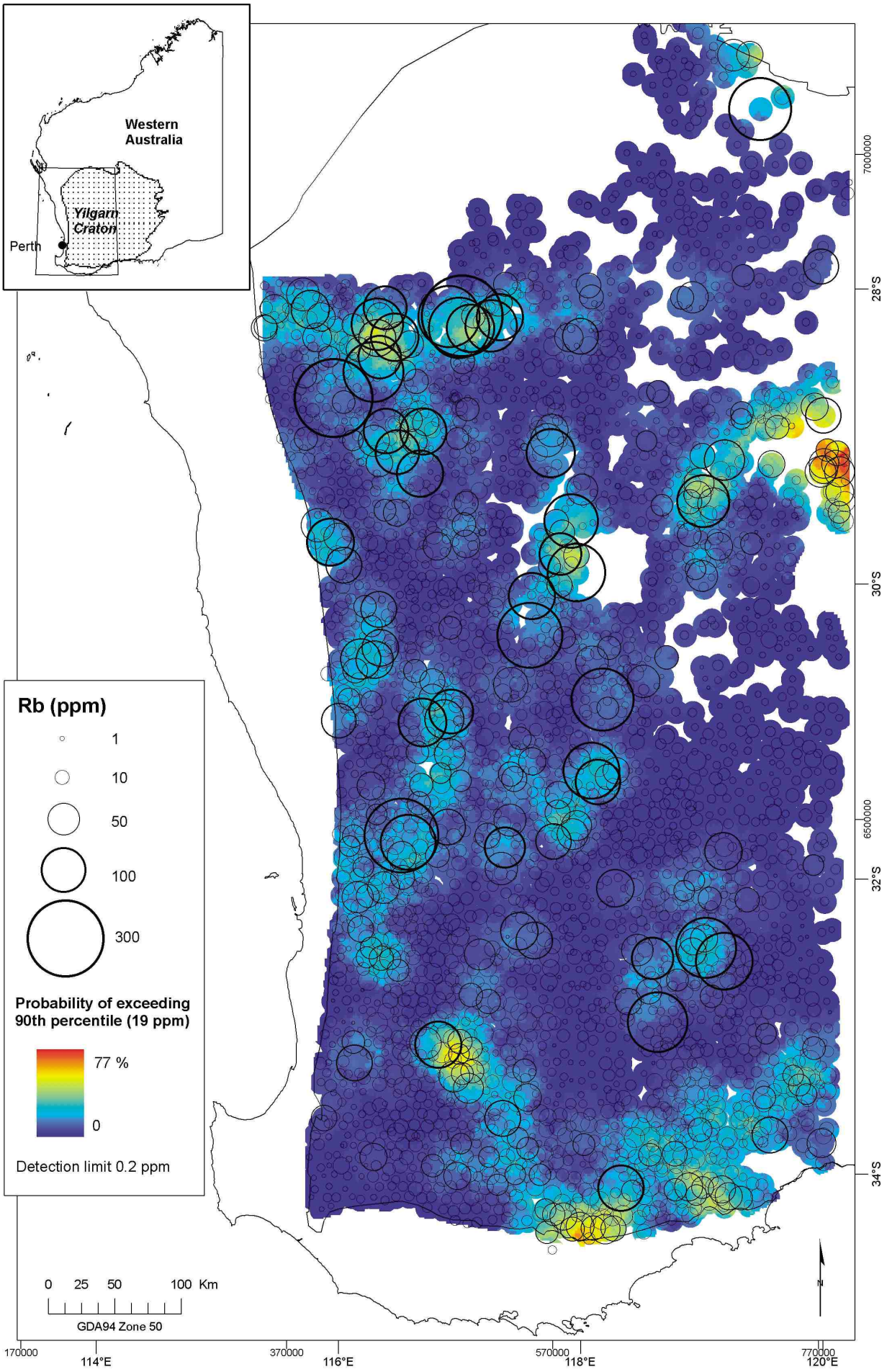
Western Australia
Yilgarn Craton
Perth
Rb (ppm)
1
10
50
100
300
Probability of exceeding 90th percentile (19 ppm)
77 %
0
Detection limit 0.2 ppm
0 25 50 100 Km
GDA94 Zone 50
170000
114°E
370000
116°E
570000
118°E
770000
120°E
7000000
28°S
6500000
30°S
32°S
34°S
N

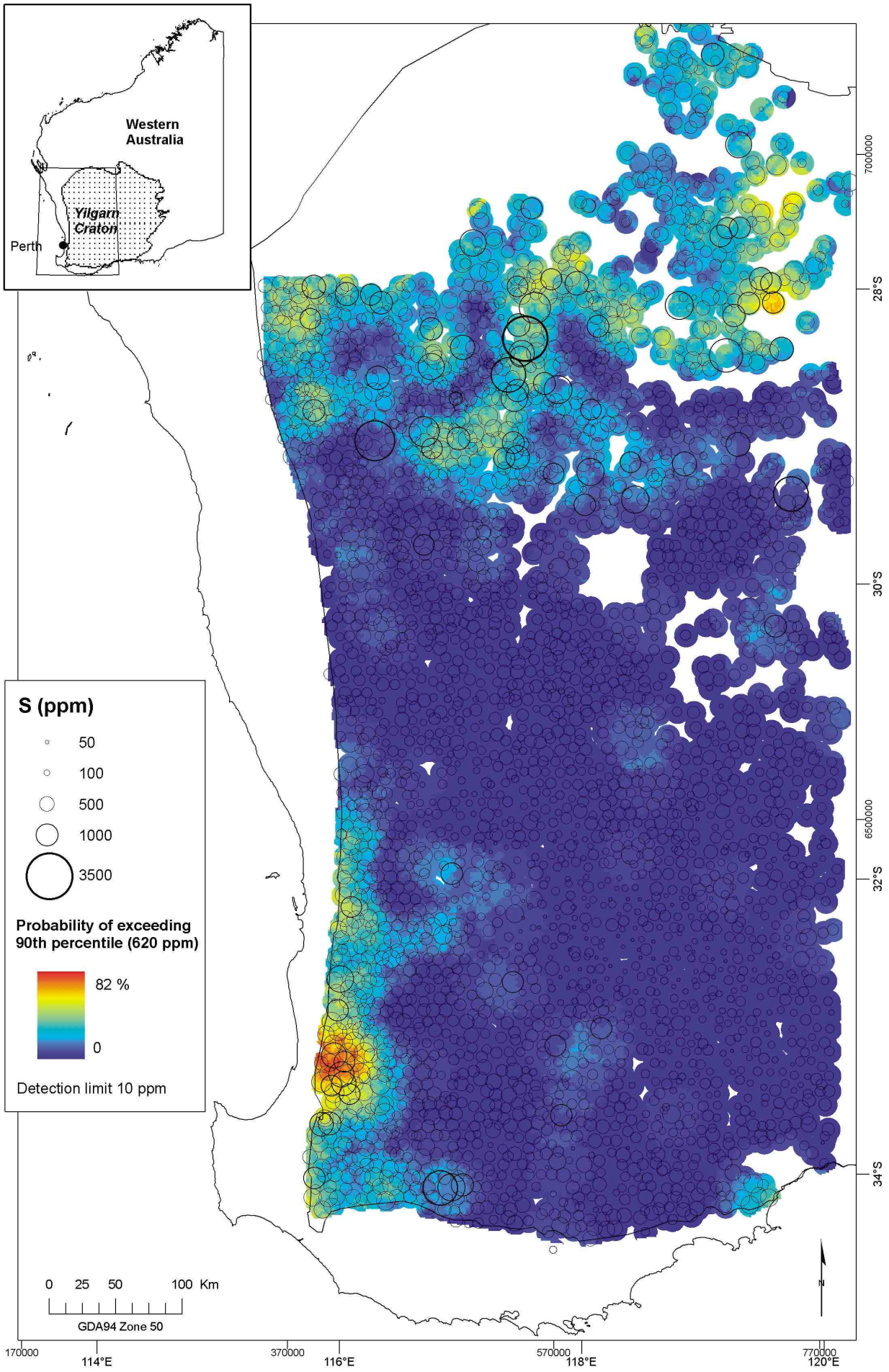
Western Australia
Yilgarn Craton
Perth
S (ppm)
50
100
500
1000
3500
Probability of exceeding 90th percentile (620 ppm)
82 %
0
Detection limit 10 ppm
0 25 50 100 Km
GDA94 Zone 50
N
7000000
28°S
30°S
6500000
32°S
34°S
170000
114°E
370000
116°E
570000
118°E
770000
120°E

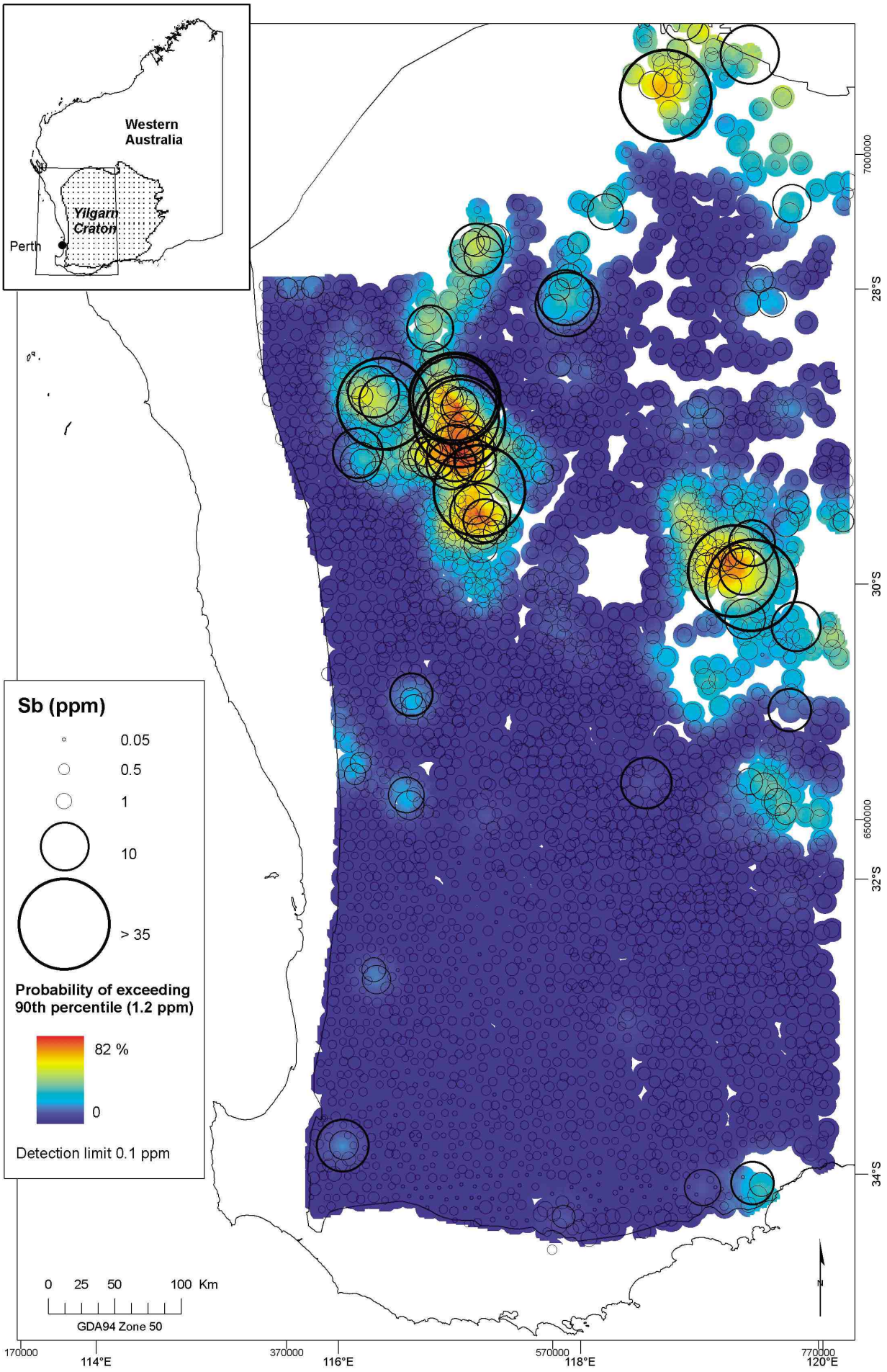
Western Australia
Yilgarn Craton
Perth
Sb (ppm)
0.05
0.5
1
10
> 35
Probability of exceeding 90th percentile (1.2 ppm)
82 %
0
Detection limit 0.1 ppm
0 25 50 100 Km
GDA94 Zone 50
170000
114°E
370000
116°E
570000
118°E
770000
120°E
7000000
28°S
6500000
30°S
32°S
34°S
N

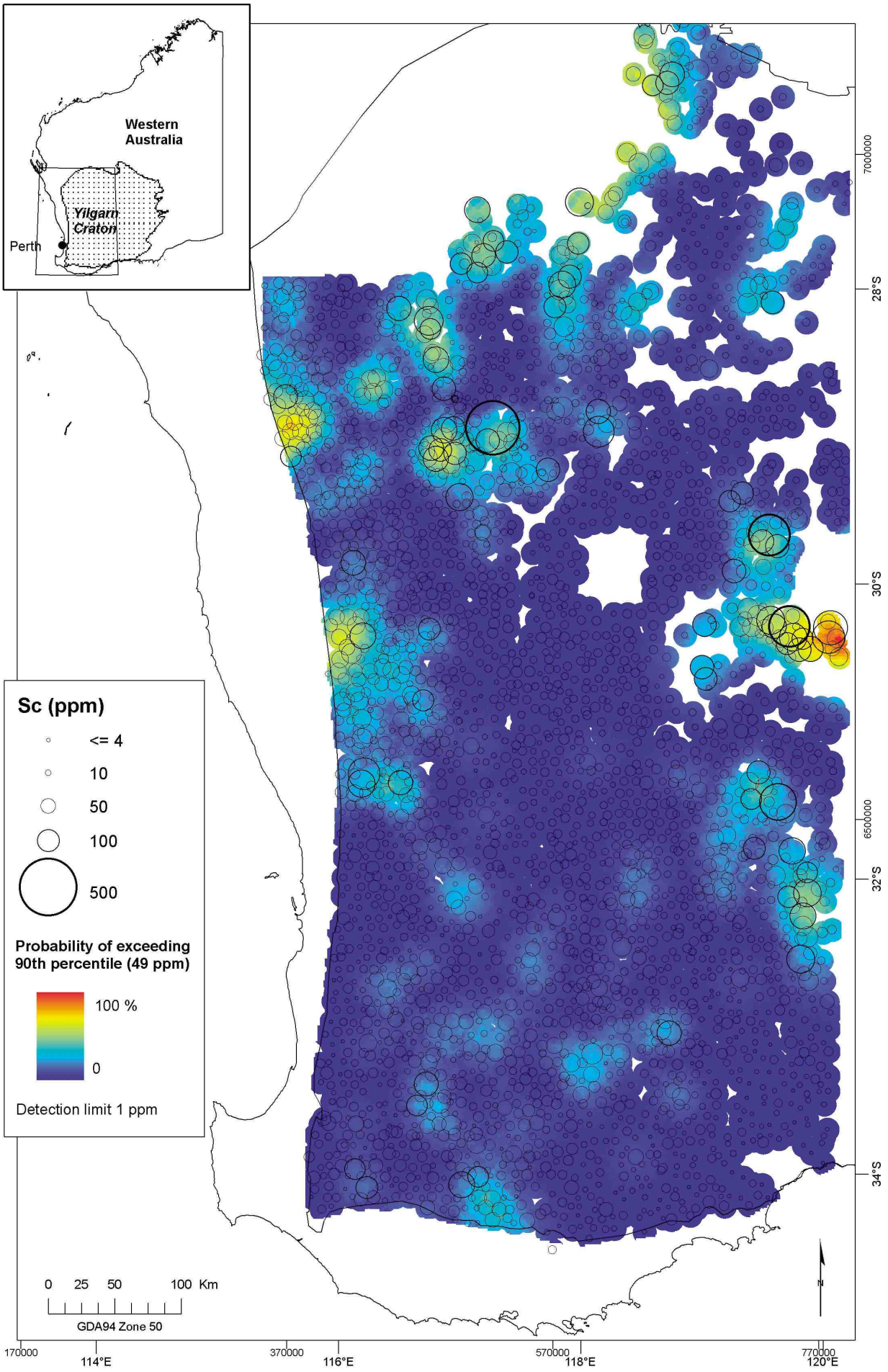
Western Australia
Yilgarn Craton
Perth
Sc (ppm)
<= 4
10
50
100
500
Probability of exceeding 90th percentile (49 ppm)
100 %
0
Detection limit 1 ppm
0 25 50 100 Km
GDA94 Zone 50
170000
114°E
370000
116°E
570000
118°E
770000
120°E
7000000
28°S
6500000
30°S
32°S
34°S
N

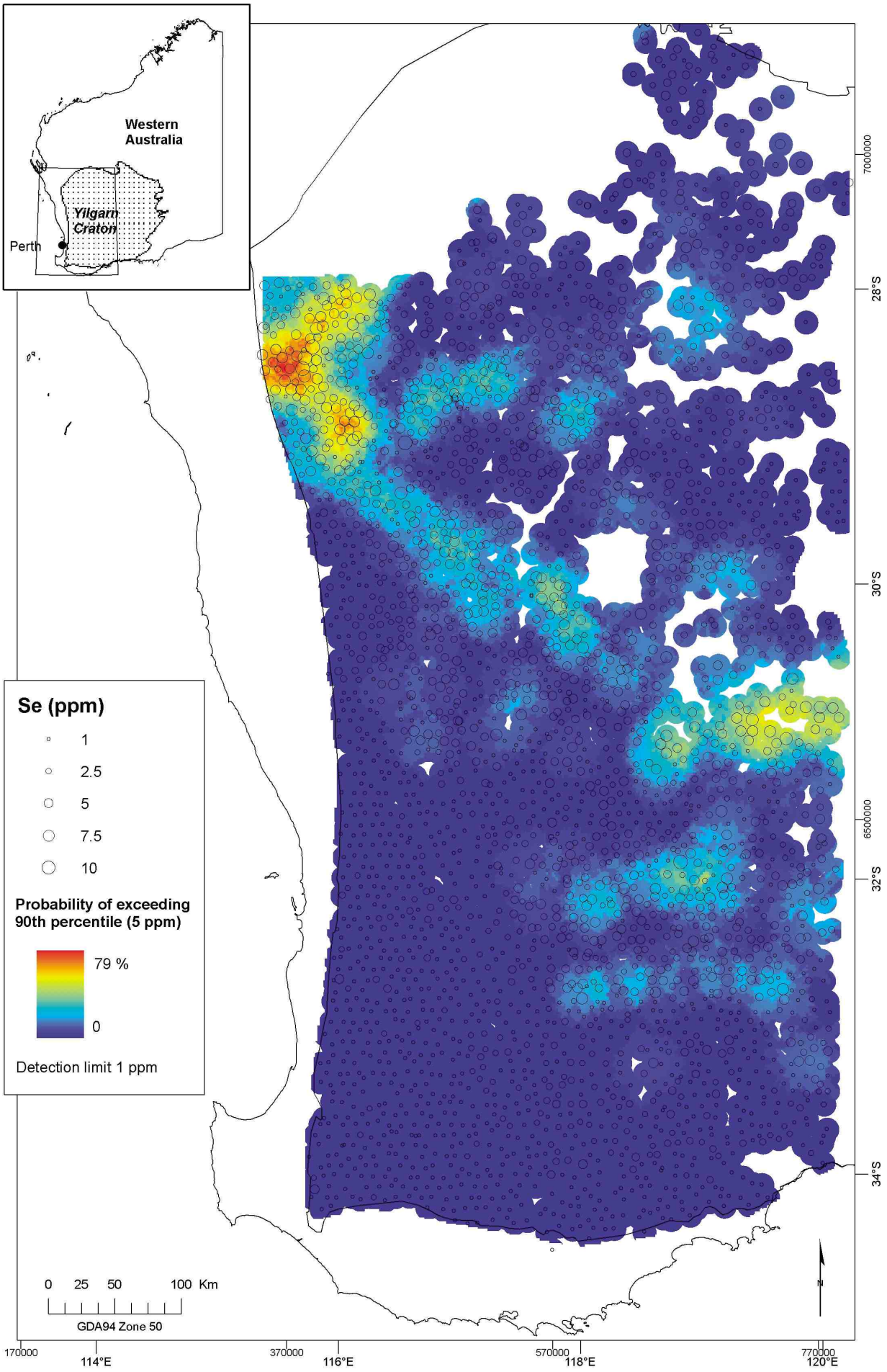
Western Australia
Yilgarn Craton
Perth
Se (ppm)
1
2.5
5
7.5
10
Probability of exceeding 90th percentile (5 ppm)
79 %
0
Detection limit 1 ppm
0 25 50 100 Km
GDA94 Zone 50
N
7000000
28°S
30°S
6500000
32°S
34°S
170000
114°E
370000
116°E
570000
118°E
770000
120°E

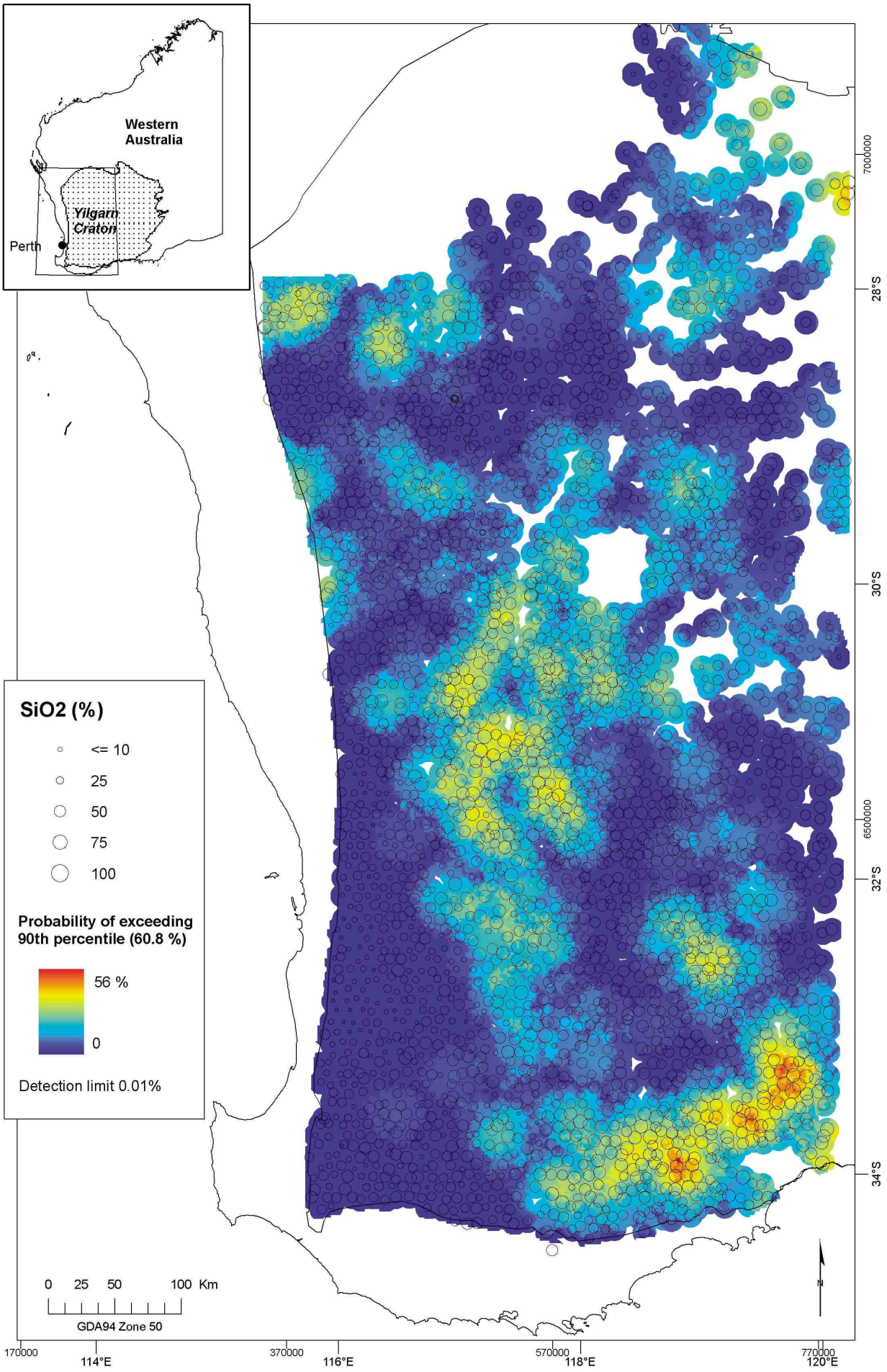
Western Australia
Yilgarn Craton
Perth
SiO2 (%)
<= 10
25
50
75
100
Probability of exceeding 90th percentile (60.8 %)
56 %
0
Detection limit 0.01%
0 25 50 100 Km
GDA94 Zone 50
170000
114°E
370000
116°E
570000
118°E
770000
120°E
7000000
28°S
6500000
30°S
32°S
34°S
N

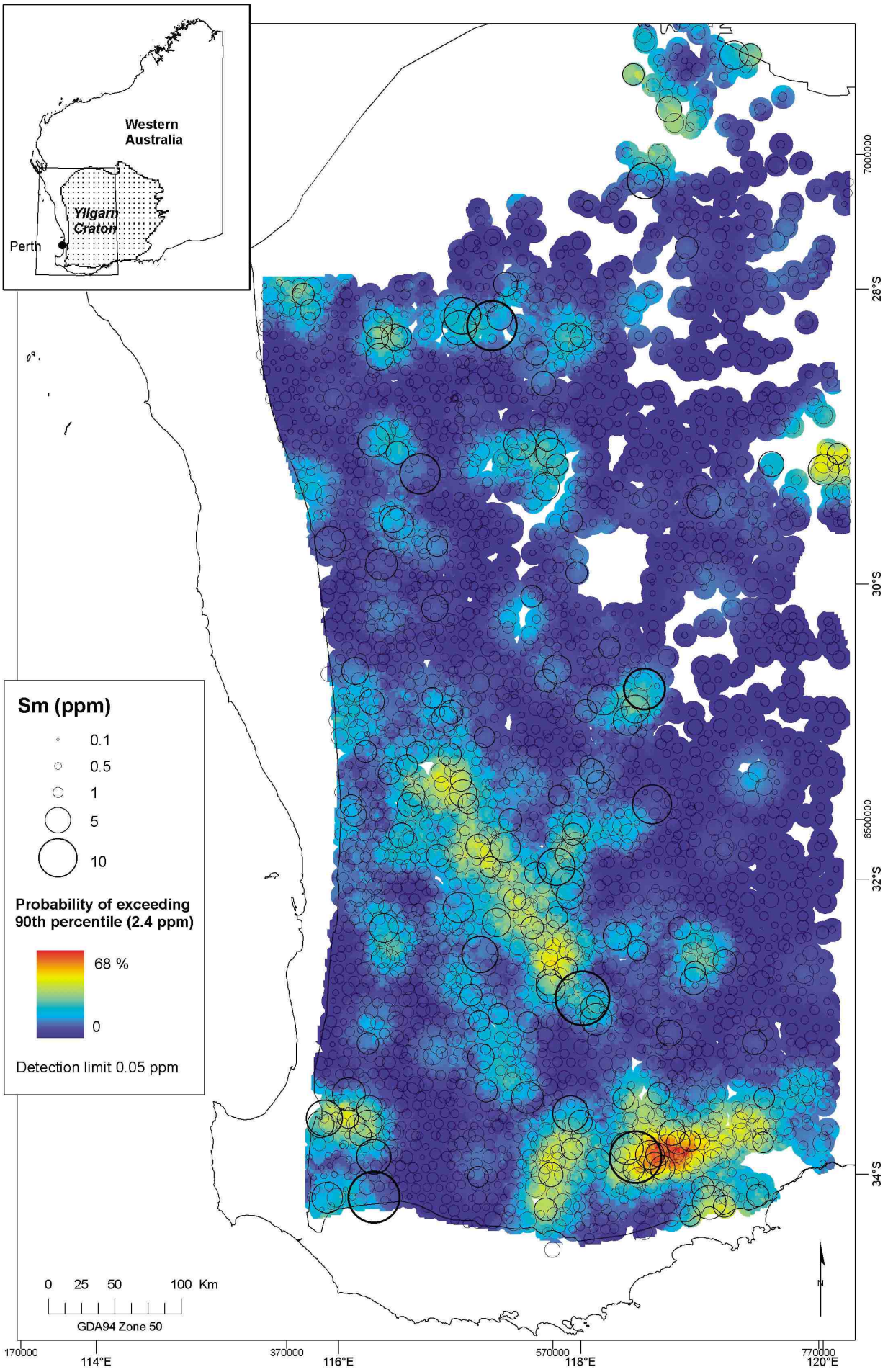
Western Australia
Yilgarn Craton
Perth
Sm (ppm)
0.1
0.5
1
5
10
Probability of exceeding 90th percentile (2.4 ppm)
68 %
0
Detection limit 0.05 ppm
0 25 50 100 Km
GDA94 Zone 50
N
170000
114°E
370000
116°E
570000
118°E
770000
120°E
7000000
28°S
6500000
30°S
32°S
34°S

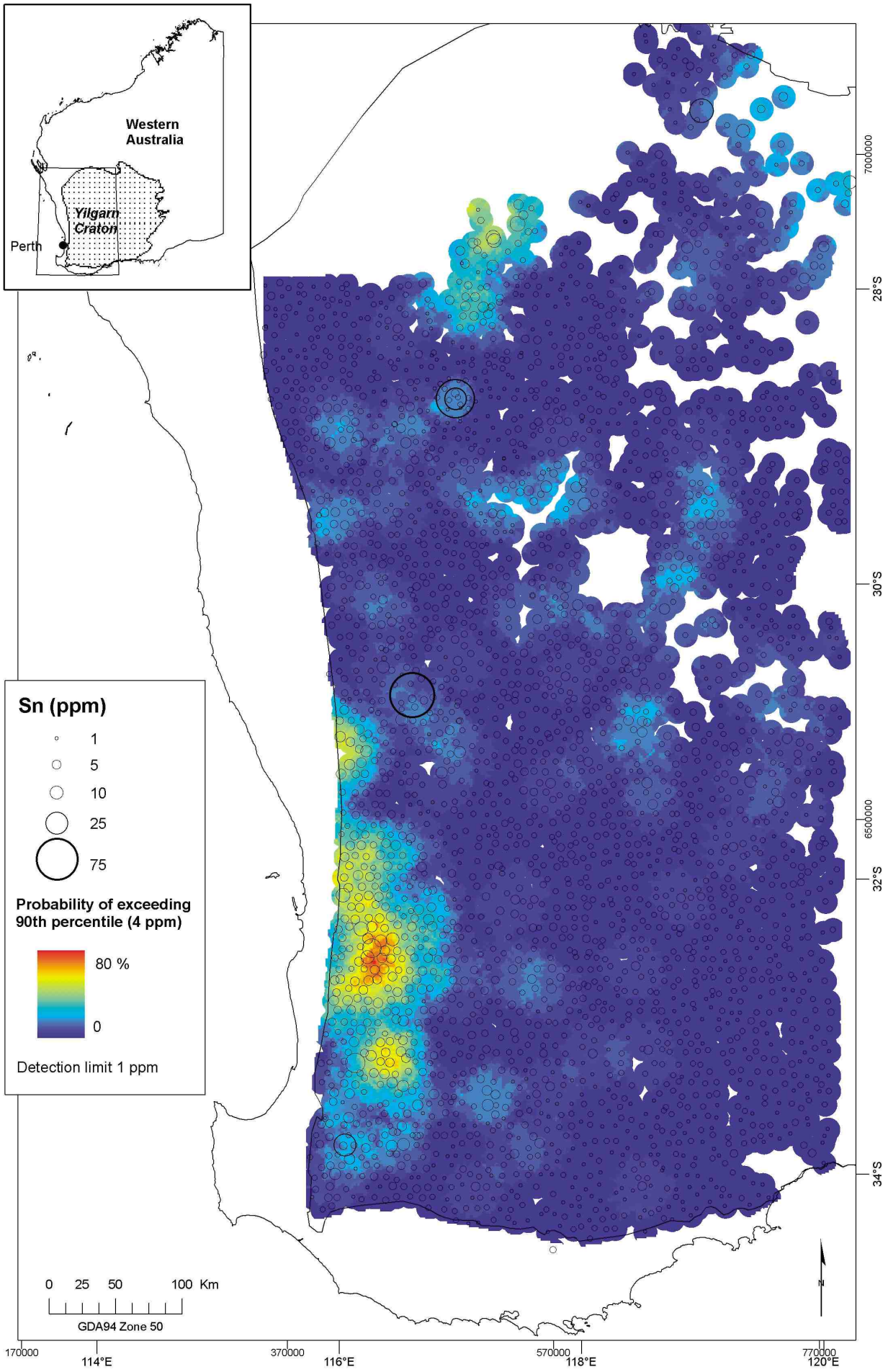
Western Australia
Yilgarn Craton
Perth
Sn (ppm)
1
5
10
25
75
Probability of exceeding 90th percentile (4 ppm)
80 %
0
Detection limit 1 ppm
0 25 50 100 Km
GDA94 Zone 50
170000
114°E
370000
116°E
570000
118°E
770000
120°E
7000000
28°S
6500000
30°S
32°S
34°S
N

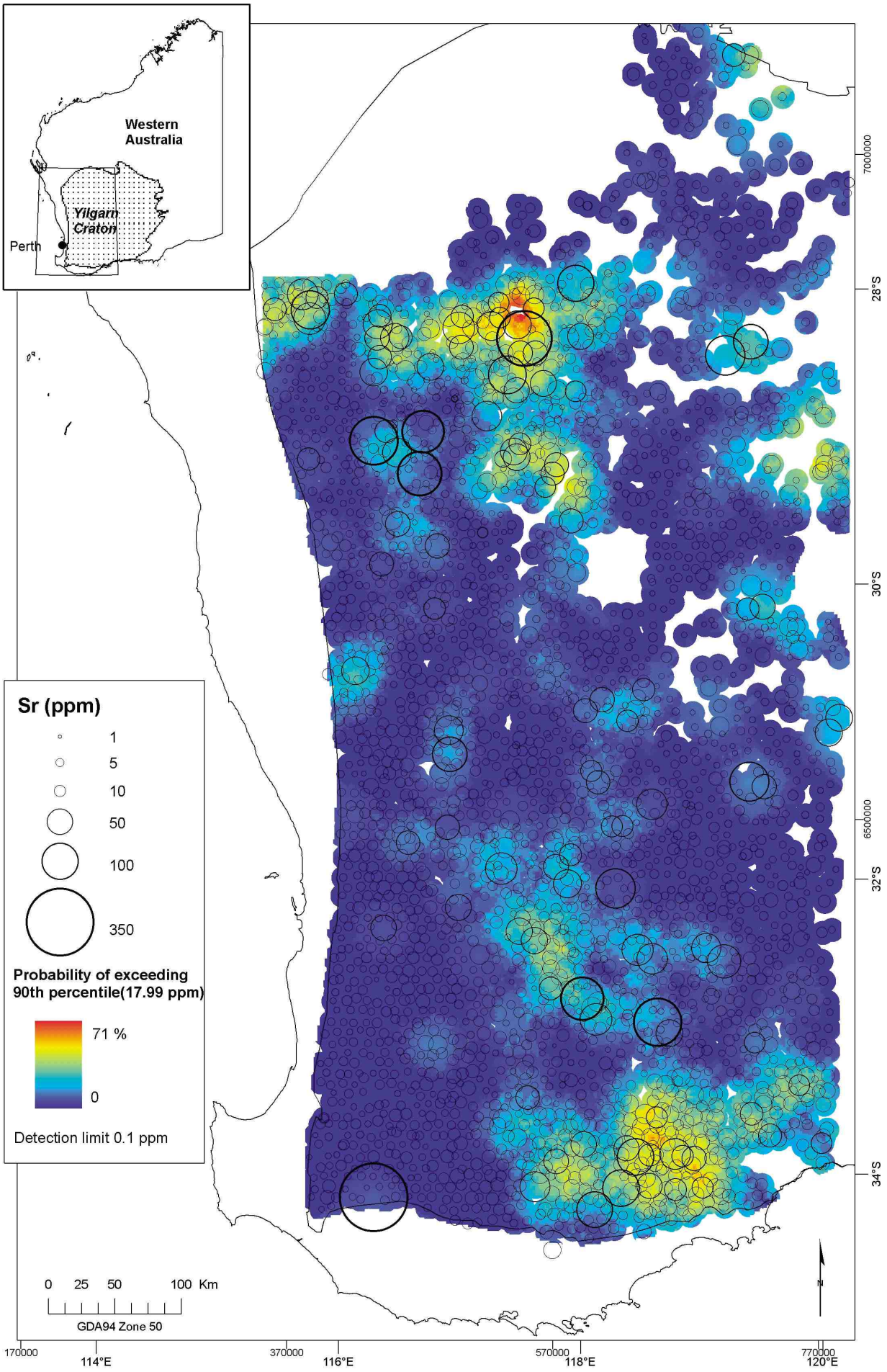
Western Australia
Yilgarn Craton
Perth
Sr (ppm)
1
5
10
50
100
350
Probability of exceeding 90th percentile(17.99 ppm)
71 %
0
Detection limit 0.1 ppm
0 25 50 100 Km
GDA94 Zone 50
7000000
28°S
30°S
6500000
32°S
34°S
170000
114°E
370000
116°E
570000
118°E
770000
120°E
N

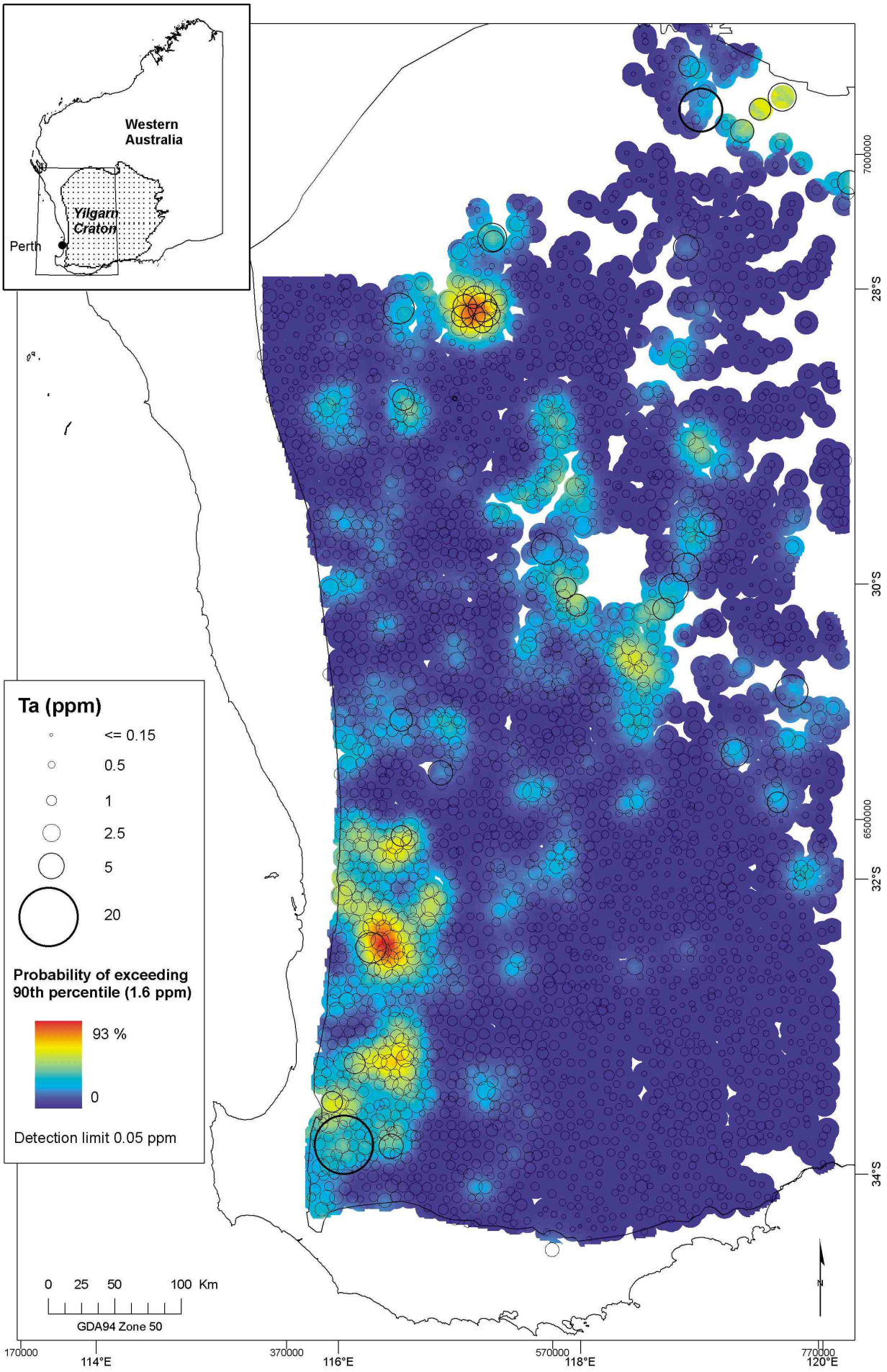
Western Australia
Yilgarn Craton
Perth
Ta (ppm)
<= 0.15
0.5
1
2.5
5
20
Probability of exceeding 90th percentile (1.6 ppm)
93 %
0
Detection limit 0.05 ppm
0 25 50 100 Km
GDA94 Zone 50
7000000
28°S
30°S
6500000
32°S
34°S
170000
114°E
370000
116°E
570000
118°E
770000
120°E

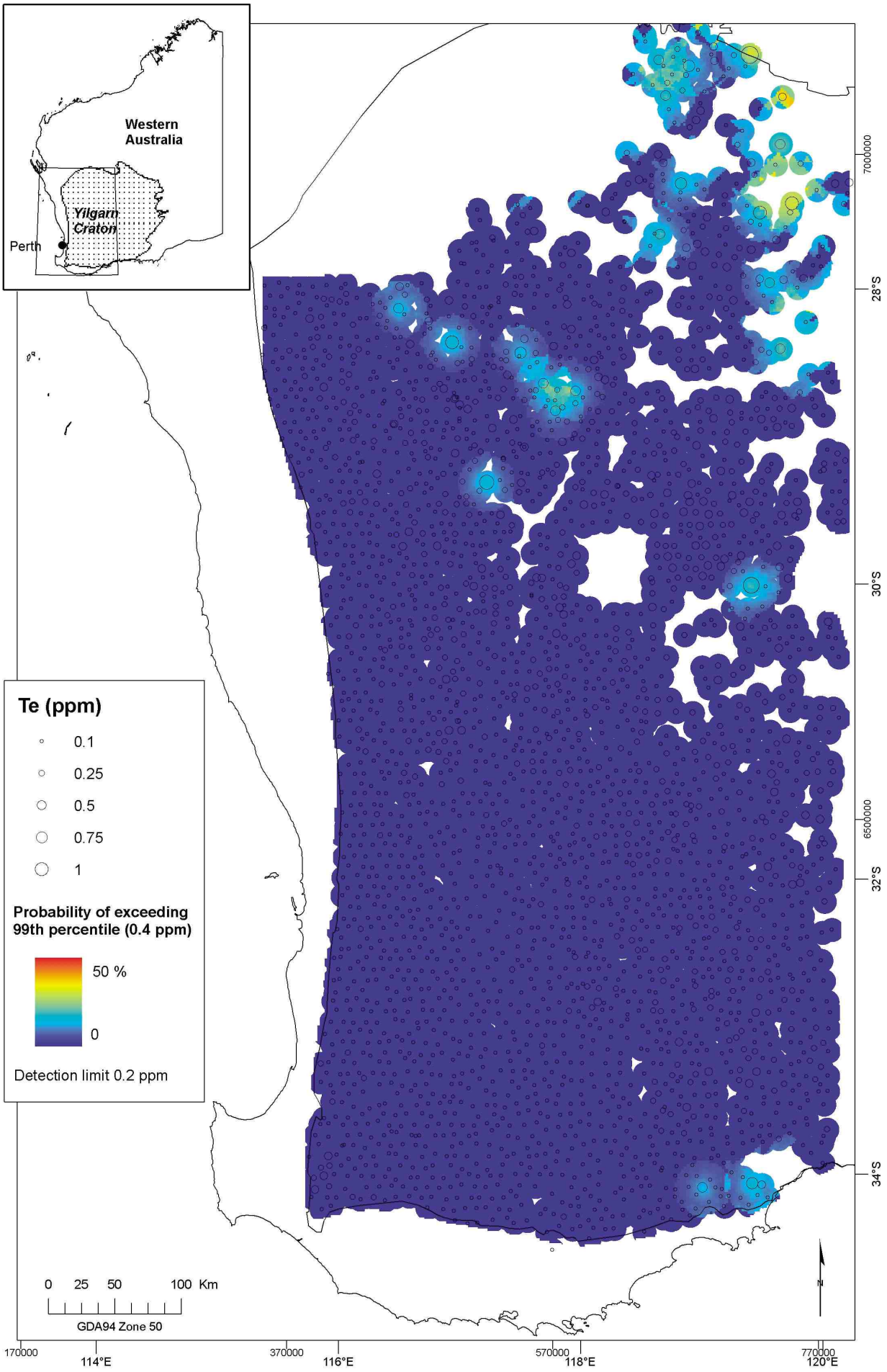
Western Australia
Yilgarn Craton
Perth
Te (ppm)
0.1
0.25
0.5
0.75
1
Probability of exceeding 99th percentile (0.4 ppm)
50 %
0
Detection limit 0.2 ppm
0 25 50 100 Km
GDA94 Zone 50
170000
114°E
370000
116°E
570000
118°E
770000
120°E
7000000
28°S
6500000
30°S
32°S
34°S
N

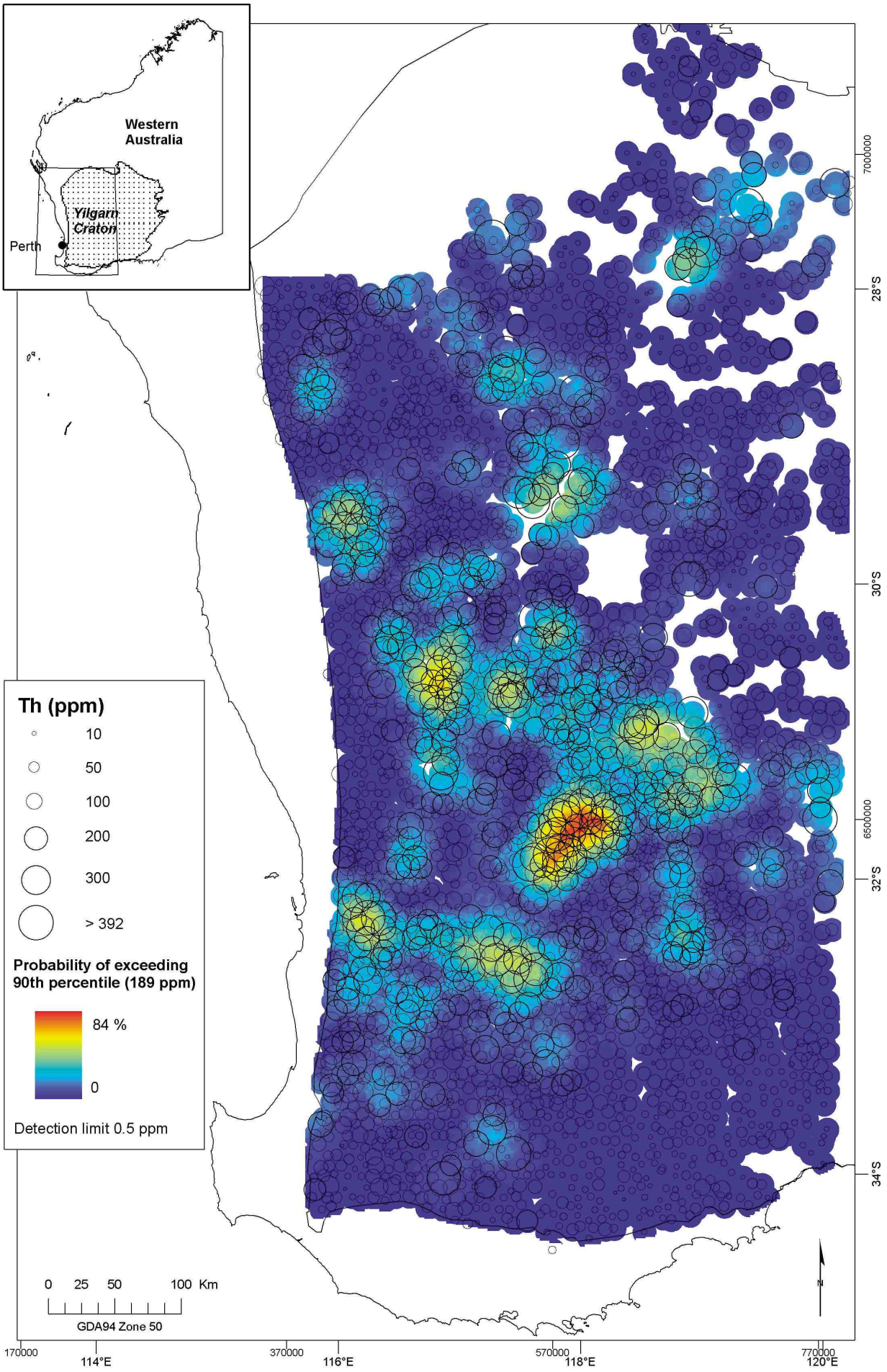
Western Australia
Yilgarn Craton
Perth
Th (ppm)
10
50
100
200
300
> 392
Probability of exceeding 90th percentile (189 ppm)
84 %
0
Detection limit 0.5 ppm
0 25 50 100 Km
GDA94 Zone 50
N
7000000
28°S
30°S
6500000
32°S
34°S
170000
114°E
370000
116°E
570000
118°E
770000
120°E

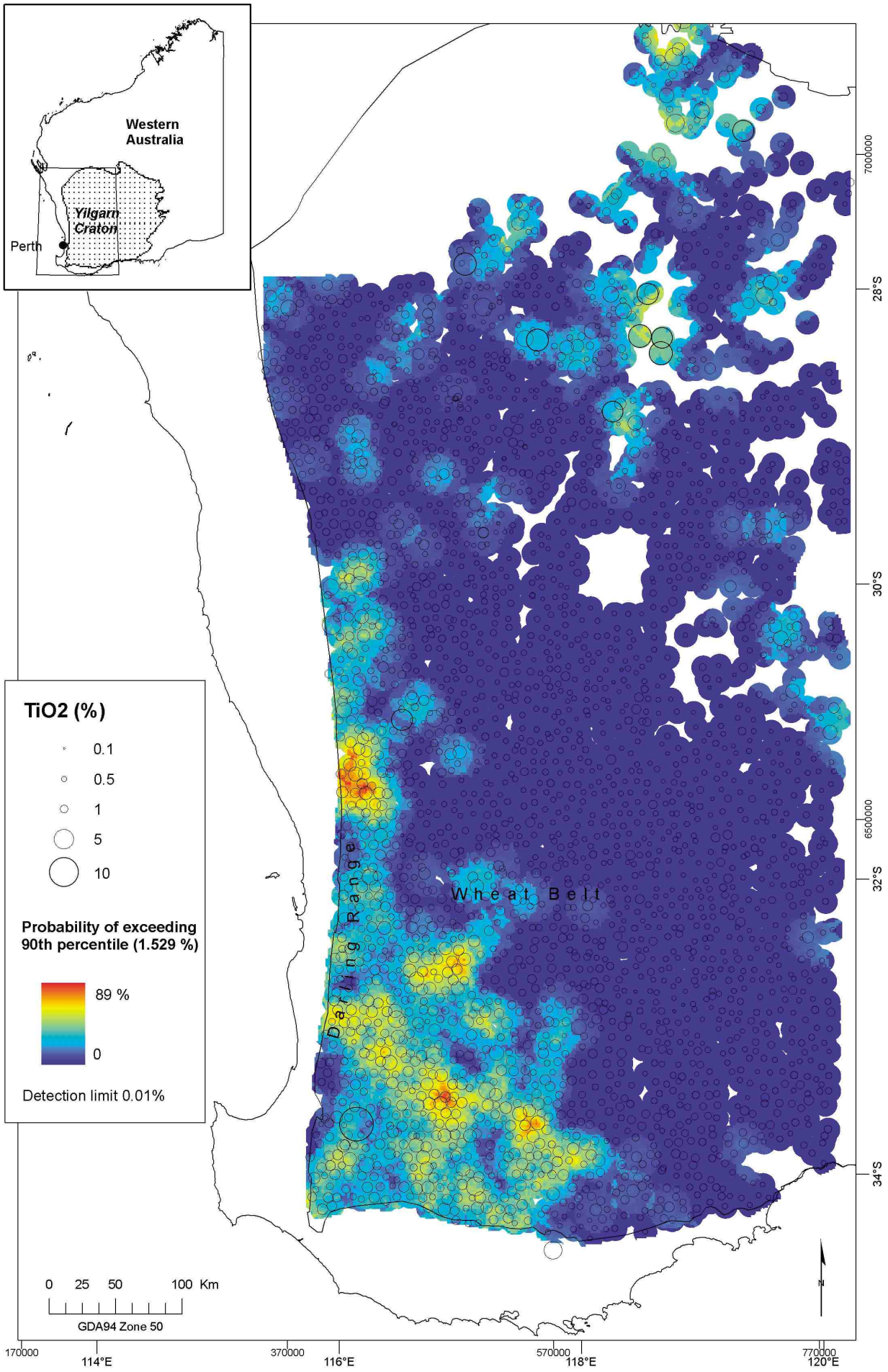
Western Australia
Yilgarn Craton
Perth
TiO2 (%)
0.1
0.5
1
5
10
Probability of exceeding 90th percentile (1.529 %)
89 %
0
Detection limit 0.01%
Darling Range
Wheat Belt
0 25 50 100 Km
GDA94 Zone 50
N
170000
114°E
370000
116°E
570000
118°E
770000
120°E
7000000
28°S
6500000
30°S
32°S
34°S

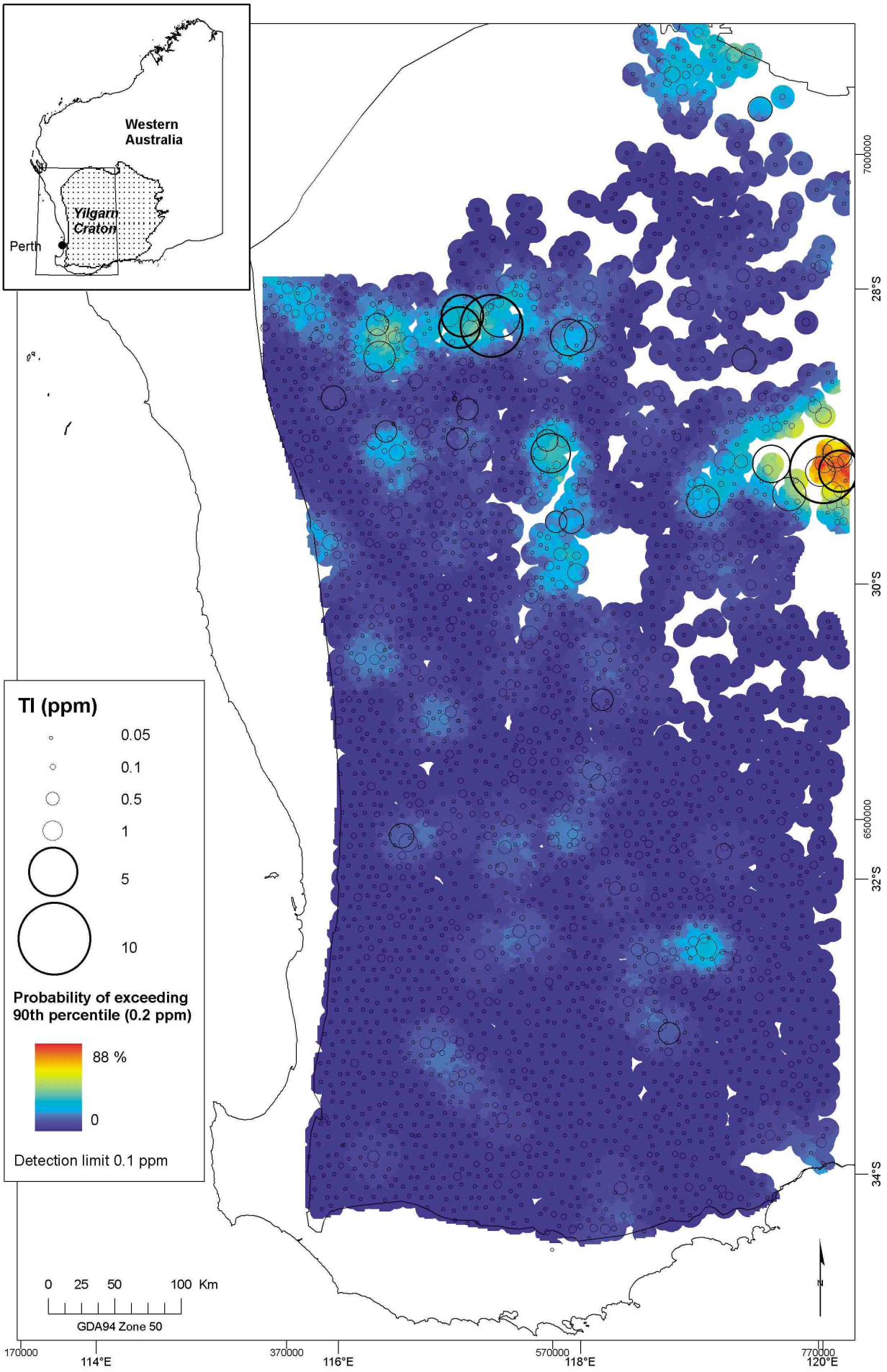
Western Australia
Yilgarn Craton
Perth
Tl (ppm)
0.05
0.1
0.5
1
5
10
Probability of exceeding 90th percentile (0.2 ppm)
88 %
0
Detection limit 0.1 ppm
0 25 50 100 Km
GDA94 Zone 50
170000
114°E
370000
116°E
570000
118°E
770000
120°E
7000000
28°S
6500000
30°S
32°S
34°S
N

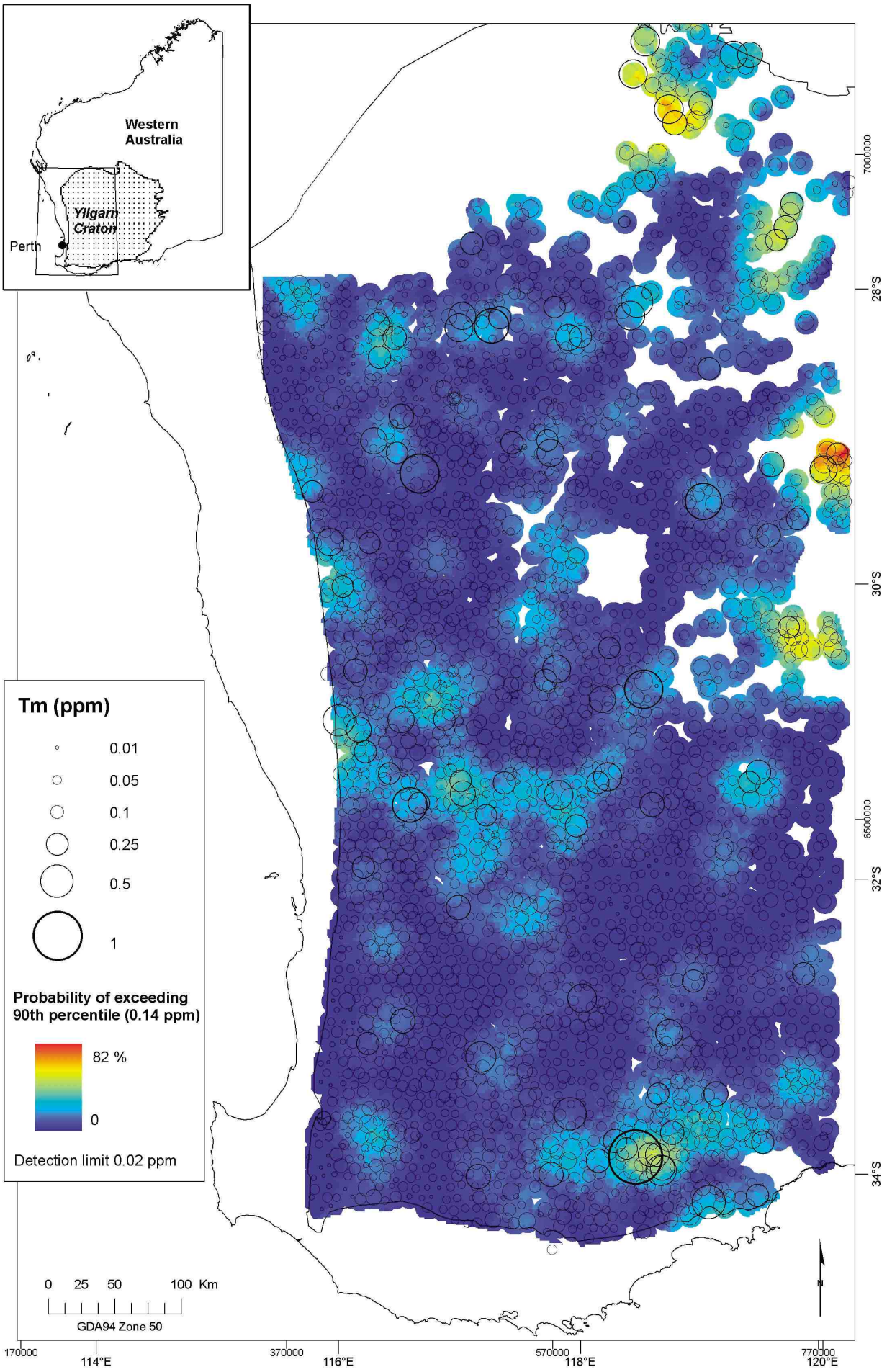
Western Australia
Yilgarn Craton
Perth
Tm (ppm)
0.01
0.05
0.1
0.25
0.5
1
Probability of exceeding 90th percentile (0.14 ppm)
82 %
0
Detection limit 0.02 ppm
0 25 50 100 Km
GDA94 Zone 50
7000000
28°S
30°S
6500000
32°S
34°S
170000
114°E
370000
116°E
570000
118°E
770000
120°E

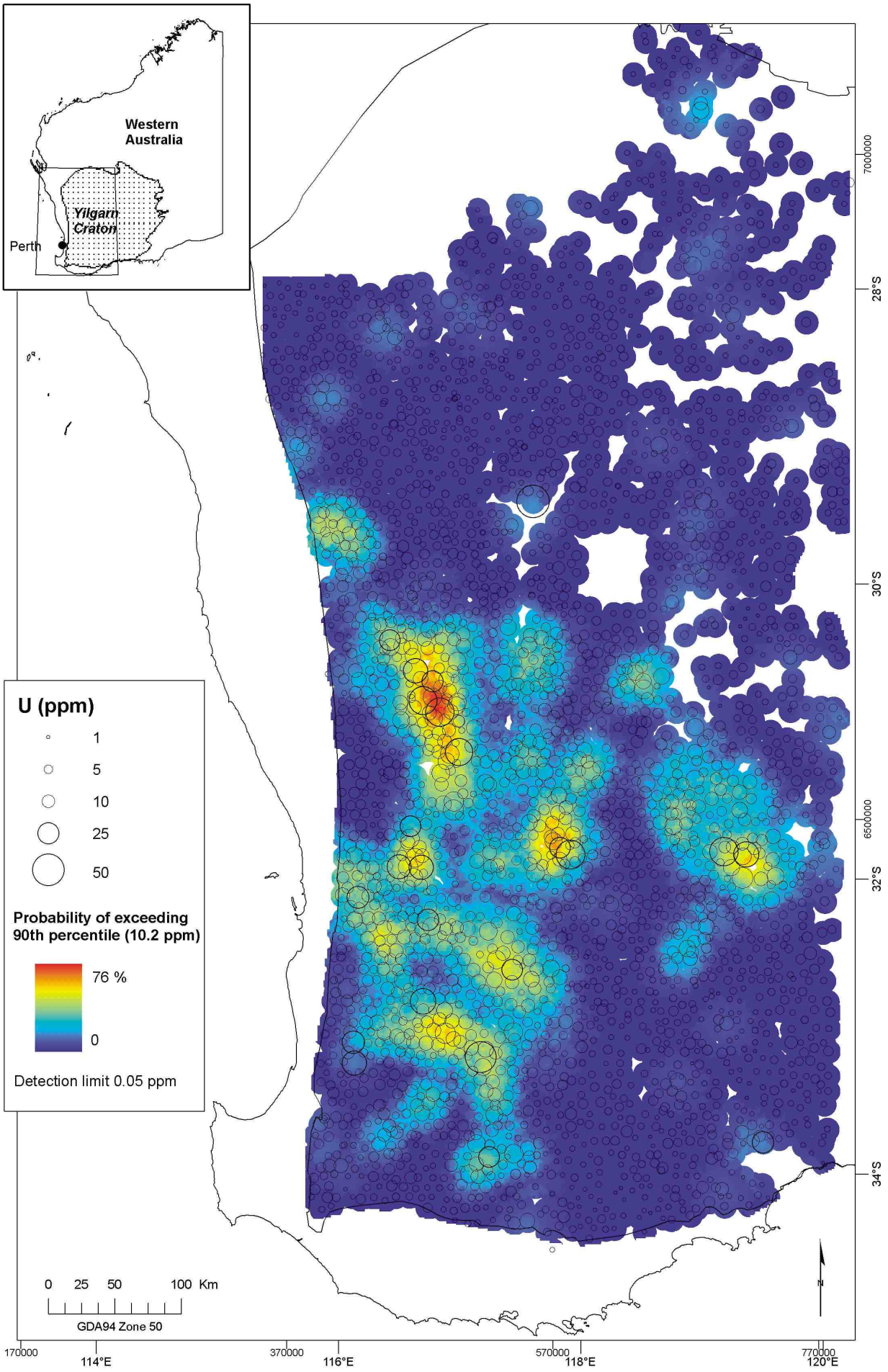
Western Australia
Yilgarn Craton
Perth
U (ppm)
1
5
10
25
50
Probability of exceeding 90th percentile (10.2 ppm)
76 %
0
Detection limit 0.05 ppm
0 25 50 100 Km
GDA94 Zone 50
170000
114°E
370000
116°E
570000
118°E
770000
120°E
7000000
28°S
6500000
30°S
32°S
34°S
N

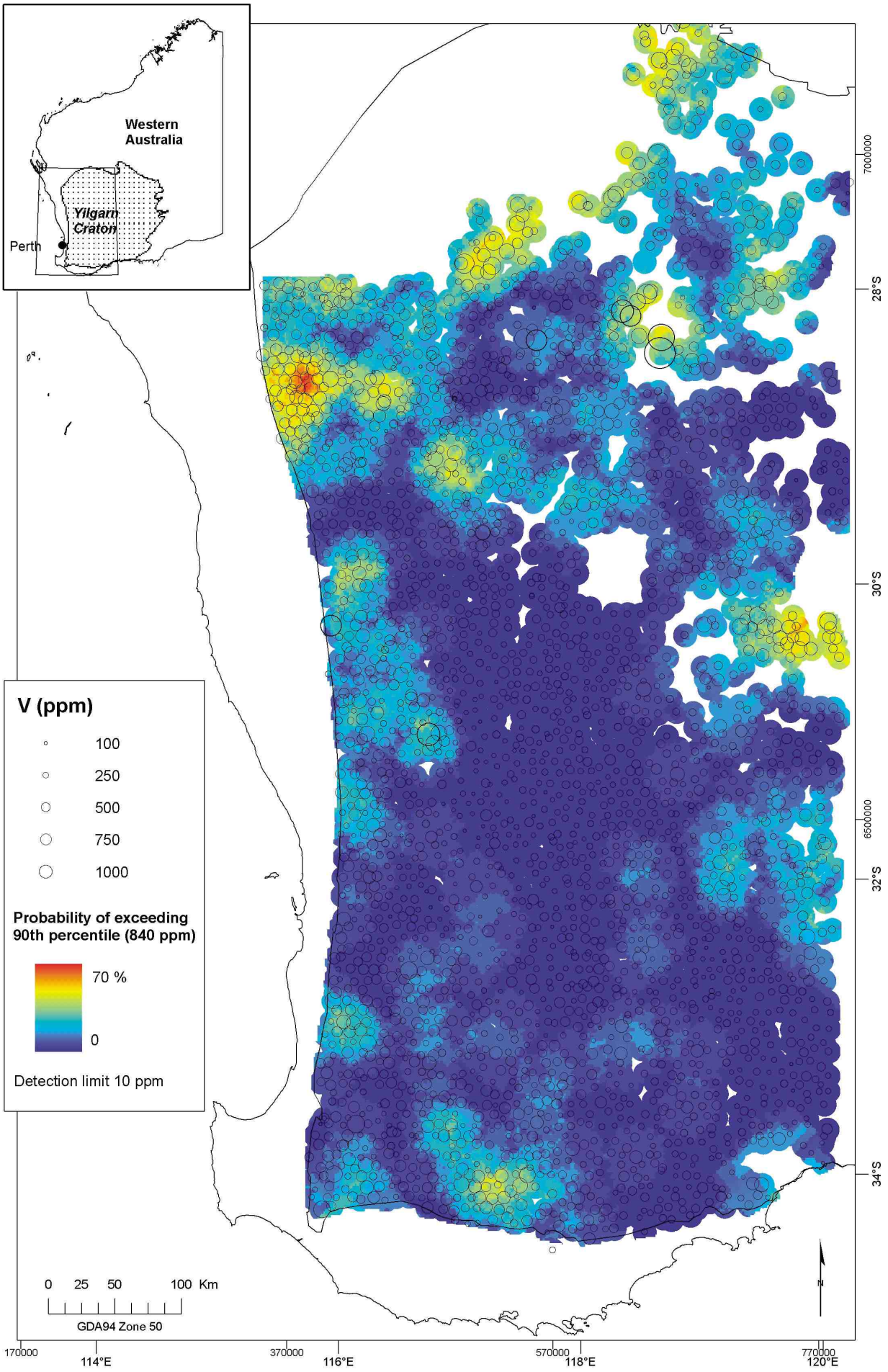
Western Australia
Yilgarn Craton
Perth
V (ppm)
100
250
500
750
1000
Probability of exceeding 90th percentile (840 ppm)
70 %
0
Detection limit 10 ppm
0 25 50 100 Km
GDA94 Zone 50
N
7000000
6500000
28°S
30°S
32°S
34°S
170000
370000
570000
770000
114°E
116°E
118°E
120°E

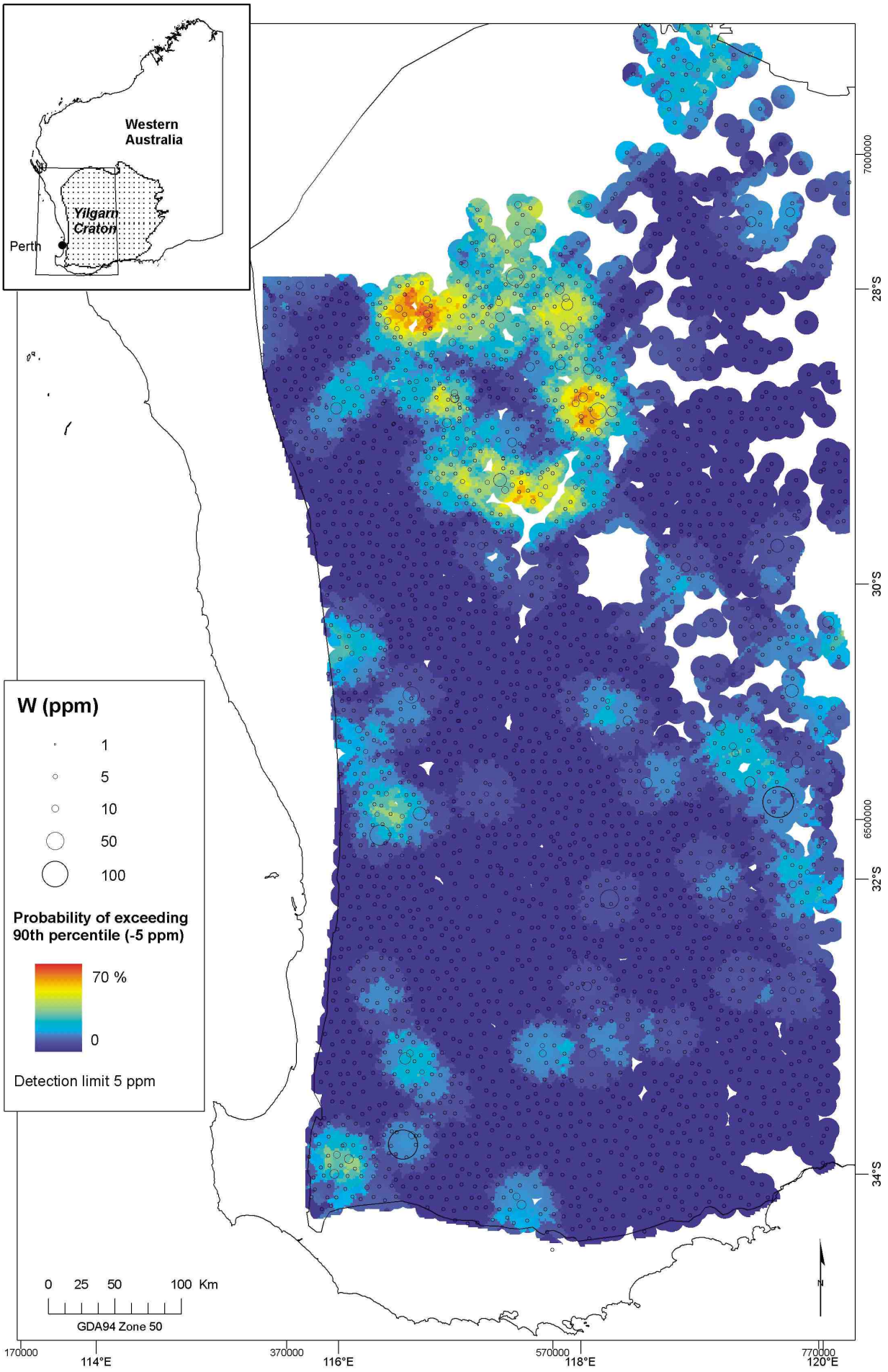
Western Australia
Yilgarn Craton
Perth
W (ppm)
1
5
10
50
100
Probability of exceeding 90th percentile (-5 ppm)
70 %
0
Detection limit 5 ppm
0 25 50 100 Km
GDA94 Zone 50
N
7000000
28°S
30°S
6500000
32°S
34°S
170000
114°E
370000
116°E
570000
118°E
770000
120°E

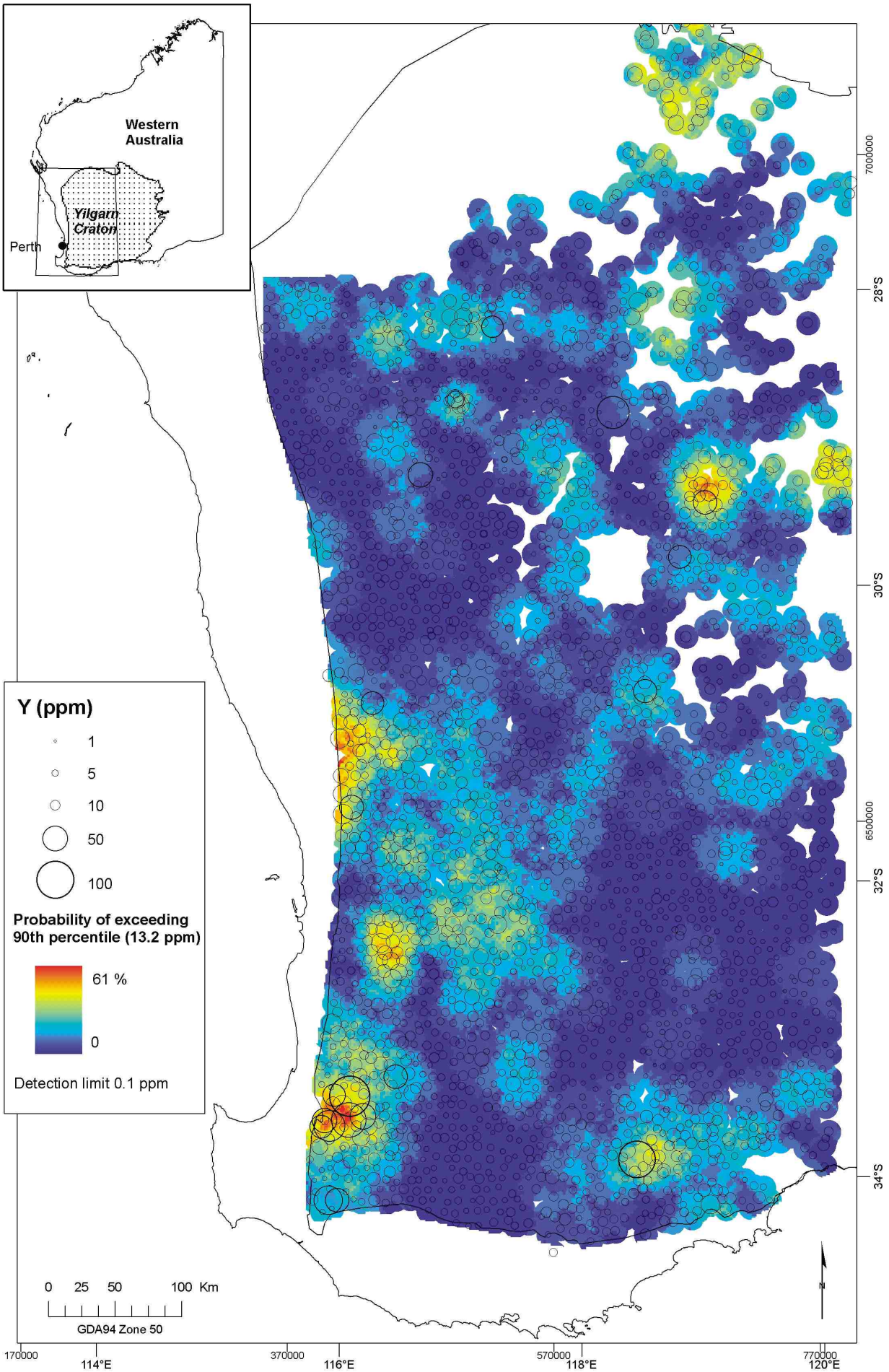
Western Australia
Yilgarn Craton
Perth
Y (ppm)
1
5
10
50
100
Probability of exceeding 90th percentile (13.2 ppm)
61 %
0
Detection limit 0.1 ppm
0 25 50 100 Km
GDA94 Zone 50
7000000
28°S
30°S
6500000
32°S
34°S
170000
114°E
370000
116°E
570000
118°E
770000
120°E
N

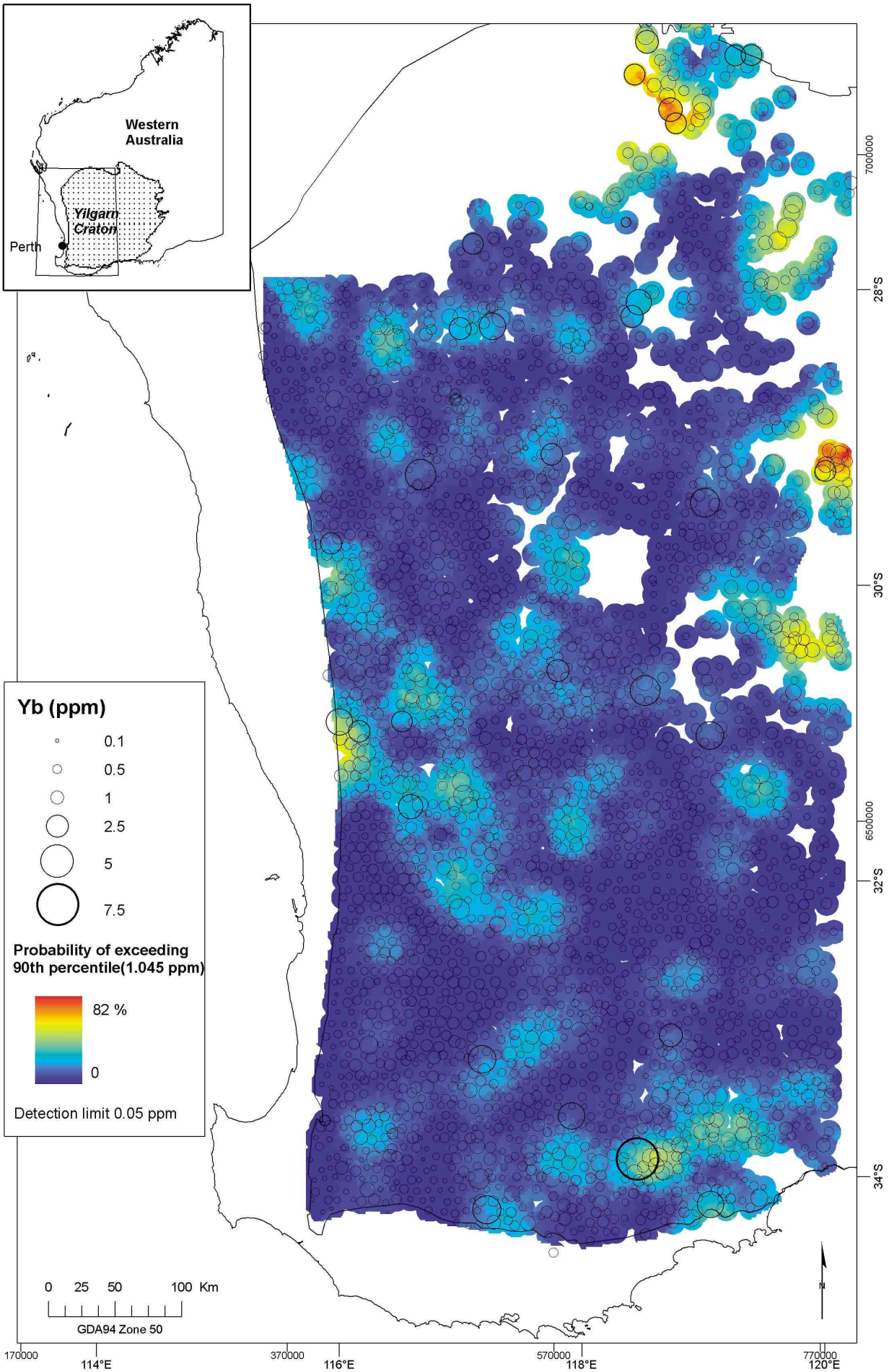
Western Australia
Yilgarn Craton
Perth
Yb (ppm)
0.1
0.5
1
2.5
5
7.5
Probability of exceeding 90th percentile(1.045 ppm)
82 %
0
Detection limit 0.05 ppm
0 25 50 100 Km
GDA94 Zone 50
N
7000000
6500000
28°S
30°S
32°S
34°S
170000
370000
570000
770000
114°E
116°E
118°E
120°E

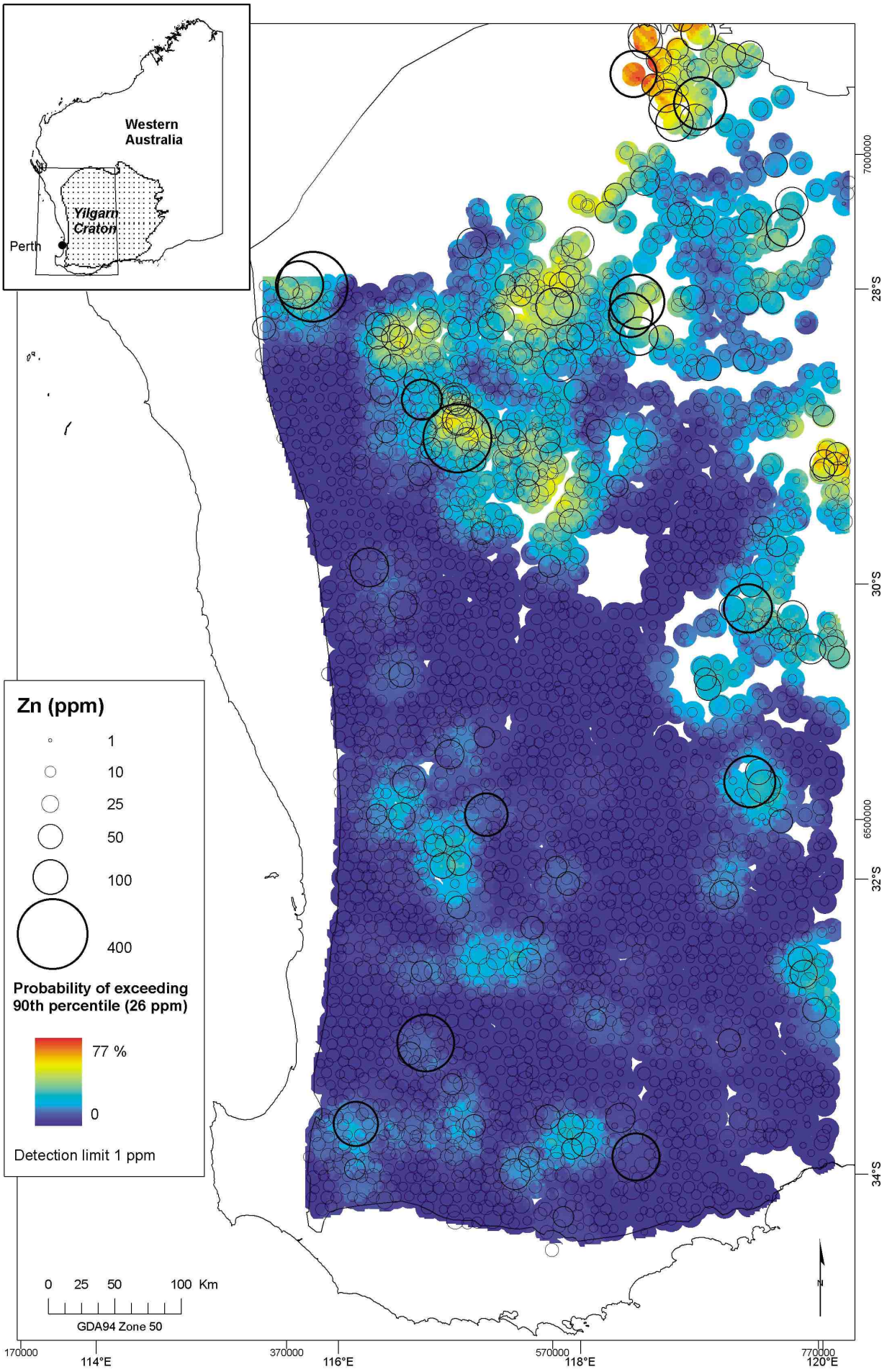
Western Australia
Yilgarn Craton
Perth
Zn (ppm)
1
10
25
50
100
400
Probability of exceeding 90th percentile (26 ppm)
77 %
0
Detection limit 1 ppm
0 25 50 100 Km
GDA94 Zone 50
N
7000000
28°S
30°S
6500000
32°S
34°S
170000
114°E
370000
116°E
570000
118°E
770000
120°E

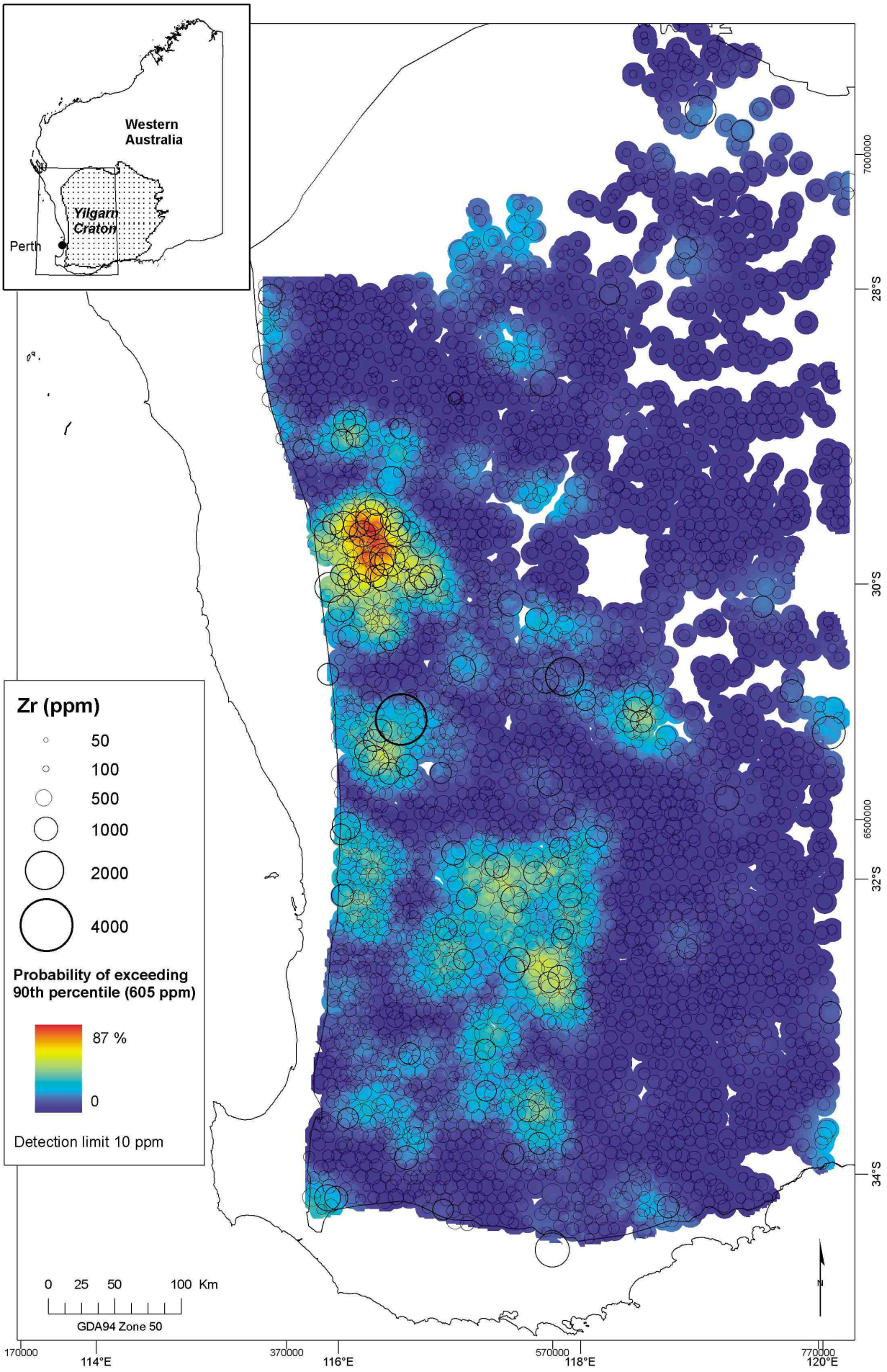
Western Australia
Yilgarn Craton
Perth
Zr (ppm)
50
100
500
1000
2000
4000
Probability of exceeding 90th percentile (605 ppm)
87 %
0
Detection limit 10 ppm
0 25 50 100 Km
GDA94 Zone 50
170000
114°E
370000
116°E
570000
118°E
770000
120°E
7000000
28°S
6500000
30°S
32°S
34°S
N

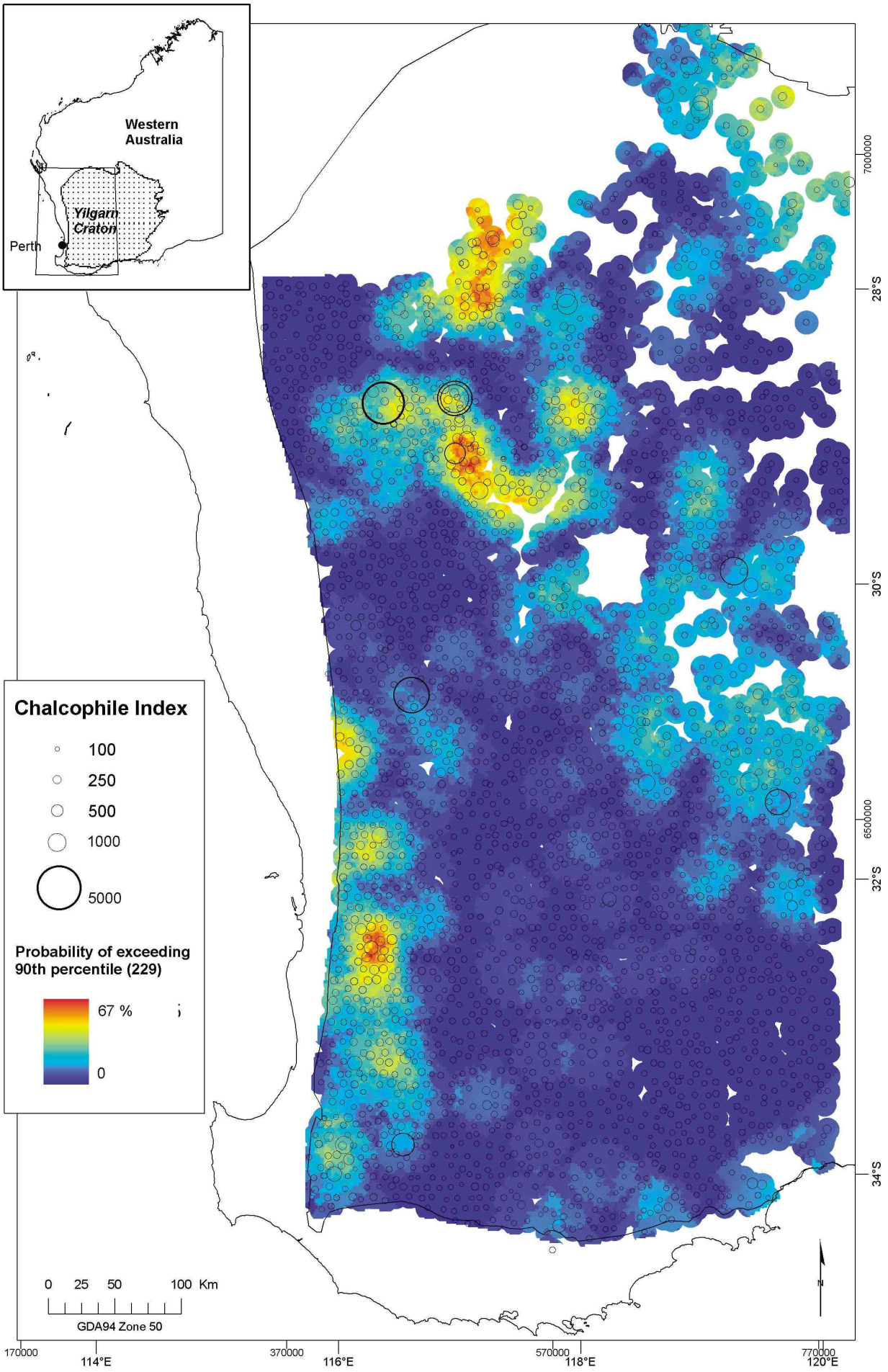
Western Australia
Yilgarn Craton
Perth
Chalcophile Index
100
250
500
1000
5000
Probability of exceeding 90th percentile (229)
67 %
0
0 25 50 100 Km
GDA94 Zone 50
170000
114°E
370000
116°E
570000
118°E
770000
120°E
7000000
28°S
6500000
30°S
32°S
34°S
N

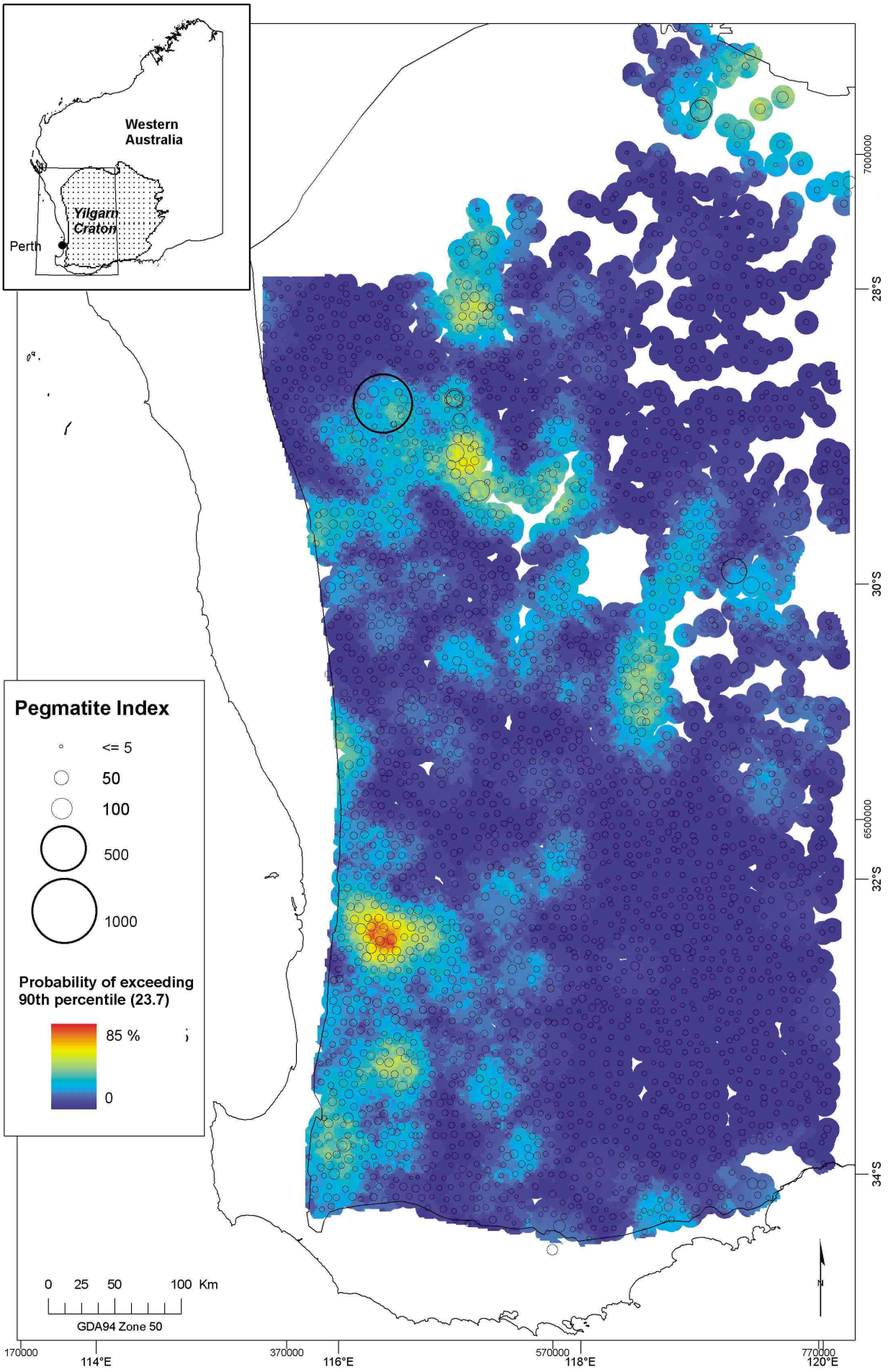
Western Australia
Yilgarn Craton
Perth
Pegmatite Index
<= 5
50
100
500
1000
Probability of exceeding 90th percentile (23.7)
85 %
0
0 25 50 100 Km
GDA94 Zone 50
N
7000000
6500000
28°S
30°S
32°S
34°S
170000
370000
570000
770000
114°E
116°E
118°E
120°E

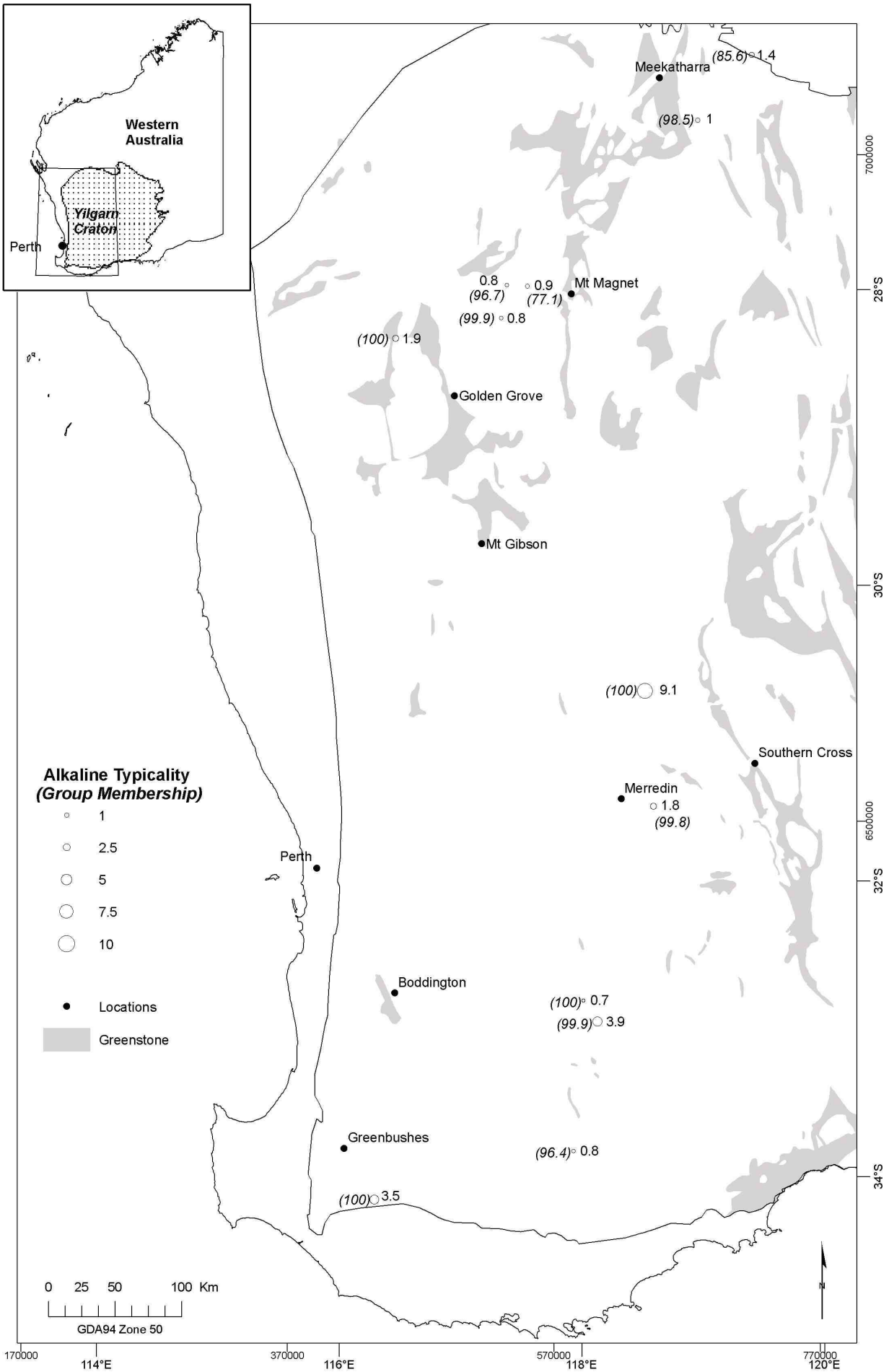
Western Australia
Yilgarn Craton
Perth
Meekatharra
(85.6) 1.4
(98.5) 1
0.8
(96.7)
0.9
(77.1)
Mt Magnet
(99.9) 0.8
(100) 1.9
Golden Grove
Mt Gibson
(100) 9.1
Southern Cross
Merredin
1.8
(99.8)
Perth
Boddington
(100) 0.7
(99.9) 3.9
Greenbushes
(96.4) 0.8
(100) 3.5
Alkaline Typicality
(Group Membership)
1
2.5
5
7.5
10
Locations
Greenstone
0 25 50 100 Km
GDA94 Zone 50
N
7000000
6500000
28°S
30°S
32°S
34°S
170000
370000
570000
770000
114°E
116°E
118°E
120°E